STUDIES OF PHOTOCONDUCTIVITY AND ASSOCIATED PHENOMENA IN CADMIUM IODIDE

by

D. K. WRIGHT

A Dissertation Submitted to the
University of Warwick for
Admission to the Degree of
Doctor of Philosophy.

CONTENTS

ABSTRACT

The photoconductivity of cadmium iodide is described in this dissertation. Measurements have been made at temperatures between 300°K and 10°K on high quality single crystals grown from solution. A sensitive electrometer, with a noise level of less than 10^{-16} amps enabled low currents to be measured and low illumination intensities to be used; the photocurrent was then proportional to the intensity. The photoresponse has been determined at energies up to ~6.5eV; at high energies, near 5.6eV, where exciton effects become important, the photoconductivity is comparable to that in the adjacent band to band transition regions.

Reflectivity measurements have been made in the same apparatus, many of the reflectivity features appeared in the photoconductivity spectrum in particular the high energy exciton reflectivity peaks appeared as photoresponse dips. The reflectivity spectra enabled the photoresponse to be corrected for photons lost by reflection. When the photoresponse for absorbed photons was plotted against absorption coefficient a smooth curve was obtained. The points corresponding to the exciton lines at 5.7eV and 6.2eV did not fall on the curve, however, the exciton photoresponse was some 100% greater than that predicted on the basis of absorption coefficient. The smooth curve may be interpreted in terms of the De Vore model and the increased photoresponse at the exciton lines in terms of an exciton diffusion process.

A semi-empirical electron energy level scheme has been given, this is based upon the correspondence between the optical spectra obtained from many metallic iodides. The scheme is consistent with the available optical information and agrees with the photoconductivity results.

The measurements of photoconductivity, particularly those made at low temperatures, were involved with the polarisation of the sample caused by the trapping of charge carriers. This polarisation was found to be both intensity and energy dependent, so that it could influence the shape of the photoresponse spectrum. An explanation has been given for these effects, in particular the energy dependence was explained in terms of the variation of the absorption coefficient.

The thermally stimulated current curve method has been used in an investigation of trapping levels. Illumination took place at $10^{o}K$, subsequent warming indicated that many different trapping levels were active. The trapping level energies were determined and glow peaks compared in two different electrode geometries. Some peaks were enhanced when a volume sensitive electrode geometry was used; it was therefore possible to distinguish volume and surface distributed traps. These conclusions were substantiated when a thin film was used, since only surface traps would then be important. Spectrographic analysis of typical crystals showed that the impurity content was low, the chief impurity was iron with 3 ppm.

A discussion of the effects of intense ultra-violet illumination, i.e. photodecomposition, on cadmium iodide is given in Chapter Seven. These experiments indicated that decomposition occurred most readily at crystal imperfections. After visible decomposition the surface resistance of typical crystals fell by many orders of magnitude to a value of $\sim 10^{6}\Omega$. This resistance was not strongly temperature dependent, the current was thought to be carried along filaments of decomposition products. Part of the photodecomposition investigation lead to the discovery of the diffusion of silver in CdI_2 at temperatures near $250^{o}C$. This result indicated that silver electrodes were not suitable for photoconductivity or ionic conductivity measurements at high temperature and explained why previous high temperature measurements were unreliable. Evaporated gold has been shown to give ohmic contacts and to be stable at high temperatures even after prolonged use.

The electronic and optical properties of CdI_2 were summarized in Chapter Eight. Proposals have been made for future experiments to investigate these properties. Amongst these a new technique for the measurement of photoconductivity and simultaneous correction for reflectivity loss was described.

ACKNOWLEDGEMENTS

The studies described in this thesis were carried out in the School of Physics of the University of Warwick. I am therefore grateful to Professor A.J. Forty of this department for the generous provision of laboratory facilities and for his encouragement and advice.

The assistance of the laboratory staff of the University is gratefully acknowledged. I am particularly grateful to Mr. S. Spry (late of this department) for the construction of the liquid helium cryostat and to Mr. H.G. Ellacott for technical advice.

I would like to thank Miss Christine Avril of the School of Engineering Science for assistance with the diagrams used in this dissertation, Mr. A. Whitehead for photographic work and Mrs. G.M. Butler for skilfully typing the manuscript.

I am grateful to my colleagues in the School of Physics for many helpful discussions and to Professor J. Malinowski of the University of Sofia for several stimulating conversations. Dr. R.M. Yu of the University of Hong Kong provided the 150 UV photocell.

A formidable debt is owed to Dr. M.R. Tubbs who guided this work, for his friendship and constructive criticisms and for the benefit of his scientific perception.

I would also like to thank Mr. M.J. Redman for checking much of the manuscript.

I am grateful to the Central Electricity Generating Board for their financial support throughout this work.

Finally, it is a pleasure to thank my wife for her patient encouragement.

- o O o -

CHAPTER ONE

INTRODUCTION

1.1 General

The electronic properties of a crystalline solid, consisting of a periodic array of atoms, are very different from those of the isolated atoms. In particular, those properties that are determined by the electronic energy levels and the behaviour of electrons moving under the influence of applied fields have been extensively studied. In order to fully understand the electronic behaviour of a solid it is first necessary to achieve some understanding of the arrangement of electron energy levels in that material. It is natural, although not essential, to begin by considering the nature of atomic electronic levels. In an isolated atom or ion electrons are assumed to exist in discrete energy levels, motion between energy levels taking place only under the influence of an external field and subject to selection rules.

In single crystals, however, the atomic energy levels are broadened into bands of closely spaced levels which may not have the same sequence in energy as the isolated atomic levels (fig. 1.1). The selection rules governing transitions between states are affected by the perturbation from the large number of atoms in the crystal. Any given energy level derived from N atoms of the same species has an N-fold degeneracy which may be removed by perturbation of the lattice. Several basic procedures have been adopted in order to calculate the positions of the energy levels.

We begin by considering the valence-bond treatment. On this model, which is based on the atomic orbitals, the crystalline electron states are treated as linear combinations of atomic orbitals (Ziman 1964). This treatment is applicable only when the electrons are tightly bound to the individual atoms. It may, for example, be applied to the inner levels or to low lying bands in ionic crystals.

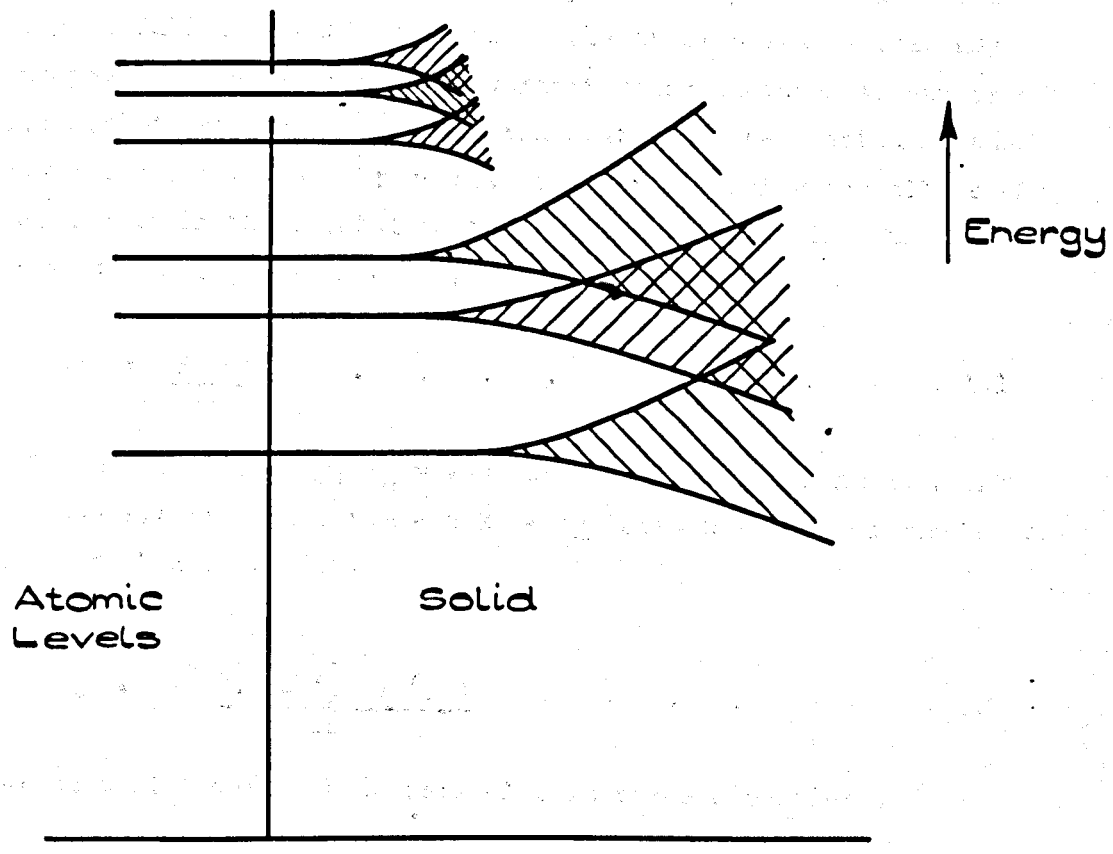

ONE-ELECTRON ATOMIC ENERGY LEVELS SPLIT INTO BANDS IN SOLID.

Fig. 1.1

1.2 Electron Energy Bands

In the one-electron scheme the electron distribution in the solid is considered to be non-localised. The outermost electrons of the isolated atoms cease to belong to particular atoms and are able to move through the crystal. The lattice periodicity allows any wave property to fulfill Bloch's Theorem. This theorem states that any wave property of the lattice is invariant under an integral number of lattice period translations. Electron states may be treated in this way and are Bloch waves. If we now consider a model which allows the free electrons in the crystal to behave as 'electrons in a box', we find that the energy of an electron is given by

$$E = \frac{\hbar^2 k_n^2}{2m} \quad . \quad . \quad . \quad . \quad . \quad . \quad . \quad . \quad . \quad . \quad 1.1$$

where E = electron energy, k_n = wave number, m = electron mass. $\hbar k$ is then the electron momentum and $k_n = \frac{n\pi}{L}$ where n is the quantum number and L is the box dimension.

More generally

$$E = \frac{\hbar^2 (k_x^2 + k_y^2 + k_z^2)}{2m} \quad . \quad . \quad . \quad . \quad . \quad . \quad . \quad 1.2$$

This means that E versus k is parabolic in three dimensions.

The free-electron model neglects the lattice periodicity and the individual atoms. If we now introduce the lattice as a set of periodic potential wells and treat the electrons by the Bloch method then discontinuities appear in the E versus k parabola. The discontinuities appear at values of k corresponding to electrons at Brillouin Zone edges. The parts of the E versus k curve which are allowed energy regions are called energy bands. Electrons may not, therefore, have energies between the energy extremes of successive bands. Electron states in the forbidden regions correspond to imaginary values of k.

Since there is a finite number of electrons in a crystal, all of which obey Fermi-Dirac statistics, we may say that all allowed energy states are filled up to an energy E_F, the Fermi Energy. It can be shown

that only electrons in partly filled bands contribute to electrical current. Empty or full bands do not, but an empty state in an otherwise full band may behave as a positive charge and is called a positive hole.

1.3 Insulators and Semiconductors

An insulator is a crystalline solid which has no partly filled electron energy bands. It is a necessary condition that the uppermost filled band be sufficiently separated in energy from the next empty band so that thermal excitation between them is improbable. An intrinsic semiconductor is an insulator in which the second condition is not fulfilled, electrons may, therefore, be thermally excited into empty bands (fig. 1.2). Extrinsic semiconductors have impurity energy levels in the forbidden gap between the energy bands. Thermal excitation may raise electrons from impurity levels to the conduction band or raise positive holes to impurity levels. In a metal, however, the Fermi-level lies in an unfilled band and thermal excitation takes place in this band. There are, therefore, carriers available at all temperatures.

It is important to realise that the distinction between semiconductors and insulators is quantitative not qualitative since semiconductors may behave as insulators at low temperatures. The reverse effect applies in principle at high temperatures but it is often masked by ionic conduction. It is usual for intrinsic semiconductors to have band gaps of 1.5eV or less (e.g. Ge~0.7eV, Si~1.5eV).

1.4 Optical Transitions

Consider an electron in an energy state E_o with momentum $\underline{k}_o$; this electron may be excited to a state $\underline{k}_1$ of higher energy provided the transition probability is sufficiently large. The transition probability will depend upon the energies of the states and the joint density of states function. If such a transition takes place and if the excited

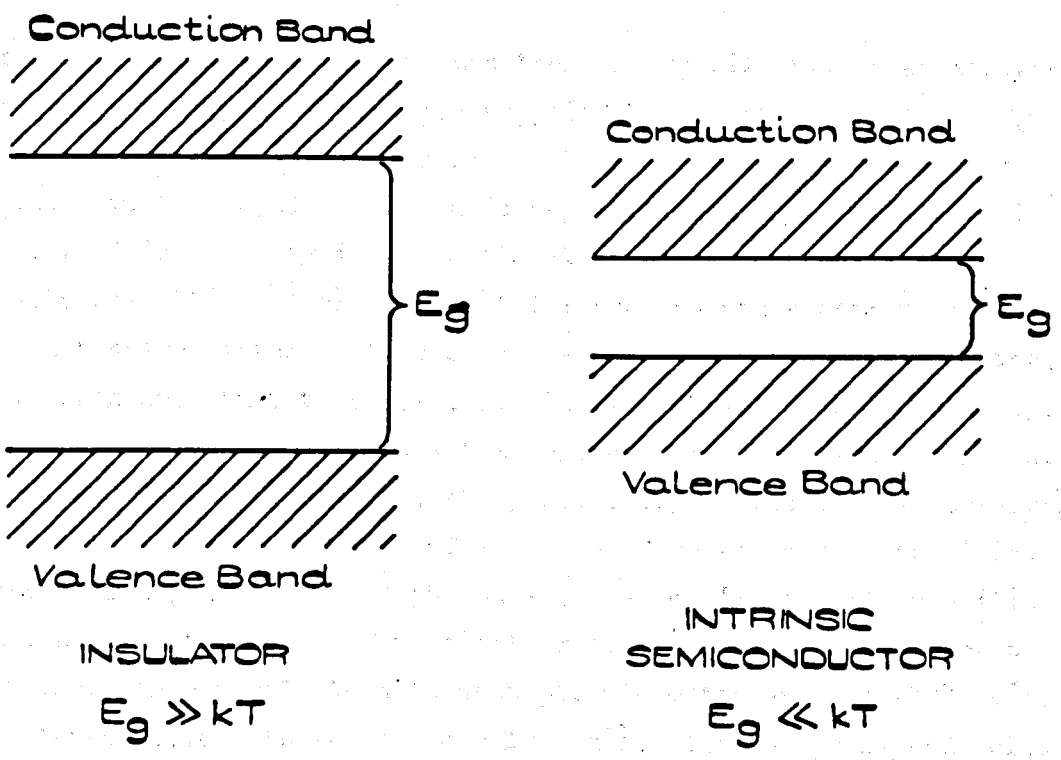
Conduction Band
E_g
Valence Band
INSULATOR
$E_g \gg kT$
Conduction Band
E_g
Valence Band
INTRINSIC
SEMICONDUCTOR
$E_g \ll kT$

Fig. 1.2

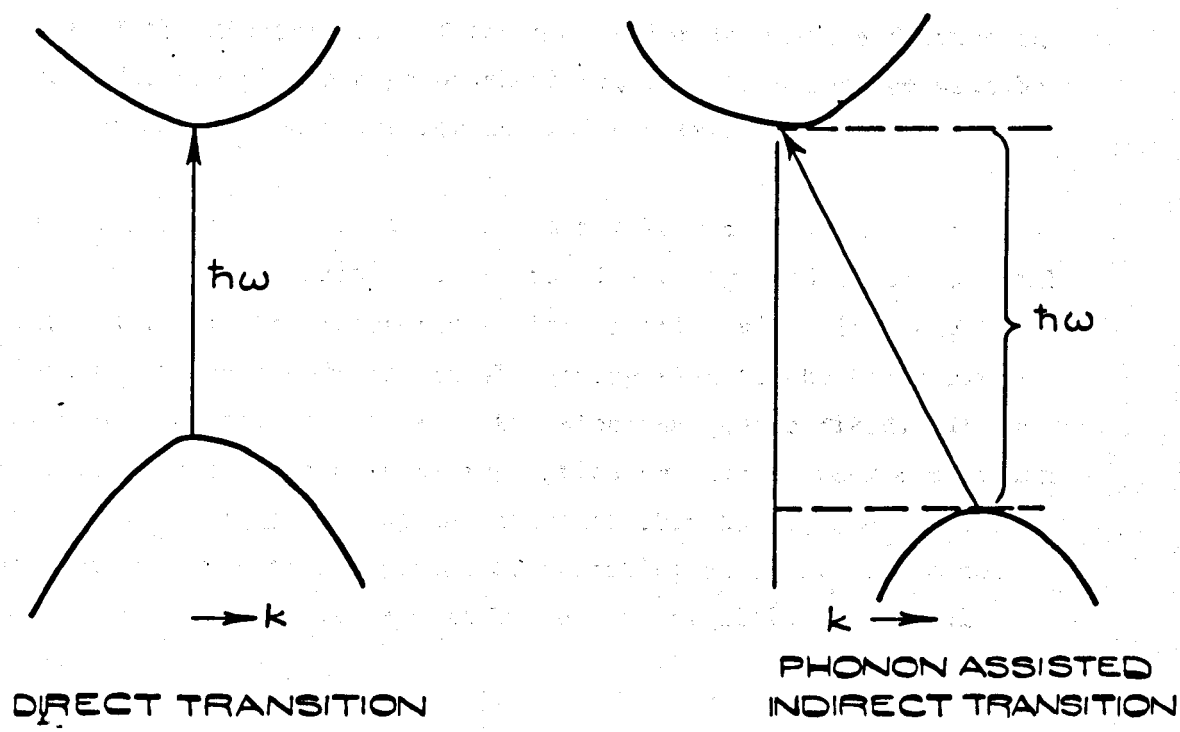
$\hbar\omega$
k
DIRECT TRANSITION
$\hbar\omega$
k
PHONON ASSISTED
INDIRECT TRANSITION

Fig. 1.3

electron goes into an unfilled band then energy will have been absorbed. The required energy may have been supplied by an optical photon. Optical photons have energies of the order of electron volts. The momentum associated with an optical photon is negligible compared with the electron momentum. This quantity is proportional to the wavenumber which is typically some 10^4 cm^{-1} and 10^8 cm^{-1} for photons and electrons respectively. Although total momentum must be conserved in an electronic transition, the electron momentum, therefore, is also essentially unchanged in optically induced transitions. This means that optical transitions are vertical in $\underline{k}$ space. There is, however, the possibility of inducing a non-vertical transition by the intervention of a phonon of non-zero momentum (fig. 1.3). The transition probability of phonon assisted or 'indirect' transitions is much smaller than that of vertical or direct transitions. Direct transitions consequently lead to absorption coefficients of $\sim 10^5$ cm^{-1}, indirect transitions to values near 10^3 cm^{-1}. The energy dependencies of the two types of transition process are different. It is possible to use this difference to distinguish between the processes by plotting curves of log α against log E, where α and E are the absorption coefficient and photon energy respectively. A feature of indirect transitions which derives from the phonon assistance is the strong temperature dependence of the absorption. If the absorption leads to a feature in a spectrum, for example an edge or shoulder, then this feature will be strongly temperature sensitive for an indirect transition process.

The absorption of photons in solids may lead to several processes other than interband transitions. At the low energy end of the optical spectrum, usually in the infra-red region, lattice vibrations may be excited in the transverse mode thereby giving rise to the Restrahlen bands by direct coupling of ions to the electromagnetic field. It is also possible for defects such as impurities to lead to weak absorption bands on the low energy side of an interband threshold. Such absorption is dependent upon the concentration of absorbing centres. It is not characteristic of the ideal crystal but may be significant in real specimens.

1.5 Exciton States

At energies higher than those described above, but just below the corresponding absorption edge, exciton formation is possible. Exciton states are formed as a result of the degeneracy of the lattice, they cannot be described by a one electron scheme. An exciton may be described as the lowest excited state of the lattice, Dexter and Knox (1965), Knox (1963). If an electron is excited from a valence band to the conduction band then the photon energy absorbed must equal the difference in electron energies between the two bands at the $\underline{k}$ value required for the process. The energy required to form an electron and hold as a bound entity will be less than that required for the band to band transition. The electron-hole binding is similar to the binding of a hydrogen atom. The exciton absorption lines lie below the absorption threshold which in many ionic materials corresponds to exciton ionization.

The Wannier model of the exciton treats the electron and hole as wave pockets and finds a series of energy eigenvalues determined by the coulomb interaction. The hydrogenic series of levels is given by

$$E_n = \frac{-2\pi^2\mu e^4}{h^2\varepsilon^2 n^2} \quad . \quad . \quad . \quad . \quad . \quad . \quad . \quad . \quad . \quad . \quad 1.3$$

where μ = reduced mass of electron-hole entity, e = electron charge, ε = dielectric constant, n = quantum number.

The series of levels is of the same form as that found for the hydrogen atom. Many of the properties of excitons in the presence of external fields are analagous to those found in the case of the hydrogen atom. The Wannier model is usually applied to materials with a large dielectric constant, where the exciton binding is weak and the electron orbits are much larger than a lattice parameter, so that a continuum approximation is justified.

In the Frenkel model the exciton is described as an excited state of an atom. The exciton may move by a resonance transfer process because of the N-fold crystalline degeneracy. The Frenkel model is usually confined to molecular solids and tightly bound crystals. In many crystals,

however, the exciton absorption may be of the hydrogenic type, but the innermost orbits (where the principal quantum number n = 1) may not fit the series. The inner orbits, being more tightly bound approach the Frenkel description. In these orbits the electron 'sees' a non-continuous lattice and the low frequency value of the dielectric constant no longer applies. There are also central-cell corrections because of the exchange interaction in s-like states. In many cases, therefore, the first line will not fit a hydrogenic series. Since the oscillator strengths of exciton lines for allowed transitions vary as $\frac{1}{n^3}$ then the 1st, 2nd, 3rd and 4th line strengths are in the ratio $1 : \frac{1}{8} : \frac{1}{27} : \frac{1}{64}$. The absence of the first line therefore means that the final lines necessary to fit a series will be very weak. Very high quality samples and low temperatures are therefore necessary.

At photon energies higher than the absorption edge it is possible for excitation of the so called 'core electrons' to take place. The energies required are of the order of 20eV in many cases. This core excitation is a property of the atoms rather than of the crystal lattice and will not be further discussed.

1.6 Optical Spectroscopy

We have described above some of the elementary electronic processes which may occur in crystals when optical radiation is absorbed. In atomic spectroscopy it is usual to equate photon absorption or emission with electron energy change, and to hence determine the energy levels of the atom involved. The same principle should apply in the case of solid state spectroscopy but in this case interpretation is somewhat more difficult because of problems concerned with band structure calculations (Phillips 1966) and the multi-valued nature of $E(\underline{k})$.

Ideally, simple materials could be studied whose electron energy band structure has been calculated. It should then be possible to compare the optical absorption spectrum with this structure. The optical features could then be assigned to transitions between symmetry points in the band scheme. At these critical points there are singularities in

the joint density of states function, leading to strong transition probabilities.

In practice the above approach is impossible. The band structures of the majority of solids are not known. Seemingly simple non-metallic solids have been found to have complicated band schemes, which have only recently begun to be calculated. Even when the band structure has been calculated it is difficult to assign transitions unambiguously because of the possible occurrence of more than one transition having the required energy.

Optical absorption is therefore used as an aid in calculating and checking band calculations. It is clear that a theoretical scheme must agree with the experimental evidence. At the same time only extremely careful experiments are useful since many transition thresholds may be obscured by poor experimental technique. Where possible more than one technique should be utilised.

Studies of the ejection of electrons by photons (photoemission) can give information about the density of electron energy states in the bands. These experiments are extremely difficult because of the necessity for Ultra-High Vacuum and Vacuum Ultra-Violet techniques. It is possible to alleviate the latter difficulty by Caesium coating to lower the work function, and therefore the photon energy required. This procedure tends to complicate the already difficult interpretation.

Cyclotron resonance has been used to give information over small regions of k space. More recently derivative techniques such as electro-reflectance have been used to provide additional information on energy band structure.

1.7 Techniques for the Study of Optical Properties

In order to study the absorption of light by a solid several techniques may be used. Perhaps the most fundamental approach is to determine the real and imaginary parts of the dielectric constant $\epsilon = (n - ik)^2$.

The difficulty in determining n and k is that the absorption constant may be of the order of 10^5 cm^{-1}. In standard methods of determination of n using interference techniques; and of k, by the measurement of the variation of transmission with sample thickness; it is necessary to measure the transmitted light. At such high values of k this is impossible on samples of usual dimensions e.g. m.m. thickness. In highly absorbing regions it is possible to use the reflectivity of the sample surface as a means of determining the constants. One method uses the reflectivities for the electric vector parallel to and perpendicular to the reflecting surface. Polarised light at non-normal incidence must therefore be used. It is also possible to use the fact that n and k are connected by dispersion relations. Then $n(\nu)$ and $k(\nu)$ satisfy the Kramers-Kronig relationships and hence if either is known for all values of ν then the other may be determined from these relations. In practice one or other is determined over as large a range of ν as possible.

Many optical absorption experiments are performed on thin specimens of ~1000Å thickness by the use of evaporated films. Great care is necessary in the extrapolation of results from thin films to bulk specimens. There are often differences of structure and even of stochiometry between the two sample types. There is justification for this extrapolation if the thin film can be shown to be monocrystalline or textured. Reflection from the rear surface causing interference may complicate the results in regions of low absorption.

Many experiments on single crystals are performed using normal incidence in order to determine the reflectivity spectrum. The reflectivity at normal incidence is R where

$$R = \frac{[(n-1)^2 + k^2]}{[(n+1)^2 + k^2]} \quad . \quad . \quad . \quad . \quad . \quad . \quad . \quad . \quad . \quad 1.4$$

In regions of very strong absorption where $k^2 >> n^2$ then $R \to 1$ and for negligible absorption $k \to 0$. This means that very strong absorption is accompanied by a marked increase in reflectivity. The situation is more complicated in intermediate regions where n and k are comparable. One of the main difficulties of reflectivity techniques is that sample in - sample out measurements are impossible. It is possible to replace the

sample with a specimen of known reflectivity e.g. Aluminium. In order to measure the absolute reflectivity without the possibility of error introduced by comparison or secondary reflection it is necessary to measure both incident and reflected intensities. In the case of anisotropic crystals difficulties arise because of the dependence of the reflectivity on the orientation of the electric vector. In many optical experiments structure is more readily resolved at low temperatures. Exciton lines are particularly temperature sensitive. It is therefore necessary to use cryostats capable of maintaining and reproducing low temperatures; window materials of low absorption are also required.

1.8 Photoemission

When light is absorbed and excites electrons to the conduction band, these electrons are free to move under the influence of an applied field. If a field is present at the crystal surface then electrons of sufficient energy will be emitted. In a semiconductor or insulator it is necessary for the light quanta to have sufficient energy to raise electrons from the valence band to the vacuum level. The energy required is called the photoemission threshold. In photoemission measurements the energy of the emitted electrons may be determined and the energy distribution of emitted electrons may then be calculated. The quantum yield of electrons as a function of radiation energy is also an important parameter. The initial and final state energies of the excited electrons and the selection rules governing the transitions may be determined from the photoemission measurements.

If photoemission data is augmented by reflectivity or other optical data it is possible to make deductions concerning the energy band structure (Kindig and Spicer 1965). This extremely powerful technique has not been extensively used because of experimental difficulties. Ultra High Vacuum facilities are necessary in order to achieve atomically clean surfaces. Samples must therefore be able to withstand high temperature degassing at some 400°C. Also, high photon energies are necessary in many cases in order to excite electrons

from the crystal. The energy required depends upon the initial electron energy relative to the Fermi level and the depth of the Fermi level below the vacuum level. It is necessary in many cases to use Vacuum Ultra Violet light in order to provide sufficient energy.

1.9 Photoconductivity

If the absorption of a photon creates an electron-hole pair then the absorption process may be detected by measuring the charge release per incident photon. It is usual to apply an external field to the sample which must therefore be able to support this field. The charge movement or current produced by the application of a measured number of photons is then recorded. It is clear that zero absorption leads to zero photocurrent and that absorption of one photon should lead to the detection of one electron charge.

Photoconductivity was first observed in 1873 but a systematic research programme was not undertaken until the 1920's when Pohl and his co-workers studied natural crystals of the alkali halides and diamond (Pohl 1937). They were concerned with the 'primary' photoconductivity i.e. the current which flows on application of the light. This method is probably the most direct for determining the quantum efficiency of electron production.

1.10 Primary Photoconductivity

Consider an insulating sample of length ℓ. The sample must be insulating in order that charge does not move in opposition to the field before the application of the light. The sample is illuminated in a narrow region at a distance x_o from the anode. The initial charge released into the conduction band is ηN where N is the number of photons incident and η is the quantum efficiency of electron production. The charge released [assumed for simplicity to be electrons only] will drift towards the anode. Some charge will then be trapped in the process of drifting and some will reach the anode. The electrodes used are

'blocking' so that no charge leaves or enters the crystal via the electrodes. Insulating spacers are normally used to avoid electrical contact.

The charge measured by the electrometer is then Q where

$$Q = \frac{q\omega}{\ell}\left(1 - e^{\frac{-x_o}{\omega}}\right)\eta N \quad . \quad . \quad . \quad . \quad . \quad . \quad . \quad . \quad . \quad . \quad 1.5$$

cf Mott and Gurney (1948)

where q is the electron charge and ω = electron schubweg or mean free path.

This equation was derived assuming that all incident photons were absorbed. It is therefore necessary to take account of the proportion reflected. The number of photons reflected is NR, hence after reflectivity correction equation 1.5 becomes

$$Q = \frac{e\omega_o E}{\ell}\left(1 - e^{\frac{-x_o}{\omega_o E}}\right)\eta N(1-R) \quad . \quad . \quad . \quad . \quad . \quad . \quad . \quad . \quad 1.6$$

(assuming that $\omega = \omega_o E$).

In an experiment Q is measured. It is usual to vary E and to fit the value of ω_o to the experimental curve of Q against E. The curve saturates at large values of E corresponding to the condition when all electrons are pulled to the anode. The value of ω_o may therefore be determined. The quantum efficiency may be determined by increasing E to saturation and measuring the saturation value of Q as a function of photon energy.

1.11 Experimental Primary Photoconductivity

This method of determining the quantum efficiency may be applied in similar form to the case of an applied field in the direction of the illumination. The primary photoconductivity has been used successfully by Teegarden and co-workers. Their thin film results on the alkali halides are particularly interesting since they clearly show the relationship between optical absorption and photoconductivity at 80°K and 10°K (Huggett and Teegarden, 1966). The photoconductivity data together with

the optical data on RbI give the band gaps of the material and show that the first low energy peak is excitonic in nature. In the alkali halides exciton effects are strong and there is some difficulty in determining the position of the first band edge from optical data. This edge, however, corresponds to the onset of photoconductivity since the exciton peaks do not lead to appreciable photoresponse.

This work was the result of prolonged studies begun by Ferguson unsuccessfully in 1944, and continued more recently by Taylor and Hartman (1958). Primary photoconductivity is involved with low current $<10^{-12}$ amps since larger currents lead to space charge polarisation. Photons of such high energies lead to photoemission necessitating elaborate precautions and careful design.

It was not until 1961 that reliable results appeared (Nakai and Teegarden, 1961, Kuwabara and Aoyagi, 1961), although Teegarden had made preliminary experiments in 1958. The results of Huggett and Teegarden have since been substantiated by Sydor (1967).

The primary photoconductivity method which necessitates the use of low currents is therefore extremely difficult. The difficulty is increased in the far ultra-violet; because of weak light sources, currents as low as 10^{-16} amps are often found. These difficulties, coupled with others previously described, make studies in the fundamental regions of ionic crystals somewhat scarce. However, once reproducible results are obtained they may be used to analyse and supplement optical data to show which transitions lead to appreciable number of free electrons. Crystals other than the alkali halides have been studied with success. In particular AgCl and TlCl have been studied by Heyningen and Brown (1958) and Kawai et al (1965). Since few of these materials are suitable as practical photoconductors and because of the experimental difficulties, the bulk of research has been directed towards semiconductors.

1.12 Photoconductivity in Semiconductors

The situation in semiconductors is somewhat less straightforward than in insulators. In semiconductors the thermal generation of free

carriers leads to appreciable dark currents. The dark current may cause the build up of space charge and will tend to swamp the photocurrent. The primary photoconducting technique is therefore inappropriate. It is usual in semiconductors to use electrodes which maintain a steady dark current flow. The contacts should also ensure that the photoconductivity is ohmic (Bube, 1960). The effect of illumination at wavelengths where free carriers are formed is to change the carrier concentration of the sample. We assume for simplicity that only electrons are mobile then

$$\Delta\sigma = e\mu\Delta n \quad . \quad . \quad . \quad . \quad . \quad . \quad . \quad . \quad . \quad . \quad 1.7$$

$\Delta\sigma$ and Δn are the changes in electron density and μ is the electron mobility. The equation is readily modified to take account of non zero hole mobility.

This relationship means that the change in conductivity is proportional to Δn, which is in turn proportional to the incident light intensity. The relationship holds at low light levels only in general. At higher intensities recombination becomes important and the current ceases to vary linearly with light intensity. The relation then changes to

$$I_p = Ai^{\beta} \quad . \quad . \quad . \quad . \quad . \quad . \quad . \quad . \quad . \quad . \quad 1.8$$

where I_p is the photocurrent due to illumination intensity i. The value of β is determined by the intensity and wavelength of the illumination. At very high values of i direct recombination takes place and the value of β tends to $\frac{1}{2}$.

In order to correct for the above effects precise experiments should determine the current-intensity curve at each wavelength. In many experiments the quantum flux is maintained constant and the effect on the photocurrent of varying wavelengths determined. It is preferable, however, to maintain constant absorbed quantum flux although this necessitates a knowledge of the reflectivity spectrum. In regions of strong absorption and hence high reflectivity, the surface recombination is important. In low absorption regions the bulk recombination parameters apply. It is therefore difficult to accurately correct the I versus energy curves for the reflectivity loss unless the I_p versus i curves have been plotted. Even with these complications many interesting experiments have been performed on semiconductors.

1.13 Exciton Photoconductivity

In ionic materials it is unusual to find strong exciton effects throughout the region of fundamental absorption. In semiconductors exciton effects are weaker. Semiconductor spectra are dominated by edges and peaks due to singularities in the joint density of states for interband transitions, (Phillips 1966). A large number of materials do not fall into either category and exhibit exciton effects together with interband edges.

Some of these intermediate materials having practical importance have been extensively studied, in particular CdS and Cu_2O. Many other materials have shown interesting exciton structure including hydrogenic series. In many cases the exciton structure leads to similar or reversed structure in photoconductivity. The work of Gross in U.S.S.R. and Nikitine in France has been particularly extensive. Gross' paper in the 1964 Paris conference is interesting because it relates optical absorption, photoconductivity and luminescence in the exciton peaks and shows some of the complications involved.

Among the intermediate materials is a group known as the layer structured metallic halides. This group, which includes PbI_2 and CdI_2, exhibits strong exciton effects. Some of these materials have also been shown to have practical importance.

1.14 The Layer Structured Metallic Halides

Materials of the MX_2 type, for example PbI_2 and CdI_2, have the well known sandwich-layer structure. In these crystals close packed layers of halide ions have the smaller metallic ions sandwiched in the octahedral interstices. The bonding between the opposite charges is largely ionic, whereas that between the halide ions of adjacent sandwiches is largely of the Van der Waal's type.

The structure of these materials leads to marked anisotropies in their physical properties. In both PbI_2 and CdI_2, for example, the ionic conductivity along the layers is some three orders of magnitude larger than that in the perpendicular direction.

The optical properties of PbI_2 and in particular the exciton spectrum have been studied by Tubbs (1964). The photoconductivity spectrum has also been studied and a peak in photoconductivity assigned to exciton absorption. Closely connected with both photoconductivity and optical absorption is the photodecomposition process. In PbI_2 this process is linked to exciton formation.

Recently, Tubbs (1968a) has shown that the optical spectra of many of the metallic iodides of this group have remarkable similarities. All of the materials used exhibited strong exciton absorption peaks. The positions of the exciton lines were found to agree with a proposed iodide ion excitation model, Tubbs (1968b).

CdI_2 has similar electronic and crystal structure to PbI_2. In the case of CdI_2 extremely interesting optical reflectivity spectra were presented by Greenaway and Nitsche (1965). The present work was stimulated by this and by the relationship between CdI_2 and other members of the above group.

1.15 The Optical Properties of CdI_2

Preliminary experiments were performed by Fesefeldt who measured the optical absorption spectrum of CdI_2 thin films. The spectrum was determined at RT and is fairly smooth with a peak at 5.2eV and a smaller one at 3.8eV. Further experiments of a preliminary nature were performed by Gross and Kapliankii (1955), Putseiko and Tevenin (1949), (1953) and by Fotland (1959). It was not until 1963 that Best reported the optical absorption of thin films of CdI_2 prepared on substrates at various temperatures, so that a reliable spectrum exhibiting strong exciton lines could be observed.

Single crystals of high quality were used by Greenaway and Nitsche (1965) to record reflectivity spectra at room and liquid nitrogen temperatures. They found strong exciton peaks which they designated X_1 and X_2. These peaks were some 3eV above the onset of intrinsic absorption at ~3eV. The low energy edge was shown to be due to indirect transitions from a valence band to a conduction band. In order to explain the shape of the exciton lines occurring near 6eV, Greenaway and Nische suggested that Phillips' model of metastable excitons be invoked. It has also been suggested that a lower lying valence band coupled with two conduction bands might lead to a similar spectrum involving only transitions at k=0 (Tubbs 1968a). The assignation of these peaks to exciton formation was made because of their sharpness and marked dependence on temperature and crystal structure. The spectrum found by Greenaway and Nitsche has since been substantially verified by Brahms (1965) and by Tubbs (1968a).

In the high energy region near 6eV the optical absorption coefficient is so large that it is impossible to measure the optical absorption in single crystals of normal dimensions. Thin films must, therefore, be used. In the case of CdI_2 the structure of vacuum deposited thin films has been studied by Best (1963) and by Yu (1967). Yu reported that films of thickness ~1000Å were largely composed of single crystal regions several microns in lateral dimension. There is, therefore, some justification in using thin films for absorption measurements in CdI_2. Thin film absorption measurements are in fact in good agreement with single crystal reflectivity data.

In view of the interesting optical spectra of CdI_2, particularly the high energy exciton peaks, it was decided to study the photoconductivity response at higher energies and lower temperatures than those used by previous investigators.

1.16 Photoconductivity in Cadmium Iodide

Previous photoconductivity experiments on CdI_2 have been confined to room temperature and above. Fotland (1959, 1960), for example, made a quantitative study of optical absorption and photoconductivity up to 3.4eV. No appreciable structure was found, the experiments being largely

concerned with anisotropy effects, in particular those concerned with ionic conductivity. Values of $4 \times 10^{7}\Omega$cm and $4 \times 10^{11}\Omega$cm were measured perpendicular to and parallel to the 'c' axis. The crystals used were mainly prepared by the Bridgmann technique although some were obtained from aqueous solution. In solution grown crystals the resistivity increased to $20 \times 10^{11}\Omega$cm parallel to the 'c' axis. This result indicates that crystals grown from the melt tend to have a higher content of defects than those obtained from solution.

Fotland's work was repeated by Yu who used solution grown crystals of high quality. The electrometer sensitivity limited these measurements to room temperature and above and necessitated the use of high light levels ($\sim 10^{13}$ quanta/cm^2/sec). The photoconductivity is not linear with intensity at such high light levels and interpretation is therefore difficult.

Our experiments on photoconductivity in solution grown crystals have extended the spectrum into the exciton region. Measurements have been made at energies up to 6.5eV using an electrometer with a sensitivity of $\sim 5 \times 10^{-17}$ amps. The experiments were performed using low light levels. Although this made room temperature measurements difficult, at low temperature the photocurrent was found to be proportional to the light intensity. Spectra have been obtained at liquid helium and liquid nitrogen temperatures as well as room temperature. The reflectivity spectra of single crystals have also been determined in the same apparatus. The photoconductivity spectra were found to reproduce many of the features of the reflectivity spectra.

As a result of the work of Fotland (1959) and of Yu (1967) on CdI_2 papers, photodecomposition has been studied in CdI_2 single crystals. The crystals were found to be very insensitive to decomposition even at the optimum temperature near 250°C. We have also studied the effect of photo-decomposition on the photoconductivity spectra. One interesting aspect of the decomposition studies was the discovery of a silver diffusion effect in CdI_2.

Closely allied to the study of photoconductivity is the study of trapping levels. The method of thermally stimulated current has been used to determine the energy levels of traps.

The results of the experiments briefly described above will be discussed in later chapters.

REFERENCES

Best, K.J., 1963, Phys.Kondens.Materie. 1, 316.

Brahms, S., 1965, Phys.Lett. 19, 272.

Bube, R.H., 1960, Photoconductivity in Solids (Wiley), p.117.

Dexter, D.L., and Knox, R.S., 1965, Excitons (Interscience).

Ferguson, J.N., 1944, Phys.Rev. 66, 220.

Fesefeldt, H., 1930, Zeits.f.Phys. 64, 741.

Fotland, R.A., 1959, Thesis, Case. Inst. of Technology.

Fotland, R.A., 1960, J.Chem.Phys. 33, 956.

Greenaway, D.L., and Nitsche, R., 1965, J.Phys.Chem.Solids 26, 1445.

Goto, T., 1965, J.Phys.Soc.Japan 20, 1654.

Grass, E.F., and Kaplianskii, A.A., 1955, Zhur.Tekh.Fiz. 25, 2061

Gross, E.F., Akopian, JKn., Kreingold, F.I., Novikov, B.V., Titor, R.A. and Shekmametiev, R.I., 1964, Proc.Int.Conf. on The Physics of Semiconductors, Paris, p.957.

Heyningen, R.S., and Brown, F.C., 1958, Phys.Rev. 111, 462.

Huggett, G.R. and Teegarden, K., 1966, Phys.Rev. 141, 797.

Kawai, T., Kobayashi, K., Fyita, H., 1966, J.Phys.Soc.Japan 21, 453.

Kindig, N.B. and Spicer, W.E., 1965, Phys.Rev. 138, A 561.

Knox, R.S., 1963, Theory of Excitons, Solid State Physics, Vol. 5.

Kuwabara, G. and Aoyagi, K., 1961, J.Phys.Chem.Solids 22, 333.

Mott, N.F. and Gurney, R.W., 1948, Electronic Processes in Ionic Crystals (Oxford).

Nakai, Y. and Teegarden, K., 1961, J.Phys.Chem Solids 22, 327.

Nikitine, S., Coret, A., Zielinger, J.P., Jeandaude, C., Boehm, C. and Zouaghi, M., 1965, J.Phys.Chem. 69, 745.

Phillips, J.C., 1966, Solid State Physics 18.

Putseiko and Terenin, 1949, Zhur.Fiz.Khim. 23, 676.

Putseiko and Terenin, 1953, Doklady.Akad.Nauk. 90, 1005.

Sydor, M., 1967, Phys.Rev. 163, 873.

Taylor, J.W. and Hartman, P.L., 1958, Phys.Rev. 113, 1421.

Tubbs, M.R., 1964, Proc.Roy.Soc. A280, 566.

Tubbs, M.R., 1968a, J.Phys.Chem.Solids. 29, 797.

Tubbs, M.R., 1968b, Phys.Stat.Sol. 28, 135.

Yu, R.M., 1967, Thesis, Bristol.

Yu, R.M., 1967, Phil.Mag. 16, 1167.

Yu, R.M., 1969, J.Phys.Chem.Solids. 30, 63.

Ziman, J.M., 1964, Principles of the Theory of Solids (Cambridge).

CHAPTER TWO

EXPERIMENTAL TECHNIQUES

2.1 Introduction

In Chapter One CdI_2 was introduced as a material of interest because of the remarkable structure in its high energy optical properties. Several workers have found high energy exciton peaks in this material whose properties are intermediate between those of strongly ionic and covalent crystals. CdI_2, however, is of interest not only for its own sake but because of its relationship with other layer structured materials, such as PbI_2.

Since the optical properties of CdI_2 are now well documented it is of some importance to compare and contrast these properties with information obtained from photoconductivity experiments. We have indicated in Chapter One how successful this approach has been in other materials.

Previous experiments concerned with photoconductivity in CdI_2 were limited in scope by the lack of sensitivity of the current measuring instruments. The measurements were therefore confined to large currents of $\sim 10^{-11}$ amps and to temperatures above $\sim 290^{\circ}K$. The lack of sensitivity also restricted the spectral range obtainable and in fact no spectra were recorded at energies above 3.4eV, the indirect absorption edge being at ~3.2eV. These experiments had indicated a fall in sensitivity at photon energies above the absorption edge. Greater intensities or sensitivity were apparently necessary to allow measurements to be made at higher energies. The latter course was adopted since high intensity continuous light sources were not available in the Ultra-Violet region.

There were other more fundamental reasons for the choice of increased sensitivity. At low intensities the photocurrent is proportional to the illumination intensity whereas in general, at high intensities, this is not so and there are then difficulties in correction for energy dependent photon flux. High intensity illumination may also lead to localised heating of the specimen, a particularly troublesome effect at low temperature. At higher temperatures intense illumination may produce photodecomposition.

Once the low current method had been chosen to measure photoconductivity it was necessary to decide between a direct or an alternating current measuring technique.

2.2 Current Measurements

Many photoconductivity experiments have been performed on semiconductors using modulation techniques, whereas the direct current technique has usually been found to be more suitable for studies of insulators.

In semiconductors or ionic conductors the dark current may be comparable with or greater than the photocurrent. In these circumstances if the light intensity cannot be increased then some means must be found of amplifying the photocurrent but not the dark current.

The dark current may, for instance, be stabilised and then offset, leaving the photocurrent to be amplified. Since the dark current usually varies exponentially with temperature, stringent temperature control is necessary in this case. It may be possible to offset the dark current by the use of a bridge method. This technique has been used by Apfel and Portis (1959) in Cu_2O. Large samples of uniform properties are required since three electrodes are placed on the front surface to give two resistors of the same material. The two resistance regions may then be used as arms of a bridge circuit. Illumination in one region leads to an unbalance in the bridge and hence to a photocurrent signal. The effect of temperature drift on the dark current is therefore reduced.

If the incident light is modulated then the photocurrent may be amplified by a tuned amplifier and phase sensitive detector. The dark current, which is not modulated, will not be amplified. This technique reduces the effects of dark current drift and scattered light.

In insulating crystals the photocurrent may be large compared with the dark current and the combined current may therefore be amplified for measurement. One complication which then arises is the decay of photocurrent with time for steady illumination. This effect is caused by the

trapping of the photo-generated carriers leading to a polarisation field in the sample. The effect of the polarisation may be reduced by the use of an alternating field technique which reduces the mean value of the polarisation field to zero.

It is usual, however, for measurements of the smallest currents to be made with a direct current electrometer. Measurements may then be made with a single light pulse and steady electric field. The alternate measurements may be made with a reversed field. A depolarisation procedure may also be adopted between measurements. This technique essentially measures charge displacement and may be used in non ohmic conditions.

The choice of a particular technique was based on the information available from previous photoconductivity experiments on CdI_2. Some indication of time dependent room temperature photocurrents and dark currents had been given by Fotland (1959). This effect was probably caused by space charge polarisation. The conductivity of melt-grown crystals was high so that the resistivity at room temperature was some $10^7 \Omega$cm along the cleavage plane, increasing to $10^{11} \Omega$cm in the perpendicular direction. The resistivity of solution grown crystals was some $2 \times 10^{12} \Omega$cm in the latter direction. It was therefore clear that at low temperatures the material would behave as an insulator. The direct current electrometer method was therefore chosen to measure photoconductivity in CdI_2. This method, as well as having the advantages described above has the benefit of versatility since transient effects may be readily observed.

2.3 Electrometer Techniques

The absence of previous low temperature, low light level measurements meant that a highly sensitive instrument was desirable. An E.I.L. Vibron Vibrating Capacitor Electrometer Model 62A was therefore chosen. The sensitivity of this instrument was $\sim 5 \times 10^{-17}$amps corresponding to ~300 electrons/second, a typical sensitivity for electrometers of this type. Measurements of such small currents require special techniques.

Two basic methods of measurement were used. The first was that of passing the unknown current through a standard resistor (usually of the order of $10^{12}\Omega$) connected across the electrometer input. The sample, standard resistor and applied potential were then in series (see fig. 2.1). If the sample resistance is large compared with the standard resistor then the potential drop across the standard will be small compared with the applied potential.

The second method measures current by recording the rate of change of voltage, at a standard capacitance, due to the applied current. The standard capacitance may be the electrometer input capacitance or the electrometer in conjunction with standard capacitors. The Vibron electrometer was equipped with switched input capacitors of known value.

The resistance method registers a fixed voltage for a steady current whereas the capacitance method registers a voltage increasing uniformly with time. The first method is therefore more suitable for measuring current changes superimposed upon steady or slowly varying currents. This method was therefore used in the majority of experiments. The electrometer was equipped with a facility for backing-off voltage which could be used for offsetting dark currents. This facility also amplified the difference between the applied voltage and the voltage offset.

The capacitance method was used to advantage with small currents when the time constant of resistance circuits became large. The time constant is proportional to the circuit capacitance and the input resistance. Negative feedback in the electrometer effectively reduced the value of this product by a factor of 100. In many experiments using the $10^{12}\Omega$ resistor the response time was of the order of seconds.

2.4 The Electrical System

Currents of the order of 10^{-16} amps due to applied potentials of 1000V correspond to effective sample resistances of $10^{19}\Omega$. The insulation in parallel with the sample must therefore have a resistance greater than $10^{19}\Omega$ if such small currents are to be measured.

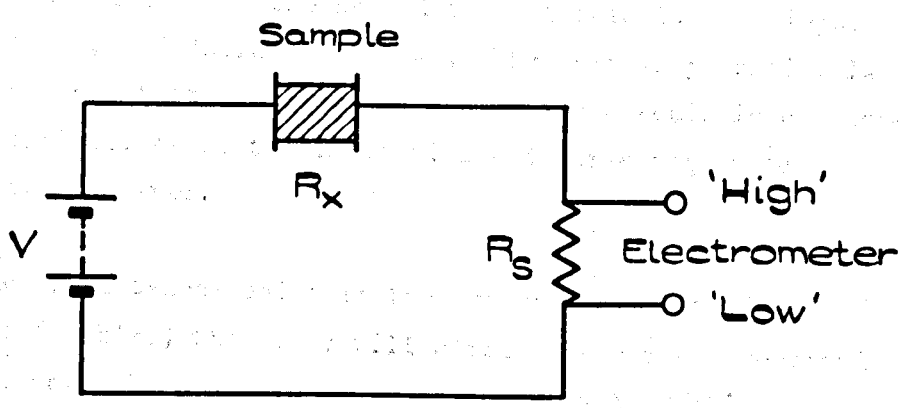

Fig. 2.1

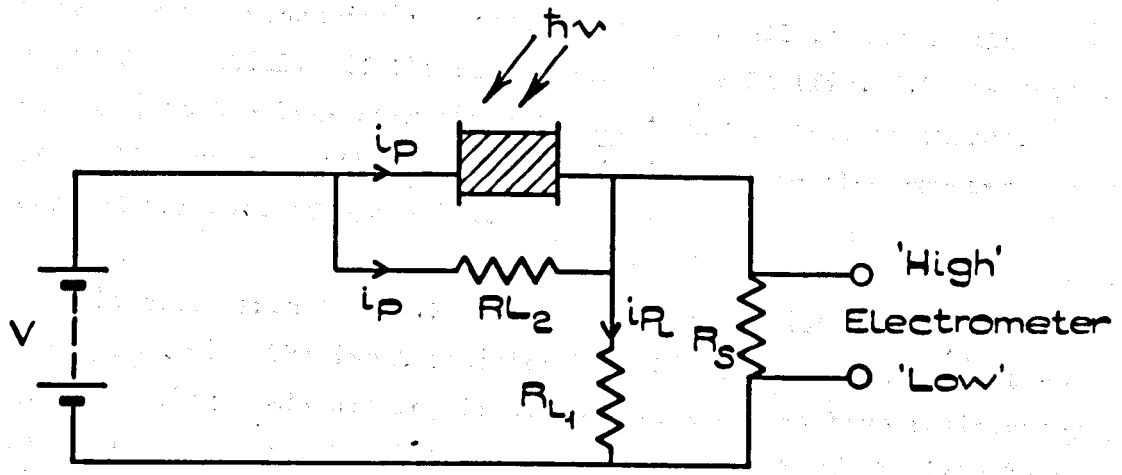

Fig. 2.2

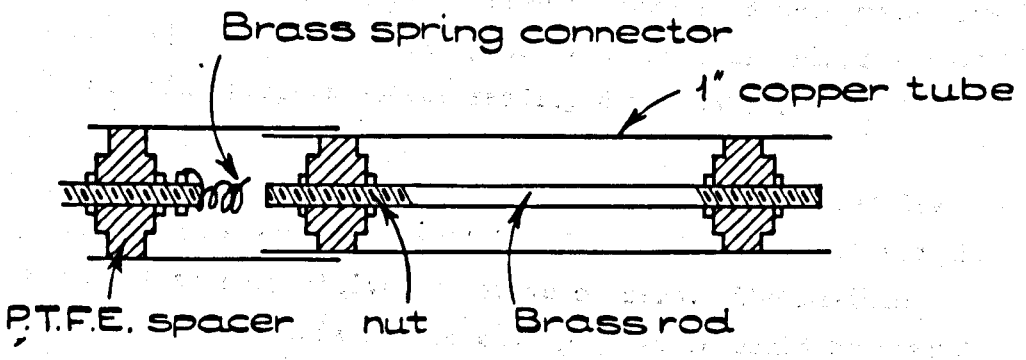

INTERLOCKING SCREENED LEAD.

Fig. 2.3.

The electrometer measures potential at its highly insulated and screened terminal relative to the second input terminal. The input terminals are designated 'High' and 'Low'. The unknown potential is applied in such a way that the grounded end of the circuit is connected to the 'Low' terminal, since the insulation and screening is less efficient at this terminal.

If leakage resistances exist in the external circuit (in, for example, co-axial cables) then they will affect the current recorded by the electrometer. In order to minimise the effect of this resistance in the lead to the electrometer input the cable outer was fixed at 'Low' potential. The voltage across the leakage resistance was therefore the measuring voltage, which was small compared with the applied potential. If the sample resistance Rx (fig. 2.2) is equal, for example, to the leakage resistance R_{L1} then the leakage current ip^{L} is small compared with ip. The 'low' side of the electrometer was earthed for ease of operation.

It is clear from fig. 2.2 that the leakage resistance R_L, must be large compared with the input resistor R_S. Since R_S may be $10^{13}\Omega$ then highly insulating leads are required. Co-axial cables have resistances of the required order but all are susceptible to mechanical disturbance. A rigid demountable co-axial connecting system was therefore designed.

The current carrying inner conductor was of brass rod, the outer screen being of 1" diameter copper tubing. P.T.F.E. insulation was used as shown in fig. 2.3. Straight pieces of this screened conductor were push fits into elbows. Connections between brass rods were made with helical brass springs. The entire system was therefore rigid and of excellent insulating properties but readily demountable.

The potential applied across the sample was from several dry batteries wired into a reversing switch. A second switch allowed the applied potential to be positive, negative or zero. The maximum potential available from this source was ~540V which could be varied in steps of 90V. No attempt was made to vary the potential by means of resistances. The potential was therefore remarkably steady, varying by less than one volt in many months.

The most likely source of leakage in the circuit was between the sample connections since the full applied potential appeared between them. A P.T.F.E. sheet was therefore used as a support for the sample. This sheet was some $\frac{1}{32}$" thick. It was attached to the copper finger of the cryostat by small screws, a thin smear of silicone grease was used to ensure good thermal contact. Extremely careful handling and cleaning of the sample holder was necessary to eliminate grease smears which could cause leakage. The cleaning procedure adopted was to clean first in trichloroethylene and to then dry quickly with tissue, repeating the procedure with acetone and absolute alcohol. This procedure minimised leakage currents.

The liquid nitrogen temperature cryostat was of the cold finger type (fig. 2.4). The copper finger was fixed to a Kovar seal. The glass vessel was evacuated by means of a 12" NGN vacuum coating unit. The ultimate vacuum obtainable was of the order of 10^{-5} torr or $<10^{-6}$ torr with liquid nitrogen in the oil vapour trap. It was possible to dispense with the rotary pump and to pump the diffusion pump with a vacuum reservoir to reduce vibration. It was, however, rarely necessary to make use of this facility.

All measurements, including those taken at room temperature, were recorded with the specimen in vacuo. Atmospheric moisture tends to reduce insulation resistances and could damage highly soluble crystals such as CdI_2.

2.5 The Optical System

Three light sources were used in the course of the investigations. The most important of these was a Deuterium Arc Lamp supplied by Hilger and Watts Ltd.. This lamp gave a continuous emission spectrum from 200mμ to near 360mμ. Lines became apparent in the spectrum near 380mμ. The stability of this lamp was adequate for the photoconductivity experiments. The intensity at a given wavelength changes by less than 1% over the period of an experimental run. The output of the lamp was low, so that for some measurements it became necessary to use a Mercury Discharge Lamp. The output of the discharge lamp, which was a Philips High Pressure Spectral Lamp, varied with time. This variation was probably caused by

Fig. 2.4

wandering of the arc. The lamp was therefore unsuitable for precise experiments. It was necessary to use this lamp in conjunction with some thin films because of the low sensitivity of these samples. The spectral lines of this lamp were used to calibrate the monochromator wavelength scale. It was also used to calibrate a 150UV photocell against a vacuum thermopile since high intensities were required to operate the thermopile.

A Quartz-Halogen tungsten filament lamp was used to investigate photoconductivity at long wavelengths in some samples. The deuterium and mercury arc lamps were unsuitable because of the strong lines in their spectra at wavelengths above 380mμ.

2.6 Intensity Measurement

The spectral variation of the output from the monochromator was determined with a Mullard 150UV photocell. The photocell was provided by Dr. R.M. Yu for whom it was calibrated by the National Physical Laboratory. The N.P.L. calibration is illustrated in fig. 2.5, it extends from 248-600mμ. Since in our experiments the region below 248mμ was of particular interest, it was necessary to extend the calibration. A vacuum thermopile was therefore used to calibrate the photocell to wavelengths near 200mμ. This instrument was a Hilger-Schwartz type FT16 with two 0.95cm x 0.05cm elements, one of which was shielded. The response of the elements was 25μV/μ Watt. A Keithley Electrometer Model 150B with a maximum sensitivity of <0.1μV was used to measure the thermopile output. The thermal fluctuation noise of the thermopile was of the order of 0.2μV and was greater than the electrometer noise.

The mercury discharge lamp was used to provide sufficient intensity for the thermopile. The monochromator output was then much too great for the photocell except near 200mμ where the thermopile ceased to respond. The light beam from the monochromator was therefore split by a suprasil silica plate at 45° (fig. 2.6). The transmitted beam was incident on the thermopile whereas the reflected (and therefore attenuated) beam was incident on the photocell after being further attenuated by a rotating sector. The overall attenuation was of the order of 1000. The thermopile

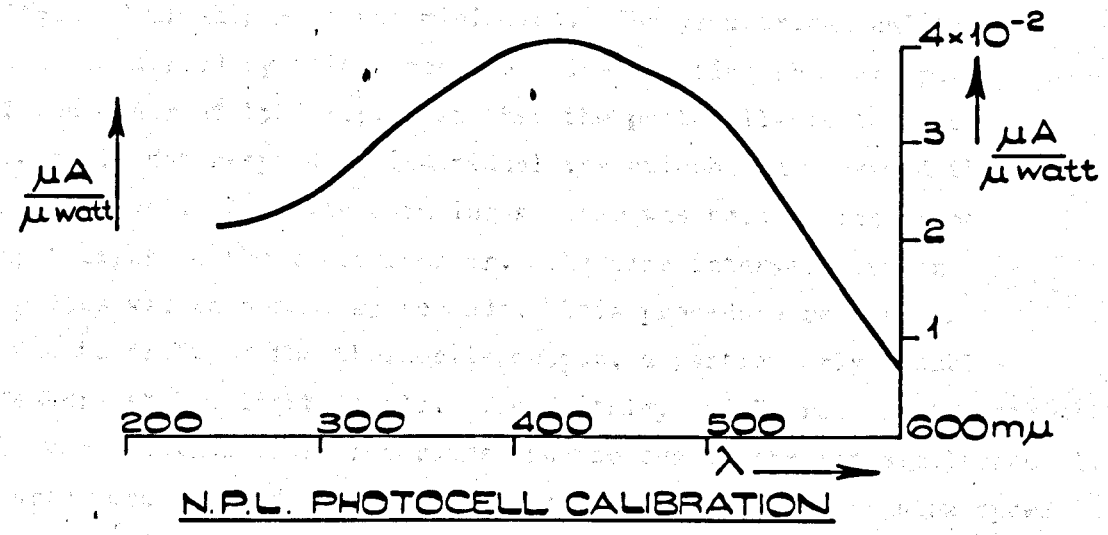

N.P.L. PHOTOCELL CALIBRATION

Fig. 2.5

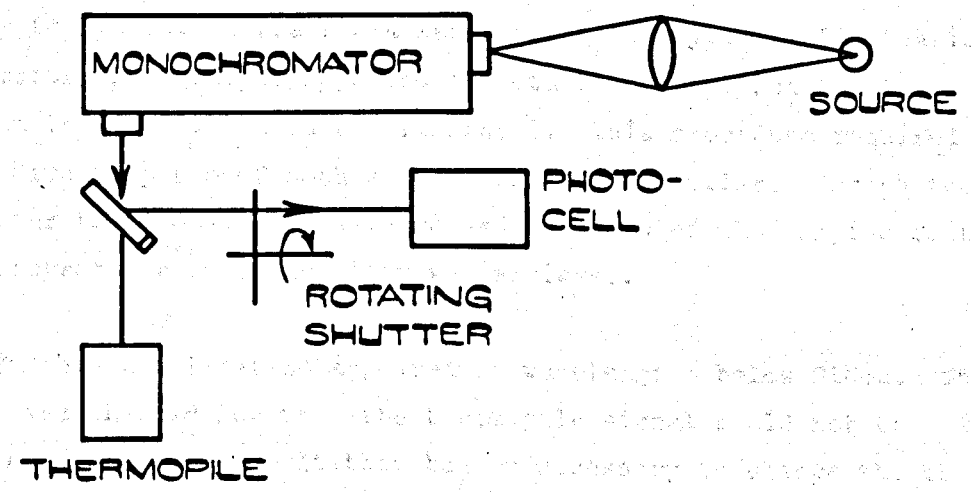

Fig. 2.6

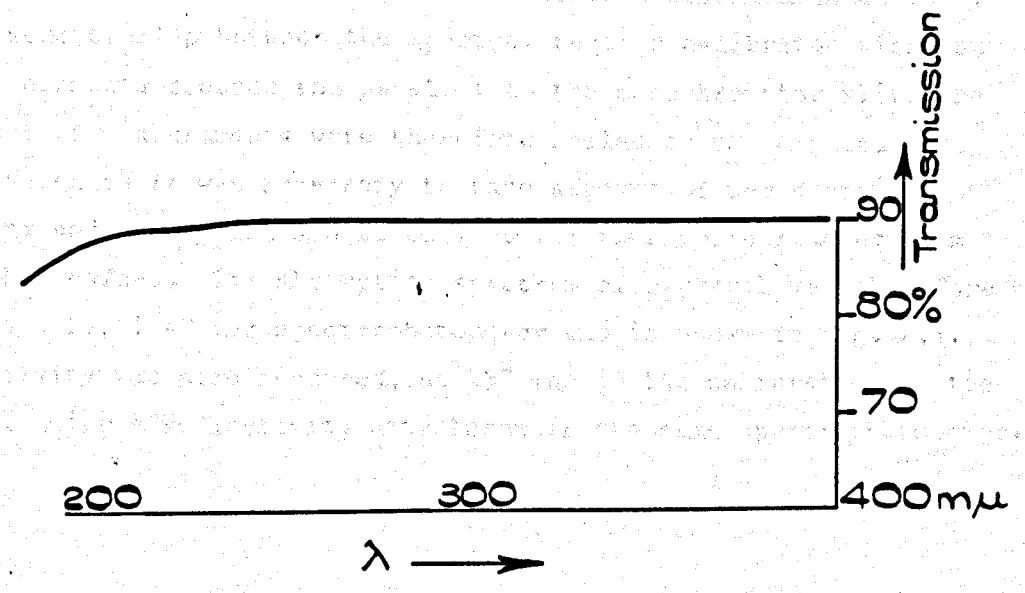

Fig. 2.7

elements and monochromator slits were mutually perpendicular so that the effect of misalignment was minimised. The geometrical calibration was also simplified by this procedure. The rotating shutter speed was of the order of 1500 r.p.m. so that the photocell-electrometer circuit could not respond to individual variations and measured the mean light level. A slowly rotating shutter was used to interrupt the input light to the monochromator. The time interval between light pulses was then some 25 seconds. This procedure reduced the error due to drift of the thermopile output, a particularly troublesome feature at low light levels. The Keithley and Vibron Electrometer outputs were fed into chart recorders and the two charts ran simultaneously. The charts were allowed to run for a number of cycles of the slow speed shutter at a given wavelength, the monochromator wavelength was then changed. At short wavelengths where the intensity was low it was necessary to run the charts for a large number of cycles. Fluctuations in the mercury lamp output appeared on both charts so that the the error from this source could be eliminated. This procedure required that the time response of both systems should be similar. The photocell-electrometer time constant was increased by means of the damping control of the electrometer until equality was achieved.

A further complication appeared at wavelengths below 210mμ. The intensity was then so low that the thermopile signal could not be measured above the noise. It then became necessary to change the thermopile orientation until the slits of the monochromator were parallel to the thermopile elements. The calibration was then extended to 202.5m . There was some overlap between the spectral regions calibrated with the thermopile elements crossed and parallel to the monochromator slit, the parallel set of measurements were therefore scaled to the crossed set. At each wavelength it was necessary to take account of the suprasil reflectivity and absorption and to convert the thermopile reading from watts to photons/sec. The absorption spectrum of suprasil was therefore measured in a Perkin-Elmer spectrophotometer and is shown in fig. 2.7. The reflectivity was also measured, at 45° (as in the calibration of the photocell), using a reflectivity attachment in the same spectrophotometer.

2.7 Sample Preparation

Single Crystals

Following Fotland (1959) several attempts were made to grow single crystals by the Bridgmann technique in evacuated Pyrex crucibles. The crucibles were sealed to maintain stochiometry. The method was partially successful in that some crystals were obtained. The crystals tended to have small cavities and specks of black precipitate (probably Cd metal). Excess iodine was added to the crucible before crystallisation but the crystals did not improve appreciably. It was apparent that much refinement was necessary to obtain crystals of the same quality as those obtained from aqueous solution.

Attempts were also made to prepare crystals by deposition from the vapour phase. A glass combustion tube was electrically heated and cadmium iodide placed inside the tube close to one end. Nitrogen or argon could then be admitted at this end and exhausted at the other. Small flakes of CdI_2 condensed at the cooler end of the tube near to the gas outlet. These flakes were of the order of 1mm across.

Growth from solution was therefore found to be the most successful crystallization procedure. All crystals used in the experiments were prepared from solution in the following manner.

A solution of Analar grade CdI_2 was prepared by dissolving approximately 1 kilogramme of the material in Analar grade water by heating the liquid to boiling point. Additional water was added when necessary to completely dissolve the CdI_2. The solution was then concentrated by evaporation until it became saturated at boiling point. Precipitation then occurred. The evaporation was allowed to continue and the mixture allowed to cool. Approximately one third of the CdI_2 had then precipitated. The solution was then decanted and discarded and the precipitate redissolved in Analar water. The new solution was heated near boiling point until a film of CdI_2 precipitate appeared on the surface of the solution. The liquid was then allowed to cool over the period of a day or more when a small proportion of precipitate occurred. The solution was then diluted by the addition of approximately one fifth by volume of water. The nearly saturated solution was then filtered through Whatman No.6 filter paper into 20cm diameter crystallizing

dishes. The entire procedure took place in dark room conditions and after filtration the crystallizing dishes were placed in a dark cupboard away from mechanical disturbance. Several weeks were allowed to pass before the dishes were inspected. Great care was taken to ensure that the dishes were not disturbed during this time. Large filter papers were used to exclude dust from the dishes at all stages of the preparation.

Large high quality single crystals were obtained in this way. The crystals were clear and colourless and occurred in about 20% of the bowls. The crystals that were used cleaved readily, any crystals that did not were rejected. Many of the crystals had growth spirals on their upper surface. In many cases drops of solution, which were left on the crystals, later evaporated, leaving small surface crystallites. The majority of samples were therefore cleaved in order to remove growth spirals and surface crystallites.

Initially crystals were cleaved with a stainless steel razor blade. In later experiments, however, they were cleaved by means of adhesive tape. The crystal to be cleaved was held in position on a sheet of clean perspex by evacuation through a small hole in the sheet. Sellotape was placed lightly onto the top surface of the crystal to which it adhered. The surface of the crystal could then be pulled away with the adhesive tape. Surfaces formed in either case were highly reflecting, the failure rate was however lower with the method using adhesive tape.

The crystal was then carefully placed in the NGN vacuum coating unit where it was supported on a piece of clean molybdenum sheet. This sheet was also used as a mask during the evaporation to fix the electrode spacing. The separation used was $\sim$0.6cm and remained constant for all experiments using evaporated electrodes. PTFE jigs were used to locate the specimen on the molybdenum. Gold electrodes were evaporated until the gold layer was highly reflecting and almost opaque. The sample was then placed on a PTFE sample holder and retained by gold spring clips (fig. 2.8). The contact pressure was minimised to avoid undue mechanical stress. The spring clips were cemented to the sample by 'silver dag' paint. This method gave mechanically strong contacts which did not seriously deform the crystal. It was found during the investigations

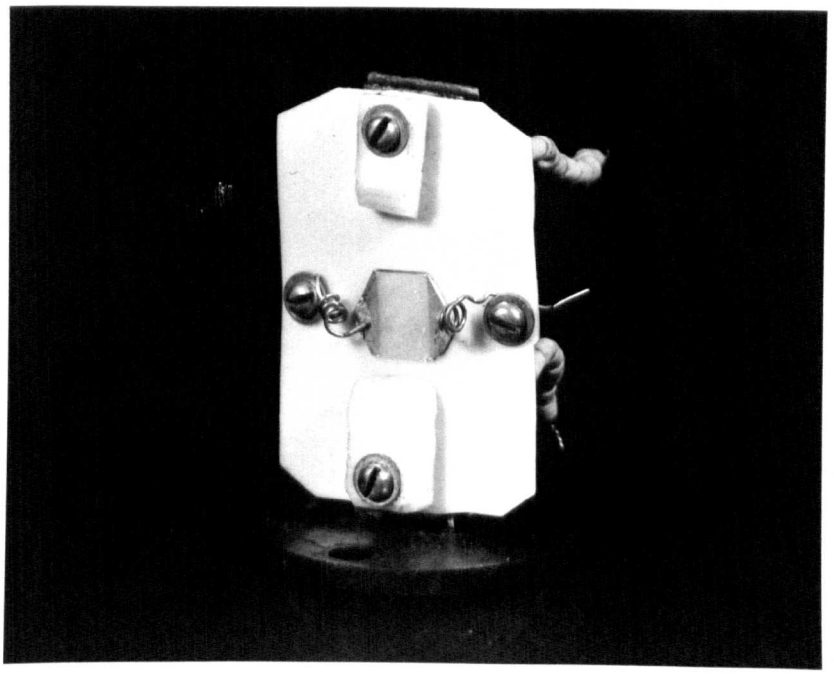

Fig. 2.8

that silver diffused into the crystals at high temperature. Contacts onto crystals for high temperature studies were therefore cemented with 'carbon dag'. Silver dag was retained for all measurements on crystals not subjected to high temperatures since carbon dag was less reliable mechanically. The silver dag was applied to the thick layer of evaporated gold and was not in direct contact with the crystal.

In the above discussion we have been concerned with electrodes deposited onto the crystal 'front' surface. The electric field was therefore parallel to the cleavage plane. This configuration is designated the 'a axis' configuration. In many experiments the electric field was applied parallel to the 'c axis' of the crystal and a different geometry was required. In this case the copper finger of the cryostat was exchanged for the type shown in fig. 2.9. The incident light was transmitted through the slit in the copper finger onto the crystal surface. The front electrode was of nickel sheet or evaporated gold. Both types had a narrow slit to allow light to penetrate into the sample. Semi-transparent electrodes were not used because of problems of transmission and reflectivity losses. The slit in the electrode was somewhat narrower than that in the copper finger. A quartz cover glass could be interposed between the sample and copper finger to reduce the effect of contamination of the sample. The sample was at a temperature close to that of the copper finger which acted as a cold trap for any pump oil or other vacuum contaminants present. The quartz plate increased the minimum sample temperature attainable since it increased the thermal resistance between sample and cryostat.

Small nichrome heating coils were wound onto mica formers so that samples in either geometry could be heated. The temperature of the sample holder could be measured with a copper–constantan thermocouple and potentiometer.

2.8 Evaporated Layers of CdI_2

In Chapter One thin films of CdI_2 were briefly mentioned. Films of thicknesses greater than 200Å prepared at room temperature were shown by Yu (1967) to be largely crystalline in structure. Best (1963) and Tubbs (1968) have shown that their optical spectra, particularly in the

'c axis' Sample Holder.

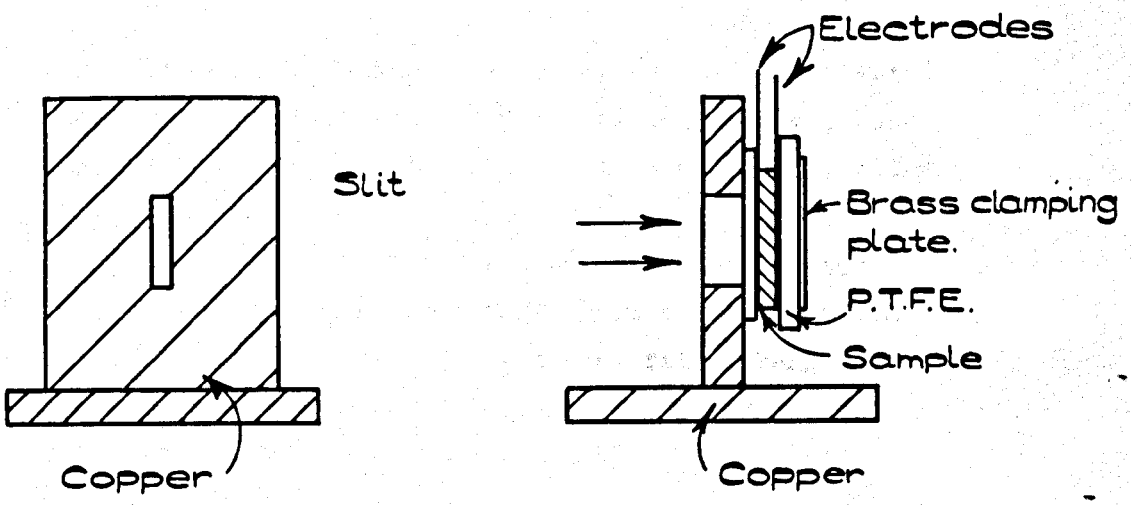

Fig.2.9

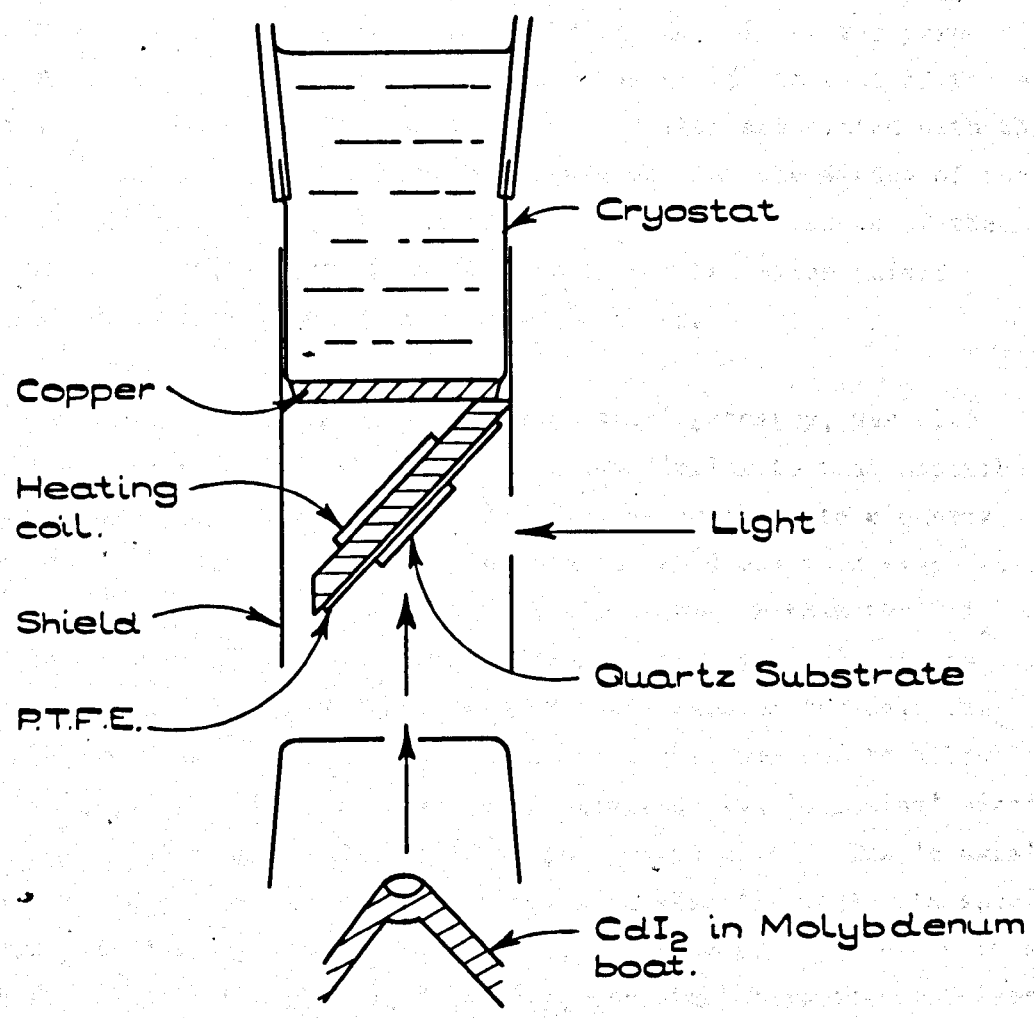

Fig.2.10

exciton regions, improve if the films are deposited at high temperature. The temperature in question is close to 100°C.

Initially films of CdI_2 were prepared in vacuo and transferred to the photoconductivity apparatus. It was noticed, however, that some films apparently changed from a colourless to a slightly milky form during the transfer. A modified apparatus was constructed to eliminate the possibility of contamination by atmospheric water vapour. Films of thicknesses greatly exceeding 1μ tended to become flaky. The flakiness was not immediate and many films changed form over the period of a minute or more. The milkiness found in some films could be attributed to this effect.

The films used in the 'a' axis geometry were prepared in situ by means of the apparatus shown in fig. 2.10. Cadmium iodide (Analar grade) was evaporated from a molybdenum boat through an aperture in a cylindrical tube. The direction of the incident light was perpendicular to the evaporation direction. The sample was at 45° to each of these directions. There were many experimental problems associated with this technique. Careful screening was necessary so that the window of the vacuum vessel was not contaminated with CdI_2. The thickness of the films was difficult to determine since a copper radiation shield prevented the observation of interference colours.

A second film configuration, the 'c axis' geometry, was also attempted. The experimental arrangement was similar to that described by Huggett and Teegarden (1966). CdI_2 was evaporated onto a quartz (spectrasil) disc 1" in diameter. A layer of gold was then evaporated onto the CdI_2. The gold layer was larger in diameter than the CdI_2 so that it covered the sample film. The gold then behaved both as an electrode and as a protective layer for the cadmium iodide. The front electrode was a nickel sheet in which a slit was cut to allow light transmission onto the film. This electrode was 'blocking' since it was insulated from the CdI_2 film by the quartz plate. The 'c axis' crystal sample holder was used in conjunction with 'c axis' film specimens. Many very careful experiments were performed using this technique in an attempt to measure the photoconductivity, but without success. Silver and aluminium were also tried as electrode materials but both appeared to attack the CdI_2 layer.

We attributed the failure of the 'c axis' film method to the very high field strength in the sample and to the ionic and electronic polarisation. Since the method uses one blocking electrode no ionic or electronic carriers may leave the specimen. The probability of polarisation is therefore increased. It might be possible to prevent the ionic polarisation by the use of lower temperatures. The number of defects such as vacancies is likely to be large in films at high temperature and the conductivity may then be orders of magnitude higher than that predicted on a bulk crystal basis. The use of liquid helium temperatures might then be necessary to prevent ionic polarisation. Very short light pulses might also be necessary to prevent polarisation due to photo-generated carriers. At liquid helium temperature the quartz substrate would be inappropriate because of its poor thermal conductivity.

2.9 Experimental Photoconductivity Techniques

Several measurement procedures were adopted for photoconductivity experiments.

The simplest method was to apply a square pulse of light to the sample with the field applied so that the resulting change in current was recorded. The procedure was then repeated after an interval of a few minutes at a second wavelength until the spectrum had been traversed. This method is described as the "point by point method without depolarisation" since the field was applied between light pulses.

In many experiments this method was inapplicable, since successive applications of the same illumination resulted in progressively decreasing currents. The released charge had been trapped and was causing a polarisation field which reduced the effective field in the sample. The polarisation field remained until the next light application when further polarisation occurred. This phenomenon did not always occur and its occurrence could be readily identified.

At room temperature the polarisation due to ionic charge carriers is more serious than the photocurrent polarisation. The former decays exponentially with time rendering photoconductivity measurements impossible unless the photocurrent is large compared with the ionic current value at equilibrium.

Ionic polarisation reduces the internal field thereby reducing the photoconductivity. This polarisation could be eliminated by lowering the specimen temperature since at low temperatures vacancies cease to be mobile. The photoconductivity polarisation then became acute but could be reduced by a reduction in the light intensity. This reduction enabled more readings to be taken before significant polarisation occurred. It was not always possible to reduce the intensity because of the corresponding reduction in photocurrent. It was therefore necessary in many experiments to adopt a depolarisation procedure.

The field was applied in a given direction at a low temperature so that there was negligible dark current. The illumination was then applied and the current recorded on a strip chart recorder. The illumination ceased and the dark current was recorded. The sample electrodes were then shorted so that the applied field was zero. Strong visible or ultra-violet light was then used to illuminate the sample. This depolarising illumination continued until the current, which was still being recorded, reached a steady value. The sample was then allowed to cool for a few minutes and the procedure was repeated. Successive readings of the same wavelength then indicated no progressive polarisation. It was possible to take alternate readings with the applied field reversed but no noticeable improvement resulted. The chief difficulty of the above procedure was that readings were not sufficiently reproducible. The error between readings was of the order of 20%, this made the determination of spectral structure very difficult. Each measurement cycle took many minutes so that some eight hours were required to traverse the spectrum from 200mμ to 400mμ. In many cases unexplained charges occurred between measurements.

After many spectra had been recorded using combinations of the above techniques the outline of the photoconductivity spectrum became clear. The structural details, however, were not resolved in some spectra. A continuous scanning apparatus was therefore adopted in an attempt to improve the resolution.

2.10 Continuous Scanning Apparatus

In this technique the monochromator pass band was scanned continuously through the spectrum and the corresponding photocurrent measured simultaneously. In the point by point measurements described

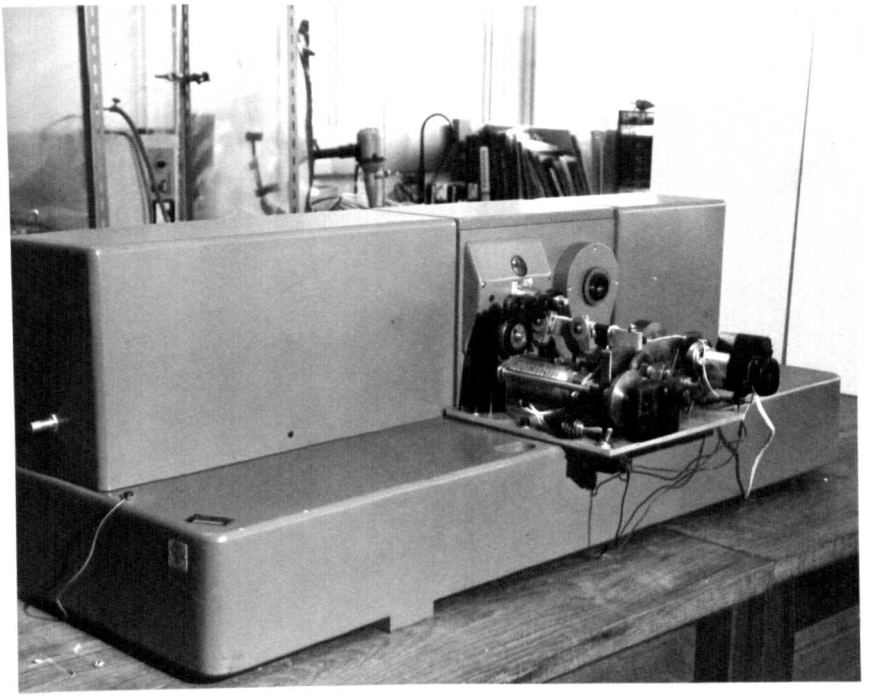

MONOCHROMATOR WITH SCANNING MECHANISM

Fig. 2.11

above it was usual to adjust the width of the monochromator slit to give a bandwidth of 10Å. This was found to give a smoothly varying output over a wide range, (see fig. 3.17). If the slits were fixed at a value to give sufficient light near 200mμ then the intensity was very high near 380mμ. A monochromator slit setting of 1.5mm was required to give 10Å bandwidth at 200mμ but at 400mμ the setting required was only 0.13mm. A setting for example 1.5mm would then give a small intensity at 200mμ and a small photocurrent but at ~380mμ the intensity would be so large that the crystal would rapidly polarise. It was therefore necessary to adjust the slit width continuously with the changing wavelength. In view of the point by point experiments it was decided to gear the slit drive to the wavelength drive in such a way that a 10Å bandwidth was maintained. The direct gearing meant that the bandwidth could be correct in two positions only, the error in all other positions was, however, less than 15%. The chief disadvantage of the drive system was that backlash was present in the gear train between slit and wavelength drum. The slit opening was therefore greater when scanning from 200-400mμ than when scanning in the opposite direction, necessitating output calibration in both directions.

A synchronous motor was used to drive the mechanism and a system of gears allowed three different speeds to be used. The spectrum could be scanned in 1½, 4 or 18 minutes. The fastest speed was rarely used since the time response of the system was usually too long and because of the difficulty in establishing wavelength reference points on the strip chart.

The great advantage of the scanning method was the ease with which structure could be located compared with the methods previously described. The major disadvantages were the degree of polarisation present in some samples and the response time of the apparatus. Both of these effects were wavelength dependent.

It was, however, possible, in many cases, to scan over selected spectral regions and to reverse the scanning direction to reduce the errors due to the polarisation and response time effects. The stability of the monochromator output enabled several spectra to be recorded so that checks were readily performed. The scanning apparatus was particularly useful at liquid helium temperature where the time allowed for an experiment was short. Many other experiments, such as reflectivity spectra, were greatly facilitated by the use of the scanning technique.

REFERENCES

Apfel, J.H. and Portis, A.M., 1959, J.Phys.Chem. Solids 15, 33.

Best, K.J., 1963, Physik Kondens Materie 1, 316.

Fotland, R.A., 1959, Thesis, Case Institute of Technology.

Huggett, G.R. and Teegarden, K., 1966, Phys.Rev. 141, 797.

Tubbs, M.R., 1968, J.Phys.Chem. Solids 29, 797.

Yu, R.M., 1967, Thesis University of Bristol.

CHAPTER THREE

THE INFLUENCE OF MEASUREMENT TECHNIQUES ON THE PHOTOCONDUCTIVITY OF CADMIUM IODIDE

3.1 Introduction

When the measurements described in this chapter were initiated the photoconductivity of CdI_2 had not been extensively studied. The results of Fotland's (1959) investigations were available but these were limited in scope. In particular no measurements at low temperature had been reported and the available response curves were confined to the region near 3.2eV. The lack of sensitivity of Fotland's apparatus necessitated the use of high illumination intensities where the photoconductivity was not proportional to the intensity.

Our interest was, however, directed towards high energy optical structure, studies of which are facilitated by the use of low temperatures. Much of the work to be described in this and later chapters is therefore of a preliminary nature since it was not possible to forecast the type of results that would be obtained or the difficulties to be encountered in the measurements. The results obtained using preliminary techniques and the refinements of these techniques will be described.

Studies of intrinsic photoconductivity in other ionic materials such as the alkali halides followed a similar if rather more extended pattern. Extensive preliminary experiments were essential to establish a reliable technique giving reproducible results.

In an ideal photoconductivity experiment the number of photons required to produce one free electron would be measured. The photon energy would be varied and the variation in the electron yield determined. For simplicity of interpretation the photon flux would be small and the photoconductivity would be proportional to the intensity. A uniform electric field would exist in the crystal but would not affect the properties of the material. Narrow bandwidth low intensity illumination containing no scattered light would ensure high resolution and reliable measurements. The experimental technique would be simplified by the absence of dark current.

It is clear that this ideal situation cannot be achieved in practice. Attempts were made in our investigations to either approach the ideal or to determine the effect of each departure from the ideal situation. The dimensions of the crystals were large on an atomic scale so that they were effectively infinite crystals. The effect of the electrodes was investigated by the use of different electrode materials and the most suitable was selected. Great care was taken to ensure that the purity and perfection of the crystals was of the highest standard available. The experimental difficulties involved in the obtaining of reliable spectra and the measures taken to overcome them are discussed below.

3.2 Electrode Materials and Contact Phenomena

Initially 'silver dag' was used as an electrode material since it had been used successfully by Fotland (1959). In particular this material was found to give ohmic contacts. Many photoconductivity experiments have been performed using parallel plate electrodes between which the sample is sandwiched. The electric field in the sample is then approximately uniform. In our experiments involving illumination perpendicular to the electric field, however, front surface contacts were used. The electric field was then constrained to the surface region of the crystal. The dark current was therefore reduced without a significant reduction in the photocurrent at high absorption coefficients.

Many of the preliminary measurements were performed using the deuterium lamp and monochromator previously described, with the monochromator slits at a fixed opening. No means of determining the monochromator output was available at that time; it was known, however, from manufacturers' data that the output varied smoothly with wavelengths up to 360mμ. Later, when a photocell calibration of the output was performed the output spectrum was found to have the smooth form indicated in fig. 3.1. The high intensity of this spectrum at low energies near the absorption edge caused strong polarisation effects. When the constant slit width output was used in a scanning experiment it was expedient to scan from high energies to low energies. Scanning in the opposite direction caused the sample to polarise before the high energy region had been reached. The high energy region referred to is that near 5.5eV where the strong exciton effects previously described had been found.

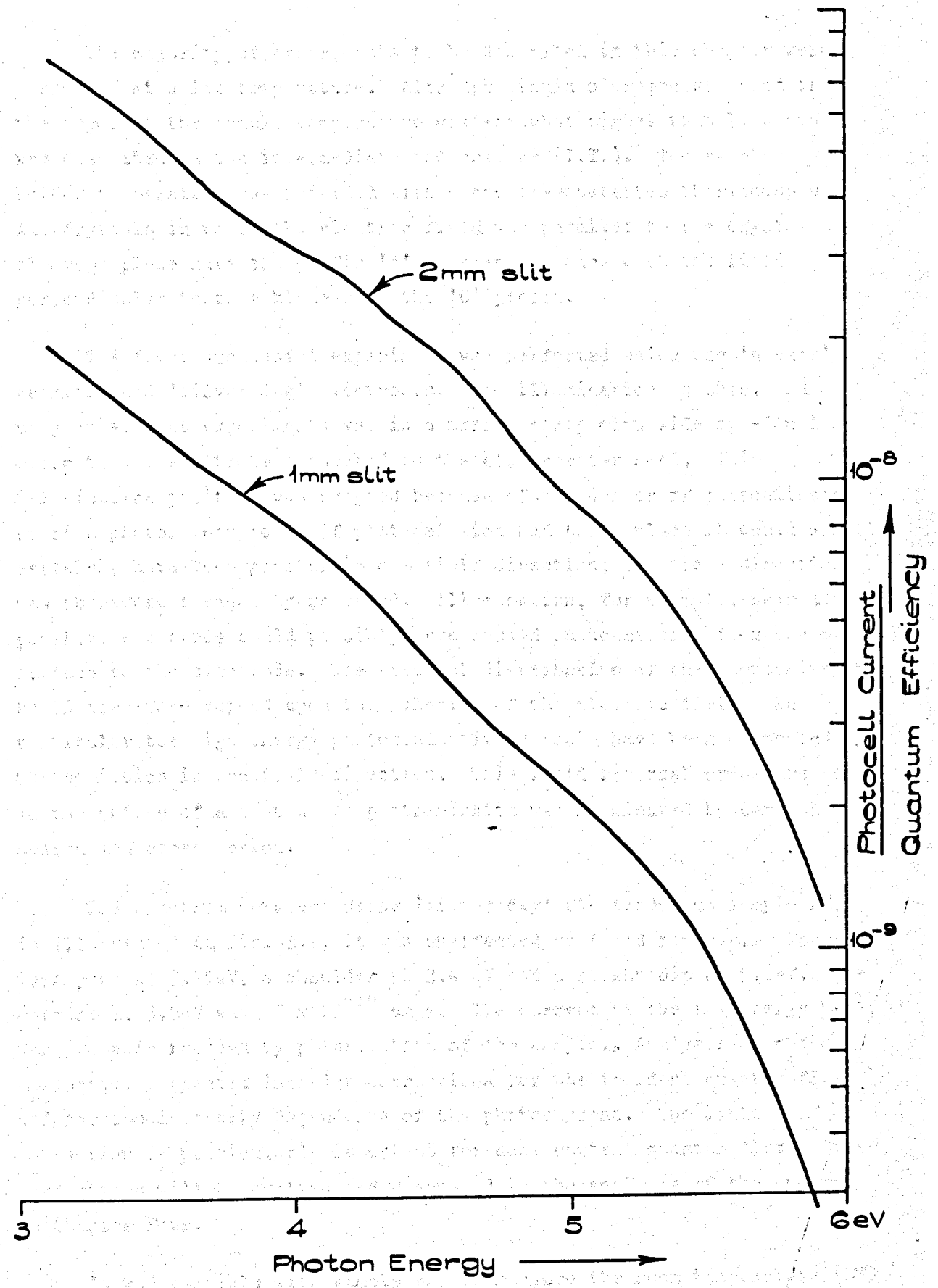
2mm slit
1mm slit
10^{-8}
10^{-9}
Photocell Current
Quantum Efficiency
3
4
5
6eV
Photon Energy

Fig. 3.1

The majority of experiments to be described in this chapter were performed at a low temperature. Although liquid nitrogen was used in the cryostat the sample temperature was somewhat higher than 77°K and was described as the intermediate temperature (I.T.). The sample holder temperature was recorded with a copper-constantan thermocouple. All crystals in which the electric field was parallel to the crystal cleavage plane have the prefix 'A' whereas the ones with the field perpendicular to this plane have the 'C' prefix.

The first successful experiment was performed using the 'a axis' geometry and 'silver dag' electrodes. The illumination in this, and many subsequent experiments was in a narrow strip ~1mm wide by ~7mm long close to the electrode connected to the electrometer head. This illumination position was adopted because of the danger of photoemission at high photon energies. If photoemission had taken place it would almost certainly have been greater in one field direction; the field direction was therefore frequently reversed. Illumination, for example, near a positive electrode could possibly have caused photoemission from the crystal surface to the electrode. The spectral distribution of the photoemission would therefore depend upon the polarity of the electric field. In particular the high energy photoconductivity would have been augmented by photoemission in one field direction. This field reversal procedure was in the nature of a test since photoemission was eliminated by careful design and construction.

The spectrum obtained using 'silver dag' electrodes on sample AX_1 is illustrated in fig. 3.2, it was unaffected by field reversal. There is a peak at 3.25eV, a shoulder at 3.45eV and a slight dip at 5.6eV. The current at 5.5eV was 5×10^{-14} amps. The current at the low energy peak was probably reduced by polarisation of the sample. Analysis of photoconductivity spectra includes corrections for the incident quantum flux and for the intensity dependence of the photocurrent. The latter correction is particularly important for non-constant quantum flux. These corrections will be applied and discussed in the analysis of the spectra in Chapter Four.

It was possible with sample AX_1 to measure the room temperature (RT) photoconductivity. The intensity at low energies was high because of the wide slit opening. The light beam was chopped by a rotating sector disc which transmitted light for one second out of every ten. This procedure

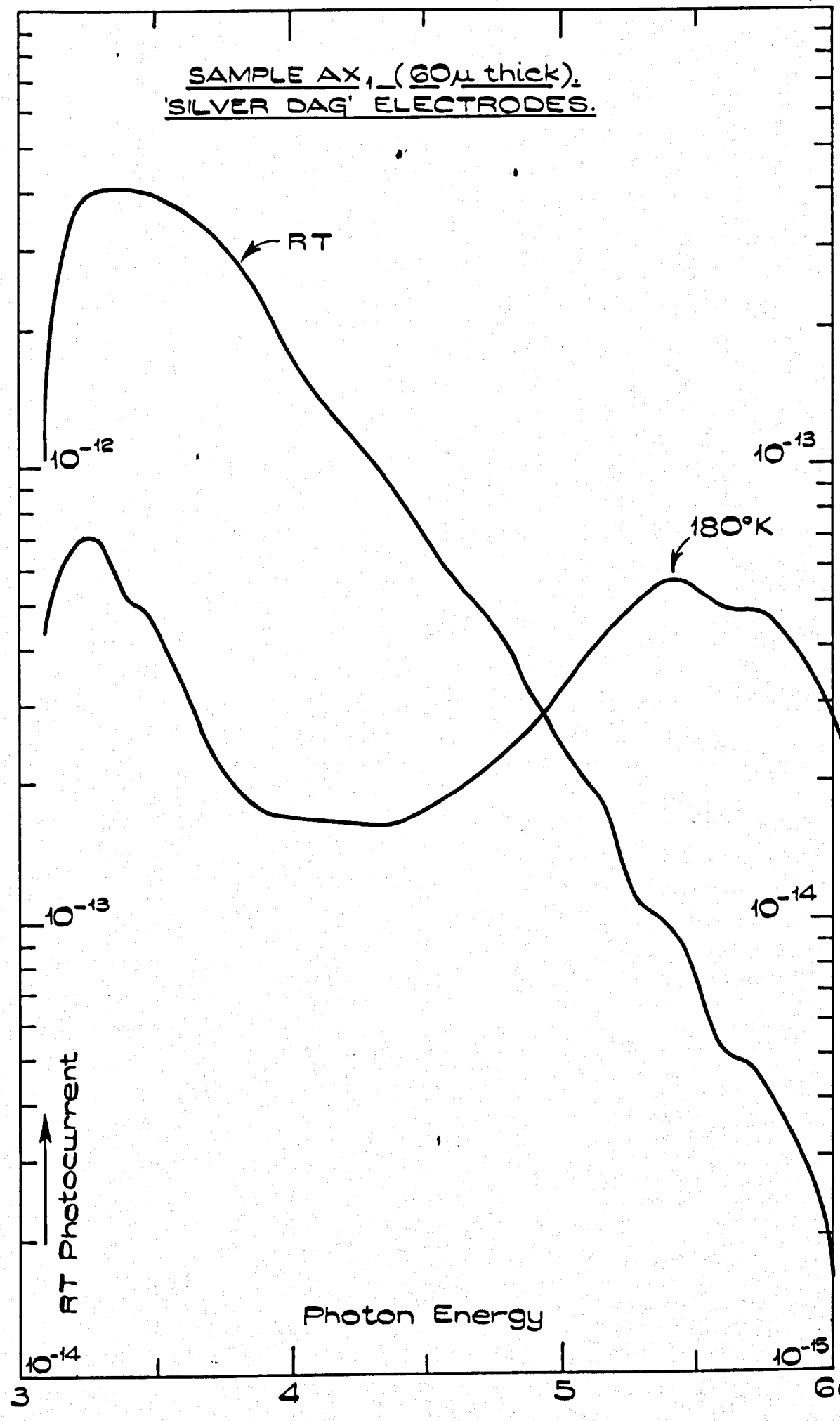
SAMPLE AX1 (60μ thick).
'SILVER DAG' ELECTRODES.
RT
180°K
10⁻¹²
10⁻¹³
10⁻¹³
10⁻¹⁴
10⁻¹⁴
10⁻¹⁵
RT Photocurrent
180°K Photocurrent
Photon Energy
3
4
5
6eV

Fig.3.2.

appeared to reduce the RT polarisation but not that which occurred at I.T..

For the next sample Molybdenum electrodes were used, they were in the form of thin spring clips some 100μ thick. In this sample, AX_2, the dark current swamped the photocurrent at RT, it was possible, however, to detect a peak near 3.2eV. The I.T. dark current was negligible and could therefore be measured. A spectrum obtained with this sample is illustrated in fig. 3.3. The spectrum has the same basic form as that obtained for AX_1 as far as could be ascertained in view of the variation between runs on either sample.

Although both of the electrode materials described above were apparently suitable as far as electrical properties were concerned, both types suffered from other major disadvantages. In the case of 'silver dag' electrodes there was some doubt concerning the stability of silver on CdI_2 at high temperatures. In particular the ionic conductivity was not reproducible at high temperature. (Yu private communication). This suspicion was later substantiated when silver was found to diffuse into CdI_2 at 250°C (see Chapter Seven). Metallic pressure contact electrodes were also far from ideal since they tended to damage the sample through excessive pressure. Attempts to reduce the pressure usually resulted in unreliable contacts or even displacement of the sample when the sample holder was cooled to I.T..

In experiments using the 'c axis' thin film technique silver or aluminium was evaporated onto the thin film CdI_2 sample as an electrode. Both materials were found to change the nature of the CdI_2 thin film specimen. No apparent change took place when evaporated gold was used. Evaporated gold, which was used in some of Fotlands experiments as a semi-transparent electrode was found to give ohmic contacts on single crystals. All future electrodes were therefore of this material, which was deposited onto a freshly cleaved crystal surface. The gold was deposited until almost opaque, the evaporation taking place in a vacuum of 10^{-5} torr. Mechanical constraint and electrical connections were provided by two gold wire spring clips (see fig. 2.8). The contacts between the spring clips and the electrodes were made with a small amount of silver dag paint.

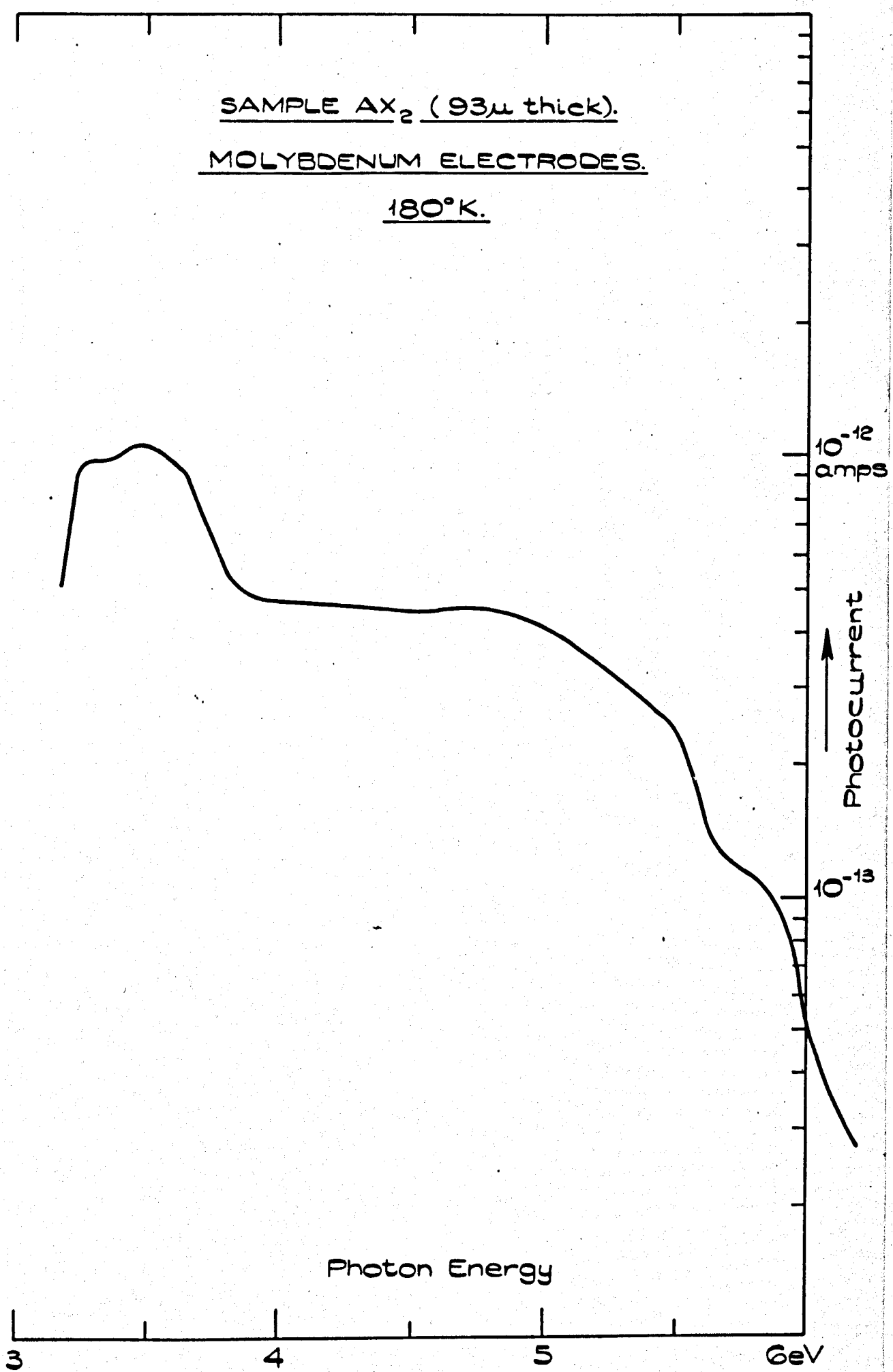
SAMPLE AX2 (93μ thick).
MOLYBDENUM ELECTRODES.
180°K.
10-12 amps
Photocurrent
10-13
Photon Energy
3
4
5
6eV

Fig. 3.3.

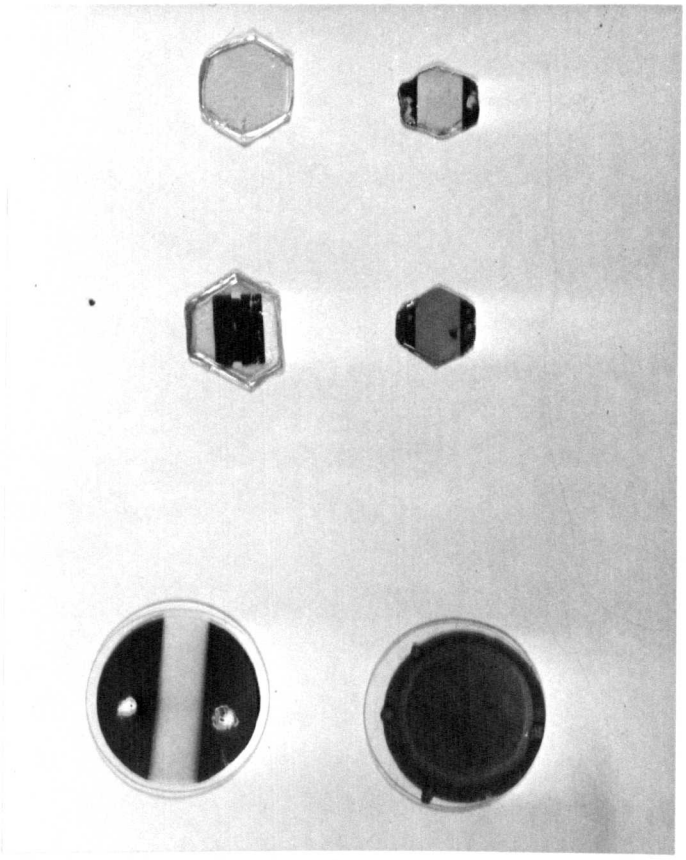

SINGLE CRYSTAL AND THIN FILM SPECIMENS

Fig. 3.4

The evaporated gold electrodes described above were used with sample AX_3. The photocurrent at RT was found to vary linearly with applied field up to a field strength of 800V/cm (fig. 3.5). Higher field strengths were not available in the 'a axis' geometry because of the limitations of the potential source. The measurements were performed using 260mμ illumination, this wavelength being chosen to give a large photocurrent and as having a high absorption coefficient. The experiment could not be usefully repeated at I.T. because of the lack of reproducibility of the results.

3.3 Preliminary Observations of Polarisation Effects

Figure 3.6 illustrates a RT spectrum recorded using a scanning procedure, it is to be compared with the point by point spectrum obtained under similar circumstances. The latter method leads to larger currents, presumably because of the effect of polarisation on the scanning spectrum.

At I.T. the corresponding scanning and point by point curves are shown in fig. 3.7. A broad dip has appeared in the scanning spectrum near 4.4eV which is absent in the other curve. This is again attributed to a polarisation effect and will be discussed in a later chapter. In this sample there was negligible polarisation at 215mμ (5.77eV), at energies below this the polarisation increased to a maximum near 300-360mμ (4.1eV-3.4eV). It seems likely that the absence of polarisation at high energies is due to the low intensity in this region. The polarisation also falls below the indirect absorption edge peak. There are three regions exhibiting different polarisation effects. The first region is at high energies near 210mμ (5.9eV) where the intensity is low and polarisation is negligible. At lower energies the higher intensities caused a pronounced polarisation effect. At still lower energies where the absorption coefficient became small the polarisation again decreased.

The preliminary measurements described above gave some indication of the photoresponse to be expected at both room and liquid nitrogen temperatures. It was clear that great care was necessary to avoid, or to make allowance for, polarisation effects. Accordingly later experiments used lower intensities to reduce the central region polarisation.

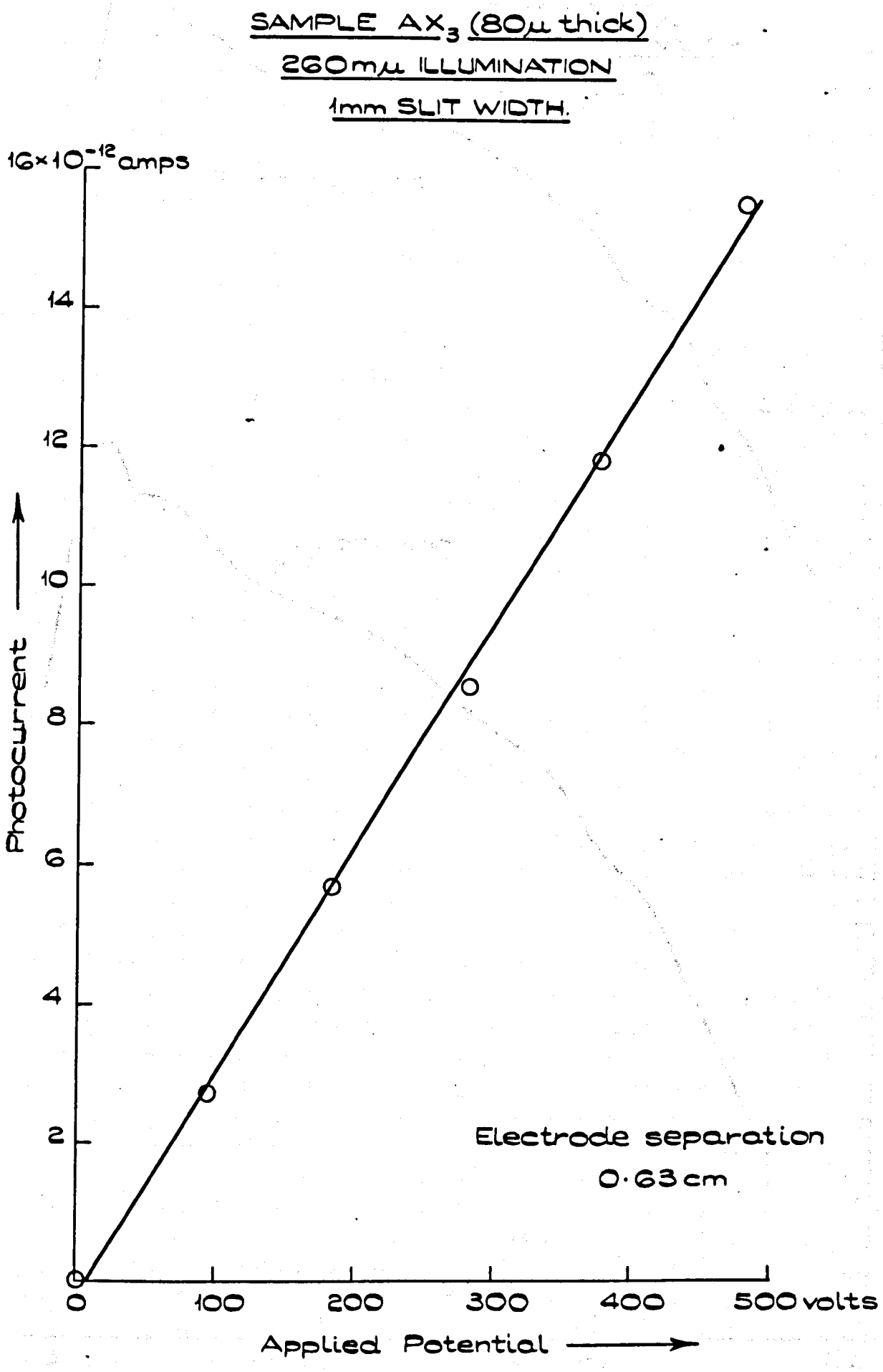
SAMPLE AX3 (80μ thick)
260mμ ILLUMINATION
1mm SLIT WIDTH.
16×10⁻¹² amps
14
12
10
8
6
4
2
Photocurrent
Electrode separation
0·63 cm
0
100
200
300
400
500 volts
Applied Potential

Fig. 3.5

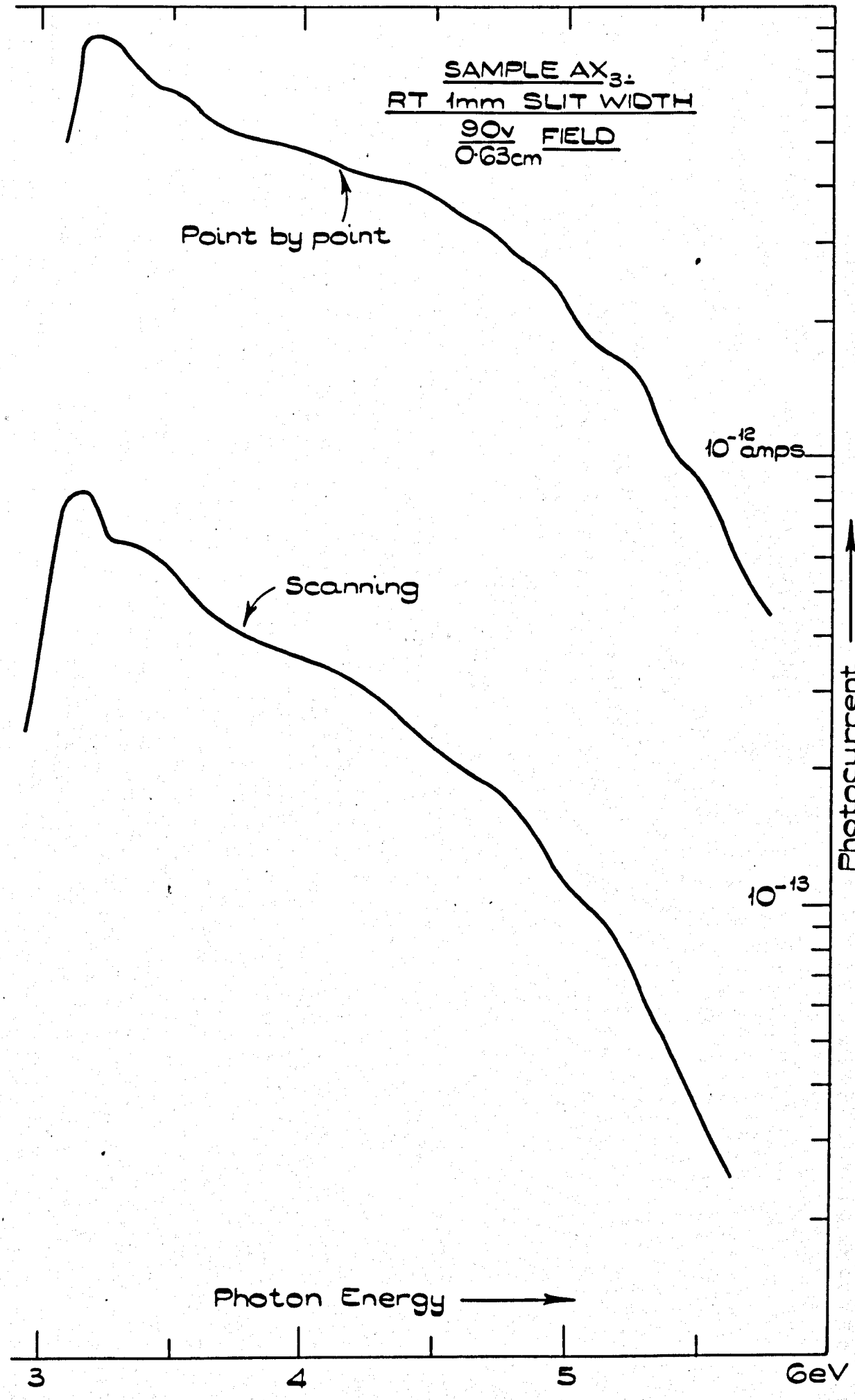
SAMPLE AX3:
RT 1mm SLIT WIDTH
90v / 0·63cm FIELD
Point by point
Scanning
10^-12 amps
10^-13
Photocurrent
Photon Energy
3
4
5
6eV

Fig. 3.6

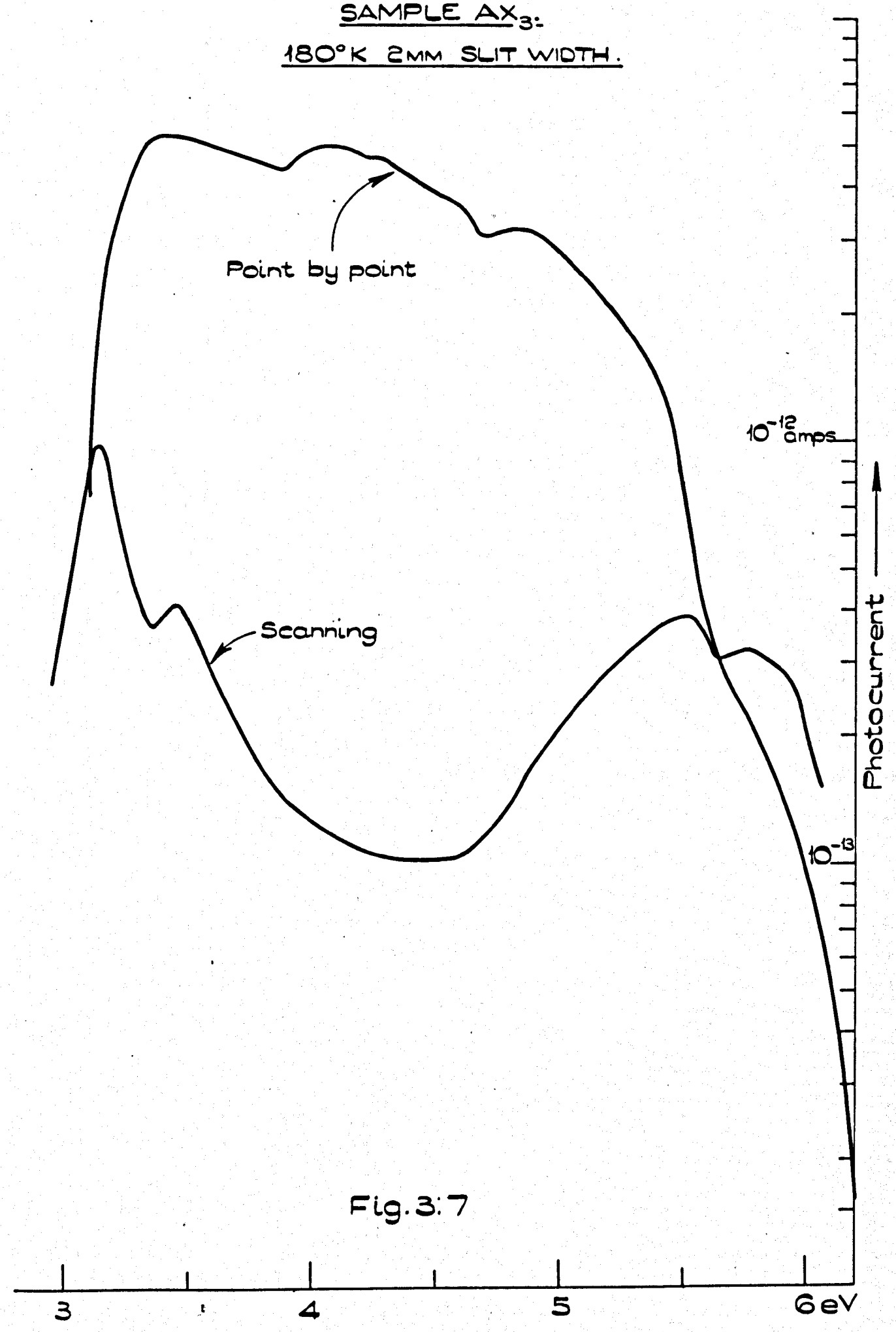
SAMPLE AX3:
180°K 2MM SLIT WIDTH.
Point by point
Scanning
10-12 amps
10-13
Photocurrent
3
4
5
6 eV

Fig. 3:7

3.4 The Elimination of Polarisation Phenomena

The reduction in intensity necessitated by polarisation elimination was achieved by adjustment of the monochromator slit opening to give 10Å bandwidth at each wavelength. The necessary slit openings were obtained from manufacturers data. In the majority of point by point measurements it was necessary to depolarise the sample between measurements. Visible or ultra-violet light from an unfiltered tungsten-filament or high pressure mercury discharge lamp was used. A spectrum obtained in this way is illustrated in fig. 3.8. A check for polarisation was made at each wavelength by repetition of the measurement. Preliminary measurements of the intensity dependence of the photocurrent were also made. They were complicated by the lack of reproducibility and the effect of polarisation, but a reliable sequence was found. One measurement was made with no attenuation of the light beam, a second measurement was then made using an attenuated intensity. The procedure was then repeated for various attenuations. In the case of sample AX_4 the wavelengths used were 230mμ and 380mμ. The relationship between light intensity I and photocurrent ip was approximately linear at 230mμ and varied as

$$ip = I^{0.7} \quad . \quad . \quad . \quad . \quad . \quad . \quad . \quad . \quad 3.1$$

at 380mμ. The low current measurements were difficult and the errors involved were of the order of 20%.

The dark current varied linearly with applied voltage (fig. 3.9) and indicated an effective sample resistance of $2 \times 10^{13}\Omega$. The resistivity of the 415μ thick sample was therefore of the order of $2 \times 10^{13}\Omega$cm along the cleavage plane.

Crystal AX_5 was much thinner being of some 40μ thickness. Spectra obtained with this sample are illustrated in fig. 3.10. There was good agreement between successive runs on this sample, the agreement being particularly good near the low energy peak. There was an appreciable dip near 218mμ (5.69eV) which fell to some 20% below the neighbouring background.

Sample AX_6 was some 200μ thick; a spectrum recorded point by point without depolarisation between measurements is illustrated in fig. 3.11. The first point recorded was at 360mμ (3.44eV) on the upper branch, it was repeated after the spectrum had been traversed to 200mμ (6.2eV). The

SAMPLE AX_4 (415 μ thick)

180°K

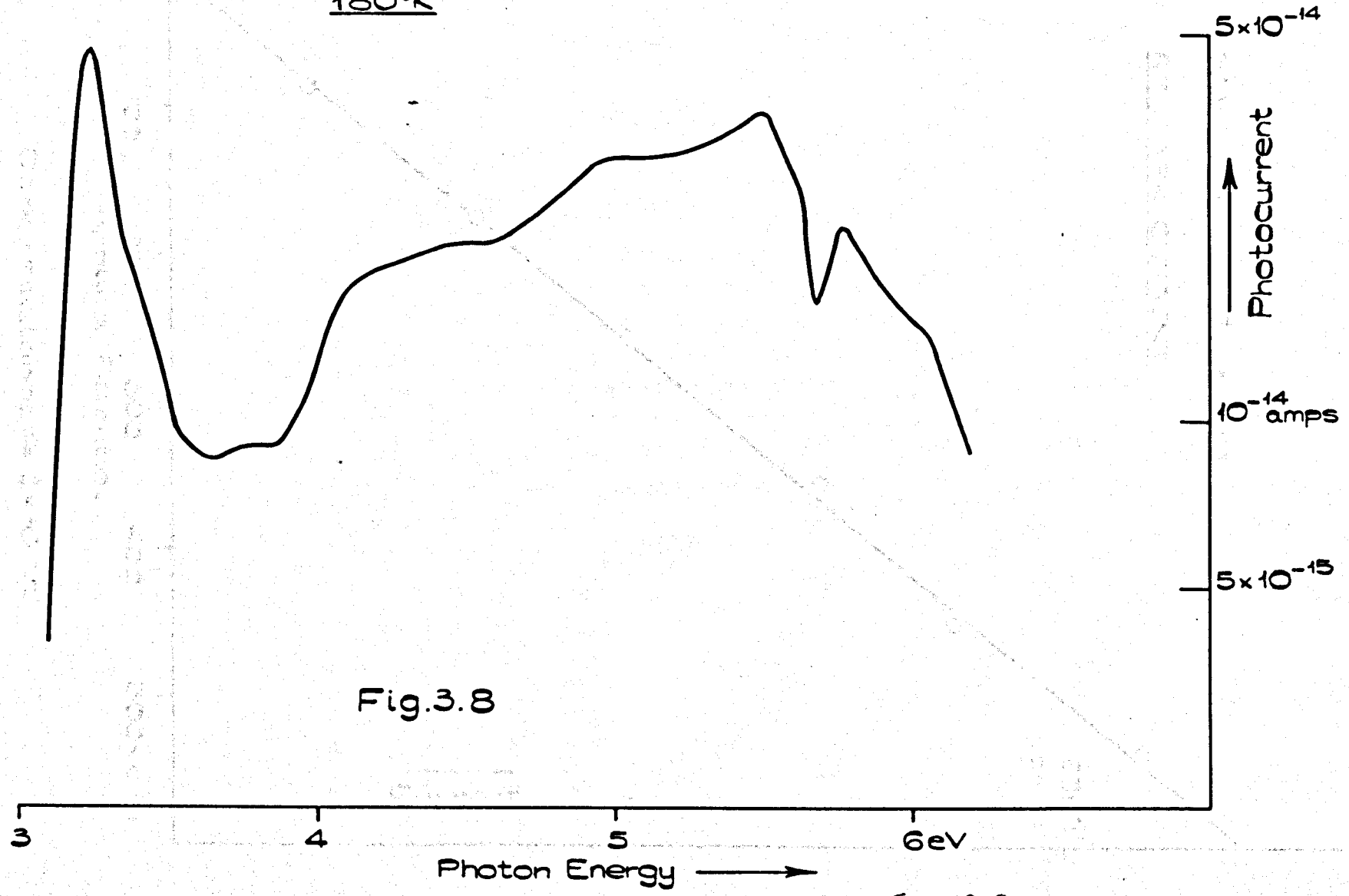

Fig.3.8

Fig.3.8

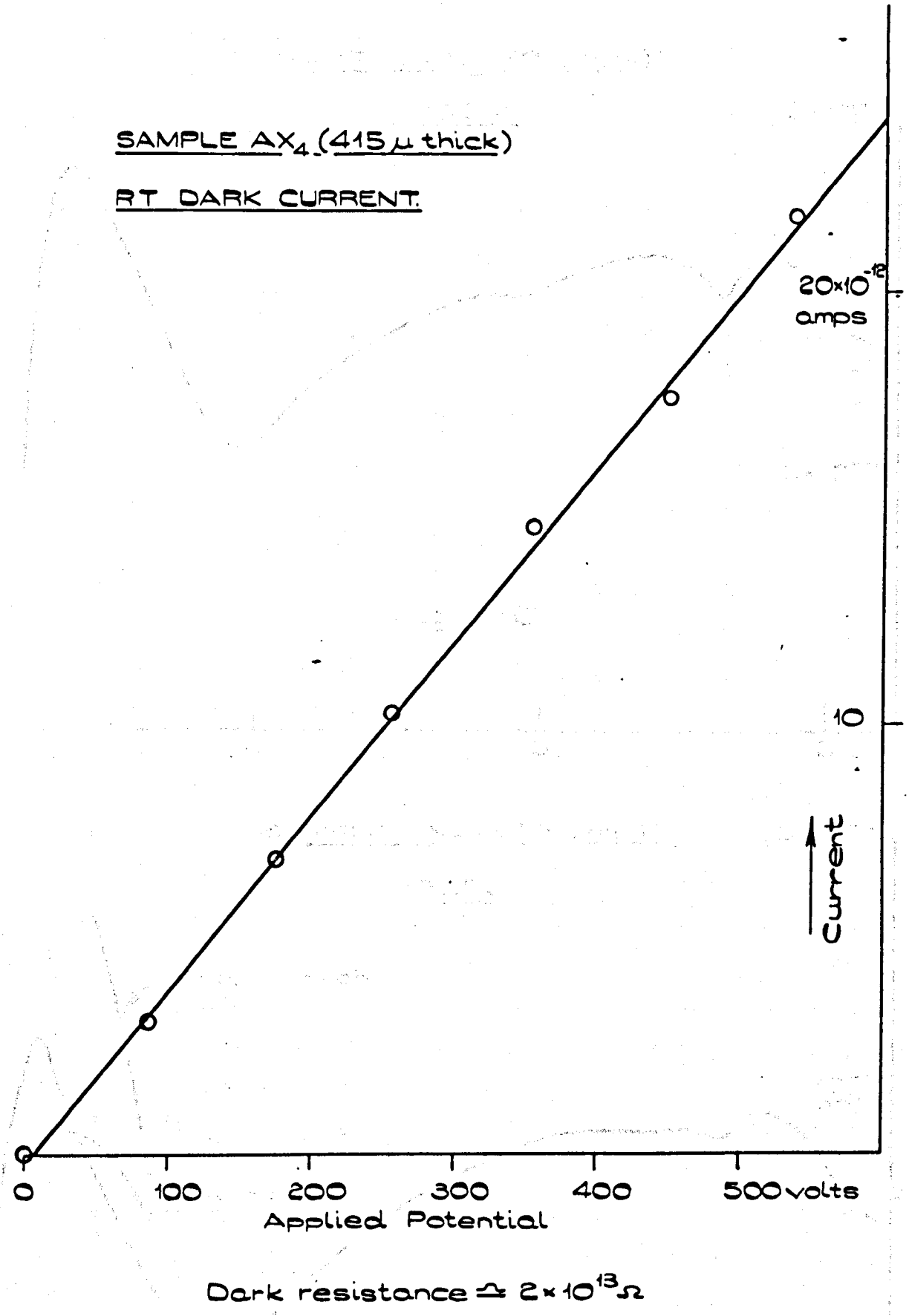

Dark resistance ≃ $2 \times 10^{13} \Omega$

Fig. 3.9

SAMPLE AX_5 (40 μ thick)

180°K

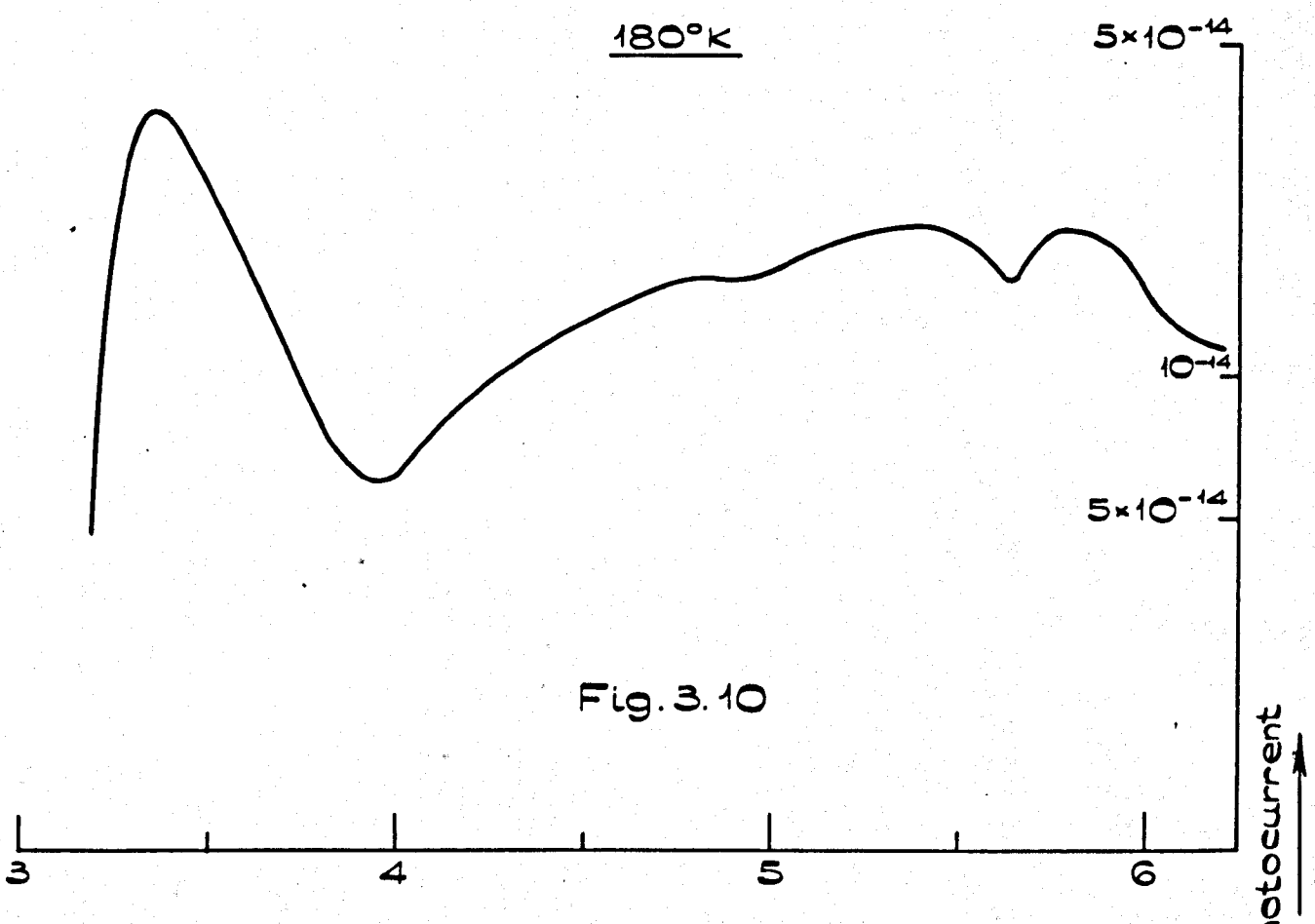

Fig. 3.10

SAMPLE AX_6 (202 μ thick)

180°K

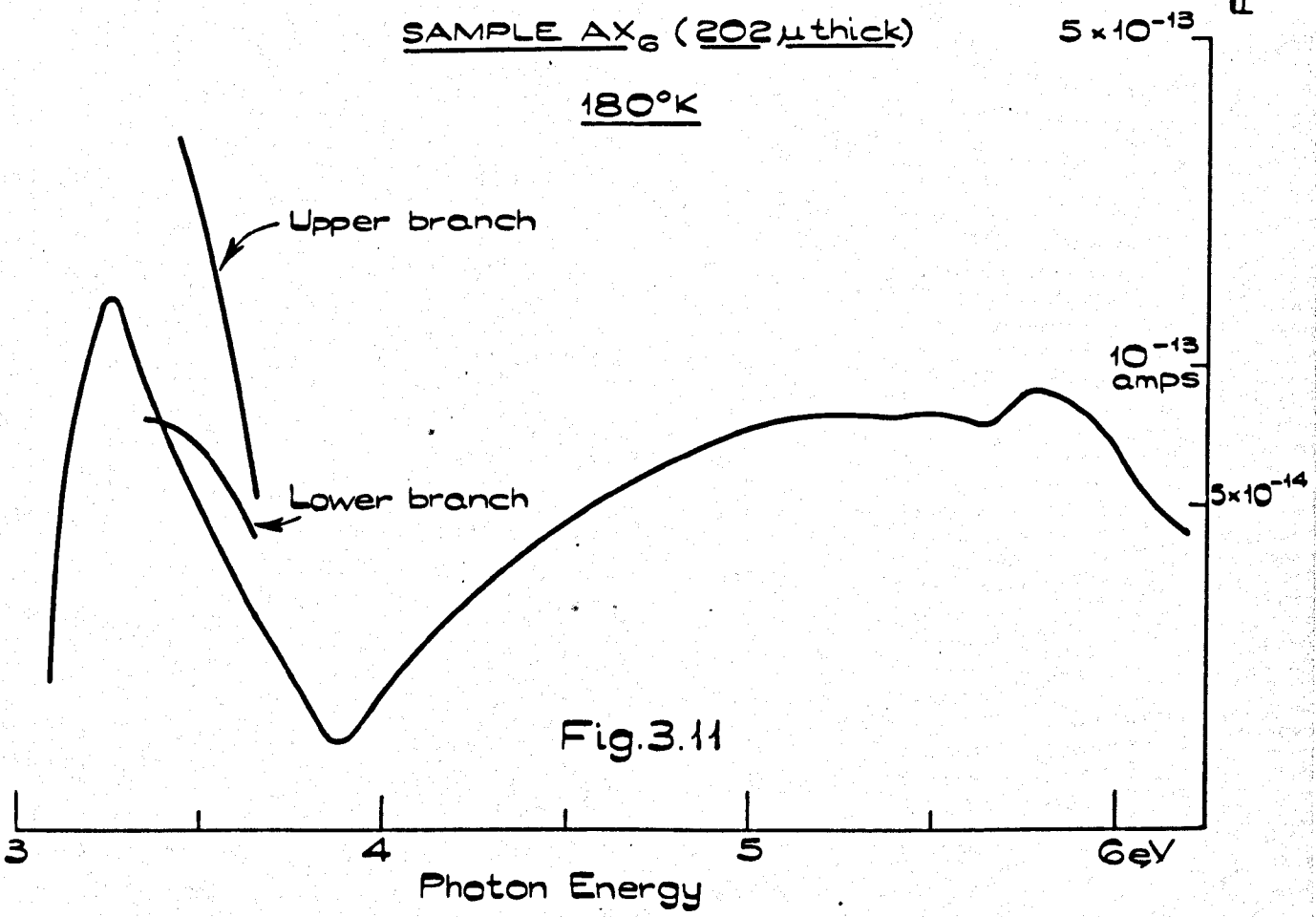

Fig. 3.11

effect of polarisation was to reduce the photocurrent from 3.2×10^{-13} amps to 7.5×10^{-14} amps. When the depolarisation procedure was used the photocurrent increased, particularly in the low energy region. The high energy spectrum was not changed significantly.

It became clear on investigations of sample AX_7 that a modification of the technique was necessary to investigate fine structure in the response spectrum. It was possible with this sample to measure the RT photoconductivity spectrum (fig. 3.12). Room temperature measurements were usually difficult because of the dark current. In particular the decay of the dark current with time was accompanied by a corresponding decay in the internal field and therefore in the photocurrent.

At I.T. the normal measurement procedure of waiting after each depolarisation was adopted, the curve shown in fig. 3.12 was then obtained. This curve was the mean of three runs which differed from the mean by less than 15% throughout the spectrum.

The current at low energies was found to increase if the measurements were taken immediately after the depolarisation. The curve also tended to lack structure.

Figure 3.13 illustrates the residual effect of a polarisation field so that illumination with zero external field led to a current in the opposite direction to the original photocurrent. The removal of the residual field by the illumination is also indicated. Measurements of the variation of photoresponse with illumination position have been made using 380mμ (3.26eV) illumination. These measurements indicate that the most rapid spontaneous fall in photocurrent (due to polarisation) occurs when the illumination is near the electrodes (fig. 3.14).

The experiments described above have justified the use of evaporated gold electrodes and indicate some of the problems associated with point by point measurements. These experiments were necessarily long and the results were not always sufficiently reproducible for the determination of fine structure.

The shape and magnitude of the photoresponse curve was however clear after the experiments described above had been performed. An improved technique was necessary to enable fine structure to be located and spectra to be obtained more rapidly.

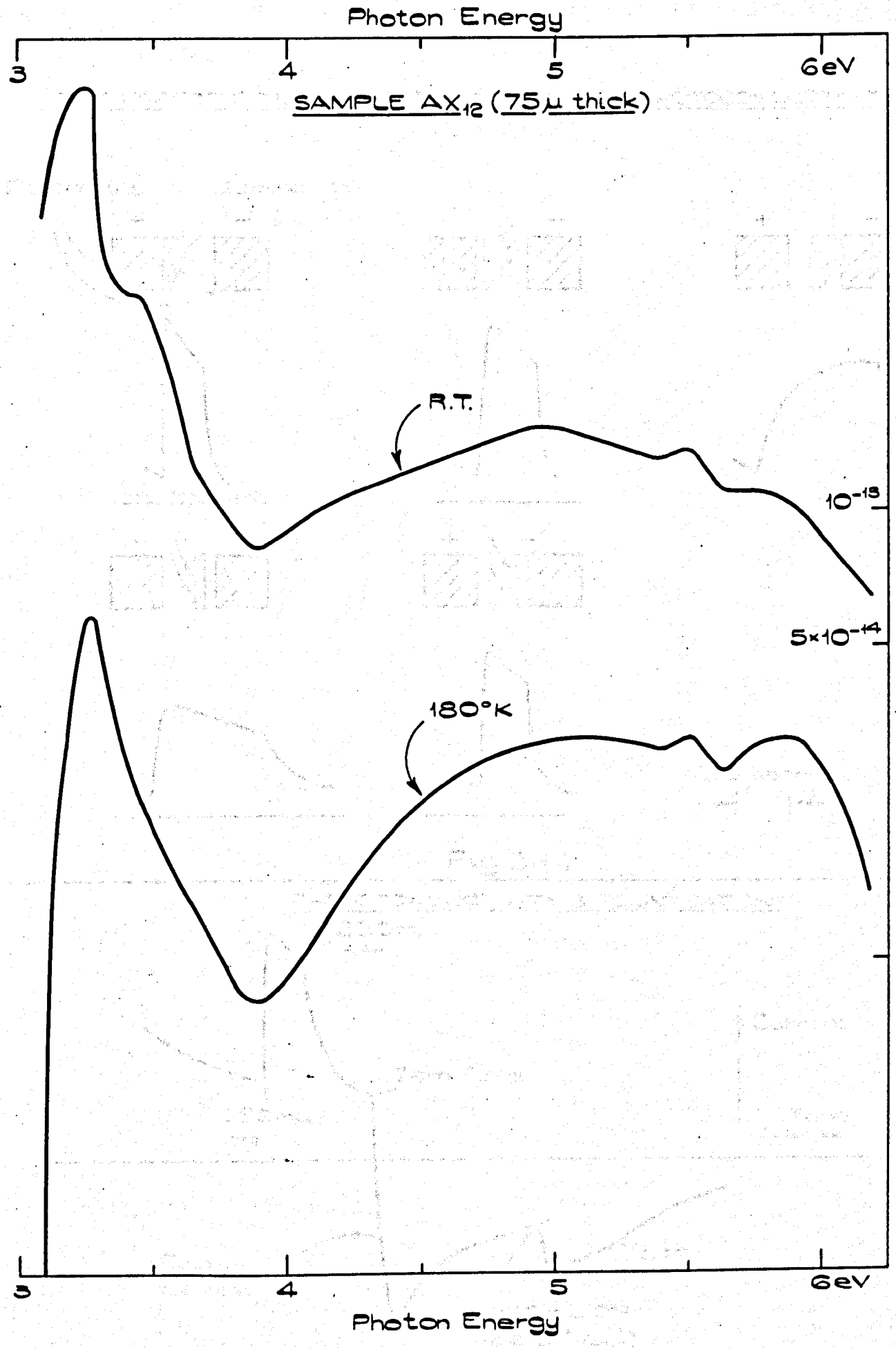
Photon Energy
3
4
5
6eV
SAMPLE AX12 (75μ thick)
R.T.
10-13
5×10-14
180°K
3
4
5
6eV
Photon Energy

Fig. 3.12

THE EFFECT OF ILLUMINATION POSITION ON PHOTOCONDUCTIVITY.

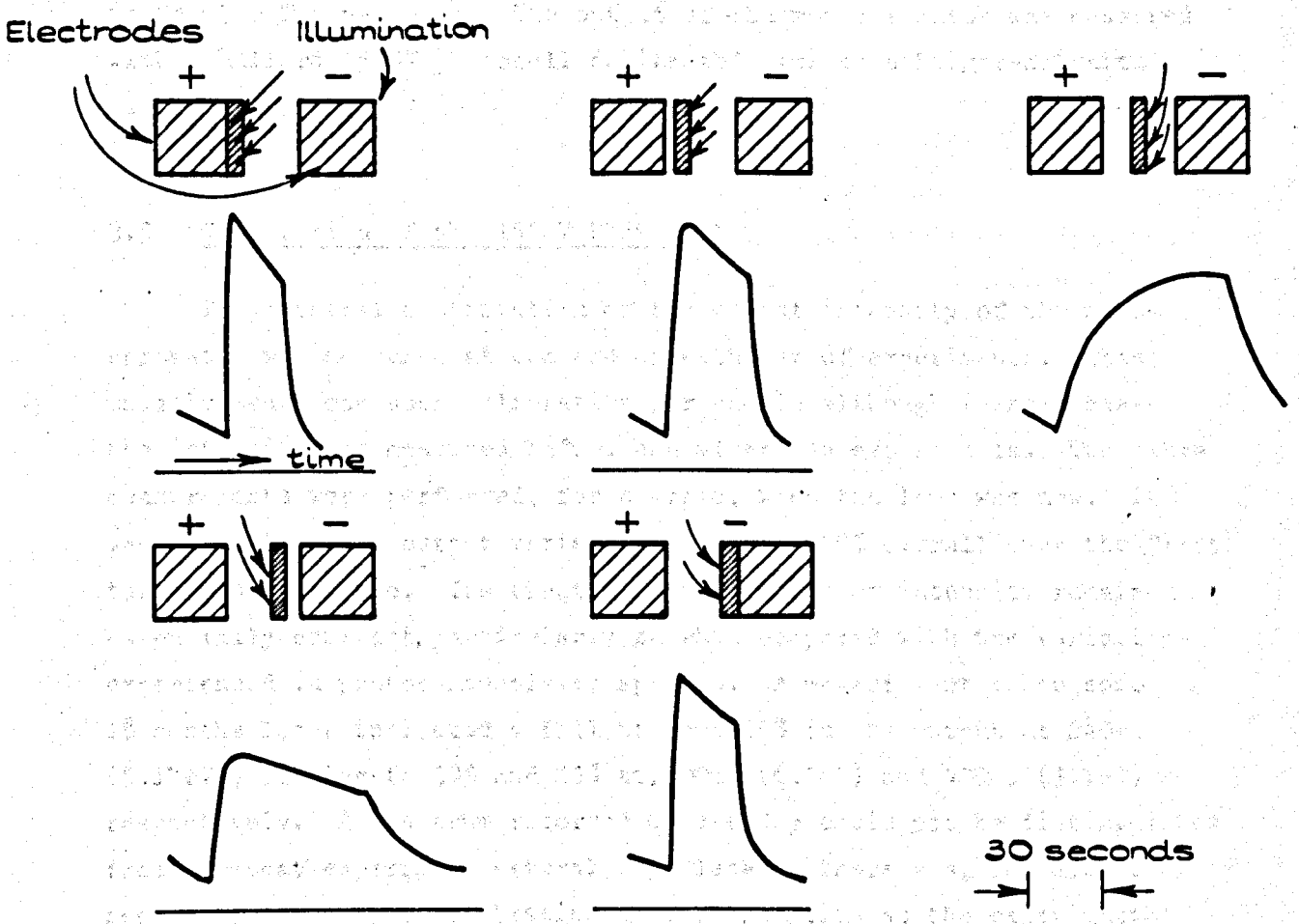

Fig.3.14

PHOTOCONDUCTIVITY & POLARISATION

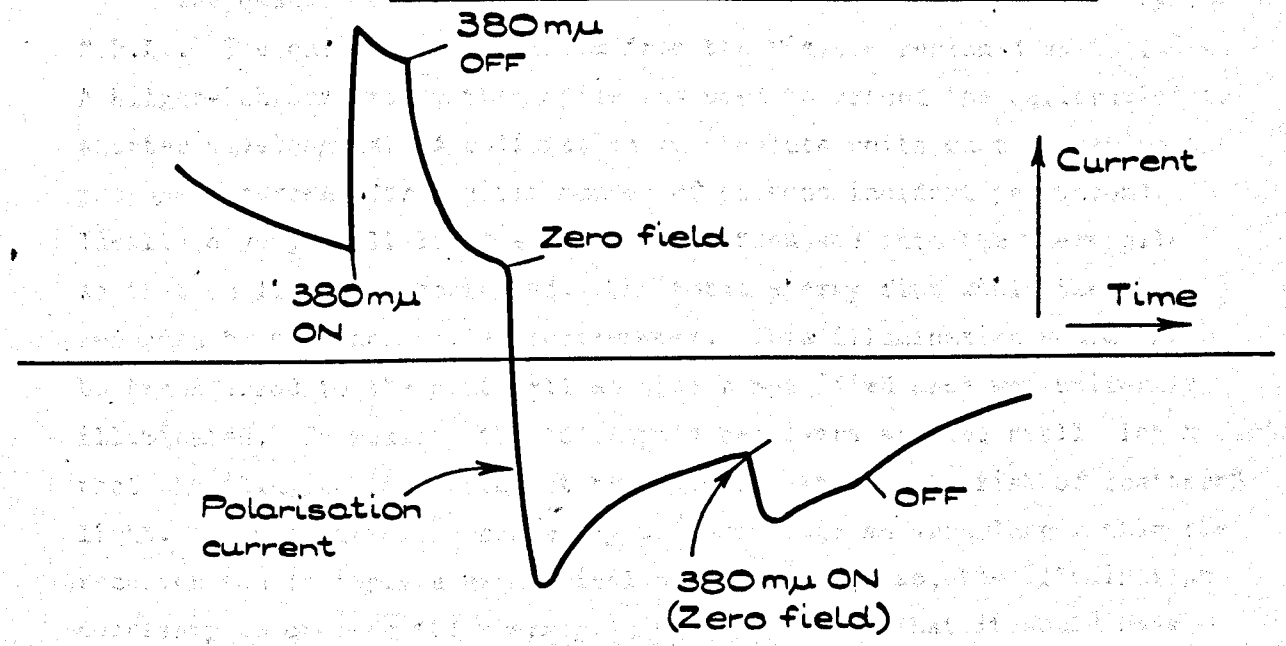

Fig. 3.13

In all of the above experiments a deuterium lamp, as described in Chapter Two was used. The output of the monochromator was measured with a Mullard 150UV photocell calibrated against a Hilger-Schwartz vacuum thermopile.

3.5 Calibration of the 150UV Photocell

The spectral distribution of the output intensity of the monochromator was measured at the end of each set of experiments. This usually meant one such calibration per sample although in some cases the intensity was measured before and after the experiments. The extra measurements were performed, for example, when the lamp was new. It was found that the output varied by less than 20% overall over the first three months of use. The spectral distribution of intensity remained essentially constant, particularly so when compared with the variations experienced in photoconductivity spectra. A measurement taken some 18 months later indicated a fall of some 50% in the output at 240mμ (5.17eV), falling to 30% and 25% at 200mμ (6.2eV) and 400mμ (3.1eV) respectively. A spectrum recorded on one day could not be distinguished from a repeat experiment several days later. There was, therefore, no necessity for output calibration at the same time as the experimental measurements were taken.

The quantum efficiency of the photocell had been determined by the N.P.L.. The calibration extended from the visible region down to 248mμ. A Hilger-Schwarz vacuum thermopile was used to extend the calibration to shorter wavelengths. A calibration in absolute units must determine the photocell current for a given number of photons incident per second. Ideally a very small light spot would be focussed onto the thermopile so that no light was scattered. The total energy flux would then be recorded by the thermopile electrometer. This illumination would then be transferred to the photocell so that a specified area was uniformly illuminated. In reality the thermopile receivers were so small 1cm x 0.05cm that the illumination could not be focussed without the risk of scattered light. It was therefore necessary to focus onto an area larger than the receiver and to apply a geometrical correction. Also, the illumination necessary to operate the thermopile was so intense that it would have overloaded and damaged the photocell. It was therefore necessary for

the illumination to be attenuated. High stability high intensity light sources were not available so that simultaneous recording was necessary. This requirement meant that a beam splitter was required. A correction factor which was wavelength dependent was used to correct for the variation of reflectivity with wavelength. A suprasil plate was used to split the beam and to attenuate the reflected beam. The reflectivity of the suprasil was measured in a Perkin-Elmer Double Beam Spectrophotometer. The suprasil was placed in a reflectivity attachment and the combined reflectivity of the attachment and suprasil place was determined. The suprasil was then exchanged for an aluminium mirror of measured reflectivity and, by comparison, the suprasil reflectivity was calculated (fig. 3.15). The curve was smoothly varying and the absorption is negligible in the region illustrated.

The errors caused by the geometry of the image on the thermopile and the size of the attenuation factors were significant but were not thought to be markedly wavelength dependent. In particular the size of the image did not change appreciably with wavelength. A luminescent screen was used to investigate this effect in the far ultra-violet. In view of these errors, which would not affect the shape of the calibration but would affect the overall magnitude, the distribution of the photocell quantum efficiency was normalised to the N.P.L. values. The values chosen to be normalised were those between 390 and 436mμ where both sets of values were fairly constant. The deviation between our results and those of the N.P.L. is less than 10% throughout the region of overlap, fig. 3.15b. The agreement is particularly good at the high energy end of the overlap.

Figure 3.16 illustrates the photocell output recorded on two separate days, the first spectrum was recorded when the deuterium lamp was almost new, the second was recorded one month later. There is good agreement between the two spectra particularly as far as their spectral distributions are concerned. The spectra were both recorded point by point.

Once the spectral distribution of the output of the monochromator could be reliably measured it became possible to improve the photo-conductivity technique. The improvement consisted of a modification to the monochromator so that the spectrum could be continuously scanned at constant bandwidths.

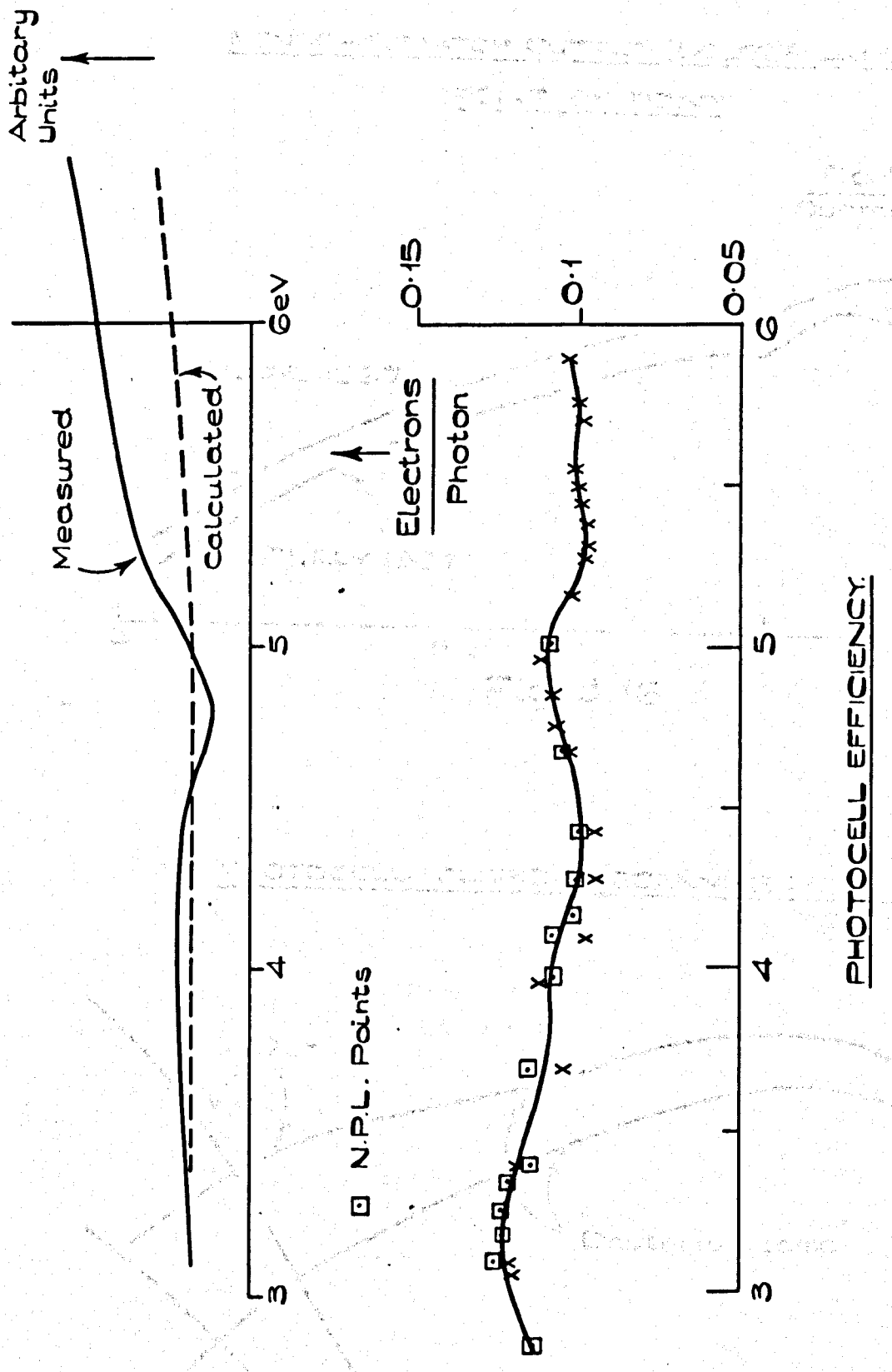

Fig. 3.15

The broken curve refers to Suprasil reflectivity calculated from the refractive indices assuming that the monochromator output was not polarised.

This assumption was verified experimentally. The discrepancy between the two curves may have been caused by a chromatic aberration in the spectrophotometer so that the calculated value was used to determine the photocell efficiency illustrated in the diagram. The difference between the two reflectivity curves was not sufficient to significantly affect the photoresponse spectra.

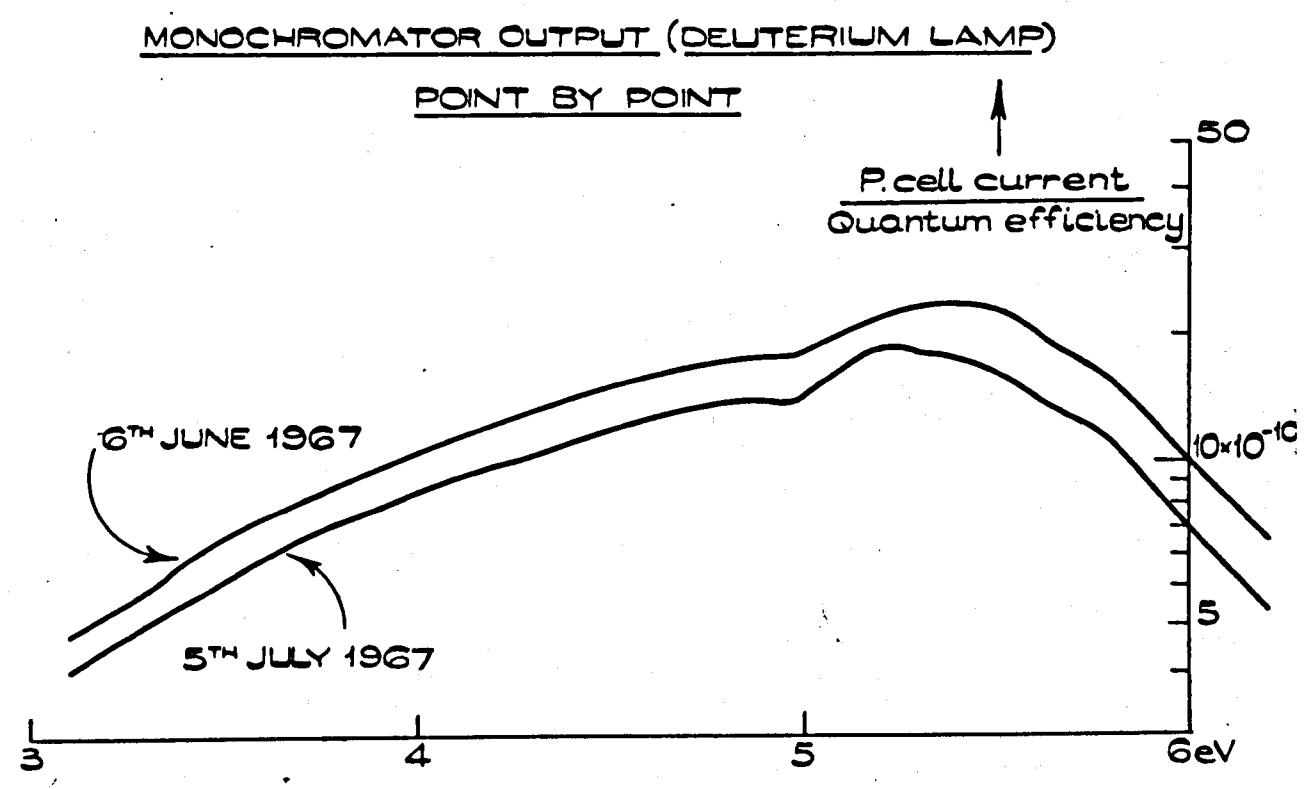

Fig. 3.16

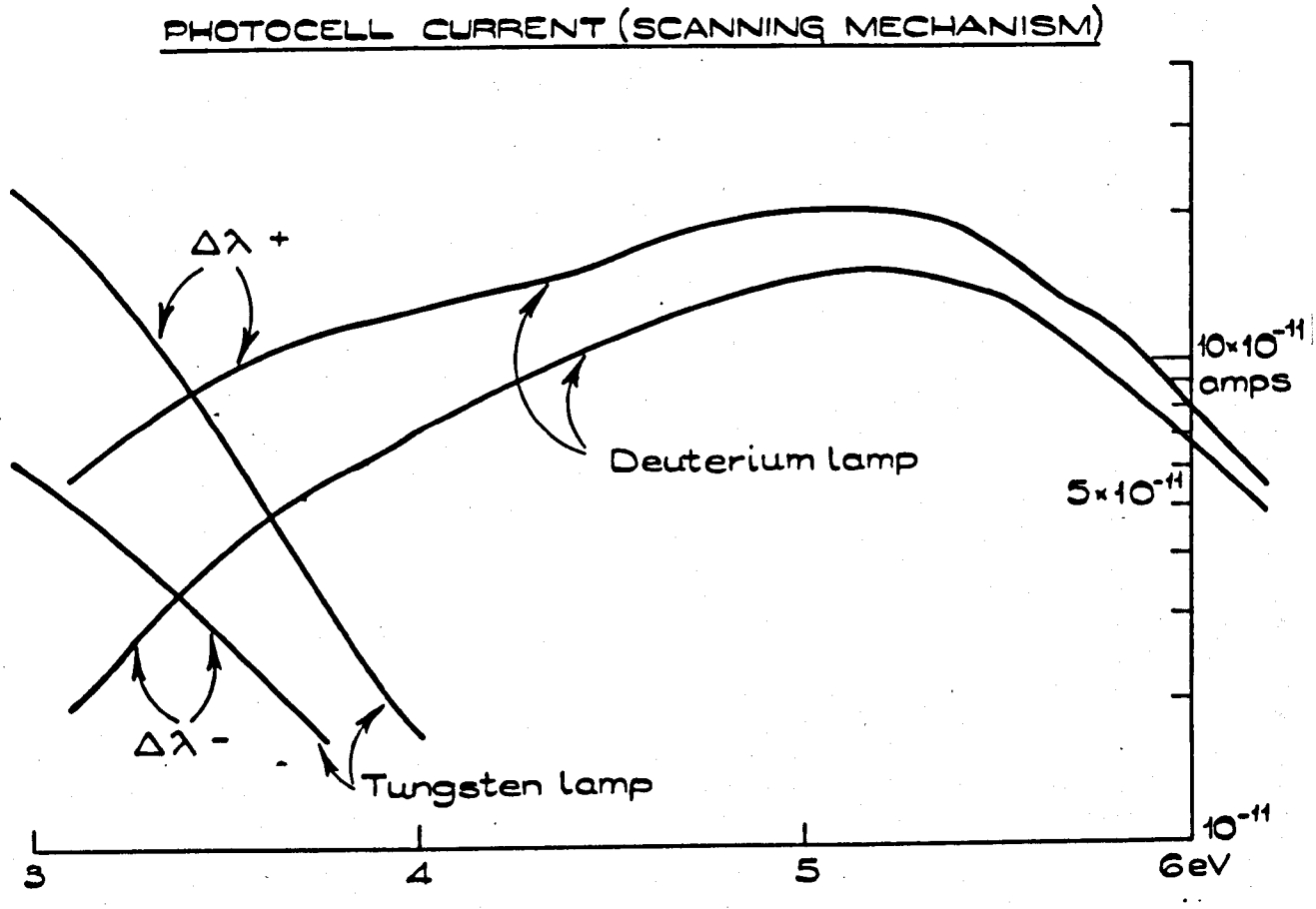

Fig. 3.17

3.6 The Constant Bandwidth Scanning Method

The difficulties apparent with the point by point spectra, particularly in the resolution of fine structure, led to the adoption of the constant bandwidth scanning technique. The output of the monochromator was constant from run to run in the same scanning direction, but depended upon the direction of scanning. This change of intensity with scanning direction, caused by backlash in the gear drive to the slit mechanism, necessitated output calibration in both directions. A typical calibration is illustrated in fig. 3.17. The scanning direction from 200mμ to 400mμ was designated $\Delta\lambda\oplus$ and the opposite direction was $\Delta\lambda\ominus$. The intensities were approximately equal for both scanning directions at 200mμ (6.2eV) but differed by almost a factor of 3 at 400mμ (3.1eV). The slit opening mechanism was adjusted to give 10Å bandwidth at 400mμ in the $\Delta\lambda\ominus$ direction. The bandwidth in the $\Delta\lambda\oplus$ direction was slightly greater than this and the output was therefore larger.

The experiments previously described had established the general shape of the photoconductivity spectra. It was therefore possible to use the scanning technique to investigate the fine structure without emphasis on the absolute magnitude of the photoresponse. It was possible, however, for direct comparisons to be made between the spectra obtained from both methods. This comparison was made for sample AX_8 which was also used to establish the reliability of spectra obtained by the scanning technique.

There was evidence of a double peak in the room temperature $\Delta\lambda\oplus$ spectrum (fig. 3.18). This spectrum did not change appreciably at higher energies on reversing the scanning direction but the 390mμ (3.18eV) peak was not apparent, a single peak at 365mμ (3.40eV) remained. There was some evidence of a double peak from the experiments of Yu (1967) so that it was of some interest to resolve the question of this peak.

A quartz-iodine tungsten filament lamp was therefore used in place of the deuterium lamp since the spectral distribution of intensity of this lamp was smooth (fig. 3.17). The spectra shown in fig. 3.19 resulted after correction for the incident photon flux. The shape of these curves suggests that effects in the region from 3.3-3.7eV were intensity dependent.

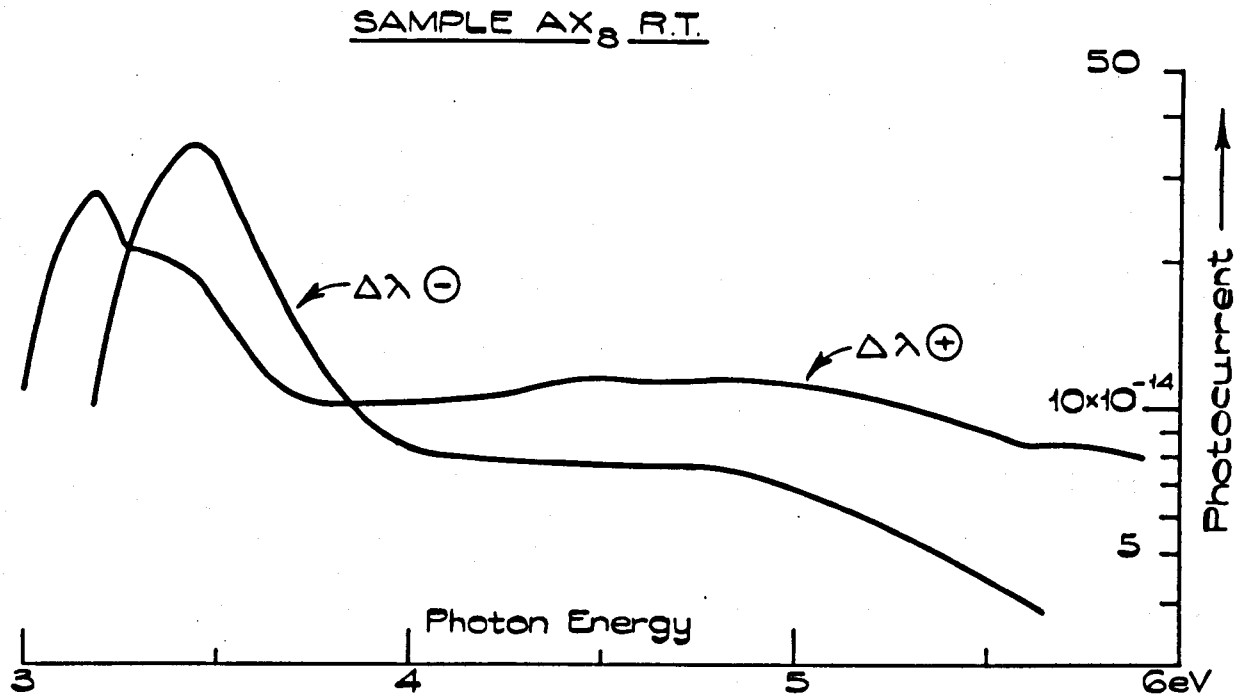

Fig.3.18

R.T. AX8:

TUNGSTEN LAMP

Fig.3.19

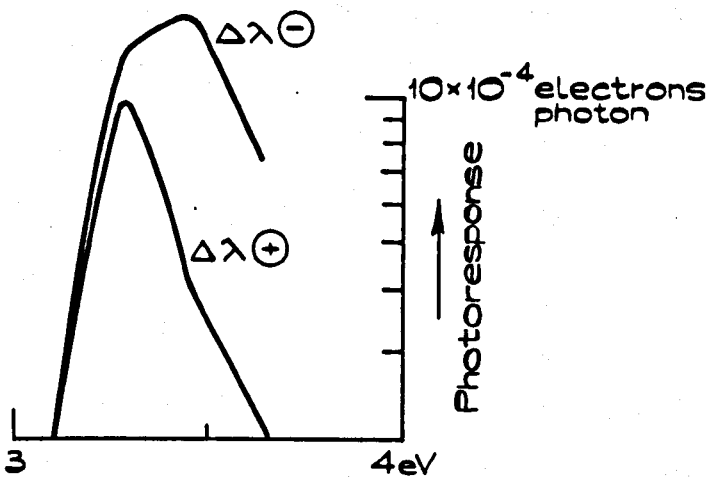

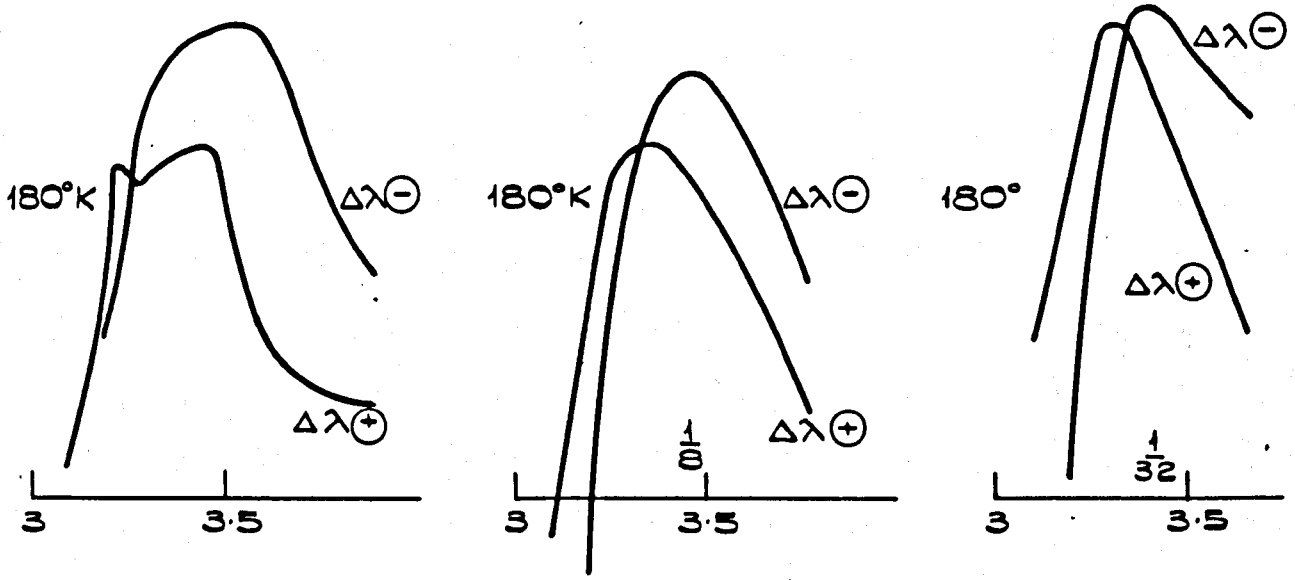

Fig.3.20

The spectrum shown in fig. 3.20 was obtained at I.T.. There is evidence for a peak at 3.22eV and a second at 3.4eV in the $\Delta\lambda\oplus$ direction. The dip at 3.27eV in the $\Delta\lambda\oplus$ curve may have been due to energy dependent polarisations. An attenuated light beam was therefore used to reduce the polarisation effect, the intensity being reduced to $\frac{1}{8}$ of its initial value. Both of the peaks shown are narrower than the original peak. The double peak disappeared in the lower curve and the peak position shifted in the upper. At still lower intensities, i.e. $\frac{1}{32}$ of the initial value, the peak value for both scanning directions tended towards the same value. The approach of the peaks and the finite separation was consistent with the effect of the response time of the system. It became clear that the low intensity measurements at (I.T.) indicated that a single peak existed and that doubling of the peak was caused by increased intensity. It seems likely that a similar explanation is valid at RT but the dark current precluded the use of low intensities. These results will be discussed and related to those of Yu and Fotland in Chapter Four.

Polarisation effects were less troublesome in the high energy region because of reduced photocurrent. Preliminary experiments performed using the point by point method are presented in fig. 3.21, the curve illustrated is the result of four runs. The effect of depolarising between measurements was marked near 360-370mμ where the current increased by 20-100%. Typical scanning spectra are illustrated in fig. 3.22. There is good agreement between the two curves particularly above 4eV.

The resolution and ease of experimentation were both improved by the scanning method but polarisation and other time dependent effects could cause structure which was not a reflection of a change in internal quantum efficiency. This structure could be readily identified by a point by point measurement which would indicate time dependent effects.

The difficulties of interpretation of photoconductivity spectra caused by non-constant quantum flux sources have been described in Chapter One. These difficulties chiefly arise from the non linearity of the intensity dependence of the photocurrent, that is, when $\beta \neq 1$. The value of β is normally energy dependent so that normalisation of spectra to uniform flux necessitates the determination of β throughout the spectrum. It is, however, sufficient for many purposes to investigate

SAMPLE AX_8

180°K Point by Point.

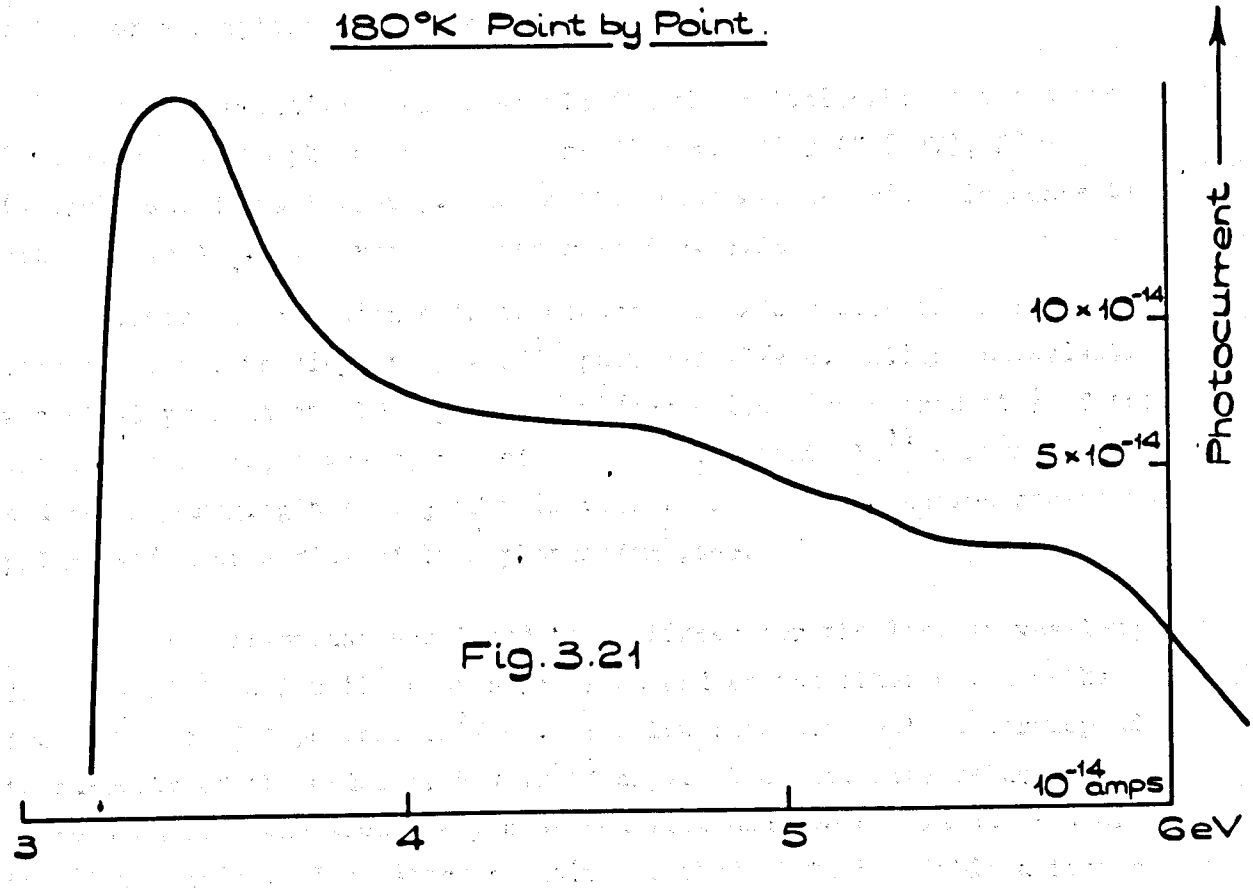

Fig. 3.21

180°K Scanning

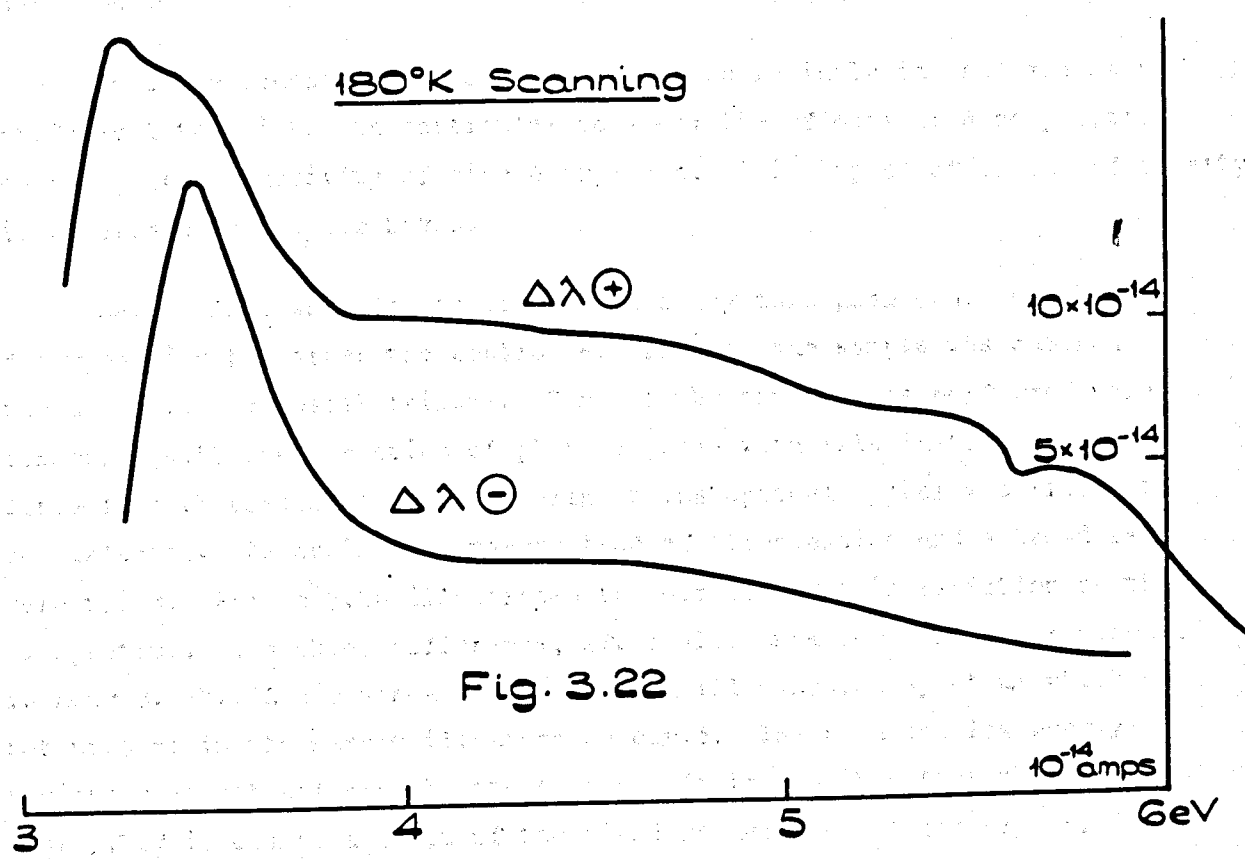

Fig. 3.22

the relationship at several values of energy corresponding to different values of absorption coefficient.

In our investigations on sample AX_8 the relationship between the intensity and the photocurrent was studied at 220mμ (5.64eV), 280mμ (4.43eV) and 370mμ (3.35eV). The method used was described in connection with sample AX_4. The results appear in fig. 3.23.

Strong polarisation effects occurred at 270mμ with the normal illumination intensity of 5×10^{10} photons/cm^2/sec. Slight polarisation was still present at 10^{10} photons/cm^2/sec which disappeared at $\frac{1}{2}$ of this value. At 280mμ, however, the effect was slight at 10^{11} photons/cm^2/sec and became negligible at $\frac{1}{4}$ of this value. 220mμ illumination caused no polarisation at a flux of 10^{10} photons/cm^2/sec.

The photoresponse was found to be linear for the longest wavelength from 5×10^{10} to 2×10^{8} photons/cm^2/sec and at the other wavelengths from 10^{11} to 10^{10} photons/cm^2/sec. The low intensity values correspond to currents of the order of 5×10^{-15} amps. The intensity values were calculated from the accurately measured flux and the estimated area of the illumination. The latter quantity is thought to be within a factor of 2 of the correct value and did not appear to be appreciably wavelength dependent.

Once the scanning method was shown to be reliable it was used as an analytical technique, in particular to study the effects of decomposition on the photoconductivity of single crystals. This aspect of photoconductivity is described in Chapter Seven.

Sample AX_{10} was also to be used to study this phenomenon of photo-decomposition but after the control experiments the sample was damaged through a vacuum vessel failure. Some of the experiments performed were concerned with the variation of photoresponse with illumination position since in a photodecomposition experiment the optical system was likely to be disturbed. Accordingly a narrow band of illumination and a broad band were tried. Figure 3.24 illustrates the effects of this variation on the RT spectrum. The chief difference, after allowance for random variations, is near 3.5eV. A dip appears in the broad illumination spectrum which was not present in the narrow illumination curve. The high and low energy regions were not affected by the change. It is possible that the change near 3.5eV is due to a facet of the field geometry or of the crystal surface sensitivity.

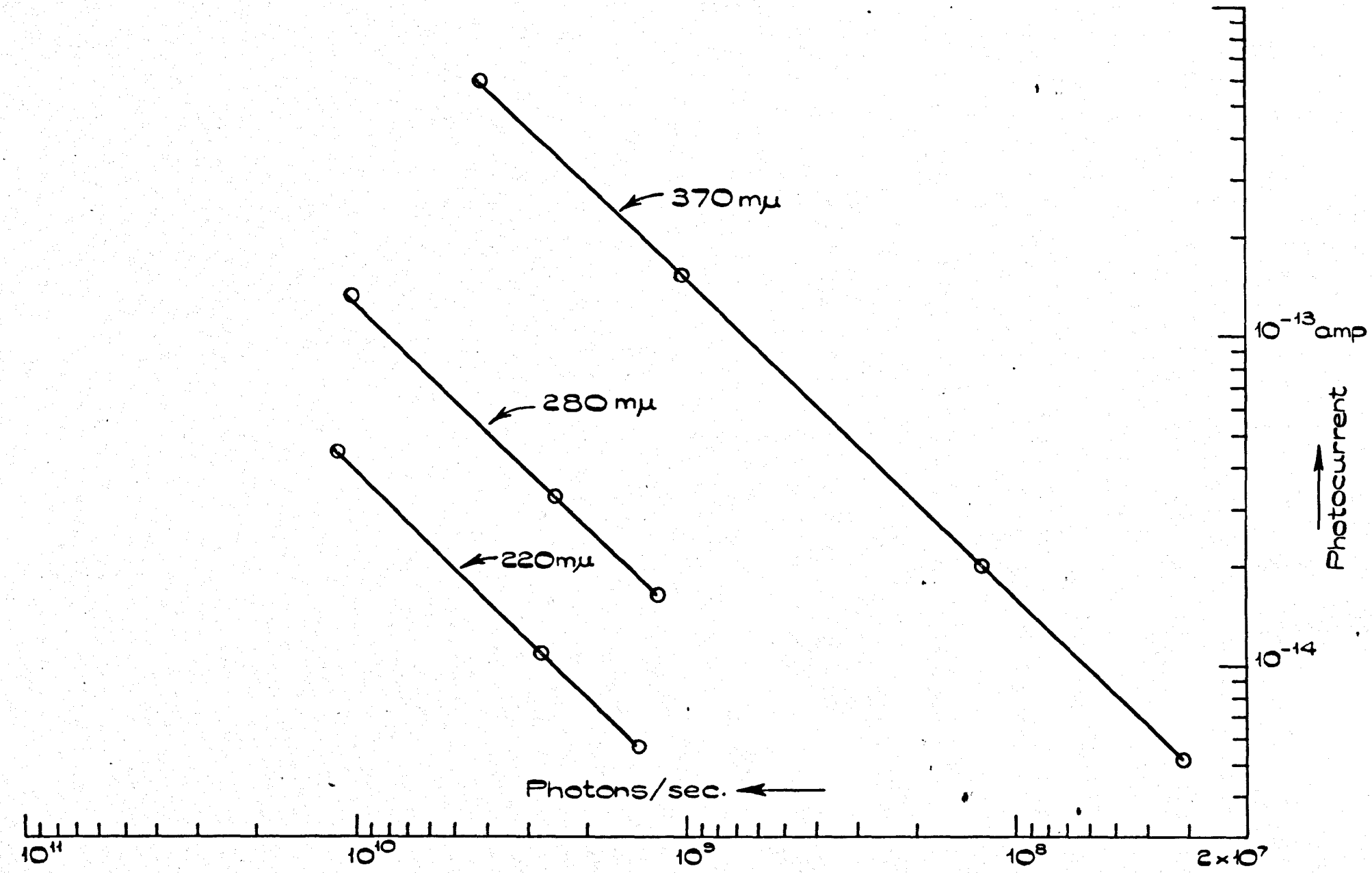
370 mμ
280 mμ
220mμ
10^{-13} amp
10^{-14}
Photocurrent
Photons/sec.
10^{11}
10^{10}
10^{9}
10^{8}
2×10^{7}

Fig.3.23

VARIATION OF PHOTORESPONSE WITH ILLUMINATION POSITION.

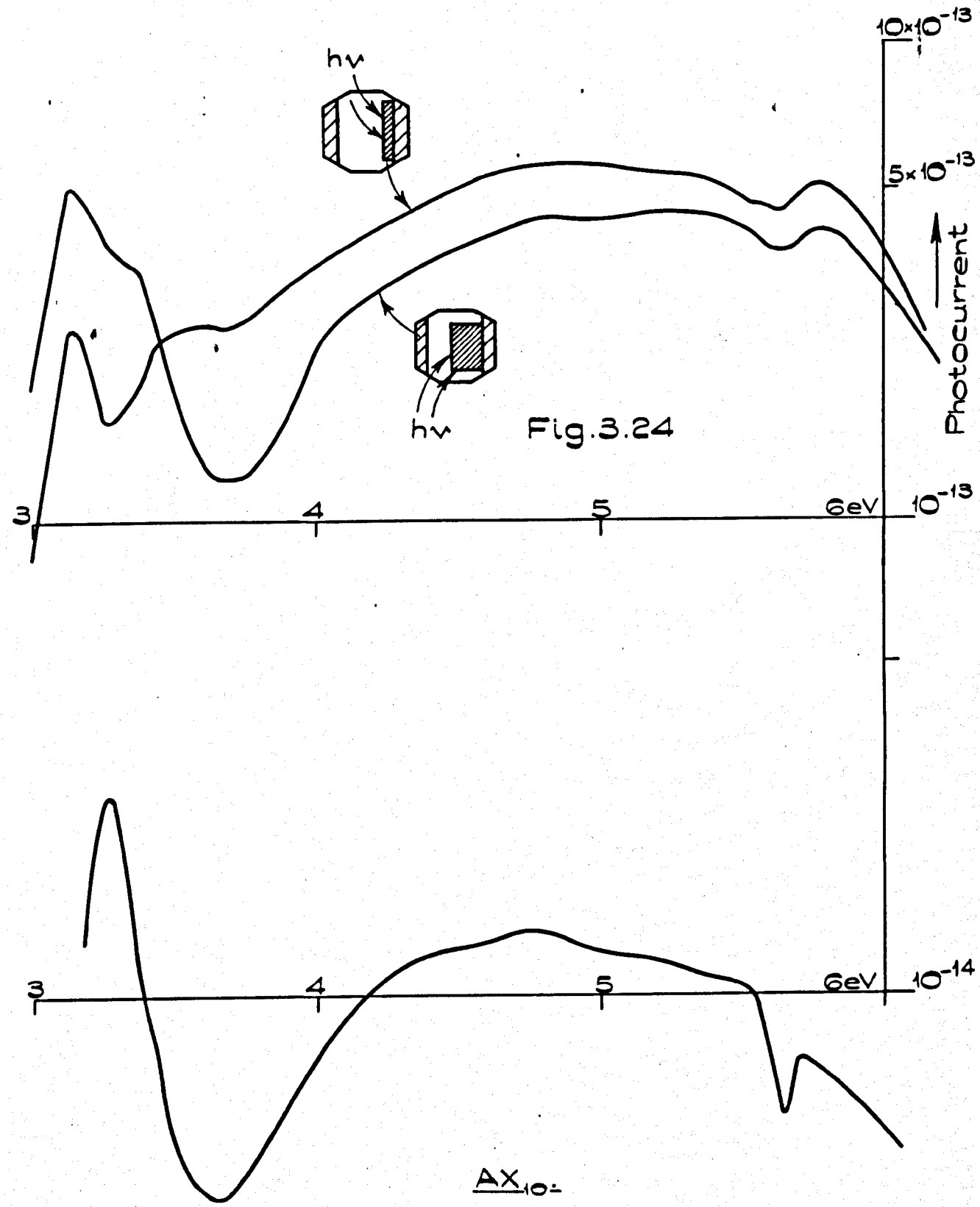

Fig.3.24

Fig. 3.25

At I.T. the illumination was as in the broad band position in all cases. In these spectra the photocurrent peak tended to be split into two, as in sample AX_8. There was strong indication of a dip near 220mμ in all spectra. The spectrum was not changed by a significant amount when the scanning direction was reversed (fig. 3.25).

3.7 Photoconductivity in Uncleaved Crystals

The results described above indicated the general features of photoconductivity spectra in CdI_2 single crystals. Structure near 220mμ was also apparent. Strong polarisation effects were found in the majority of crystals. All of these results were obtained with cleaved solution-grown crystals. Some investigations conducted by Yu had, however, been on uncleaved solution grown crystals. Crystal AX_9 was therefore used to investigate the polarisation and photoresponse of as-grown crystals at room and liquid nitrogen temperatures.

Initially the front surface electrodes were tested to ensure that the contacts were ohmic. The ionic current is plotted against applied field in figure 3.26. The relationship was linear at low fields but in some cases fluctuations occured at higher fields.

The normal procedure in measurements of ionic conductivity is to apply the potential and to then wait until the current reaches a fairly steady value. The time required for this in our investigations was usually some 15 minutes. For sample AX_9 this decay was present for the low applied fields but not for the higher fields in all cases. The current at high fields decayed from the initial value but after some 10 minutes became unsteady so that in some cases it actually increased.

The photoconductivity of the uncleaved crystals was characterised by a longer time constant than that of the other samples. The RT photocurrent took ~3 minutes to saturate. There was no evidence of polarisation since the current did not decay with prolonged illumination and represented readings at the same wavelength gave the same current value. The room temperature response curve recorded using the point by point method is illustrated in fig. 3.27. There is a peak at 370mμ (3.35eV) with a maximum current of 1.8×10^{-12} amps.

SAMPLE AX_9:-

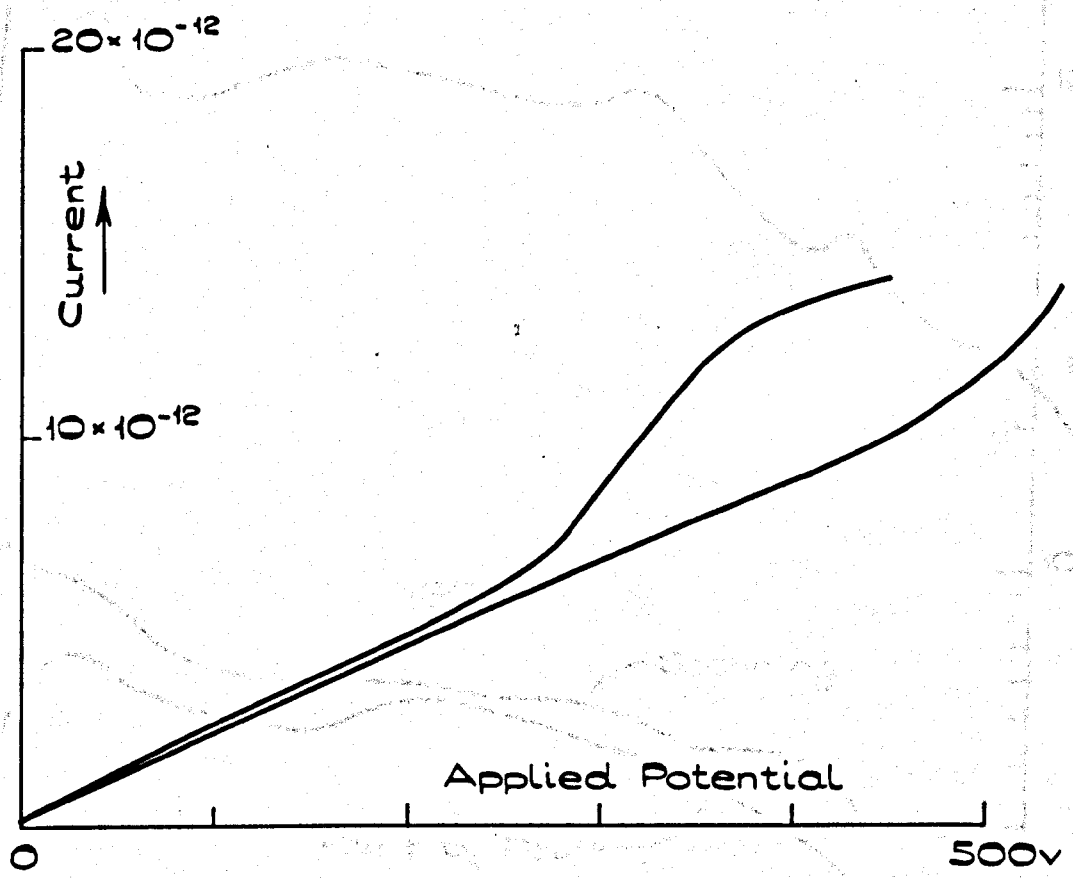

Fig. 3.26

SAMPLE AX_9 (83μ thick)

R.T. Point to Point.

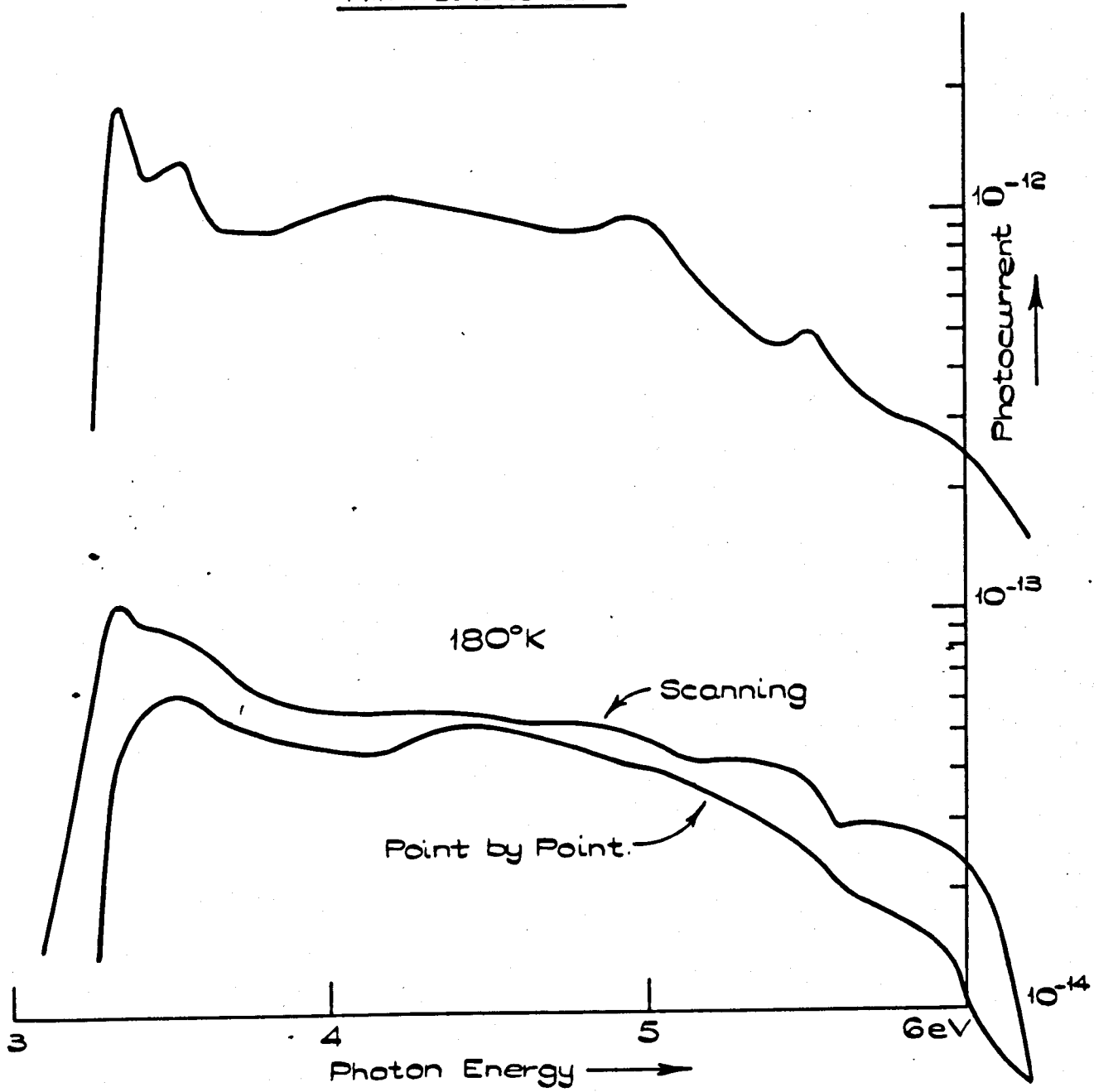

Fig. 3.27

At I.T. the corresponding peak was near 360mμ (3.44eV) with a maximum current of 6×10^{-14} amps. The shape of the scanning curve is of interest because of the good agreement with the point by point spectrum. The scanning method became possible because of the shorter response time of the photocurrent at I.T. The $\Delta\lambda\Phi$ curve peaked at ~372mμ indicating that the time constant was important in the low energy region.

The long time constant and the apparent lack of sensitivity at high energies compared with that at low energies as determined by the preliminary experiments led us to use cleaved crystals in future. Furthermore, published reflectivity spectra had all been taken with cleaved single crystal samples.

3.8 Preliminary Experiments with the Electric Field Perpendicular to the Cleavage Plane

The initial measurements of 'c axis' photoconductivity were relatively fruitless. The first sample was used with quartz plates between the crystal and the nickel sheet electrodes. The plates of quartz insulated the crystal so that the electrodes were 'blocking'. This sample suffered from rapid polarisation effects and no reliable results were obtained. Sample CX_2 with nickel sheet electrodes in contact with the crystal and CX_3, with evaporated gold electrodes, were both largely unsuccessful. The former sample suffered from spurious electrical noise and the latter from overwhelming dark currents.

Sample CX_4 was therefore the first sample of this type to produce reasonable results. The monochromator slit width was fixed for the scanning spectra since the slit drive mechanism was not available at this time.

The spectrum shown in fig. 3.28 was determined using 1mm slit width. There is a broad peak at 260mμ (4.77eV) followed by a sharper peak at 330mμ (3.76eV) and a low energy peak at 365mμ (3.4eV). The spectrum was then determined using the constant bandwidth, point by point, method. The currents near 4eV are then much larger than similar 'a axis' results. The double low energy peak is an intensity effect and is probably analagous to that illustrated in fig. 3.7 for sample AX_3. The field used in the 'c axis' samples was much greater than that used in the 'a axis' configuration because of the smaller electrode separation. The field for sample CX_4 which was 175μ thick was 2.6×10^4V/cm.

C_4X. 175 μ thick.

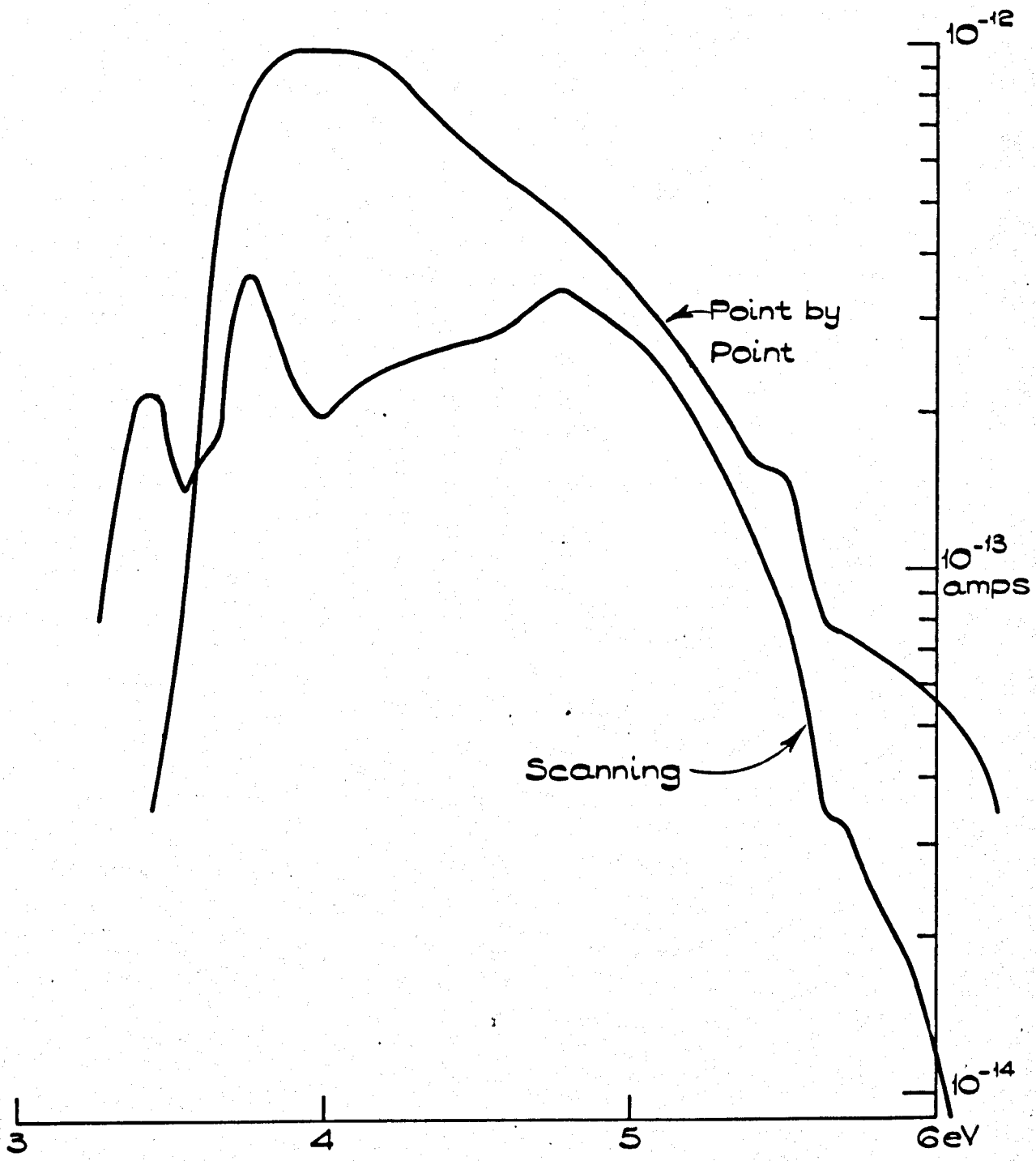

Fig. 3.28

After the initial experiments described above the point by point method was used with crystal CX_5 which had evaporated gold electrodes. Some results obtained with this sample are illustrated in fig. 3.29. Comparison may be made between measurements obtained using the depolarisation procedure and with field reversal without depolarisation. It was not possible to depolarise between field reversals because of the increased duration of the experiment.

The preliminary experiments described above indicated an entirely different low energy spectrum to that obtained at I.T. using the a axis geometry. The blocking electrode configuration was therefore repeated in an attempt to remove suspicions of polarisation effects.

3.9 The Blocking Electrode Geometry

Previous unsuccessful attempts had been made to use this geometry. In the experiments on CX_6 a thicker crystal some 845μ thick was used with a small amount of success. The currents obtained were very small, however, the peak current at RT was 10^{-14} amps. This maximum was near 390mμ (3.18eV) the width of the peak was ~20mμ at half maximum. The dark current was ~3 x 10^{-14} amps which decayed because of ionic polarisation. At I.T. the peak shifted to 368mμ with a maximum current of 4 x 10^{-14} amps. The current fell to 7 x 10^{-15} amps at 360mμ and 375mμ. There was no evidence of photocurrent polarisation at these current levels.

After these experiments gold electrodes were evaporated onto the crystal surfaces. These electrodes were found to be ohmic, see fig. 3.30. The effective sample resistance was 1.4 x $10^{14}\Omega$ which corresponded to a 'c axis' resistivity at RT of ~2 x $10^{15}\Omega$cm.

The RT non-blocking spectrum shown in fig. 3.31 is in good agreement with the blocking electrode results as far as peak position and shape is concerned. The overall current was 50 times greater in the non-blocking experiment indicating that the sample was polarised by the ionic current in the blocking experiments

The I.T. results indicate that the peak was at a lower energy in the non-blocking experiment. The experimental arrangements were very similar so that it is difficult to explain this result. The blocking

SAMPLE CX_5 (475μ thick)

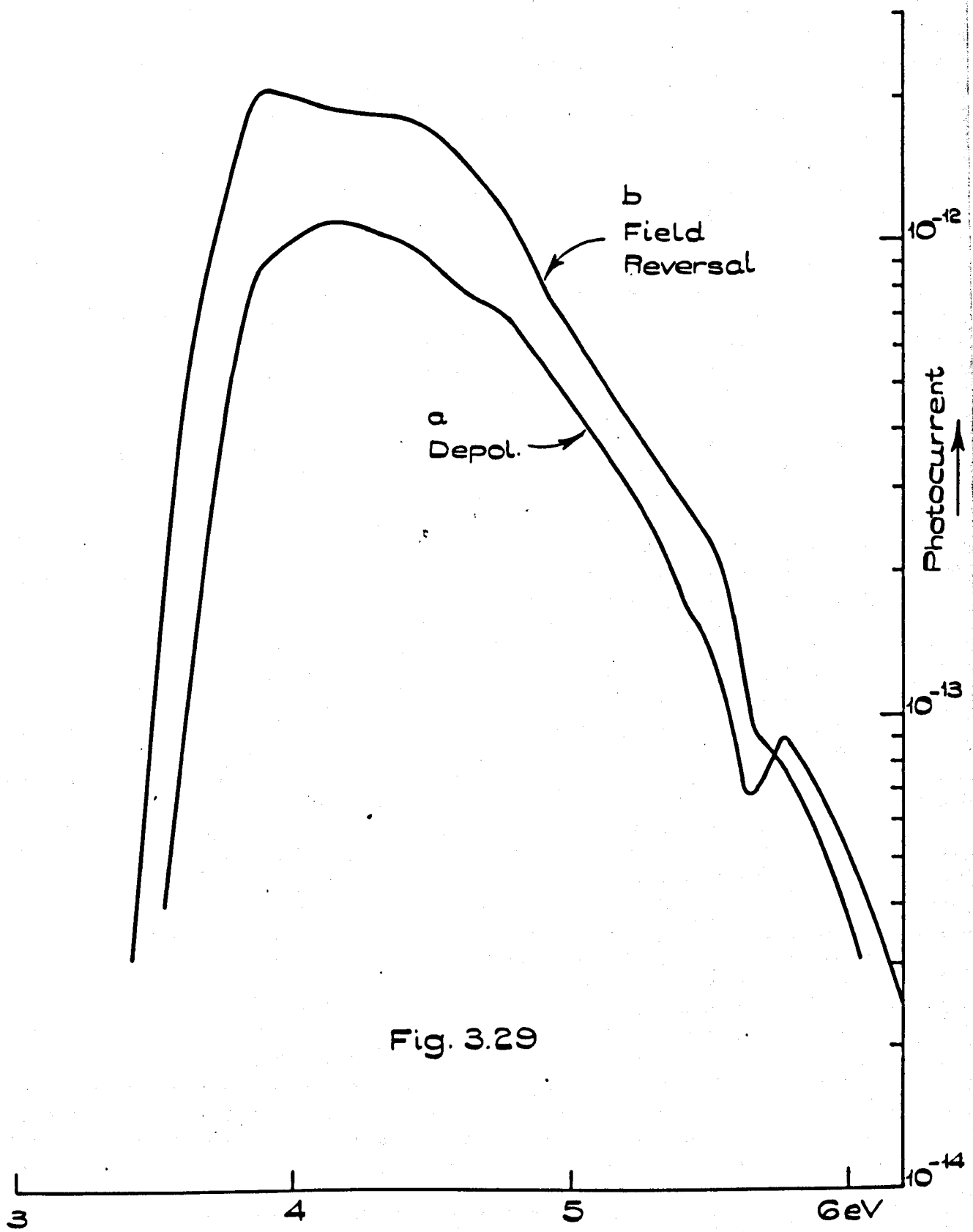

Fig. 3.29

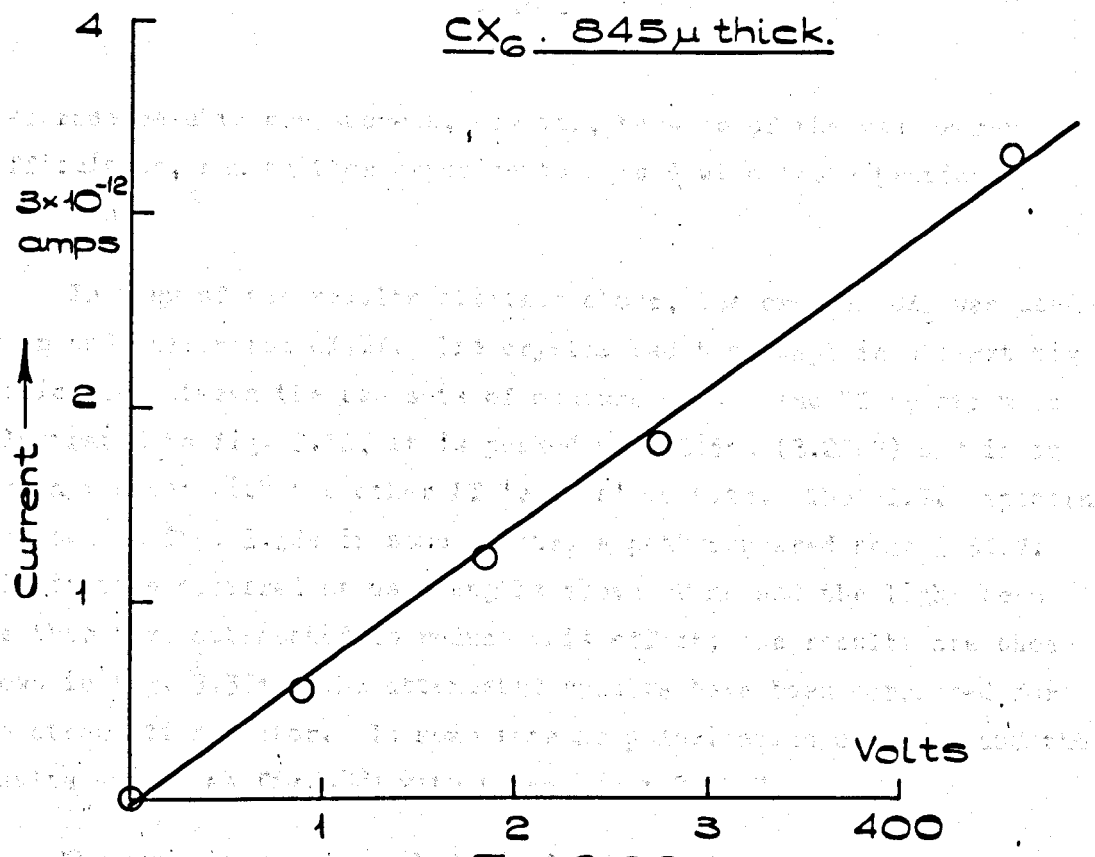

Fig. 3.30

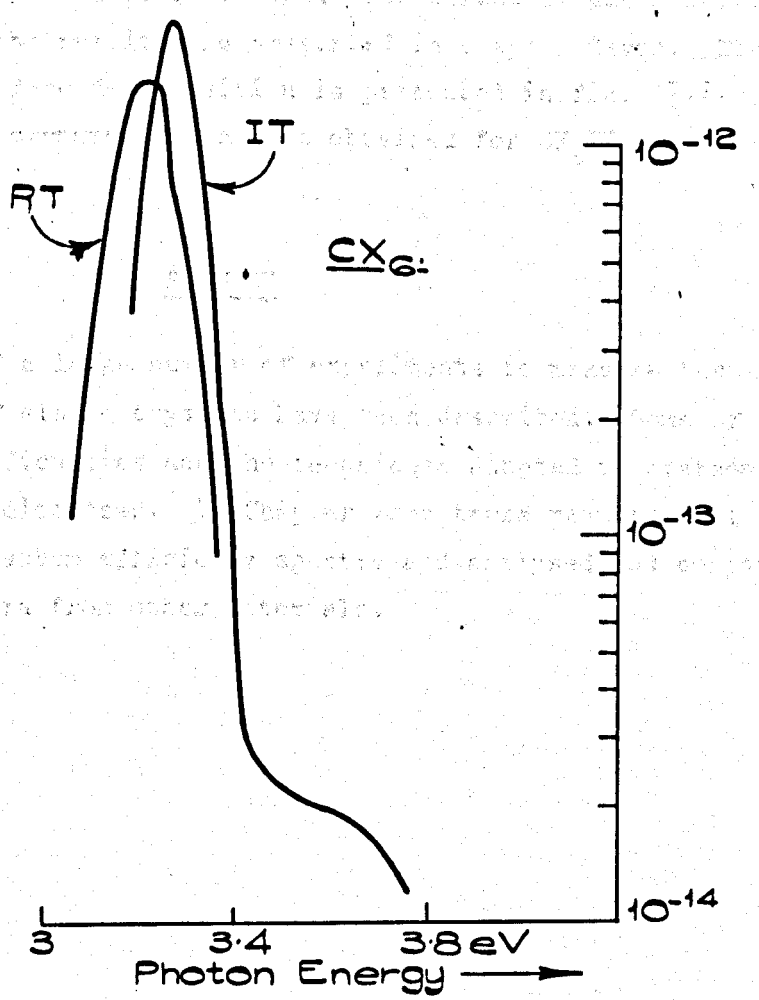

Fig. 3.31

electrode results are suspect, however, because of the measurement difficulties, and neither experiments agreed with those previously carried out.

In view of the results obtained above, the crystal CX_5 was used again and designated CX_5II. The crystal had been kept in a light tight dessicator between the two sets of measurements. The RT spectrum is illustrated in fig. 3.32, it is peaked near 385mμ (3.22eV) and is in good agreement with the other RT 'c axis' results. The I.T. spectrum is shown in fig. 3.32a in some spectra a peak appeared near 3.35eV. Polarisation occurred at wavelengths above 220mμ and the light beam was therefore attenuated to reduce this effect; the results are those shown in fig. 3.32a. The attenuated results have been corrected for the attenuation factor. In some runs no polarisation occurred and the results appear as fig.3.32b with a peak near 3.35eV.

The experiments described for CX_5II were repeated using sample CX_7. This sample was used to investigate the effect of decomposition on photoconductivity, the results are presented in Chapter Seven. The spectrum obtained before decomposition is presented in fig. 7.7. The spectrum is in good agreement with that obtained for CX_5II.

SUMMARY

The results of a large number of experiments to measure the photoconductivity of single crystals have been described. Some of the experimental difficulties and the techniques adopted to overcome them have also been discussed. In Chapter Four these results will be converted into quantum efficiency spectra and analysed and compared with published spectra from other materials.

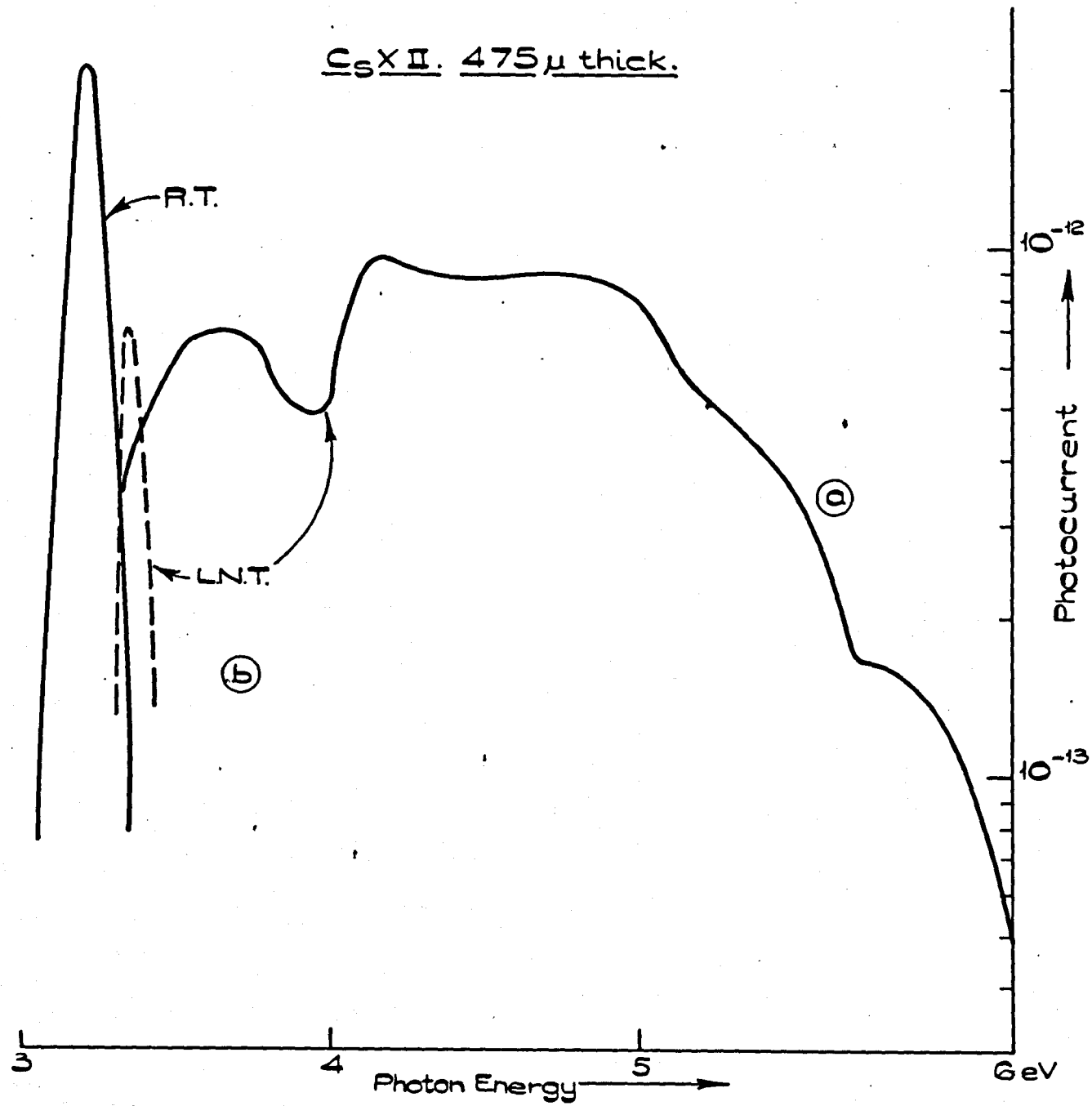
CsXII. 475μ thick.
R.T.
L.N.T.
a
b
10^{-12}
10^{-13}
Photocurrent
3
4
5
6 eV
Photon Energy

Fig. 3.32

REFERENCES

Fotland, R.A., 1959, Thesis, Case Inst. of Technology

Yu, R.M., 1967, Thesis, University of Bristol.

CHAPTER FOUR

THE INTERPRETATION OF ROOM TEMPERATURE AND 180°K PHOTOCONDUCTIVITY SPECTRA

4.1 Introduction

The results obtained from a large number of photoconductivity and associated experiments were presented in Chapter Three. Many of these experiments were intended to establish a reliable technique for the determination of structure in curves of photoconductivity.

The photoconductivity spectra were recorded using measured spectral distributions of intensity, a simple correction could be made, however, since the photocurrent was proportional to the intensity. The spectra to be described will therefore be corrected for the incident illumination intensity and presented in terms of photoelectrons detected per incident photon.

In the experimental arrangement used the photocell and sample received the same illumination so that the currents measured would be proportional to the quantum efficiency of the detector. The quantum efficiency is this context is the number of electrons measured per incident quantum and is equal to

$$\eta(\nu) = \frac{ip^{(\nu)}}{i_{p\ cell}^{(\nu)}}$$

where ip and ip_{cell} are the sample and photocell currents for a given illumination flux and $\eta_{p\ cell}$ is the photocell quantum efficiency.

The majority of the spectra described below show the spectral variation of η_{CdI_2}; the subscript will be omitted in the text. These will be compared, where possible, with published results. Since published results were confined to high temperatures (at or above RT) and to low energies (below 3.4eV) this comparison will be limited.

4.2 Room Temperature Photoconductivity Spectra 'a axis' Geometry

The quantum efficiency spectra corrected for intensity obtained at RT with six 'a axis' samples are illustrated in figures 4.1-4.6. These have been corrected assuming a linear intensity dependence. In the first

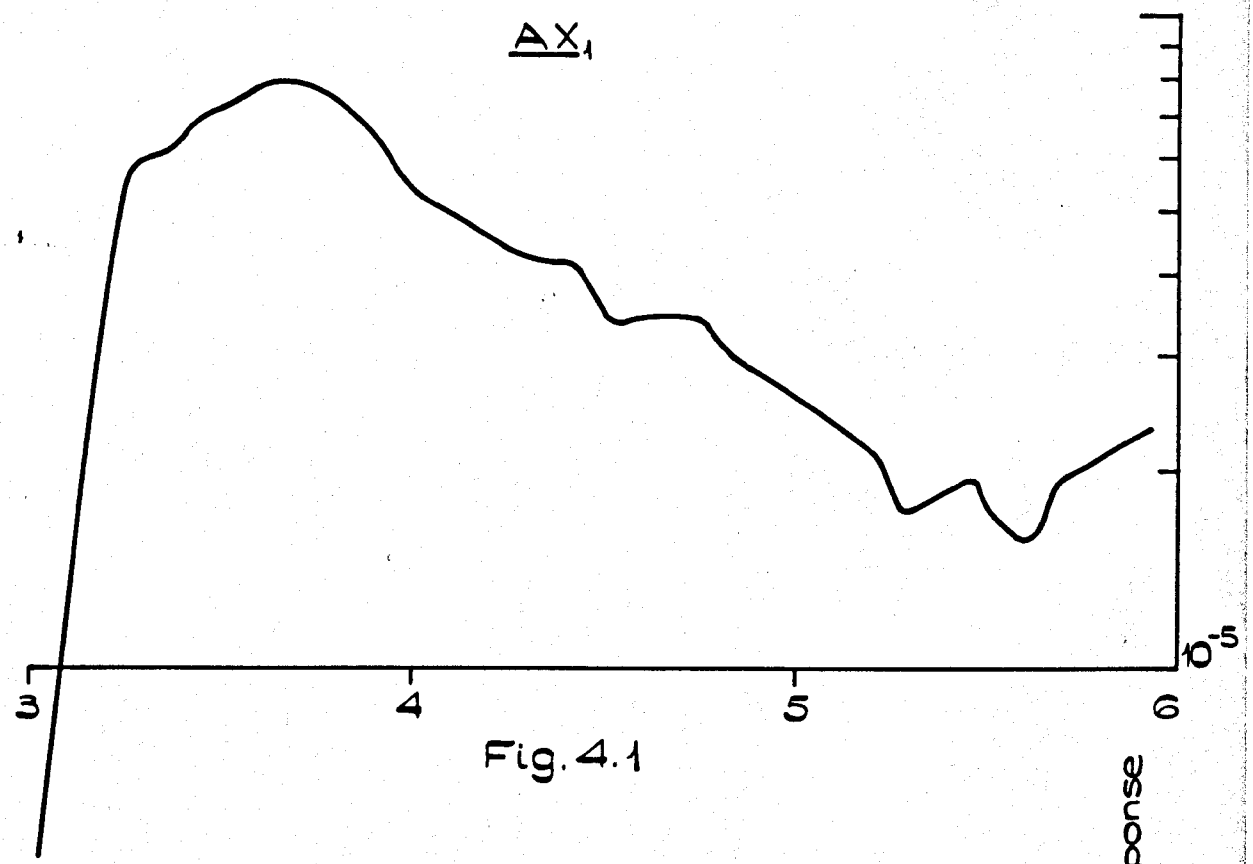

Fig. 4.1

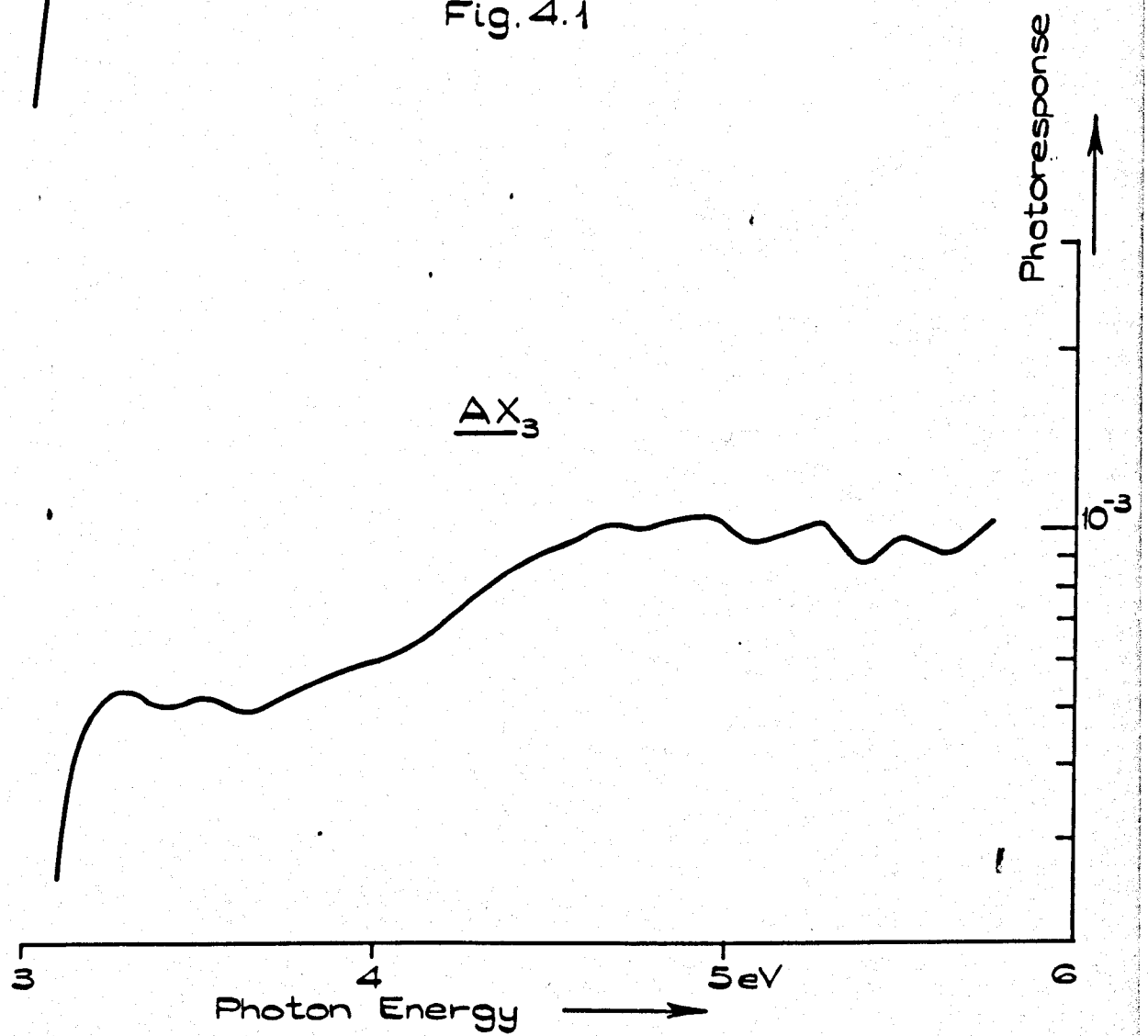

Fig. 4.2

AX 7: R.T.
(75 μ thick)

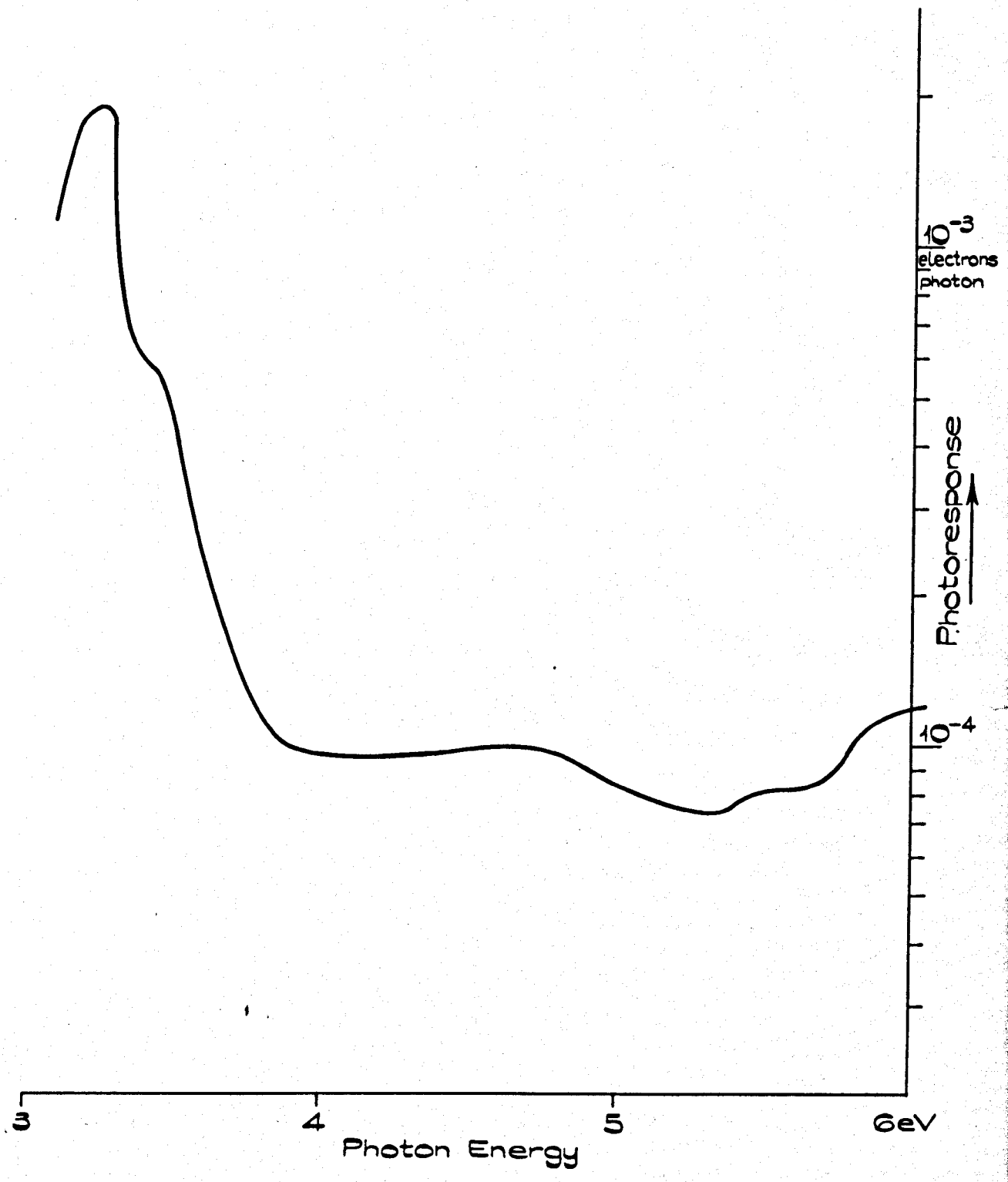

Fig.4.3

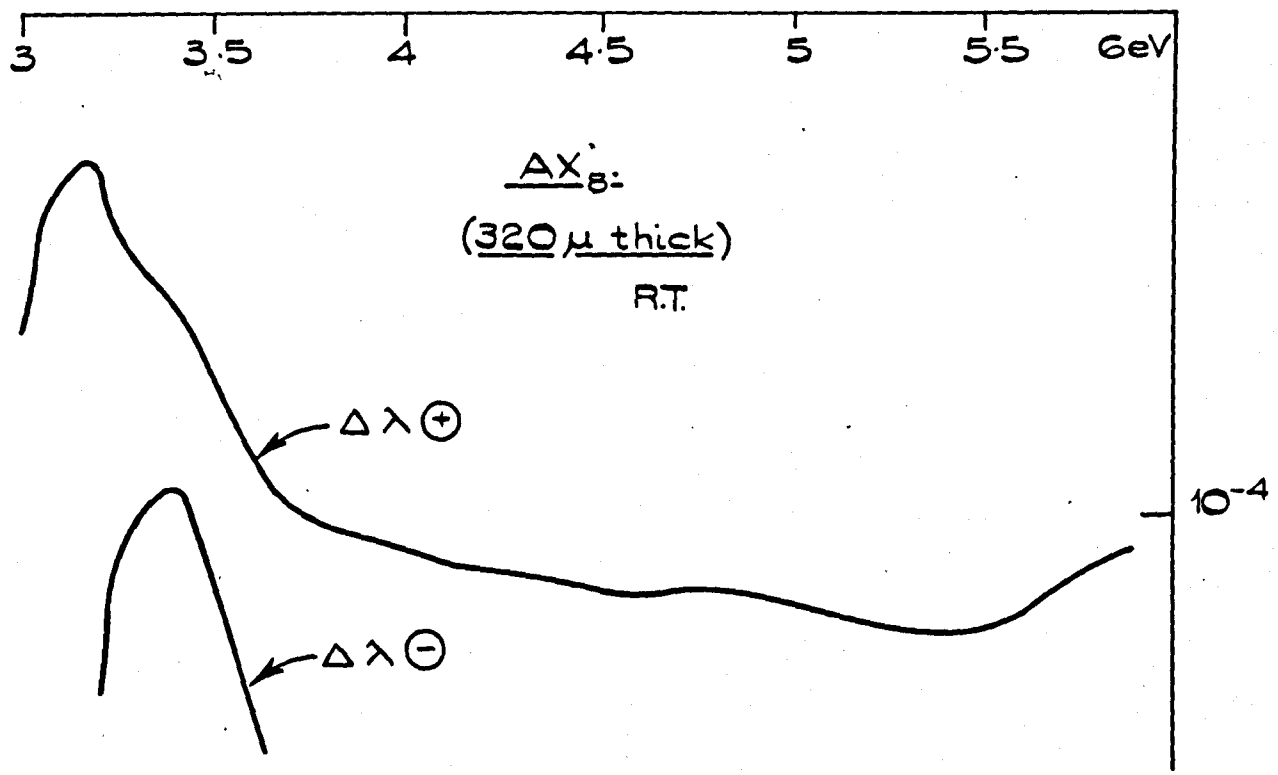
3
3.5
4
4.5
5
5.5
6eV
ΔX8:-
(320 μ thick)
R.T.
Δλ⊕
Δλ⊖
10-4

Fig. 4.4

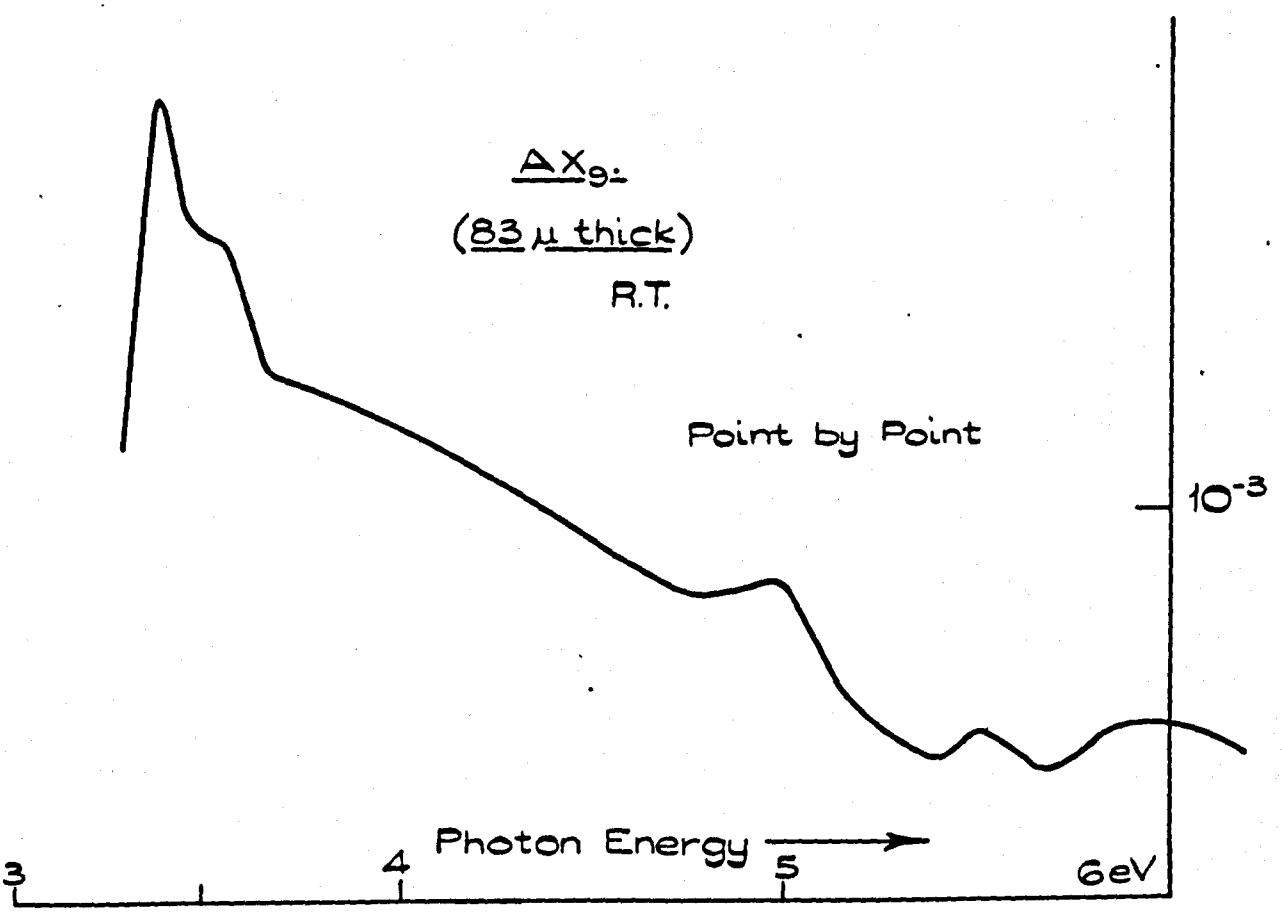
ΔX9:-
(83 μ thick)
R.T.
Point by Point
10-3
Photon Energy
3
4
5
6eV

Fig. 4.5

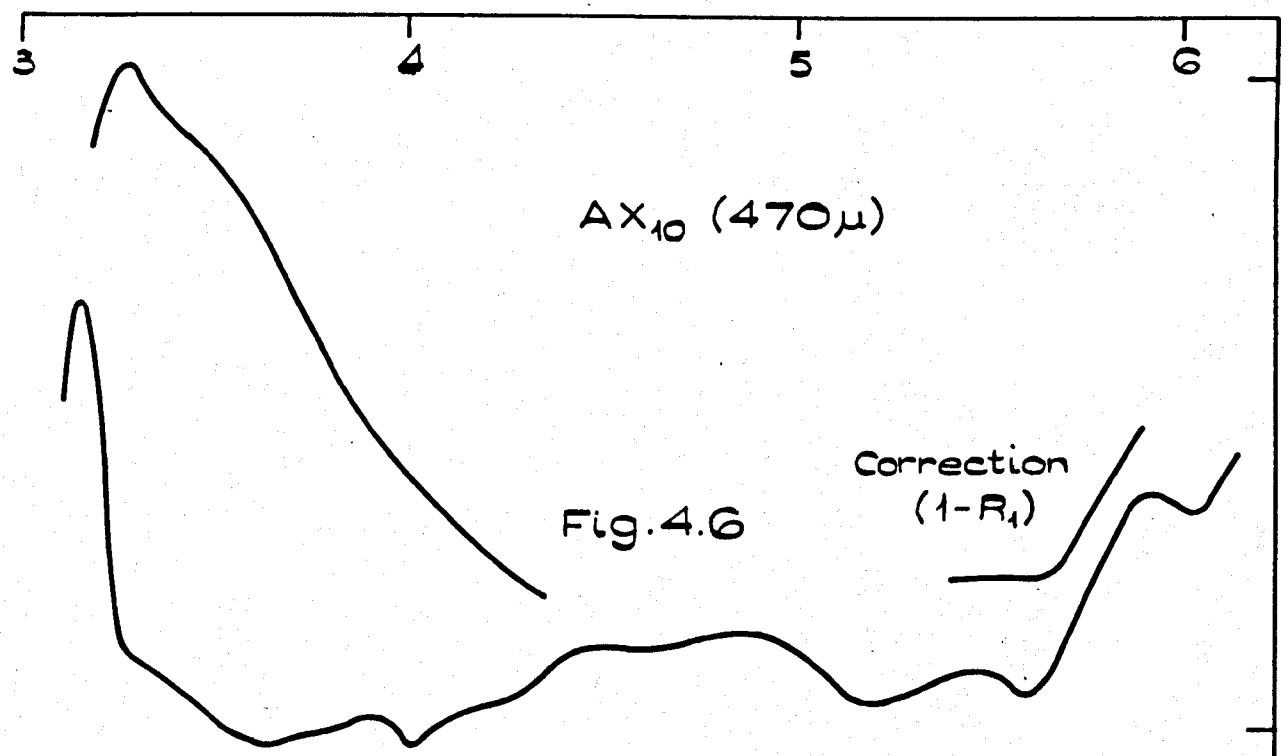

Fig. 4.6

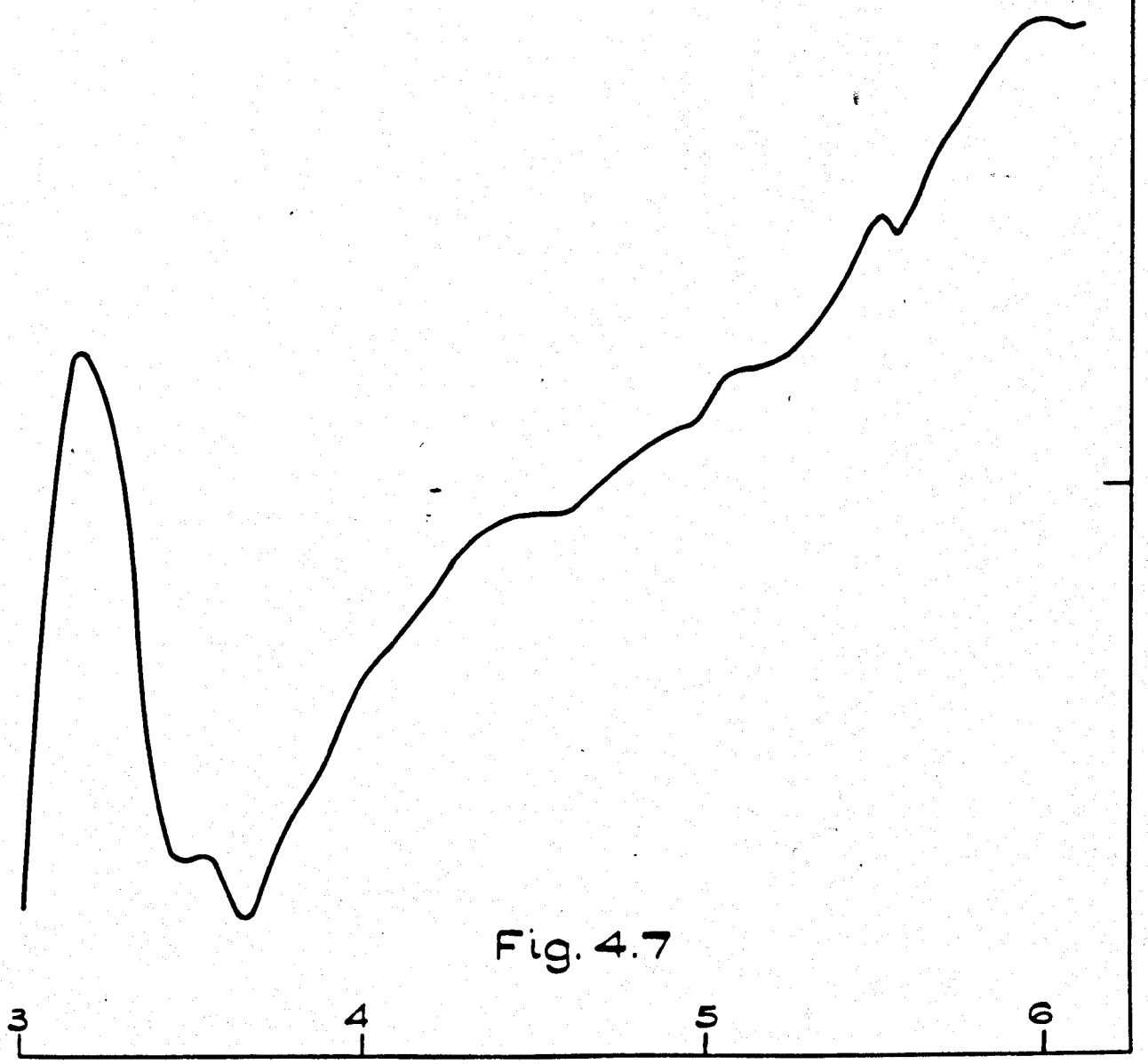

Fig. 4.7

two spectra the illumination was high and strongly energy dependent (see fig. 3.1) so that this approximation may not have been valid. The spectra shown in figures 4.3-4.6 were recorded using the constant bandwidth technique, the experimental details of which were described in Chapter Three.

In the constant slitwidth technique used on the samples AX_1 and AX_2 the intensities at 3.18eV with 2mm and 1mm slit openings were 4.5×10^{12} photons/cm^2/sec and 10^{12} photons/cm^2/sec respectively. The later samples were used with fluxes of $<5 \times 10^{10}$ photons/cm^2/sec, the photocurrent being proportional to the intensity at these intensities, (see fig. 3.23).

As well as the preliminary and constant bandwidth samples described above a sample $HCAX_2$ was used at RT in the liquid helium cryostat. This sample was accidentally destroyed because of a vacuum leak at low temperature. The thickness could therefore not be measured but was of the order of 500μ; it exhibited a low energy photoconductivity peak at 3.19eV at RT, see fig. 4.7.

4.3 Comparison with Previously Published Spectra

It is possible, in the low energy region, to make comparisons with spectra published by Fotland (1959) and more recently by Yu (1967).

Fotland reported photoconductivity in crystals of CdI_2 grown by the Bridgmann technique. These crystals were of high impurity and defect content; the total content of metallic impurities was of the order of 150p.p.m. Some solution-grown crystals, prepared from reagent grade starting material, were also used, but it is difficult to make an estimate of their purity since purification would have taken place during crystallization.

The photon flux of 2×10^{13} photons/cm^2/sec used in Fotlands investigations was much higher than those used in our experiments. The photocurrents were also larger and varied between 10^{-11} and 1.5×10^{-8} amps. Smaller currents could not be measured because of the lack of sensitivity of the electrometer used.

Yu (1967) has studied the photoconductivity of high quality solution-grown crystals in the same energy region as Fotland, i.e. 2.9-3.4eV. Two samples were used, one of 400μ and the other of 954μ thickness. They were not cleaved and silver drag electrodes in conjunction with flat spring clip mechanical contacts were used.

The low energy photoconductivity peak occurred at 3.21eV for the 400μ crystal and at 3.12eV for the 954μ crystal. There was also some indication of a feature near 3.35eV. The photon fluxes used were similar to those used by Fotland and were 5×10^{12} and 2.8×10^{13} photons/cm^2/sec. The entire area between the electrodes was illuminated in these experiments.

The important low energy peaks obtained from our experiments and those of Fotland and of Yu appear in the table below.

TABLE 4.1

Sample Number	Thickness μm	Low Energy Peak Position	Quantum Efficiency at Peak	Field Strength v/cm
AX_1	60	3.3eV	6×10^{-5}	730
AX_7	75	3.23eV	2×10^{-3}	730
AX_3	80	3.18eV	10^{-4}	140
AX_9	83	3.36eV	7.2×10^{-3}	730
AX_8	320	3.18	5×10^{-4}	730
Yu	400	3.21	4×10^{-5}	286
AX_{10}	470	3.15	4.6×10^{-4}	730
$HCAX_2$	~500	3.19	2×10^{-4}	730
Fotland	~900	3.16	$\sim 10^{-2}$	1000
Yu	954	3.12		

The quantum efficiencies shown in the table are those recorded at the low energy peak and correspond with the number of electrons measured per incident photon. This quantity was found to vary linearly with applied field. The internal field was probably not uniform (see Fotland) and although this field was proportional to the external field it is unlikely that the two were equal at all points. In particular there was a sensitive region near the electrodes; the increased field in this region was probably due to space charge effects.

In the present measurements the field strength was usually of the order of 700v/cm. The electrode separation was chosen to be large compared with the size of the image on the crystal. The upper limit was fixed by the lateral dimensions of available crystal. In this way the separation of 0.63cm was chosen. The illumination was usually confined to a region near to the electrometer 'High' electrode. This area was a region of high sensitivity and illumination near an electrode simplified tests for photoemission.

In view of the marked differences in experimental techniques and sample type, the peak quantum efficiency found by Yu of 4×10^{-5} electrons per photon for a 400μ crystal is in good agreement with our results. Yu investigated the photocurrent versus light intensity curves down to photon fluxes of 4×10^{11} quanta/cm^2/sec; this was somewhat higher than those used in the majority of our experiments. The photocurrent was not proportional to the intensity for the intensities and energies used; the relationship depended upon both quantities (Yu 1969). No attempt was made to repeat these measurements. An intensity dependence experiment was, however, performed at 180°K and the photocurrent was found to be proportional to the intensity at the low light levels used. We have assumed for the purpose of comparison that the RT relationship was also linear. Low intensity RT measurements were difficult because of the dark current.

Since Yu's experiments were performed on uncleaved crystals, direct comparison with the present results is impossible as the only uncleaved crystal was much thinner than those used by Yu. It is therefore necessary to make comparison between two different sample types.

Ionic Polarization was always present in our RT experiments. Similar effects have been observed in NaCℓ by Sutter and Norwick (1963). These authors concluded that the polarisation was not due to the build up of space charge near the electrodes, but was a result of a dielectric relaxation process. Our experiments on CdI_2 indicate that an enhanced field exists near the electrodes which was probably caused by a space charge effect. It is likely, therefore, that in CdI_2 at RT both processes occur. The time constant of the polarisation in CdI_2 was found to be reduced at high temperatures and in fact, polarisation could not be observed, (see Chapter Seven).

4.4 Room Temperature Photoconductivity Spectra 'c axis' Geometry

The room temperature results with the 'c axis' geometry were severely hampered by polarisation effects. This prevented measurements of photoconductivity in many cases. The application of an external field at RT led to a dark current which rose to a maximum value in less than 1 second and then began to decay. The decay followed a typical exponential polarisation curve. Thorough investigations of this phenomenon would necessitate measurements over many decades of current and time. The temperature must be highly stabilised since the ionic current depends exponentially on the absolute temperature.

The increased polarisation in the 'c axis' case was caused by either the increased field strength or the different field geometry. Several sets of results were obtained however, and these are illustrated in the table below and in fig. 4.8.

TABLE 4.2

Sample Number	Thickness μm	Low Energy Peak Position	Quantum Efficiency at Peak	Field Strength v/cm
CX_7	195	3.24eV	2.7×10^{-2}	23,000
CX_5II	475	3.22eV	1.12×10^{-2}	9,500
CX_6	845	3.20eV	0.78×10^{-2}	5,300

The quantum efficiencies increased with decreasing thickness, indicating that the photocurrent was approximately proportional to the field strength when the crystal thickness was altered, rather than the applied potential. The applied potential used to give the above fields was 450V.

The only previous measurements using the c axis geometry were those of Fotland, who found a room temperature peak at an energy of 3.23eV. The current at the peak was some 2×10^{-9} amps at a field strength of 17,000V/cm. The crystal thickness was probably 500μ and the quantum efficiency 5×10^{-3} electrons/photon.

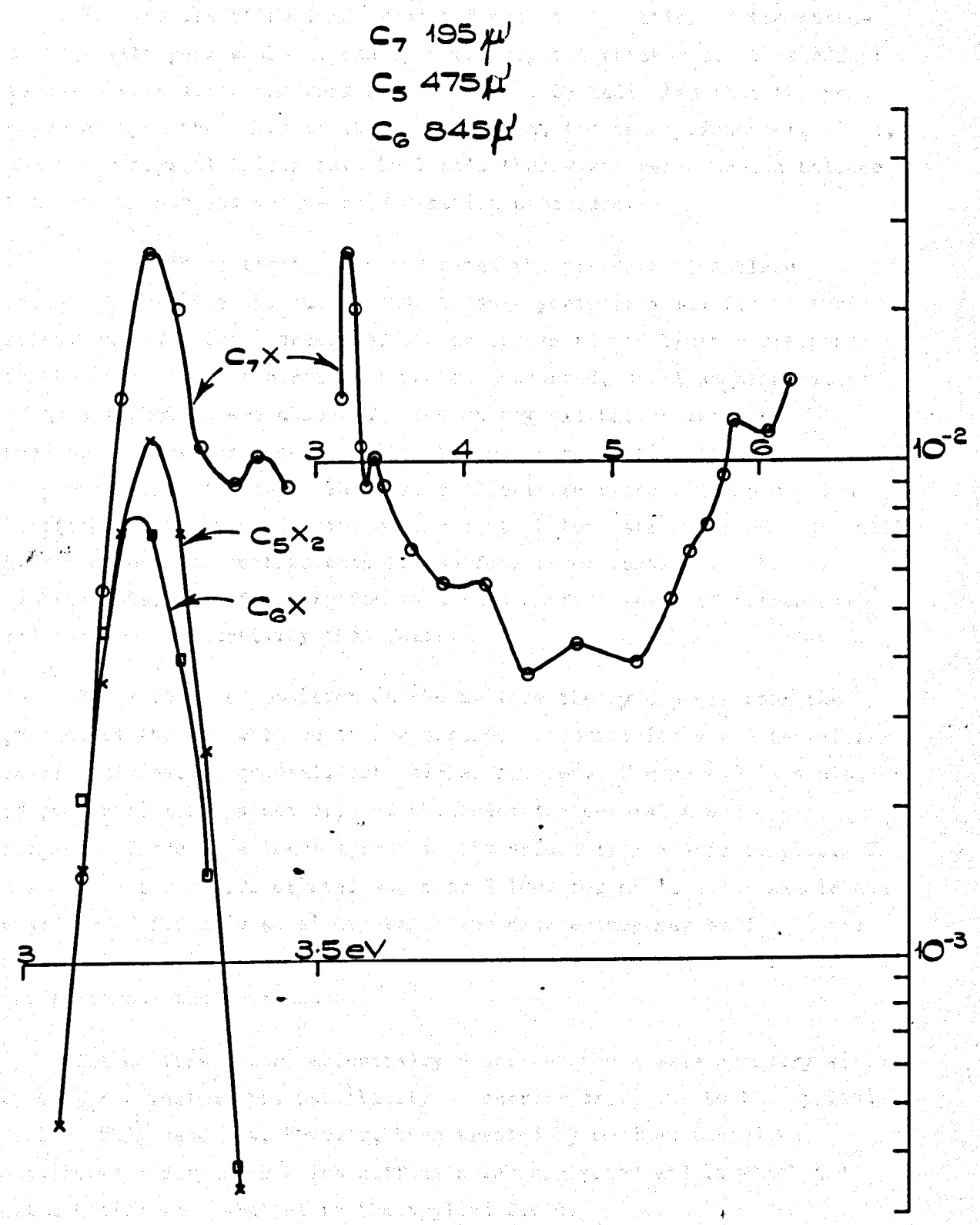

Fig. 4.8

4.5 Summary of 'a' and 'c axis' Low Energy Room Temperature Results

The results of Fotland suggested that the position of the photoconductivity peak would depend upon the crystal thickness. This effect is well known since the work of de Vore (1956) indicated that the peak depended upon the value of the product of α, the absorption coefficient, and d the crystal thickness. De Vore's theory was based upon a balance between surface and volume recombination processes.

A photoconductivity peak indicates the presence of surface recomination since the curve tends to an asymptotic value for no surface recombination. The increase of photoresponse to the limit corresponds to the increasing proportion of photons absorbed, until at high values of αd all photons are absorbed. Low energy excitation leads to negligible photoresponse, until at higher energies significant numbers of photons are absorbed. The photoconductivity rises with absorption coefficient until the majority of incident photons are absorbed. At still higher absorption coefficients the surface recombination may become important because of absorption in a thin surface layer of thickness $\frac{1}{\alpha}$ and the photoconductivity then falls.

Since the peak position on the de Vore theory depends upon the product αd then it will be at low absorption coefficients and therefore lower energies, in general, for thicker samples. Figure 4.9 is a plot of peak position against crystal thickness for several a and c axis samples. There is a large spread in the values from a axis samples. The mean value for a 400μ crystal was near 3.18eV for an 'a axis' sample and near 3.22eV for a 'c axis' crystal. The discrepancy may be due to the scatter in the 'a axis' case, or to the internal field geometries of the two electrode configurations.

The de Vore theory essentially describes the a axis geometry since it does not include the possibility of carrier drift due to the applied field. This case has, however, been treated by Goodman (1959) who considered a sample in which diffusion was neglected and in which the illumination was parallel to the applied field.

In the 'a axis' electrode geometry the electrodes were both on the front surface and the internal field was therefore depth dependent. This non uniform field distribution might have an effective penetration

AX9:-

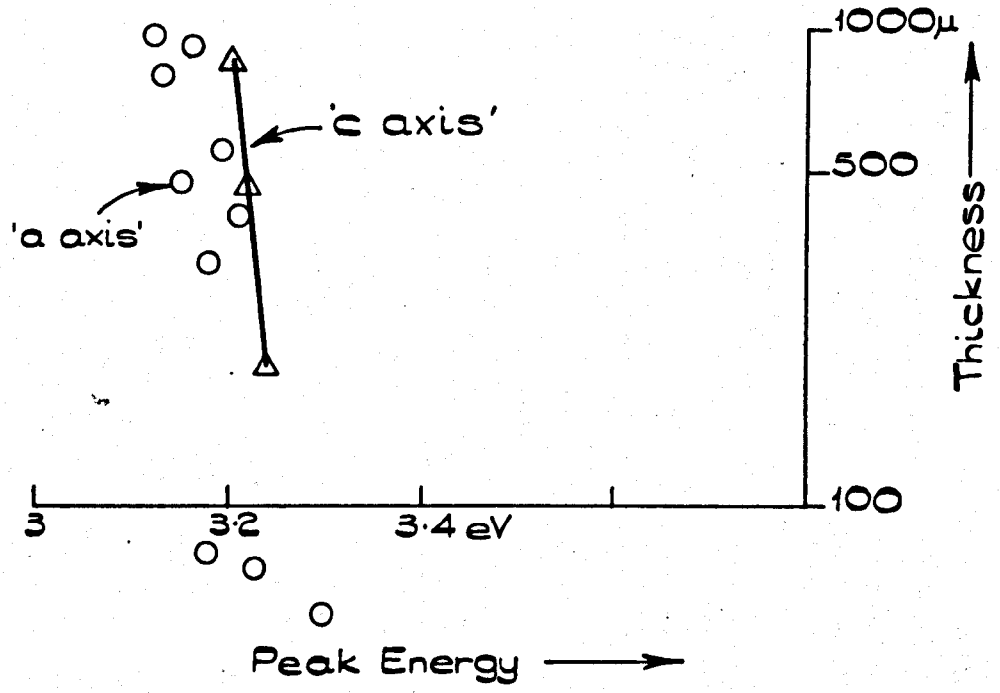

Fig. 4.9

REFLECTIVITY SPECTRUM

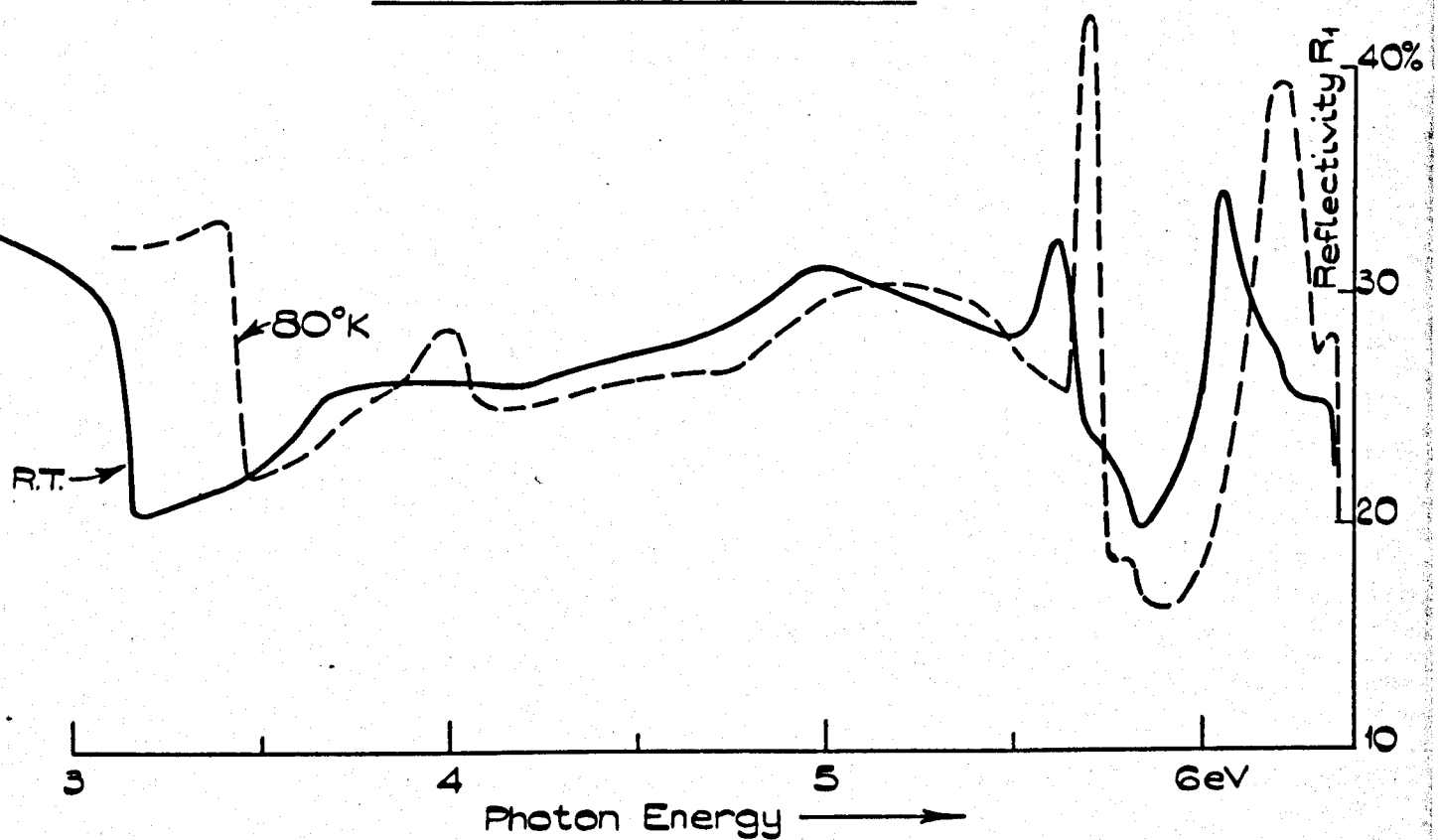

Fig. 4.10

depth γ. The depth γ need not approach the crystal thickness for large values of d the thickness, but might be related to it. If such a condition existed then the effective crystal thickness would be reduced and would not lead to a reduced energy peak. Furthermore the electrodes used by Yu and Fotland would not have caused this effect. In Yu's experiments the electrodes were on the rear surface of the crystal and would have caused a shift to low energies.

It is interesting to note that the existence of a field penetration depth might have the effect of reducing the shift of the photoconductivity peak with crystal thickness.

The peak position in crystal AX_9 was at a higher energy than that in cleaved crystal spectra for samples of similar thickness. If a field geometry effect was present in uncleaved crystals only, then the difference in peak position between these and the cleaved crystals could be explained.

Polarisation of the photocurrent did not occur in uncleaved samples however, and this difference could account for the difference in peak positions. This aspect will be discussed in more detail in a later section.

The low energy measurements of photoconductivity are in good agreement with those previously reported. No previous results had been obtained using such low intensities or on cleaved high quality crystals. Spectra obtained using two different electrode geometries are in good agreement.

The low energy peak is apparently shifted to lower energies by polarisation, since in an uncleaved crystal in which the effect was absent the peak was at a significantly higher energy.

4.6 High Energy Room Temperature Spectra

At the high energy end of the spectrum reported by Yu, there was a weak feature at 3.35eV. This feature has been found in our investigations and in many spectra was comparable with the peak near 3.2eV. The position of the peak in samples AX_3, AX_7, AX_{10}, AX_8, AX_9 and CX_7 was at 3.5, 3.45, 3.35, 3.44, 3.5 and 3.46eV. It therefore appears to be a genuine feature of photoconductivity measurements. There are no reflectivity features at this energy, hence the secondary peak cannot be explained on an optical

reflectivity basis so that the proportion of photons absorbed does not change. A similar feature appeared at I.T. and some analytical experiments were performed to investigate the nature of this feature. Both RT and I.T. secondary peaks will therefore be discussed together.

The reflectivity spectrum of CdI_2 measured at RT is presented in figures 4.10 and 4.11. The spectra were recorded using two separate samples $HCRX_1$ and $HCRX_2$. The reflectivity spectrum was also recorded at liquid nitrogen temperature and liquid helium temperature. These results and the measurement techniques used will be described in Chapter Five.

The reflectivity spectra are in good agreement with one another and with other spectra of single crystals reported by Greenaway and Nitsche (1965) and Brahms (1966).

It is instructive at this point to consider some of the features of the spectra. For convenience the spectrum illustrated in fig. 4.11 for crystal $HCRX_2$ will be discussed.

The high reflectivity at energies below 3eV is due to the low absorption of the crystal allowing reflection from the rear surface. The fall in reflectivity near 3.15eV corresponds to the onset of absorption and consequent extinction of the rear surface reflection. The reflectivity rises gradually from 3.2 to 5.15eV. There is some indication of a feature at 3.75eV. There is a broad peak at 5.2eV followed by sharp peaks at 5.6eV and 6.15eV. In this region, where the absorption coefficient is high, the variation of the extinction coefficient or absorption coefficient is reproduced in that of the reflectivity. The chief reflectivity features are summarised in table 4.3.

TABLE 4.3

THE REFLECTIVITY FEATURES, ROOM TEMPERATURE

Peaks	5.15eV,	5.61eV,		6.1eV
Shoulders	3.1 eV,	3.75-3.8eV		
Dips	3.18eV,	3.8-3.9eV,	5.51eV,	5.83eV

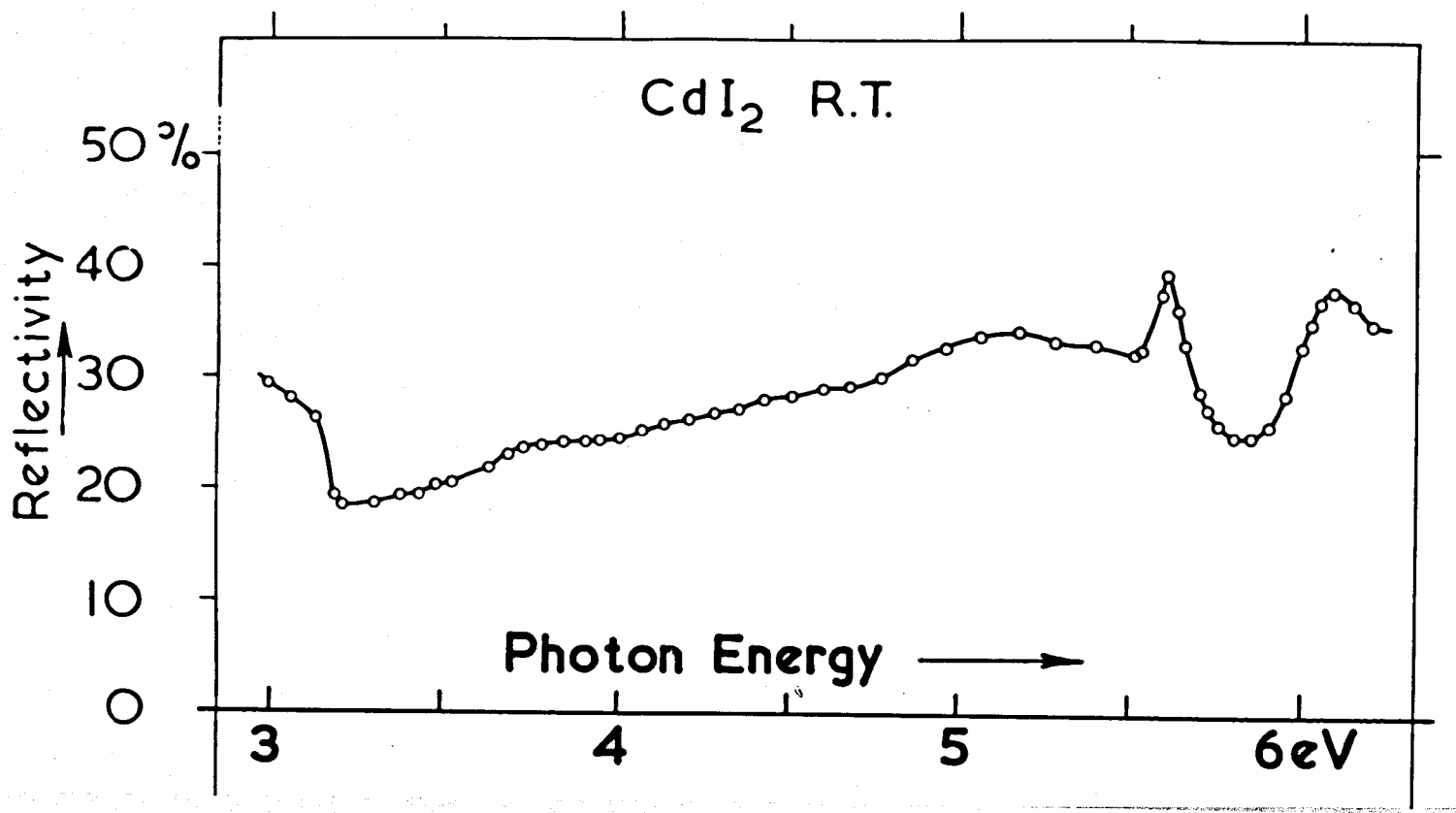

Fig. 4.11

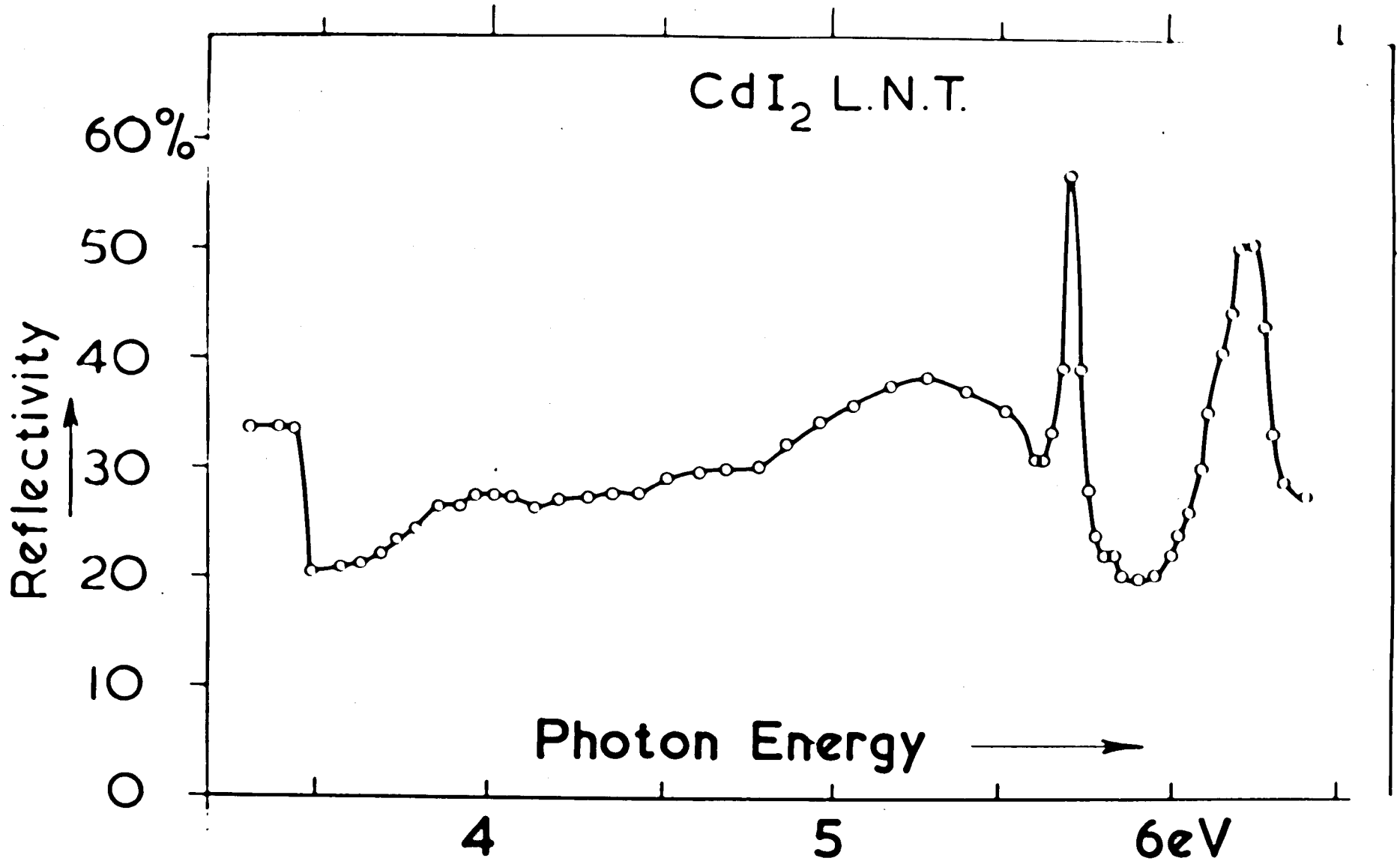

Fig. 4.11

The above information is to be compared with photoresponse spectra obtained from seven samples. The sturcture apparent in each of the quantum efficiency spectra is summarised in table 4.4.

TABLE 4.4

THE FEATURES OF THE PHOTOCONDUCTIVITY QUANTUM EFFICIENCY SPECTRUM AT RT

Crystal AX_7 75μ
Peaks at 3.23eV Shoulders at 3.45, 4.75, 5.5, 6.05eV
Dips at 4.1, 5.35, 5.65eV

Crystal AX_9 83μ
Peaks at 3.36eV Shoulders at 3.5, 4.95, 5.5, 5.9eV
Dips at 3.65, 4.75, 5.4, 5.65eV.

Crystal AX_8 320μ
Peaks at 3.18, 3.4eV Shoulders at 4.8, 5.75eV
Dips at 4.6, 5.5eV.

Crystal AX_{10} 470μ
Peaks at 3.15, 3.27eV Shoulders at 3.85, 4.45, 4.85, 5.5, 5.9eV
Dips at 3.6, 4.0, 4.6, 5.15, 5.6, 6.05eV.

Crystal $HCAX_2$
Peaks at 3.18eV Shoulders at 3.53, 4.00, 4.45, 5.07, 5.51, 5.98eV
Dips at 3.45, 3.63, 4.6, 5.15, 5.56, 6.09eV.

Crystal CX_7
Peaks at 3.24eV Shoulders at 3.4, 4.13, 5.9eV
Dips at 3.36, 4.45, 5.15, 6.05eV.

The low energy photoconductivity peaks at 3.15eV corresponds to the edge in the reflectivity spectrum at this energy. The reflectivity feature near 3.8eV is rather weak and correspondingly weak peaks were also found in some photoconductivity spectra, although in the majority there was negligible indication of structure at this energy. The high energy photoconductivity features below 5.5eV were not well resolved but shoulders were

present in many spectra at 5.5eV followed by dips at 5.6eV. The 5.6eV dip corresponds to the reflectivity peak caused by the formation of excitons.

The quantum efficiency illustrated in the curves drawn so far has been the number of electrons created per incident photon. This quantity does not take account of the number lost by reflection. If there are I_o incident photons then the number reflected is $I_o R(\nu)$ where $R(\nu)$ is the reflection coefficient. The number transmitted through the surface is then $I_o(1 - R(\nu))$. This quantity represents the number of photons absorbed provided that the absorption coefficient is sufficiently large to make the rear surface reflection negligible. The factor $1 - R(\nu)$ may be applied as a correction to the quantum efficiency for incident photons so that the internal quantum efficiency may be determined. If this quantity was independent of photon energy then the photoconductivity spectrum would reproduce the $1 - R(\nu)$ curve.

The $HCAX_2$ photoresponse spectrum has been corrected throughout for reflectivity loss and has the form indicated in fig. 4.12; the $1 - R(\nu)$ curve is also shown. The definition of both photoconductivity and reflectivity spectra at RT was generally poor so that lower temperatures were used to improve the spectra.

4.7 Intermediate Temperature Measurements

Measurements of photoconductivity were more readily obtainable with the single stage LNT cryostat because of the "freezing out" of the dark current. No previous measurements had been reported at temperatures below RT, so that there was no possibility of comparison as there was with the RT measurements.

The 180°K or Intermediate temperature (I.T.) quantum efficiency spectra were obrained by the experimental methods described in Chapter Three and are illustrated in figures 4.13-4.19. The preliminary spectra have not been plotted for the sake of simplicity and because the high intensities used make the spectra less reliable. The positions of the low energy peaks are summarized in table 4.5.

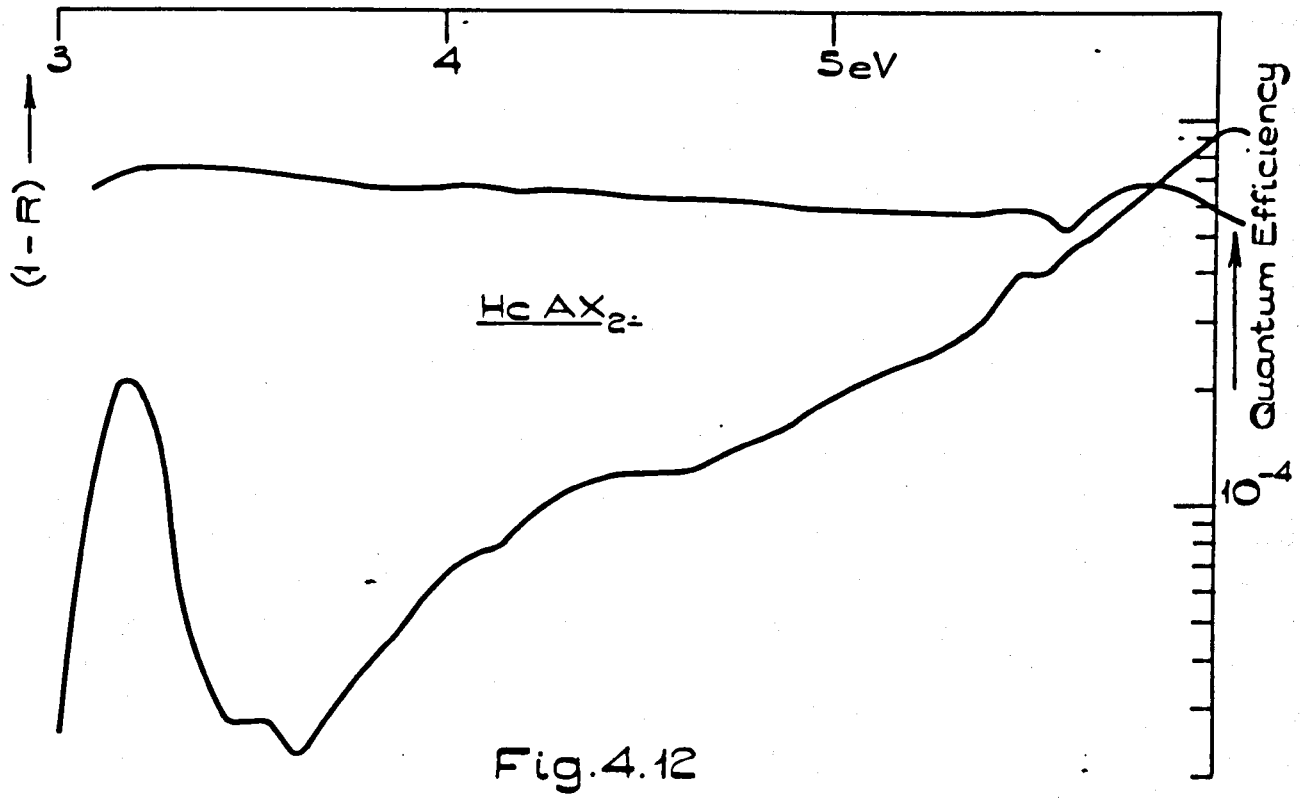

Fig.4.12

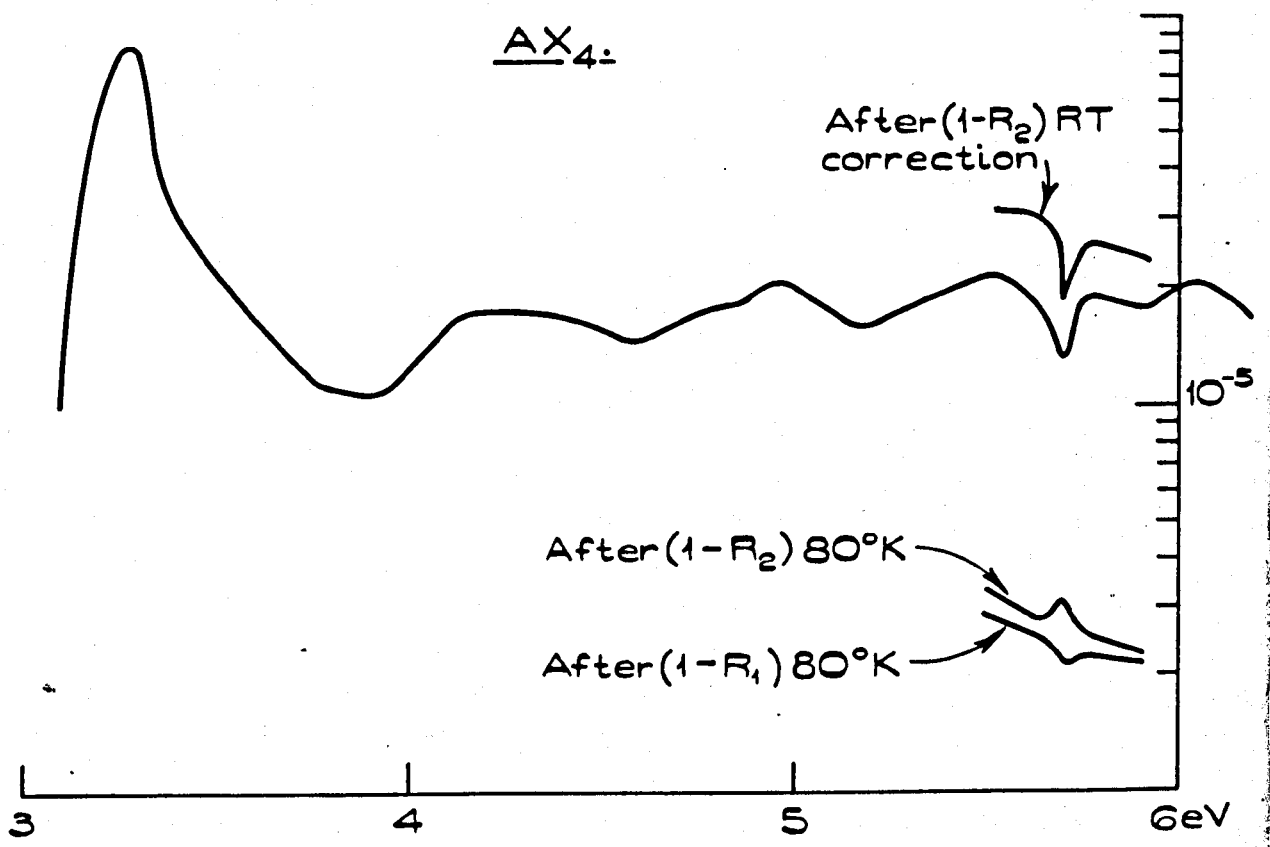

Fig.4.13

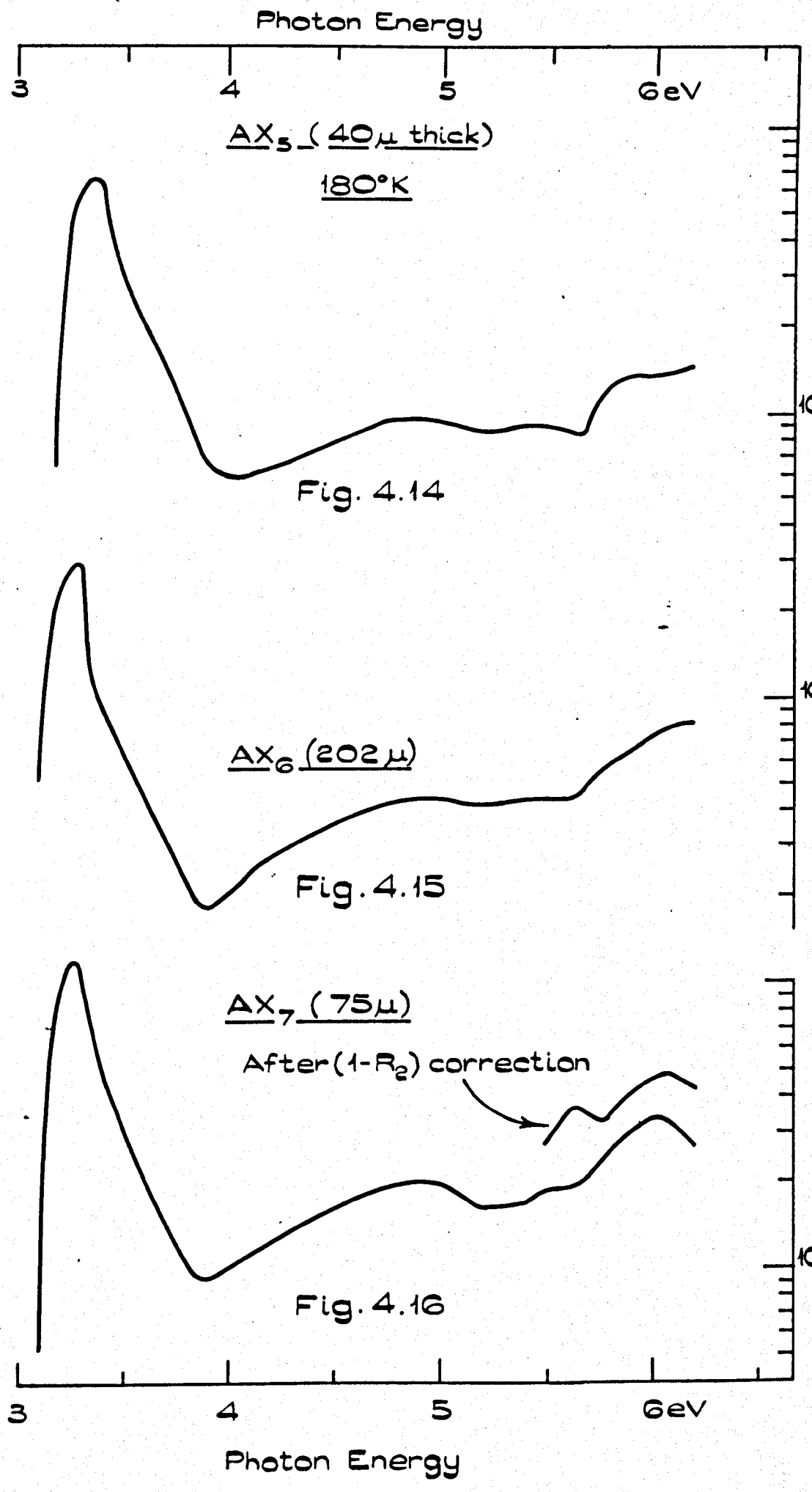
Photon Energy
3
4
5
6eV
AX5 (40μ thick)
180°K
10-5
Fig. 4.14
AX6 (202μ)
10-4
Fig. 4.15
AX7 (75μ)
After (1-R2) correction
10-5
Fig. 4.16
3
4
5
6eV
Photon Energy

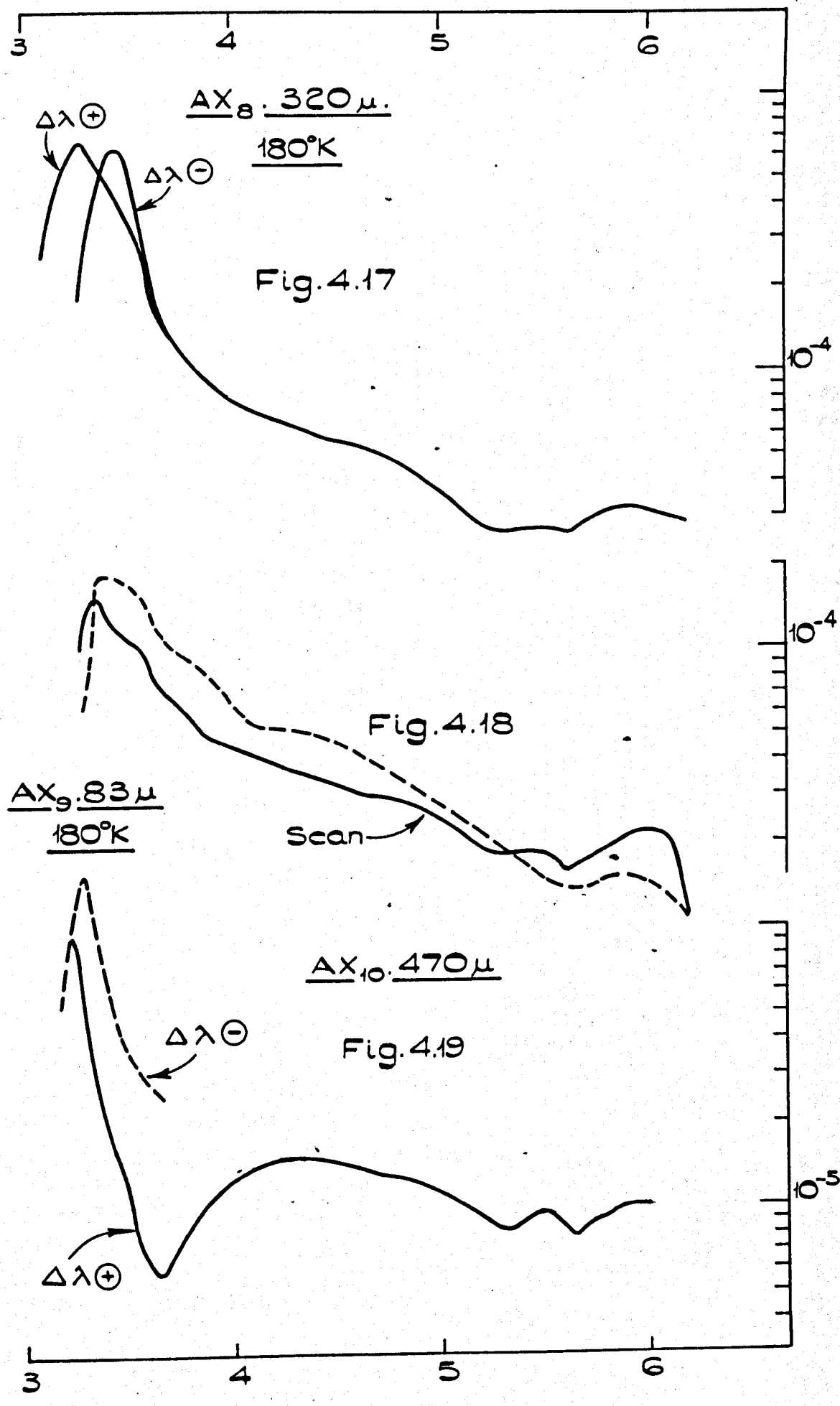

Fig. 4.17

Fig. 4.18

Fig. 4.19

TABLE 4.5

POSITION OF LOW ENERGY PEAK AT INTERMEDIATE TEMPERATURE

Sample Number	Thickness μm	Low Energy Peak Position
AX_5	40	3.36eV
AX_1	60	3.27eV
AX_7	75	3.27eV
AX_3	80	3.2 eV
AX_9	83	3.36eV
AX_2	93	3.30eV
AX_6	202	3.27eV
AX_8	320	3.27eV
AX_4	415	3.27eV
AX_{10}	470	3.22eV

The above table gives an indication of the effect of crystal thickness on photoconductivity peak energy. The peak energy decreases with increasing crystal thickness.

If the photoresponse peak is caused by increased surface recombination at high absorption coefficients then the position of the peak in terms of the product αd will be fairly insensitive to the recombination parameters. The value of αd at the peak will be between 1 and 10 (de Vore 1956). This value of αd will therefore be largely temperature independent. For crystals of typical dimensions of 100μ the value of α at the peak will be $\sim 10^3$ cm^{-1}. The peak energy consequently corresponds to the indirect absorption edge. This edge is strongly temperature dependent with a coefficient of $\sim 1.2 \times 10^{-3}$ eV/°K (Greenaway and Nitsche 1965).

The temperature measured at the sample holder in the single stage cryostat at I.T. was of the order of 130°K, the front surface may have been at an appreciably higher temperature particularly in the 'a axis' experiments. In an experiment to measure the front surface crystal temperature a copper-constantan thermocouple was cemented with 'silver dag' onto the front surface of an 800μ crystal. This procedure severely damaged the sample but enabled an upper limit to be placed on specimen

temperatures. The temperature measured was ~220°K and would be higher than the temperature of the photoconductivity specimens. It is likely that the temperature at the front surface of ~400μ crystals was near 180°K.

The RT reflectivity spectrum of typical cleaved crystals has been described above; a spectrum obtained at 80°K is also illustrated in fig. 4.11. The feature found in the RT spectrum at 3.18eV shifted to 3.45eV at 80°K. This feature corresponds to the cut-off of near surface reflections, so that the absorption coefficient will be approximately equal at the two energies. The RT photoconductivity peak was located near this feature, hence the low energy LNT peak would be expected to be near 3.45eV. Since the sample temperatures were near 180°K then significantly lower energies than 3.45eV would be expected for the peak.

It is possible to compare the reflectivity spectrum with the I.T. photoconductivity if several approximations are made. The sample temperature is assumed to be 180°K and a linear relationship between the shift of reflectivity spectral features and temperature is assumed.

The temperature difference between RT and 180°K is 113°; the low energy photoresponse peak shifted by some 0.1eV between RT and the Intermediate temperature. The temperature coefficient of the peak was therefore 10^{-3}eV/°K. The reflectivity edge shifted from 3.18eV at RT to 3.45eV at 80°K corresponding with a coefficient of 1.3×10^{-3}eV/°K. There is therefore fair agreement between the two coefficients, but the reflectivity coefficient is somewhat greater. The low temperature photoconductivity peak may not correspond with the dip in reflectivity, or the optical structure may change non-linearly with temperature.

In the 'c axis' configuration using crystals CX_5II and CX_7 at I.T. edges were found at 3.35eV and 3.36eV, see figures 3.21 and 3.22. The RT peak positions were 3.22eV and 3.24eV respectively, corresponding to shifts of 0.13eV and 0.12eV. These values are in closer agreement with the reflectivity shift. In some early 'c axis' experiments no low energy peak was apparent. The 'c axis' samples were, however, at a somewhat low temperature than the 'a axis' because of better thermal contact, there was also the possibility of an artificial shift because of chromatic aberration of the image. This aberration would be relatively unimportant in 'a axis' experiments but might be significant in the 'c axis' geometry because of the small electrode aperture.

4.8 The Nature of the Secondary Low Energy Peak

In the majority of experiments at the intermediate temperature there was a shoulder on the high energy side of the main peak. The position of this shoulder was at 3.45, 3.6, 3.5, 3.45, 3.65, 3.5, 3.5, 3.45, 3.55 and 3.4eV for samples AX_1-AX_{10}.

It is clear from fig. 4.23 that the position of the high energy shoulder is closely linked to the low energy peak position. The separation between the peaks was 0.2eV in the majority of samples.

In Chapter Three the techniques used to investigate these features using crystal AX_8 were discussed. The double peak was present even when a quartz-iodine tungsten filament lamp was used instead of the deuterium lamp. The double peak became a single peak when lower intensities were used. The position of the single peak found at low intensities was near 3.35eV for sample AX_8. (see fig. 3.20). Point by point measurements had previously indicated that energy dependent polarisation effects were present in the majority of experiments. The simple polarisation phenomena observed were of similar form to those studied by Ben Sira, Pratt, Harnik and Many in NaCℓ (1959).

4.9 Analysis of Photoconductivity Polarisation Effects

Although the basic behaviour of the polarisation phenomena was as reported by Ben Sira et al (1959) in NaCℓ there were complications because of the energy dependence of the effects.

In a typical crystal AX_4 at 180°K there was no polarisation with light levels of 10^{10} photons/cm^2/sec at 230mμ (5.39eV). At 380mμ (3.27eV) the photocurrent took 4 seconds to reach its peak value of 7.2×10^{-14} amps, and fell to 4.8×10^{-14} amps some 6 seconds later. Eleven seconds after the peak the current was 4.5×10^{-14} amps. The intensity was as for the 230mμ (5.39eV) illumination. Attenuation by a factor of 2 reduced the current to 5.1×10^{-14} amps and the peak occurred some 6 seconds after illumination began. The current fell to 4.8×10^{-14} amps 6 seconds after the peak. The maximum polarisation was found to occur for the 360-370mμ (3.45-3.36eV) illumination. The polarisation at 380mμ (3.27eV) was slight compared with that in the 3.4eV region. The time taken for the current to saturate was longer for the low intensity illumination and for weakly

polarising illumination. High intensity illumination caused strong polarisation, thereby preventing the current saturating and the current consequently decayed before reaching the saturation value.

In sample AX_7 the polarisation was again strong near 3.4eV but negligible at 3.3eV. There was negligible polarisation at 5.2eV. The polarisation was found to be strong in the region near the electrodes, see fig. 3.14.

Polarisation effects were negligible in all samples in the region above 5.4eV; at lower energies the intensity varied slowly and fell steadily to 3.1eV. If the polarisation had been simply intensity dependent there would have been a maximum polarisation near 5.4eV. It is clear that the effect will be dependent upon the number of photons absorbed rather than the number incident, consequently the effect will be reduced in regions of high reflectivity. The maximum effect was near 3.4eV however, so that since the reflectivity varies slowly in the region an additional factor must be important. Since the polarisation is dependent upon the number of carriers created, it depends upon the number of photons absorbed and the quantum efficiency of carrier generation.

If a sample is illuminated in a narrow strip perpendicular to the electric field direction, then during the illumination carriers are trapped near the illuminated strip. Since the oppositely charged carriers have moved under the influence of the field in opposite directions before being trapped there will be a net charge displacement. The displacement between opposite charges creates an electric field in opposition to the external field. This polarisation field increases with time, the rate of increase depending upon the illumination intensity, the quantum efficiency and the absorption coefficient.

Illumination of a given intensity, energy and quantum efficiency creates a given number of charge carriers. The carrier density however also depends upon the absorption coefficient. Illumination at photon energies of low absorption coefficient generates carriers throughout the crystal depth. The carrier density varies slowly with depth in this case. The same number of carriers generated by highly absorbed illumination leads to a high carrier density concentrated near the crystal surface.

Since the polarisation field is due to oppositely charged carriers on parallel regions at either side of the illuminated strip, the field is

proportional to the charge density in the chargedregions. The trapped charges in the parallel regions are analogous to the charges on the plates of a parallel plate capacitor where the field strength is proportional to the surface charge density on the plates.

Highly absorbed light leading to a high charge density consequently leads to a high electric field concentrated near the surface. Illumination of weakly absorbed light leads to a reduced polarisation field distributed throughout the crystal depth.

In the case of CdI_2 at 3.27eV the absorption coefficient is low so that the absorption length may be similar to the crystal thickness. The carrier concentration will therefore be fairly uniform and the polarisation field will be low, even though the number of charge carriers created is the same as that at 3.45eV. The absorption coefficient at the latter energy is high, consequently carriers are generated near the surface and the polarisation is strong and close to the surface.

The polarisation fields discussed have been caused by a given illumination pulse, they are therefore measures of the rate of decrease of photocurrent with time i.e. polarisation rate. Since this effect is pronounced at 3.45eV then the photocurrent will be artifically suppressed near this energy, particularly in scanning spectra. Scanning from high energies will involve traversing a region of negligible polarisation, after which the current will rise and then fall rapidly due to the strong polarisation. At lower energies no polarisation occurs and the photocurrent tends towards the saturation value. This procedure therefore leads to a splitting of the low energy peak. The two components will be at either side of the peak found in the absence of polarisation effects. This was indeed the case as found in, for example, crystal AX_8.

It is therefore apparent that the two components of the low energy feature are facets of the measurements technique and not genuine intrinsic properties of the internal quantum efficiency.

4.10 High Energy Photoresponse Structure at Intermediate Temperature

The general features of the high energy spectra are shown in figures 4.13 to 4.19. A schematic spectrum illustrating the general features is illustrated in fig. 4.20. There are shoulders or peaks at

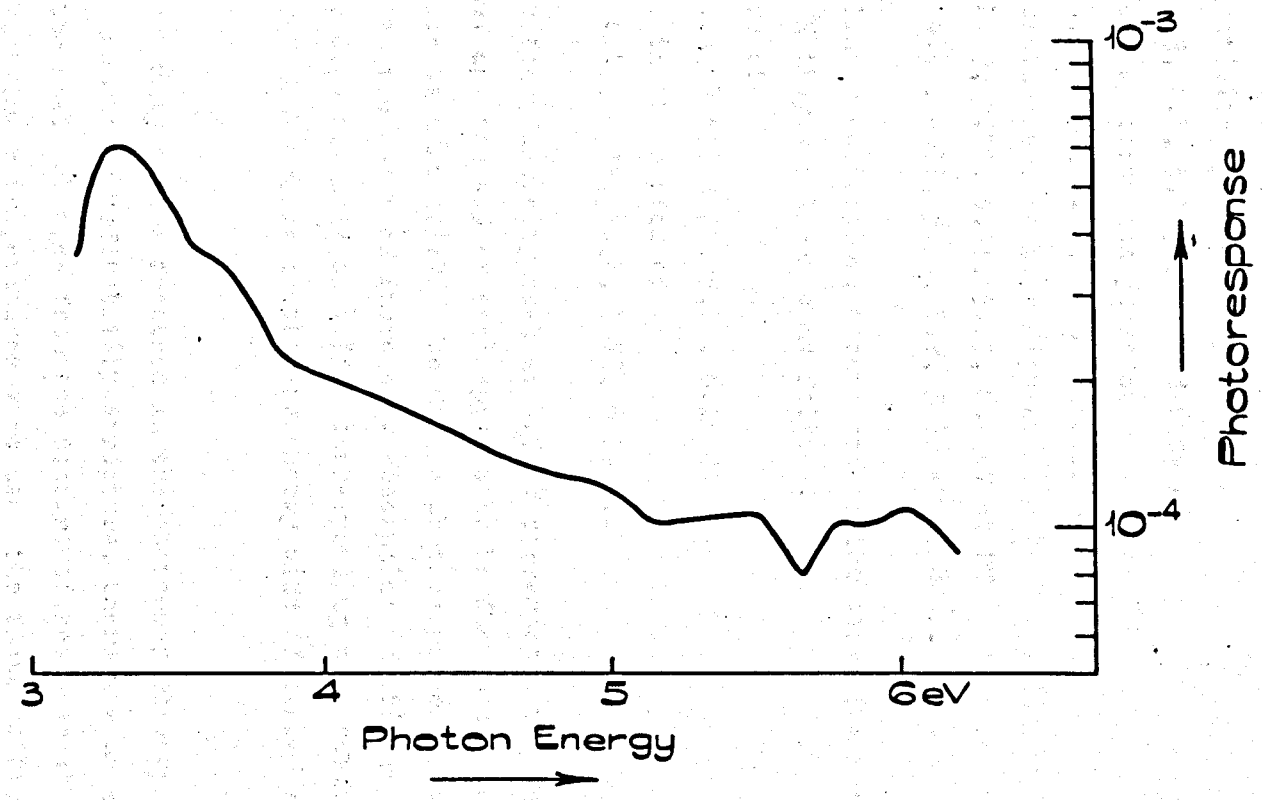

Fig. 4.20

4.95, 5.51, 6.02 eV

with dips at

3.65, 3.88, 5.15, 5.65 eV.

The RT reflectivity spectrum R peaks at

3.8, 4.3, 4.6, 5.17, 5.61 and 6.09 eV

while the 80°K spectrum has peaks at

4.0, 4.3, 4.65, 5.25, 5.70 and 6.22 eV.

The corresponding spectra have dips at

4.0, 4.43, 4.72, 5.51, 5.85, 6.2 eV at RT

and 4.13, 4.43, 4.77, 5.64, 5.9, 5.36 eV at 80°K.

If a linear temperature dependence of the above features is assumed then at 180°K they are located as follows.

The peaks are at

3.9, 4.3, 4.63, 5.21, 5.65, 6.15 eV

and the dips in the region of

4.06, 4.43, 4.75, 5.58, 5.87, 6.29 eV.

The photoconductivity peak at 4.5 eV corresponds to the reflectivity dip at 4.43eV and the 4.95eV peak appears to be due to the beginning of the absorption band at 5.2eV. The dip in photoresponse at 3.65-3.88eV corresponds to the onset of increasing absorption in this region. The; reflectivity dips slightly at 4.75eV corresponding to a reflectivity peak and the 5.12eV peak occurs on the low energy side of 5.21eV reflectivity peak.

Although many of the features in the photoconductivity spectrum in this region are due to reflectivity structure, there are uncertainties because of the small changes from the background response at these features. When lower temperatures were used the features became clearer and good correlation with reflectivity spectra was possible (see Chapter Five).

4.11 High Energy Exciton Photoconductivity

Exciton lines in the CdI_2 reflectivity spectrum are located at 5.61eV and 6.09eV at RT whereas these lines shift to 5.70eV and 6.22eV at 80°K. At 180°K they will be located at 5.66eV and 6.13eV if the temperature dependence is linear.

At RT the change in reflectivity at the first line leads to a change in (1-R) of from 0.74 at background to 0.68 at the peak. On a

second crystal these values were 0.70 and 0.61. The percentage changes in 1-R due to the peaks were therefore 9% and 16% on the two crystals $HCXR_1$ and $HCXR_2$ at RT. The corresponding charges at 80°K were 35% and 60%. We therefore take values of 12% at RT and 45% at 80°K as typical changes in 1-R at the lower energy line.

All of the photoconductivity quantum efficiency spectra exhibited dips at this energy before the reflectivity loss correction was applied.

Crystals AX_4, AX_7, CX_7 and AX_{10} were chosen to illustrate the types of photoconductivity found. They contain spectra with sharp and weak exciton line dips at the two temperatures. Sample AX_4 has a slight dip at 5.7eV at 180°K and exhibits a peak in quantum efficiency only when the 80°K $HCXR_2$ correction was applied. Since the temperature was much higher than 80°K it seems likely that the true 80°K spectrum exhibits a dip after correction for reflectivity loss. There is a sharp dip for CX_7, this time at 5.64eV, which was still apparent after the 80°K $HCXR_2$ corrections. A small peak appeared at 5.7eV which disappeared leaving a broad peak after the application of the 180°K correction.

Crystal AX_7 exhibited dips at RT and 180°K both of which became peaks after the application of the RT and 180°K $HCXR_2$ (1-R) corrections respectively. Sample AX_{10} displayed the strongest dip at RT which was smoothed out when either of the RT reflectivity corrections was applied.

4.12 Summary of Exciton Photoconductivity IN CdI_2 at RT and 180°K

Excitation at RT in the first exciton line at 5.61eV leads to appreciable photoconductivity. The efficiency of the photoresponse is as high as that in the adjacent band to band region. In some crystals the difference between the two efficiencies was ~5% in others it rose to 15%.

The situation was rather more complicated at 180°K. The strong exciton line caused a large change in the value (1-R). The strength of the peak varied from sample to sample so that the correction factor also varied.

In the case of CX_7, for example, there was a sharp dip at 3.64eV which was only reduced by the (1-R) $HCXR_2$ 180°K correction. Crystal AX_4, with a dip at 5.7eV, had a peak at 5.64eV after correction with the 180°K

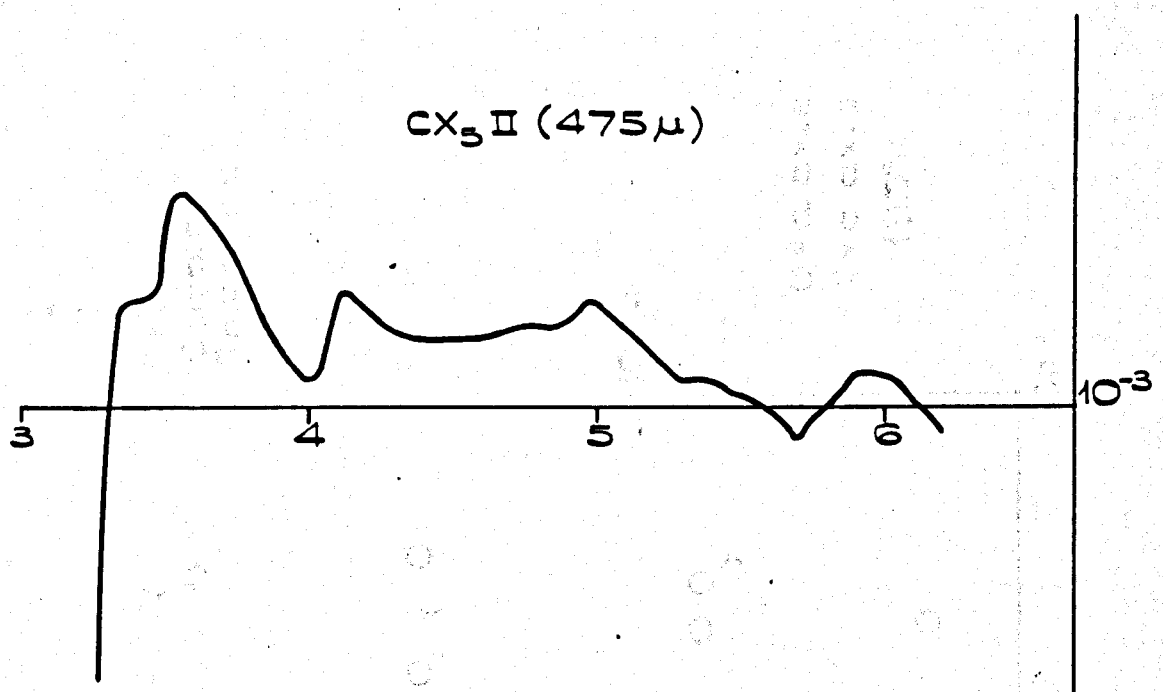

Fig. 4.21

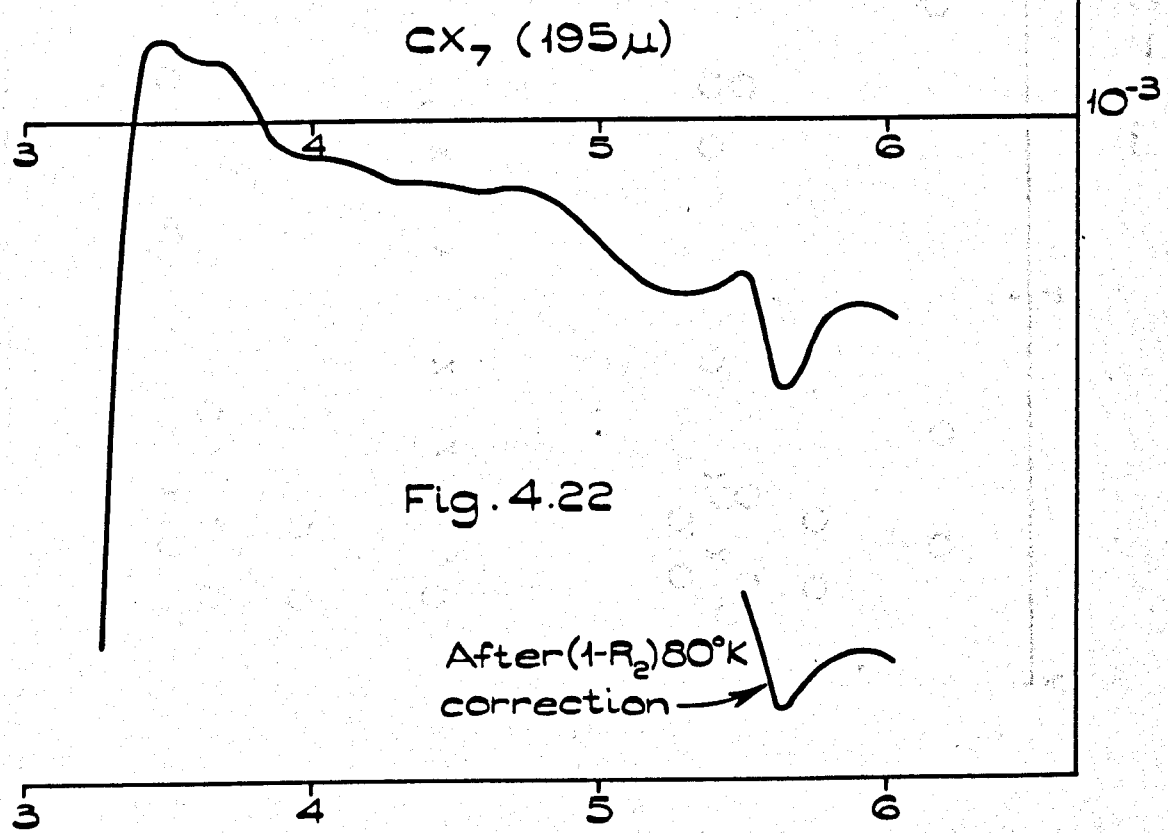

Fig. 4.22

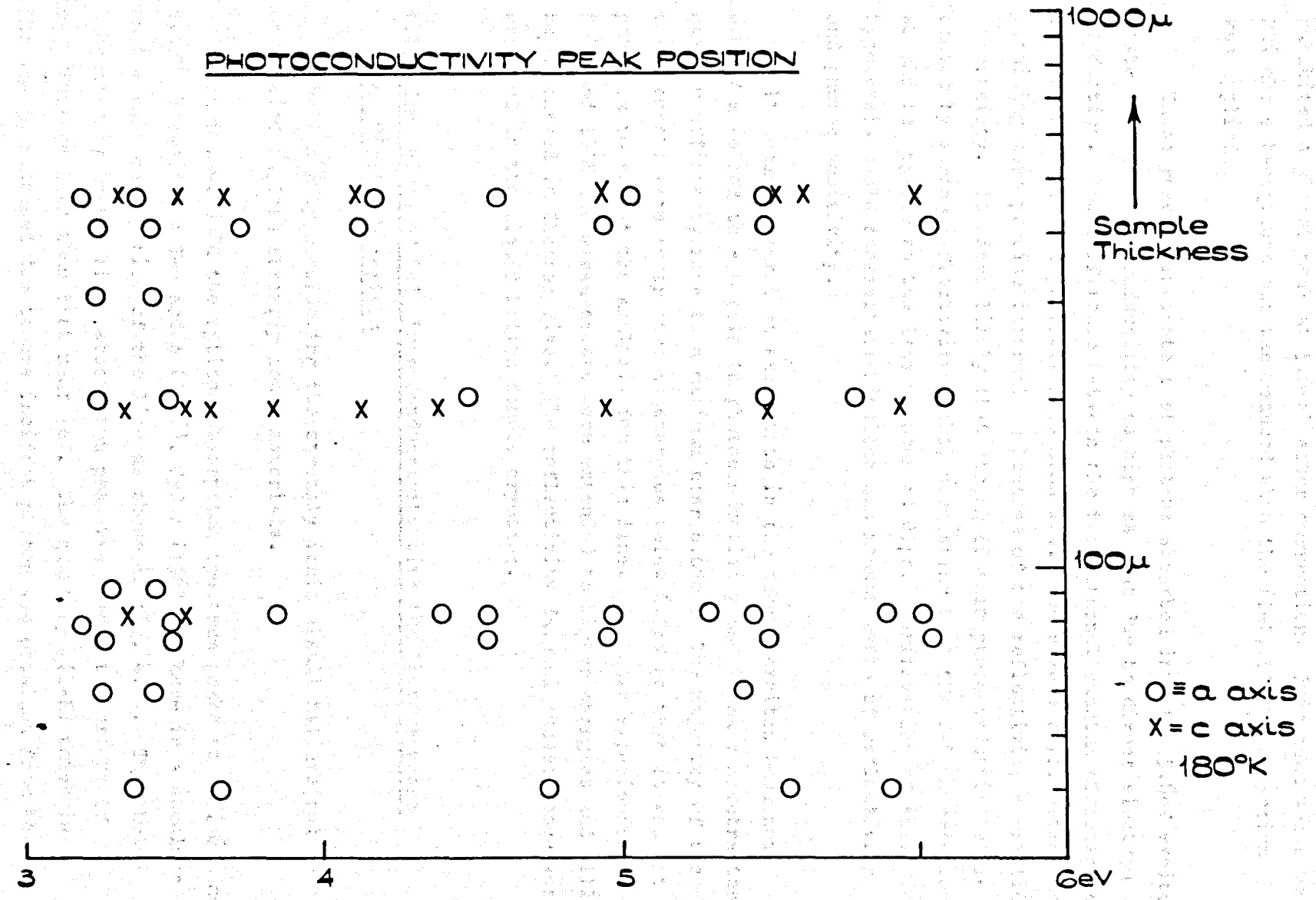
PHOTOCONDUCTIVITY PEAK POSITION
1000μ
Sample Thickness
100μ
O = a axis
X = c axis
180°K
3
4
5
6eV

Fig. 4.23

correction factor. The majority of samples followed AX_7, however, and exhibited a slight peak at 5.64eV after correction. This peak was some 20% above background but was reduced when the (1-R) $HCXR_2$ correction was applied.

These results indicate that photons absorbed into the 5.6eV exciton state lead to photoconductivity as high as that due to direct electron production. The difference between the two internal quantum efficiencies is less than 20% and probably less than 10%. There were difficulties in obtaining more precise information because of the reflectivity correction uncertainty. It seems likely that strong dips in photoconductivity are caused by strong reflectivity peaks, suggesting that the $1-R_1$ correction should be applied to the less pronounced dips. Verification of this hypothesis would necessitate simultaneous measurements of reflectivity and photoconductivity.

It became clear that excitation in the second exciton band near 6.05eV also led to appreciable photoconductivity and in many spectra the quantum efficiency rose to a maximum near 6.05eV. The majority of the measurements were restricted to energies below 6.2eV so that it was not possible to repeat the analysis for this line. In later experiments at $80^{\circ}K$ and $10^{\circ}K$ the measurements were extended to higher energies and will be discussed in Chapter Five. The reflectivity data discussed above were recorded in the liquid helium double cryostat.

4.13 Comparison of CdI_2 Photoconductivity with the Photoresponse of Similar Materials

We begin by considering the strongly ionic alkali halides and go on to discuss less strongly ionic materials.

In RbI at $80^{\circ}K$ the optical absorption spectrum peaks at 5.7, 6.1 and 6.4eV, Huggett and Teegarden (1966), Sydor (1967). There is a shoulder on the high energy side of the line as shown in fig. 4.24. The photoconductivity in the first absorption peak was almost two orders of magnitude smaller than that near 7eV. The quantity $\eta(1-R)$ which is the charge released due to one incident photon was obtained from the experimental results. These results suggest that photons absorbed in the lower energy absorption band do not readily form free carriers. The oscillator strength of the peak relative to that at 7eV suggested that excitation into this band was a different process to that in the 7eV band.

. Optical absorption spectrum of RbI at 80°K (after Baldini).

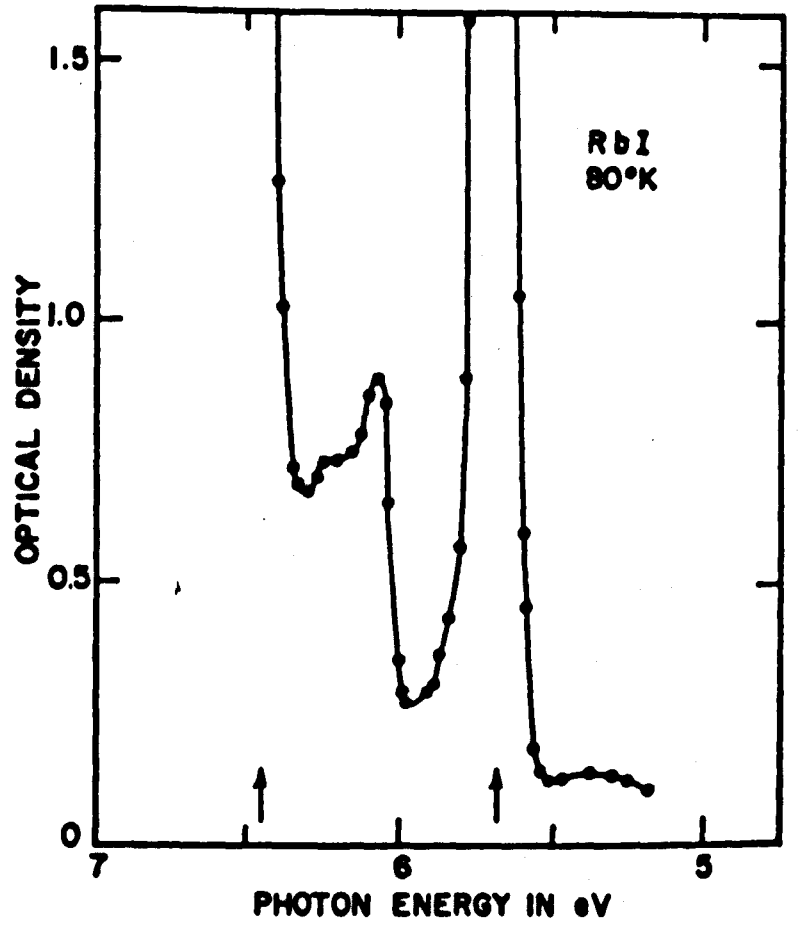

Optical absorption spectrum of RbI at 10°K (after Baldini).

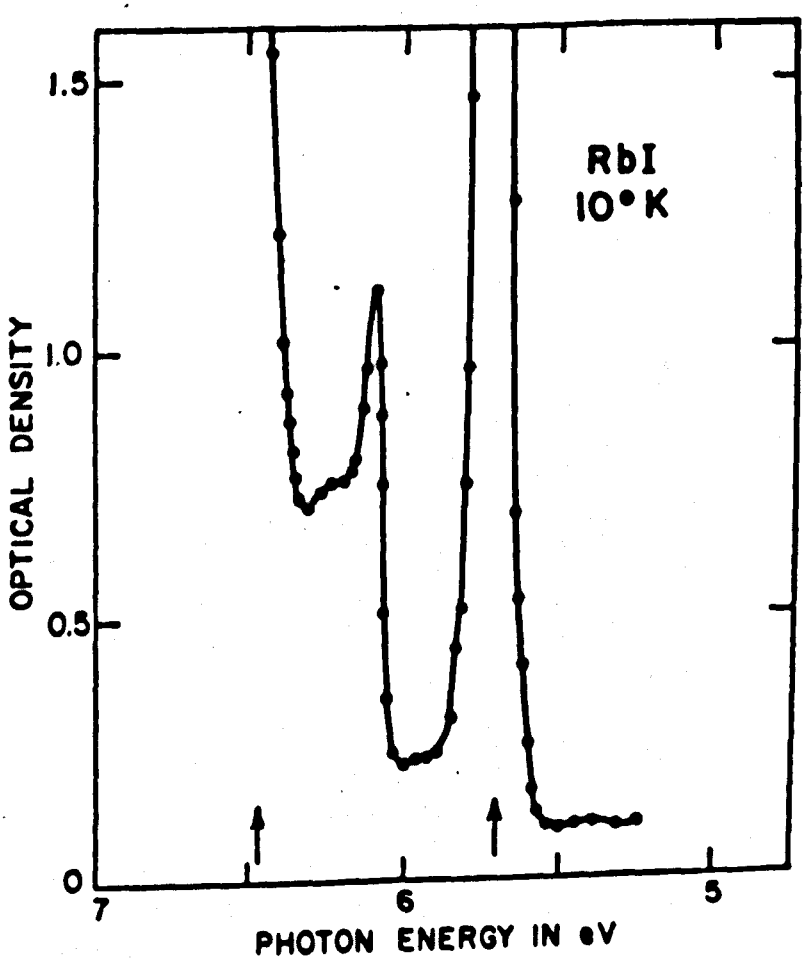

Fig. 4.24

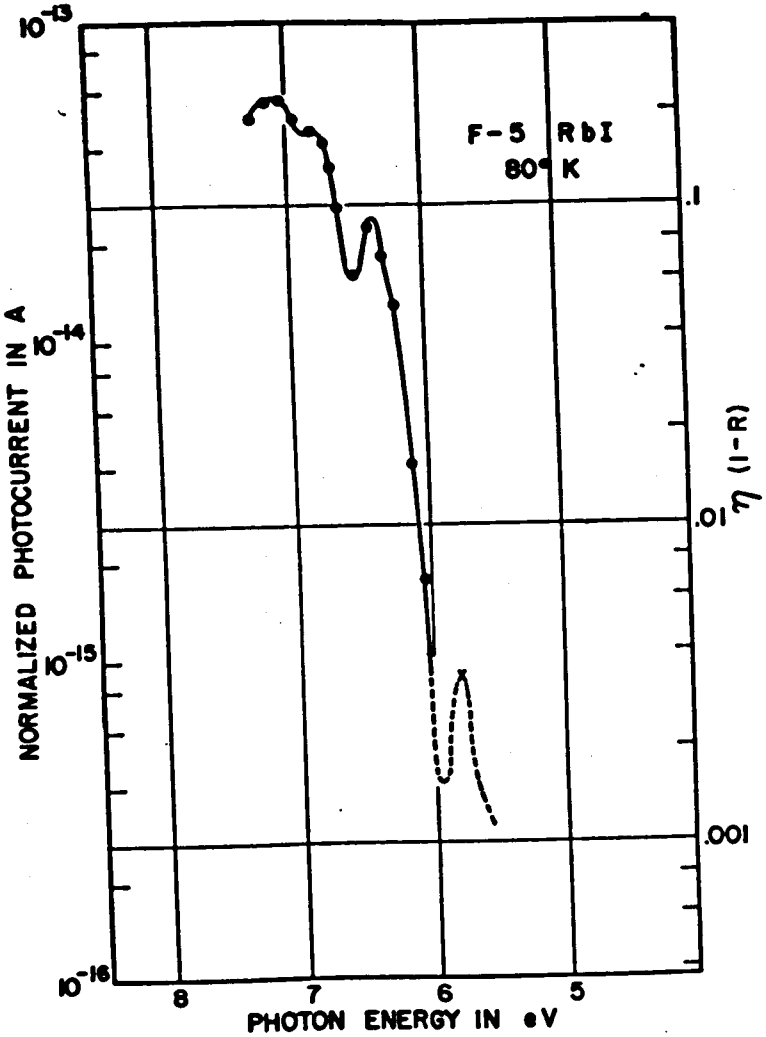

Spectral response of RbI at 80°K.

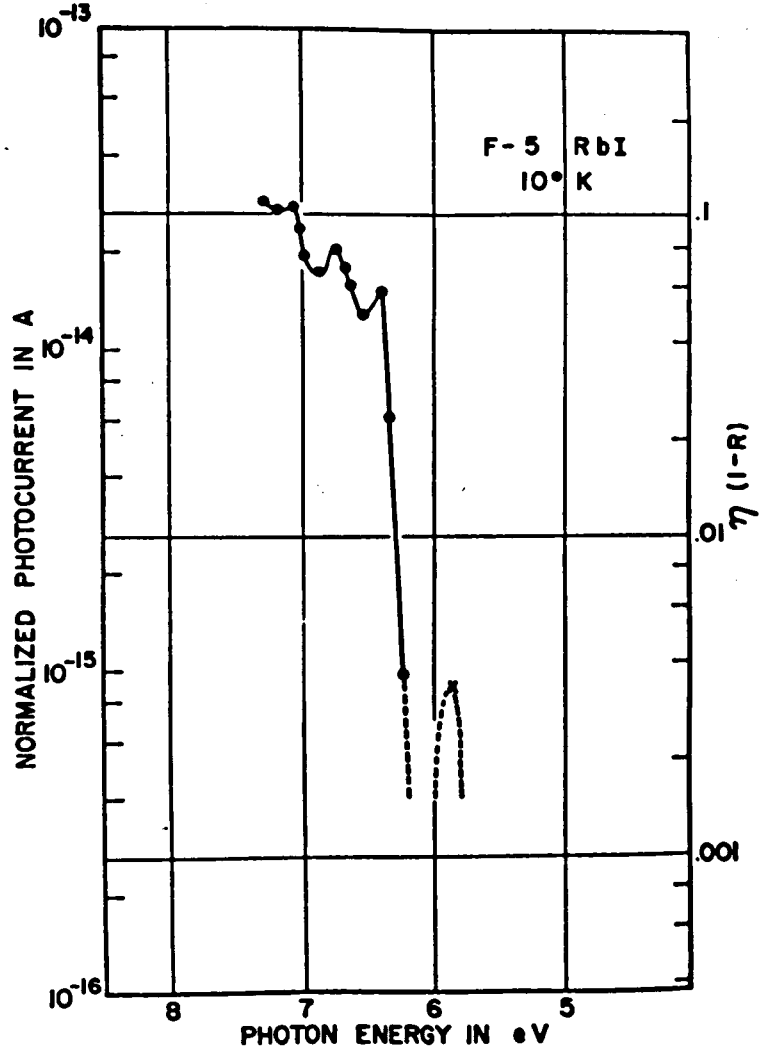

Spectral response of RbI at 10°K.

Fig. 4:24

The low energy band was thought to be due to exciton formation and excitation into this band led to the formation of non-conducting bound states. There was a dip at 6.4eV even after correction for the reflectivity loss. The internal quantum efficiencies in the first three bands, i.e. in the low energy band and the two weaker bands, were much less than that in the high energy band.

The currents at 80°K were greater than the corresponding currents at 10°K. The 6.23eV current increased relative to the 6.09eV peak indicating that if excitons were formed then the binding energy for the third state was lower than that for the second. Since exciton states are non-conducting then the photoconductivity is assumed to be due to their annihilation by interactions with the crystal lattice and impurities. The increase of photocurrent with temperature leads to a measure of the activation energy for dissociation.

In the case of RbI the activation energy was 10^{-2}eV and the ionisation limit of the exciton series was 6.36eV.

Similar techniques were utilised by Heyningen and Brown (1958) to measure the primary photoconductivity of AgCℓ single crystals. The properties of CdI_2 are closer to those of AgCℓ than to those of the alkali halides since AgCℓ has, for example, an indirect absorption edge near 3.27eV at 80°K.

The photoconductivity peak in a crystal of poor surface quality and 2mm thick was near 384mμ (3.23eV) whereas the value of K was $10cm^{-1}$ at this wavelength. The peak therefore corresponded to a value of αd of 2. The quantum efficiency of this crystal in the range from 3.4-5.6eV was only $\frac{1}{5}$ of the peak value. In higher quality crystals the high energy quantum efficiency increased and the peak became an edge. The peak in reflectivity near 248mμ (5.02eV) corresponded to an increasing value of η. The difference between the spectra from the two crystal types is in agreement with the De Vore model. The decrease of the photoresponse at high energies in the poor surface quality sample was due to increased surface recombination.

These experiments and those described for the alkali halides were performed using the primary photoconductivity technique and without detailed reflectivity data for the samples used.

Photoconductivity has also been used as a technique for investigating steady state photocurrents in the exciton region of semiconductors and semi-insulators. In particular Gross and Nikitine and their respective schools have made extensive studies.

Gross et al (1964) have studied the effect of temperature and modulation rate on the A.C. photoconductivity of CdS. They found two different types of behaviour and classified their samples accordingly. The first type exhibited photocurrent peaks at exciton lines whereas the second exhibited a line reversal effect. Some crystals however changed from the first to the second type on cooling from 77°K to 20°K. The opposite effects occurred for some samples when they were cooled. There was also a number of crystals which were type invariant under the temperature change. Similar effects were observed due to different chopping rates.

Gross has explained these effects quantitatively in terms of a De Vore type effect. This effect is a combination of the normal de Vore effect with a diffusion term to take account of exciton diffusion.

Exciton photoconductivity has been studied in Cu_2O by Apfel and Portis (1960); they found that for steady illumination at an exciton line the photoconductivity dipped, whereas for illumination chopped at 4 cycles/sec a peak occurred. Several other materials of intermediate properties, for example PbI_2, have been studied. PbI_2 is of particular interest because of its close similarity to CdI_2. There are some fundamental differences, however; the onset of optical absorption is at a much lower energy in PbI_2 and a very strong low energy exciton line has been observed.

Tubbs has investigated the optical absorption spectrum and made preliminary photoconductivity measurements. More recently Dugan and Henisch (1968) found photoconductivity from 1-7eV to 4.0eV. The photo-response peaked at 2.41eV corresponding to exciton formation and there was a shoulder at 2.64eV. There was also a peak at 3.06eV the origin of which was probably from a lower valence band. The quantum efficiency at the peak was about 10^{-4} electrons/incident photon.

In view of the above it appears that the low energy exciton lines in the alkali halides are not directly comparable with the exciton lines in CdI_2 near 6eV. These features in, for example, RbI lead to small

values of the internal quantum efficiency compared with that due to band to band transitions. The exciton binding energy in the alkali halides is large so that the probability of thermal dissociation is small.

There are similarities in the case of AgCℓ although the reflectivity data is somewhat sparse on the crystals used. The exciton line at 240mμ (5.17eV) does lead to photoconductivity in the same way as that due to the 220mμ (5.64eV) line in CdI_2.

In PbI_2, which has the same structure as CdI_2, excitation in the first exciton line leads to a peak in photoconductivity so that no comparison is possible with CdI_2. The high energy photoresponse of PbI_2 would be of great interest since the result could be compared with those from CdI_2.

The photoresponse of CdI_2 at RT and 180°K has been described. Particular attention was paid to the exciton photoconductivity which was of comparable quantum efficiency to the band to band response. Since the features of the quantum efficiency spectra improved markedly between RT and 180°K apparatus was designed to make measurements at lower temperatures. A double cryostat was therefore constructed to enable measurements to be made at liquid nitrogen and liquid helium temperatures.

REFERENCES

Apfel, J.H., and Portis, A.M., 1960, J.Phys.Chem.Solids 15, 33.

Ben Sira, M.Y., Pratt, B., Harnik, E., and Many, A., 1959, Phys.Rev. 115, 554.

Brahms, S., 1965, Phys.Letters 19, 272.

De Vore, H.B., 1956, Phys.Rev. 102, 86.

Dugan, A.E., and Henisch, H.K., 1968, Phys.Rev. 171, 1047.

Fotland, R.A., 1959, Thesis, Case Inst. of Technology.

Goodman, A.M., 1959, J.Appl.Phys. 30, 144.

Greenaway, D.L., and Nitsche, R., 1965, J.Phys.Chem.Solids 26, 1445.

Gross, E.F., et al, 1964, Proc.Int.Conf.on Physics of Semiconductors, Paris, p.957.

Heyningen, R.S. and Brown, F.C., 1958, Phys.Rev. 111, 462.

Huggett, G.R., and Teegarden, K., 1966, Phys.Rev. 141, 792.

Sutter, P.H., and Norwick, A.S., 1963, J.Appl.Phys. 34, 734.

Sydor, M., 1967, Phys.Rev. 163, 873.

Tubbs, M.R., 1964, Proc.Roy.Soc. 280, 566.

Yu, R.M., 1969, J.Phys.Chem.Solids 30, 63.

CHAPTER FIVE

THE PHOTOCONDUCTIVITY OF CADMIUM IODIDE AT LIQUID NITROGEN AND LIQUID HELIUM TEMPERATURES

5.1 Introduction

The photoconductivity measurements described in Chapters Three and Four indicated that excitation at energies well above the intrinsic absorption edge leads to photocurrents of the same order of magnitude as those produced by excitation close to the edge. Some features in the spectra could be related to structure in the reflectivity spectrum. In particular the exciton reflectivity peak at 5.6eV caused a dip in the photoconductivity spectrum which was sharper at 180°K than at room temperature.

In view of the sharpness of the features of the photoconductivity spectrum at ~180°K compared with those at RT it seemed reasonable to study photoconductivity at even lower temperatures. The reflectivity spectrum of single crystals also sharpens considerably when the temperature is lowered to 77°K (Greenaway and Nitsche 1965).

The cryostat used previously was of the single reservoir, cold finger type and suffered from two serious drawbacks. The temperature of the specimen was much higher than that of the liquid nitrogen reservoir and a temperature gradient existed in the specimen because of heat input as radiation. The sample holder of P.T.F.E. was a source of high thermal resistance so that the temperature of the sample and holder was high. A liquid helium cryostat was therefore designed to eliminate these effects and to maintain temperatures of ~80°K and 4°K.

5.2 Design of Liquid Helium Cryostat

The liquid helium cryostat was designed with the primary aim of achieving temperatures near that of liquid helium, i.e. 4.2°K.

Since poor thermal contact and high thermal resistance caused the large temperature difference between the reservoir and sample found with the single stage cryostat, a more efficient thermal connection was necessary at liquid helium temperature. This was achieved by allowing the sample holder to be in direct contact with the copper block which formed one wall of the liquid helium container (see fig. 5.1). A sheet

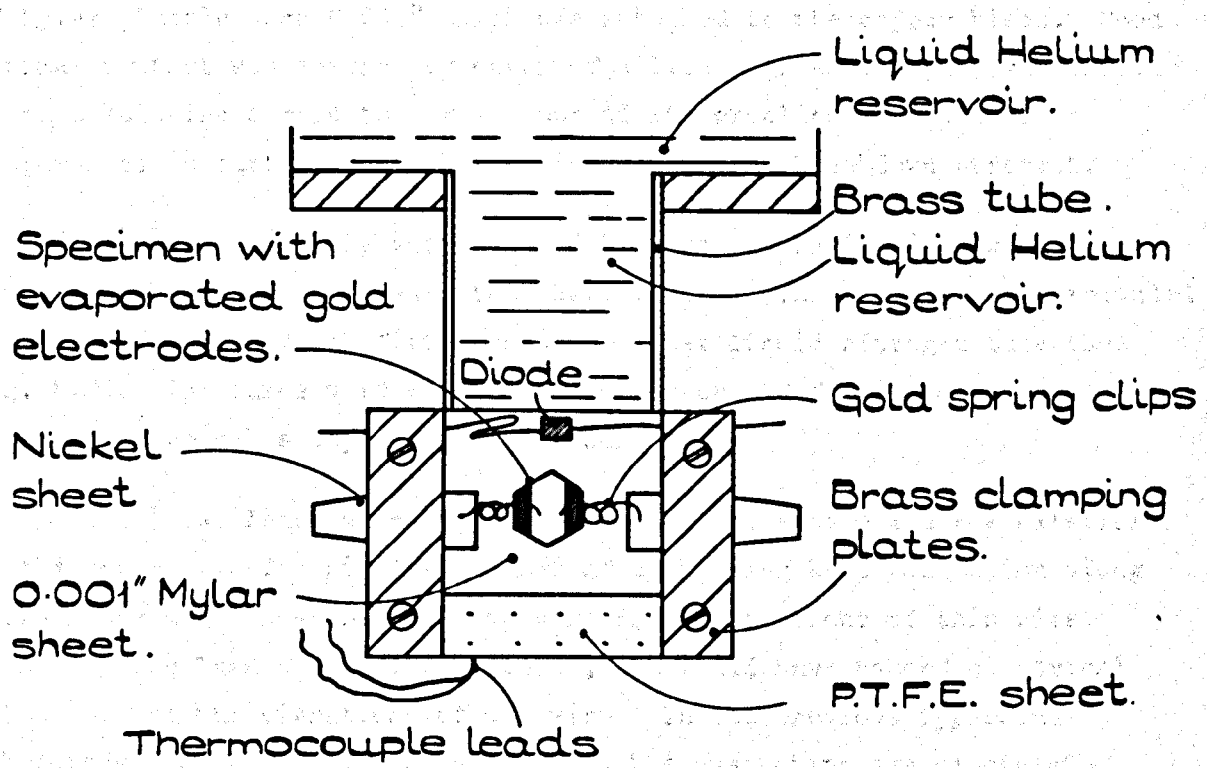

SPECIMEN HOLDER FRONT VIEW.

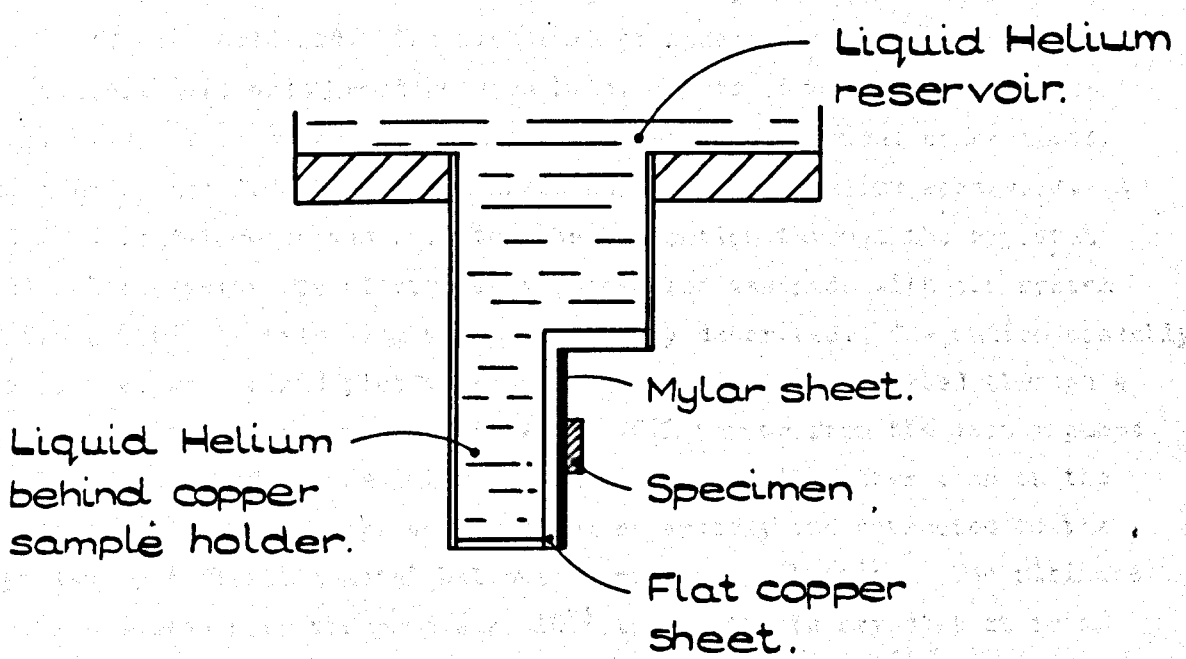

SPECIMEN HOLDER SIDE VIEW.

Fig. 5.1.

of Mylar plastic some 0.001" thick was attached to the copper block. Good thermal contact was ensured by means of silicone grease. Mylar was chosen as an insulating sample holder because of its excellent electrical properties; in particular it has a high electrical breakdown strength.

The sample assembly was enclosed by a copper heat shield which was a push fit onto the stainless steel helium tube. This shield was surrounded by a second shield which fitted onto the outer liquid nitrogen tube (see fig. 5.2). Apertures were cut in the copper shield for illumination of the sample through a suprasil outer window.

Electrical leads were necessary between the sample and the exterior of the cryostat. The simplest method of minimising heat conduction along these leads would have been to use very long connections of thin wire. Such a system lacked rigidity, however, and would have caused electrical noise through the vibrations of the wire. In the previous apparatus vibrations from external sources such as the evacuating system caused the electrical leads to vibrate, thereby generating noise signals. The optimum unsupported length was found to be ~20cm of ~36 S.W.G. wire.

The gold wire electrodes were supported by nickel sheet, to which they were soft soldered. The nickel sheet connectors were soldered to the copper wires and clamped between Mylar sheets on the sample holder (fig. 5.3). This system ensured a rigid set of electrical connections and a heat sink from the nickel sheet to the liquid helium reservoir. A P.T.F.E. lead-through was used to make connection through the cryostat wall. The cryostat to electrometer connection was made with the system of demountable interlocking wires previously described. The entire assembly was mounted on a rigid platform and the cryostat was evacuated through a side tube close to the top of the wall. Oil vapour from the vacuum pumps was then condensed on the outer liquid nitrogen wall rather than on the crystal. The vacuum pumps were mounted separately and connected to the cryostat by a flexible metal bellows to minimise vibration. The ultimate vacuum measured near the pump was 10^{-5} torr with the cryostat at room temperature.

5.3 The Specimen Holder

The central tube of the cryostat, which constituted the liquid helium reservoir, could be removed to position samples on the sample holder. A Mylar sheet was attached to the copper block by smearing silicone grease

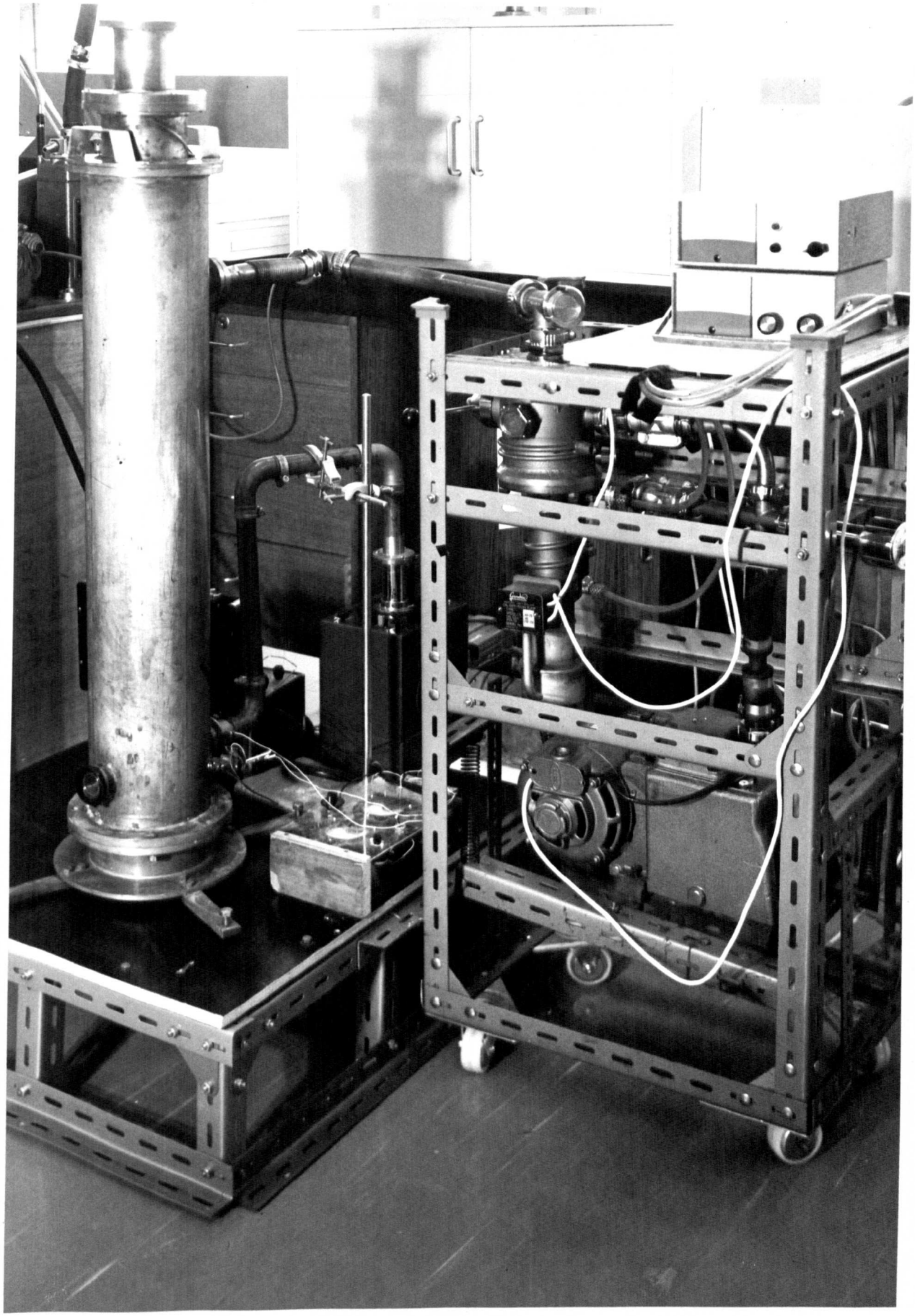

Fig. 5.2

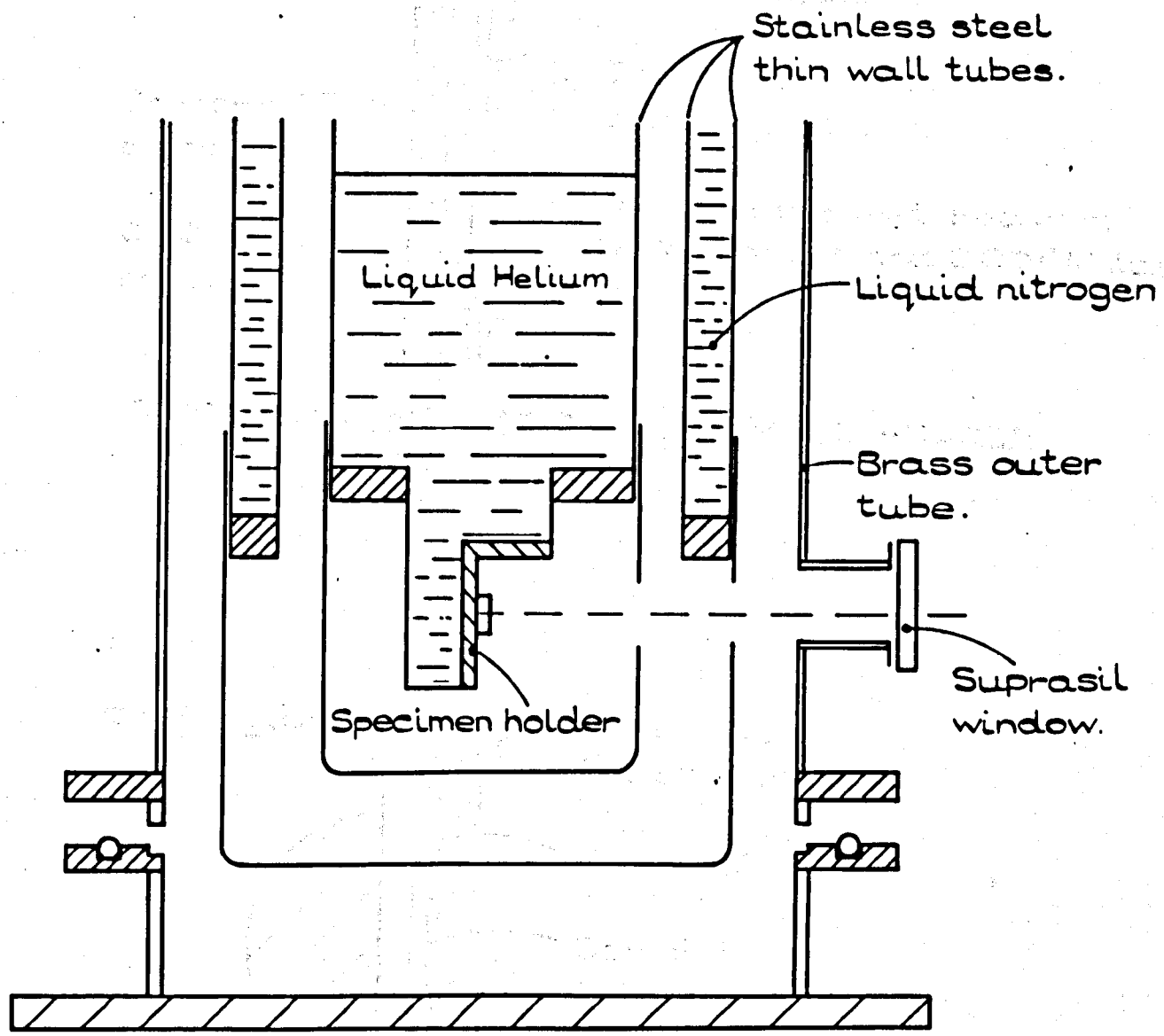

LOWER PART OF LIQUID HELIUM CRYOSTAT.

Fig. 5.2.

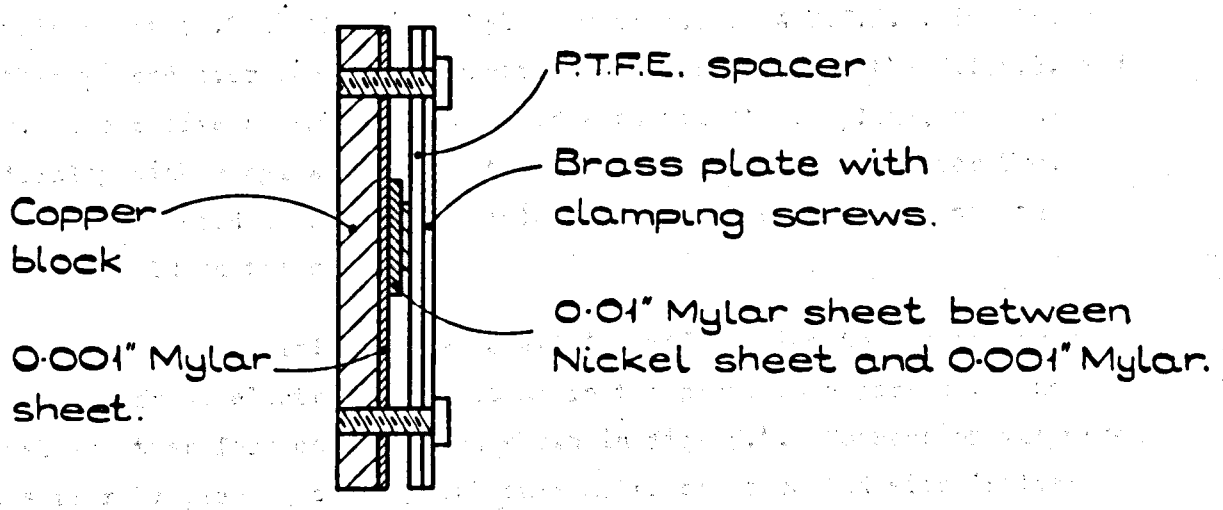

ELECTRICAL INSULATION OF SAMPLE HOLDER.
SIDE VIEW.

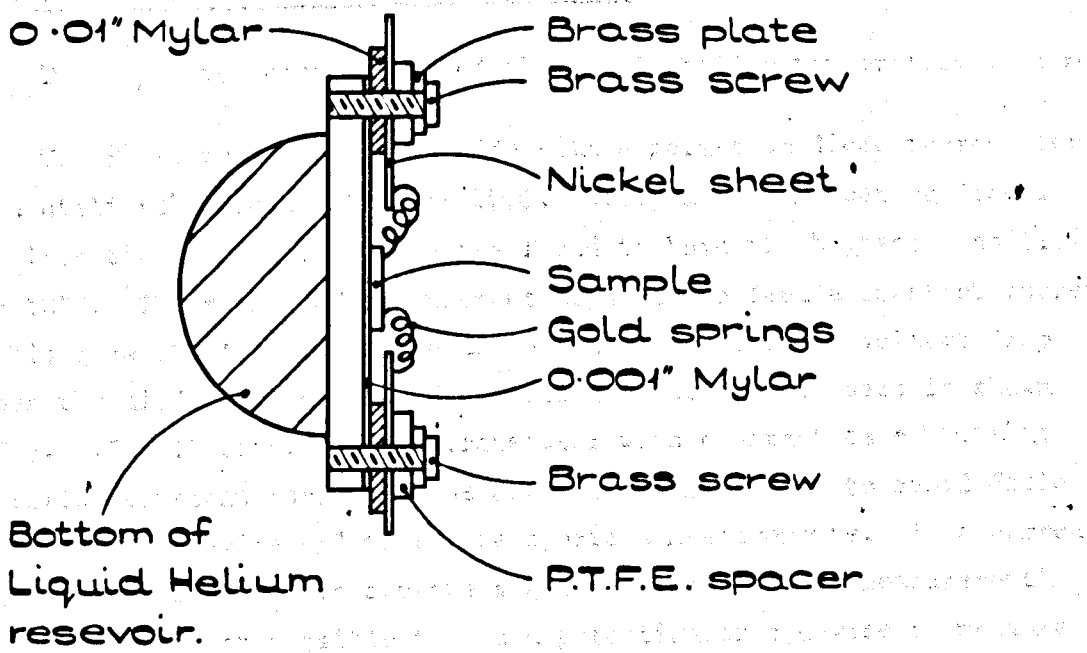

SAMPLE HOLDER VIEW FROM BELOW.

Fig. 5.3.

onto the copper. Two pieces of Mylar some 0.01" thick were placed underneath the nickel electrode holders to prevent the nickel sheet piercing the thin sheet (0.001" thick) of Mylar underneath. A P.T.F.E. insulator was then placed over the nickel electrode holders between the P.T.F.E. and Mylar. The entire assembly was cleaned with trichlorethylene, acetone and finally with ethyl alcohol in the manner described in Chapter Two. Silver dag was used to cement the gold spring clip electrodes onto the evaporated gold on the crystal.

It was not possible in the 'c axis' configuration to use the cold finger as a front electrode support as in the previous apparatus. The crystal was therefore connected as shown in fig. 5.4. Connection was made to the rear by placing the crystal on a Mylar sheet coated with 'silver dag'. The rear evaporated gold electrode was then in contact with the 'silver dag' which was in contact with a nickel sheet. The front electrode consisted of two evaporated gold strips connected by means of nickel sheet and copper wire. The rear electrode was the electrometer 'High' electrode.

5.4 The Measurement of Sample Temperature

Two separate measurements of the sample holder temperature were made.

The first measurement was made with a germanium diode thermometer, which utilised a diode I.R. type IODI. Several semiconducting diodes were investigated and this type was found to have the highest sensitivity near 10°K. The method of measurement used was to feed a constant current, in this case 100μA, through the diode and to measure the voltage drop across the diode in the forward direction. The circuit used is shown in fig. 5.5. It consists of a transistor with constant base biassing to provide constant current. The current was minimised to avoid Joule heating of the device and therefore spurious measurements. This current was, however, required to operate a galvanometer voltage measurement device. It was not possible to use a potentiometric device to measure the voltage drop because of feedback into the transistor circuit. A PYE scalamp galvanometer was used with a sensitivity of 1 Megohm/volt on all ranges. The current drain was therefore 1μA at F.S.D. and caused a negligible error, since the device was calibrated with the scalamp in circuit. The heating effect of the 100μA current was found to be negligible and was tested by observing the variation of the e.m.f. with time after switching on.

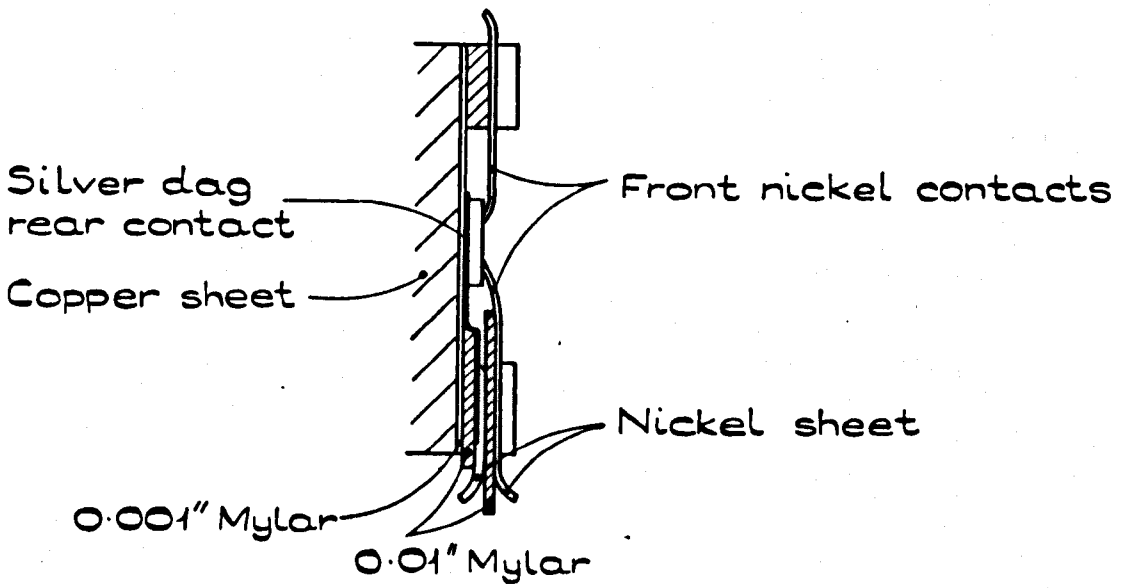

"C AXIS" SPECIMEN HOLDER FROM BELOW.

Fig. 5.4

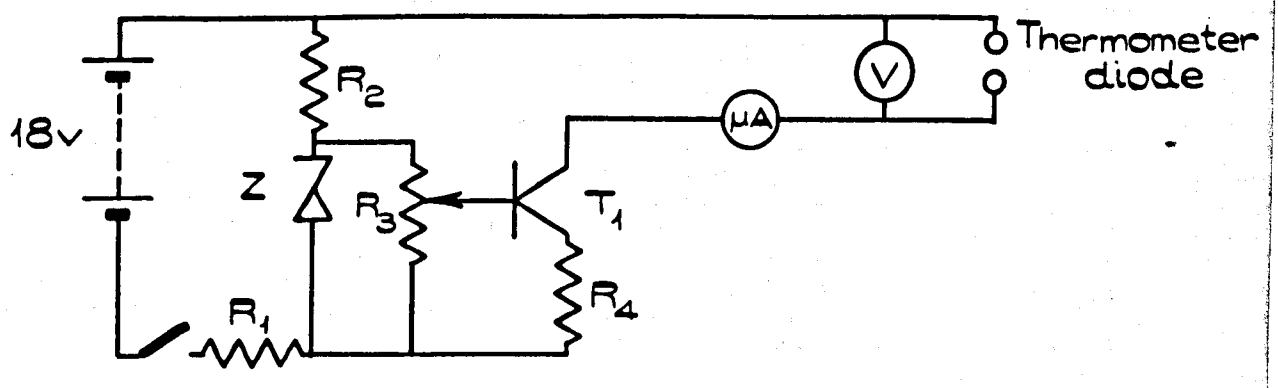

R_1 = 4,700Ω , R_2 = 510Ω , R_3 = 15KΩ , R_4 = 10KΩ,
Z = Zener Diode (9v)
T_1 = Transistor C424 NPN Type.
μA Meter 100 A F.S.D.
Voltmeter Pye Scalamp , 1MΩ Resistance.

CIRCUIT DIAGRAM OF CONSTANT CURRENT DEVICE.

Fig. 5.5

The germanium thermometer was calibrated against a copper-constantan thermocouple and using fixed points. The thermocouple junction was wrapped round one lead of the diode as close to the body of the diode as possible thereby ensuring that the two devices were at the same temperature. The assembly was placed in a copper tube of $\frac{1}{4}$" I.D., the outside of which was thermally insulated with tape. The entire assembly was then lowered into a dewar containing a quantity of liquid helium. The other thermocouple junction could be maintained at liquid helium or nitrogen temperature. The output of the thermocouple was fed into a Keithley Microvolt-Ammeter and displayed on a chart recorder. The assembly was then allowed to warm up by being slowly raised from the liquid helium reservoir. The temperature of the diode was then recorded continuously on the chart and could be compared with the potential drop across the device. In this way the diode thermometer was calibrated at 4.2°K and 77°K and at intermediate and higher temperatures using the thermocouple calibration data of Powell, Bunch and Corruccini (1961).

In the liquid helium cryostat the diode was placed on the sample holder so that it was lightly pressed against the Mylar sheet. A small quantity of silicone grease was used to ensure good thermal contact and to minimise the pressure required to maintain contact. This device was positioned near the top of the sample holder, the thermocouple was placed in a similar manner near the bottom.

The calibration curve obtained with the diode is illustrated in fig. 5.6. The sensitivity is high up to ~24°K. Between 4.2°K and 7°K the sensitivity was 0.16V/°K but fell to a lower value between 24°K and 70°K. The temperature error in the latter case was 10%. At higher temperatures the sensitivity increased. The copper constantan thermocouple sensitivity increased rapidly with temperature (fig. 5.7), so that when the diode sensitivity fell near 30°K the thermocouple potential could be measured. The Keithley electrometer was not available for the thermocouple measurements and a less sensitive Doran potentiometer was therefore used.

The leads from the temperature measuring devices were necessarily long to avoid heat input along the wires. They were thermally shunted to the liquid helium and liquid nitrogen reservoirs so that heat conducted along the wires travelled into the reservoirs and not into the thermometers.

CALIBRATION OF DIODE THERMOMETER
1R TYPE 1D21.

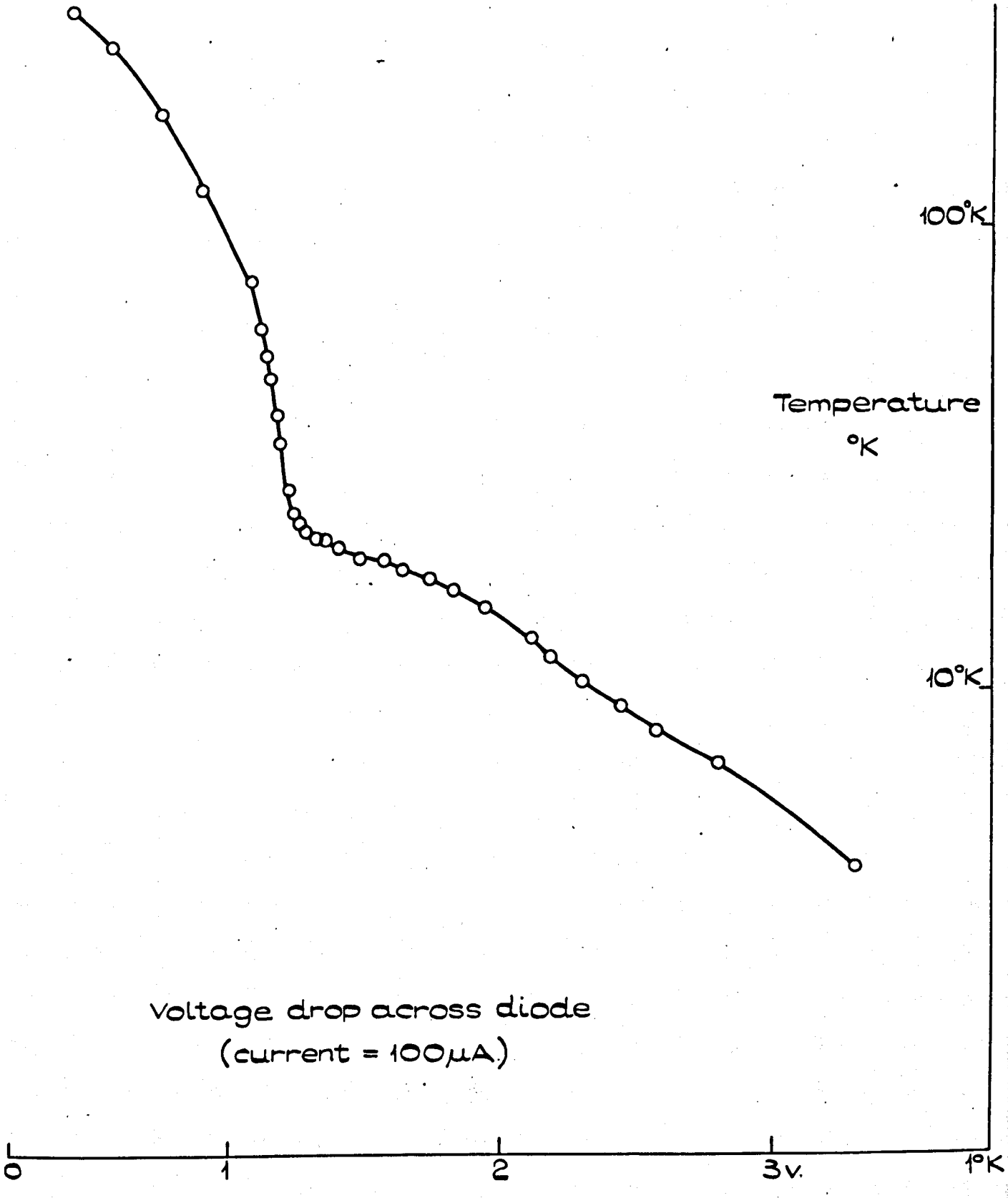

Fig. 5.6.

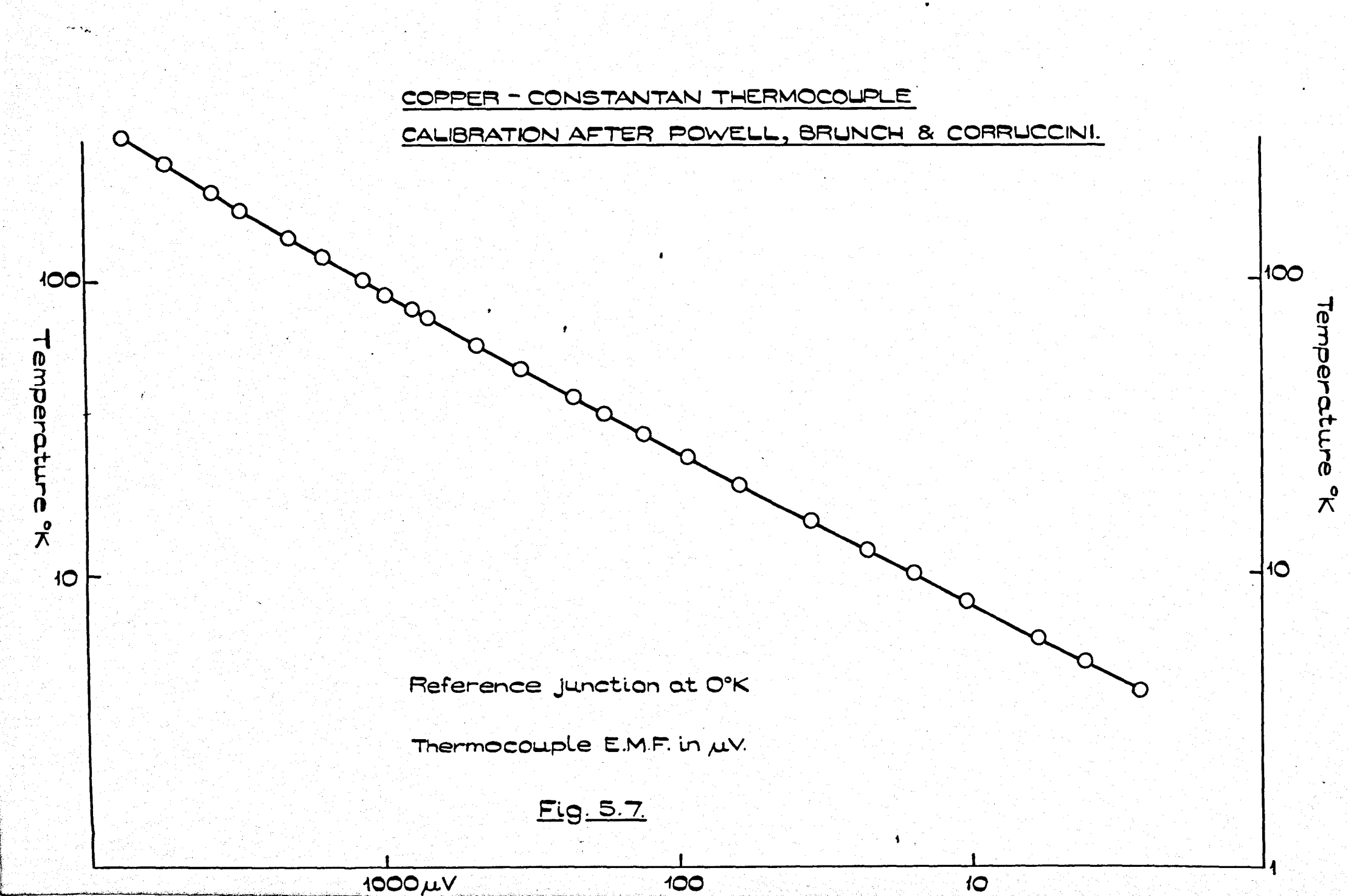
COPPER - CONSTANTAN THERMOCOUPLE
CALIBRATION AFTER POWELL, BRUNCH & CORRUCCINI.
100
10
Temperature °K
100
10
Temperature °K
Reference junction at 0°K
Thermocouple E.M.F. in μV.
1000μV
100
10
1

Fig. 5.7.

In the experiments liquid nitrogen was used to pre-cool both reservoirs, after which the inner container was emptied of liquid and flushed with helium gas before filling with liquid helium. The ultimate temperature recorded was 10°K with liquid helium in the inner vessel and 79°K when liquid nitrogen was used. Although these temperatures are not the temperatures of the sample, they represent the temperature of the diode which was in a similar position to the sample.

5.5 Room Temperature Photoconductivity Measurements in the Liquid Helium Cryostat

Initially photoconductivity measurements were made at room temperature (RT) to ensure that photoconductivity spectra obtained with this apparatus were similar to those previously obtained. There was some difficulty with early experiments because of a vacuum leak in the cryostat which occurred at low temperature only and destroyed two samples.

A room temperature spectrum is shown in fig. 5.8, it was obtained using the point by point method. The magnitude of the photocurrent, the spectral distribution, as well as the polarisation effects, were all in keeping with those found for previous samples and reported in Chapters Three and Four. One interesting effect which was noticed was a very slight dip below background when the illumination ceased. This effect occurred for 380-390mμ illumination and was probably caused by an ionic current produced by the polarisation field set up during the illumination.

A second sample used at RT with the scanning apparatus produced the spectrum shown in fig. 5.9. The spectrum although different in shape from the one shown in fig. 5.8 has many simularities, the difference was probably caused by a poorer surface quality in the first sample combined with different methods of measurement. According to De Vore (1956) increasing surface quality reduces the height of the low energy peak and in a perfect crystal there would be no peak in photoresponse. There was also a tendency for the low energy curve to be flattened when the scanning method was used.

There was a dip corresponding to the exciton line at ~5.6eV in both spectra. This dip disappeared when either spectrum was corrected for reflectivity loss. The dip was therefore a facet of the reflectivity

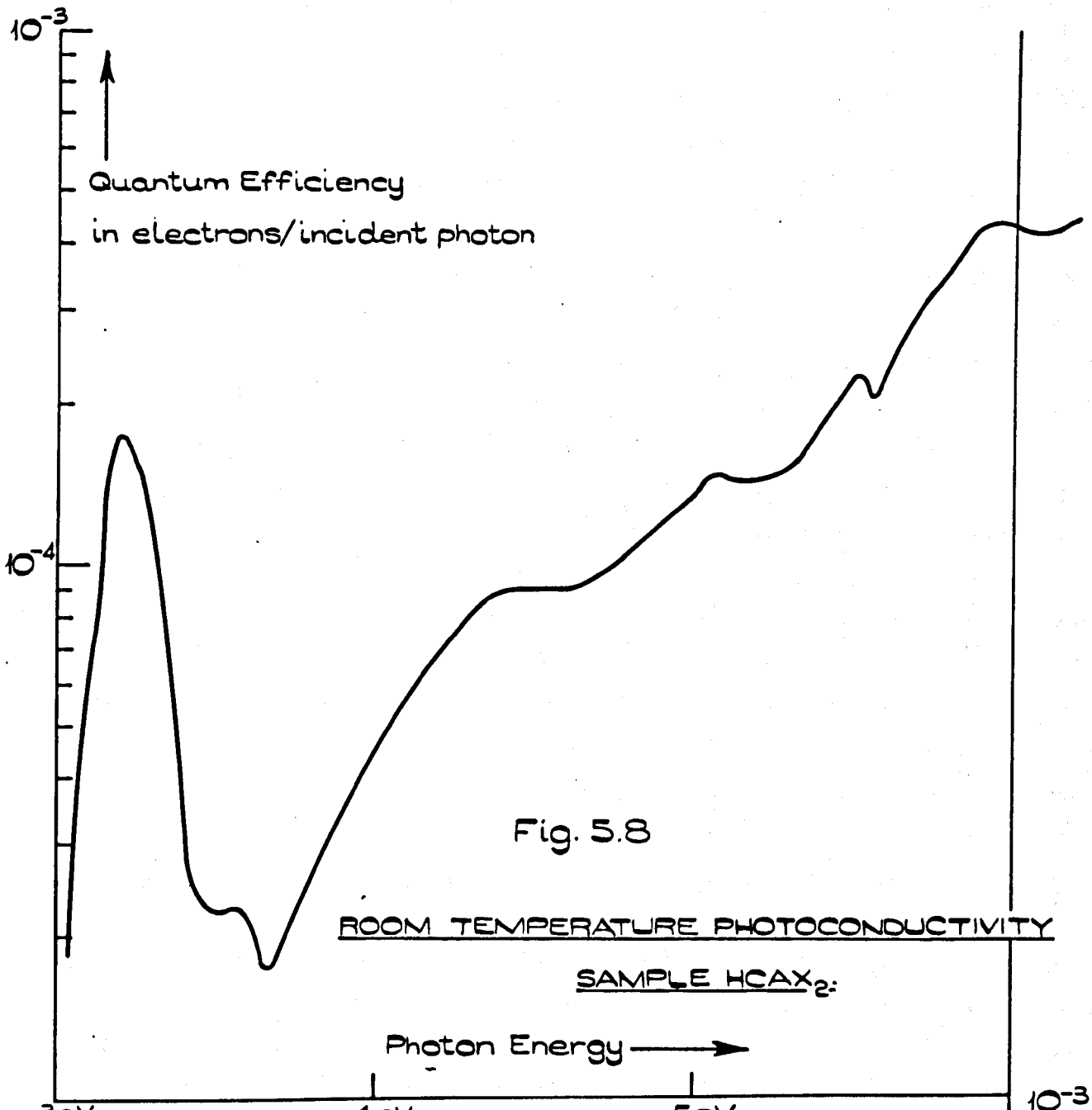

Fig. 5.8

ROOM TEMPERATURE PHOTOCONDUCTIVITY

SAMPLE $HCAX_2$:

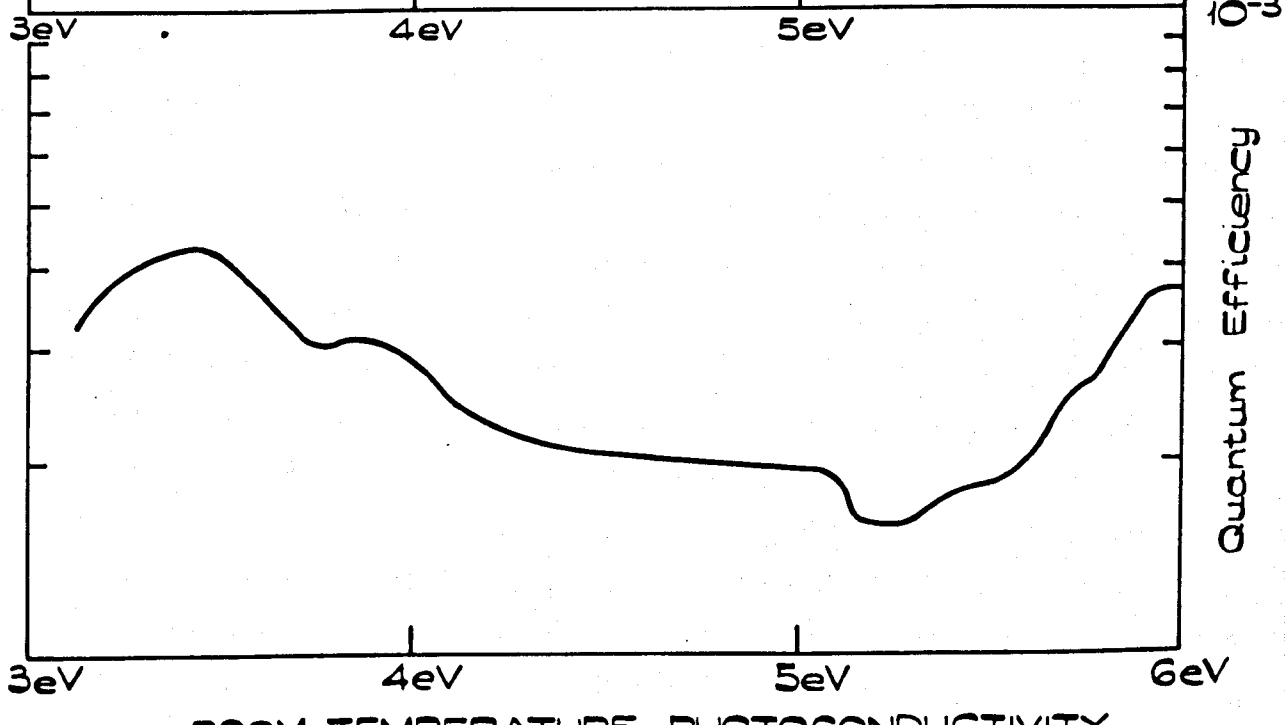

ROOM TEMPERATURE PHOTOCONDUCTIVITY.

SAMPLE $HCAX_3$:

Fig. 5.9

spectrum displayed in the photoconductivity response.

5.6 Liquid Nitrogen Temperature Measurements

The 80°K photoconductivity and reflectivity spectra have structure different from that previously described at 180°K. A typical spectrum obtained from sample $HCAX_4$ is illustrated in fig. 5.10. There are strong features in the spectrum near the exciton lines at 5.7 and 6.2eV. Also illustrated in fig. 5.10 is the reflectivity correction factor $1-R_2(\nu)$. The corresponding reflectivity spectrum was obtained using a cleaved single crystal in the liquid helium cryostat. There is a remarkable similarity between the inverse of the reflectivity correction curve and the photoconductivity spectrum before correction for the reflectivity loss. Much of the photoconductivity structure therefore appears to be caused by reflectivity loss.

One of the most significant features of the photoresponse curve is the position of the low energy photoresponse peak. The lowest energy feature of the photoresponse curve of fig. 5.10 is at 3.85eV whereas the lowest energy peak at RT was at 3.2eV. The equivalent peak at 180°K was near 3.4eV.

The high energy of the onset of photoconductivity (in $HCAX_4$) at 80°K using the scanning technique has been reproduced by the point by point method. The position of this feature is therefore independent of the method of measurement. Sample $HCAX_3$ had a low photosensitivity and it was therefore necessary to use a high intensity illumination to measure the photoresponse. A spectrum obtained using the scanning method with constant slit width is illustrated in figure 5.11. An interesting feature is the shoulder at 3.45eV, this feature was also present in some spectra obtained with the constant bandwidth technique.

It is clear from the above that the main low energy photoresponse feature is at 3.85eV at 80°K and that a faint shoulder was also present in some spectra at 3.45eV. The RT low energy peak corresponded with the position of the indirect absorption edge and with the extinction of the rear surface reflection in the reflectivity spectrum. The latter feature occurred at 3.45eV at 80°K so that the peak at 3.85eV does not correspond to the extinction of the rear surface reflection or to the indirect absorption edge.

It is therefore necessary to explain the shift of the photoresponse peak from the position of the indirect absorption edge to a higher energy and absorption coefficient when the temperature was lowered to 80°K.

5.7 Photoresponse Peak Position (De Vore Theory)

No absorption spectra were available for CdI_2 single crystals at 80°K. Thin film data have been presented (Tubbs 1968) but these do not extend to low absorption coefficients and are therefore restricted to high energies.

Since the RT photoresponse peak corresponds with the reflectivity feature at 3.18eV then the peak occurs when the extinction distance is of the same order as the crystal thickness. The peak at LNT is at a much higher value of absorption coefficient so that the peak corresponds to an extinction distance which is small compared with the crystal thickness.

The peak in photoconductivity, using the de Vore model, is caused by increased surface recombination at high values of absorption coefficient (de Vore 1956). The peak in photoresponse then appears at a value of αd corresponding to absorption throughout the sample so that $\alpha d \approx 1$, where α and d are the absorption coefficient and crystal thickness respectively. The only experimentally observed changes in the reflectivity spectrum at LNT are the higher energy (3.45eV) of the LNT step and the increased sharpness of this feature. Since the LNT step corresponds to a similar value of α to the RT step then the De Vore peak would not be affected by these changes. The photoresponse against photon energy curve, however, would be affected and the peak would in fact sharpen.

Since the peak in photoresponse has in fact shifted to a high value of αd at LNT compared with that at RT then several alternatives are possible. The surface recombination may, for instance, have been reduced relative to the volume recombination thereby increasing the surface sensitivity.

A similar effect has been observed in HgI_2 by Bube (1960, 1957) where the "surface excited" photoconductivity increased by a factor of ~100 relative to the "volume excited" photoconductivity when the temperature was lowered from 200°K to 100°K.

There was also the possibility of the electric field penetration depth being temperature dependent so that the electric field was constrained to the surface region at LNT. The 'c axis' results obtained at 80°K were in excellent agreement with those obtained with the alternative geometry so that this effect is not thought to be significant.

It is clear that the optical absorption feature near 4eV is of greater significance at LNT than at RT. This feature has been described by Tubbs (1968) as one member of an exciton doublet. He has suggested that an excitation model might be appropriate since a band-theoretical treatment has not been performed for this material or for any of the metallic layer structure dihalides. On the low energy side of the exciton line an associated band edge of the direct type was found. Tubbs' data were recorded with thin film CdI_2 specimens. Thin films of CdI_2 have been found to exhibit many structural properties similar to those of single crystals. We have also reproduced the basic features with single crystal reflectivity spectra. The spectra shown in fig. 4.11 were recorded in the same apparatus and under identical conditions to those of the photoconductivity experiments. It was necessary to use a standard reflector in place of the sample to calibrate the system. The standard used was an aluminium mirror whose reflectivity had been calibrated by measuring the incident and reflected intensities throughout the spectrum.

5.8 Photoconductivity Spectra after Reflectivity Correction

The photoresponse spectrum of sample $HCAX_4$ after correction for reflectivity loss is shown in fig. 5.12. The 3.85, 4.03, 4.75, 5.06 and 5.5eV features were still present. The strong dip in photoresponse at 5.7eV before reflectivity correction became a slight peak. It is clear that such a transformation depends upon the reflectivity correction factor at the exciton line. When a second correction, obtained from a different sample, was applied the shape in the exciton line region was noticeably different. The two reflectivity spectra were obtained under identical experimental conditions in the same apparatus so that the variation is due to a variation in the samples.

Reflectivity spectra have been recorded independently by Greenaway and Nitsche (1965) and by Brahms (1965). There is good agreement between our spectra and the other published results.

PHOTOCONDUCTIVITY AT 80°K.

CORRECTED FOR REFLECTIVITY LOSS (R_2)

SAMPLE $HCAX_4$.

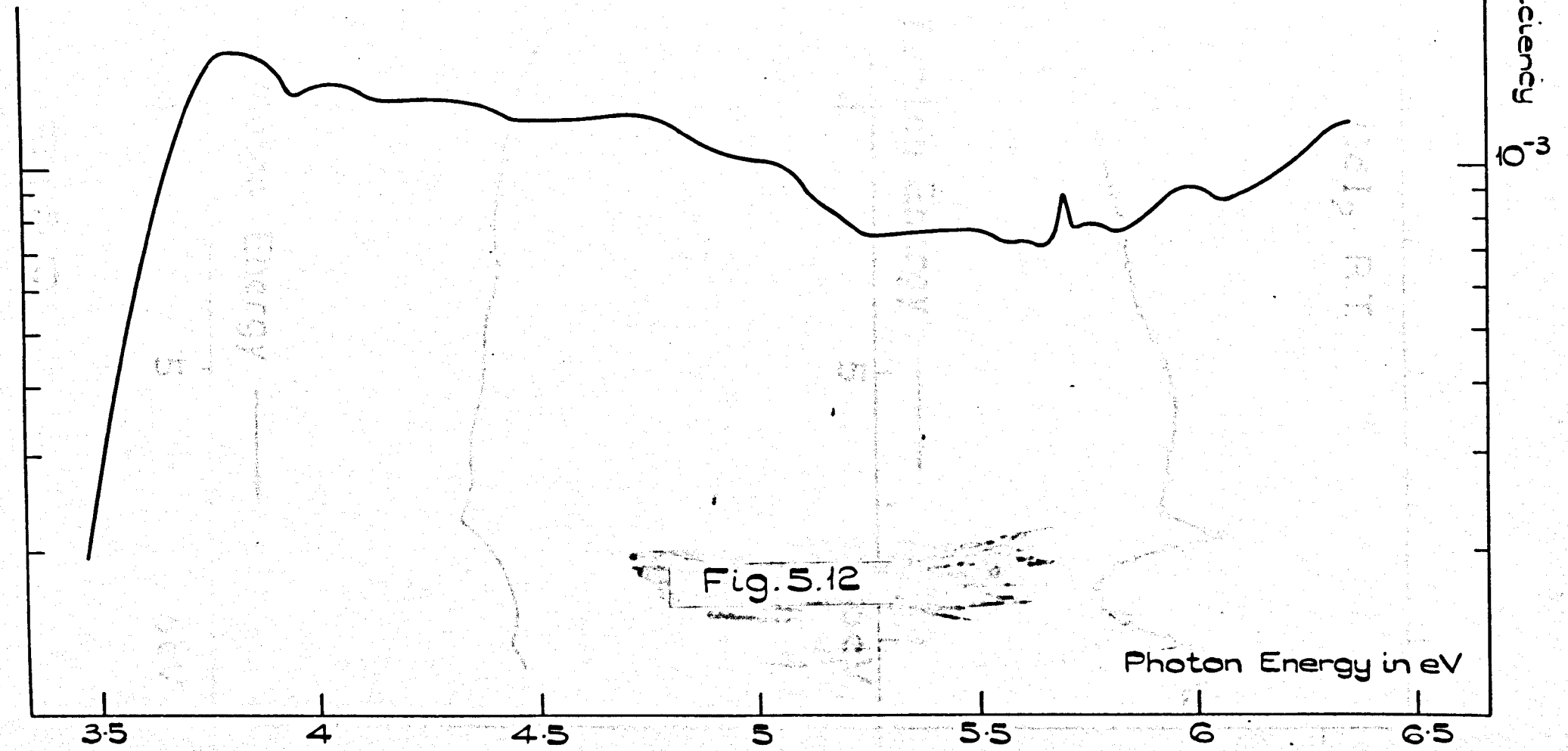

Fig. 5.12

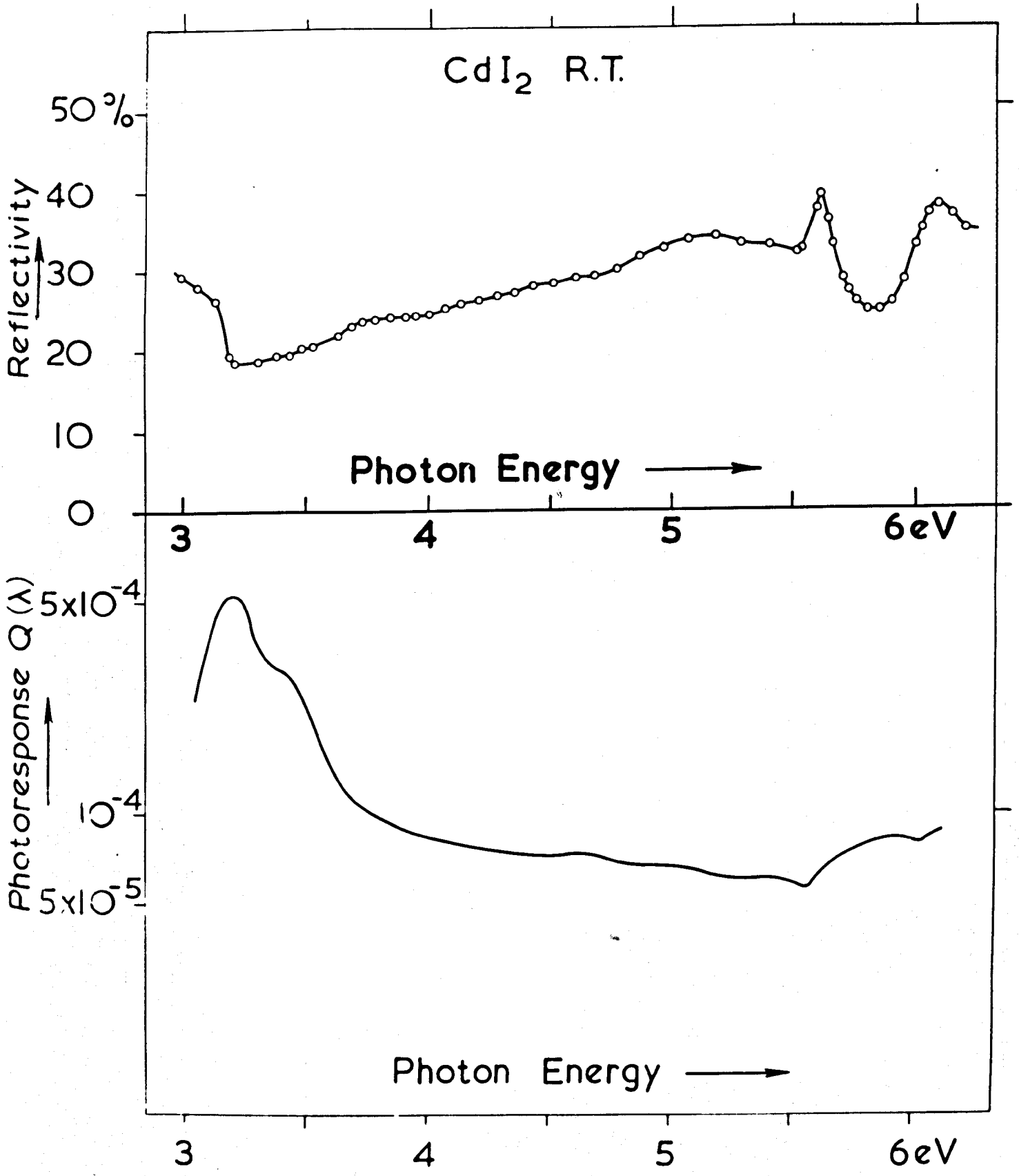
CdI2 R.T.
50 %
40
30
20
10
0
Reflectivity
Photon Energy
3
4
5
6eV
Photoresponse Q(λ)
5x10-4
10-4
5x10-5
Photon Energy
3
4
5
6eV

Fig. 5.10

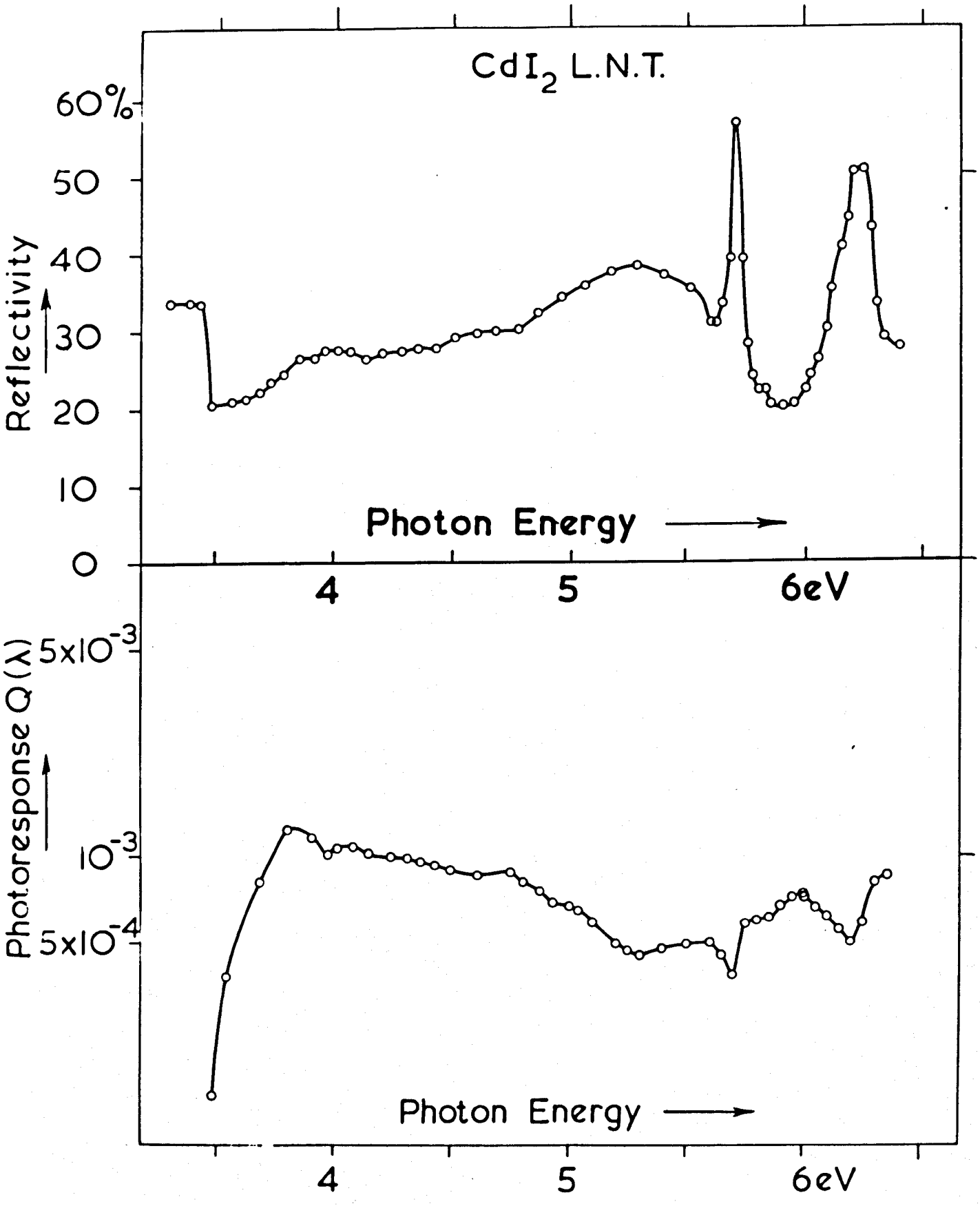
CdI2 L.N.T.
60%
50
40
30
20
10
0
Reflectivity
Photon Energy
4
5
6eV
5x10-3
10-3
5x10-4
Photoresponse Q(λ)
Photon Energy
4
5
6eV

Fig. 5.10

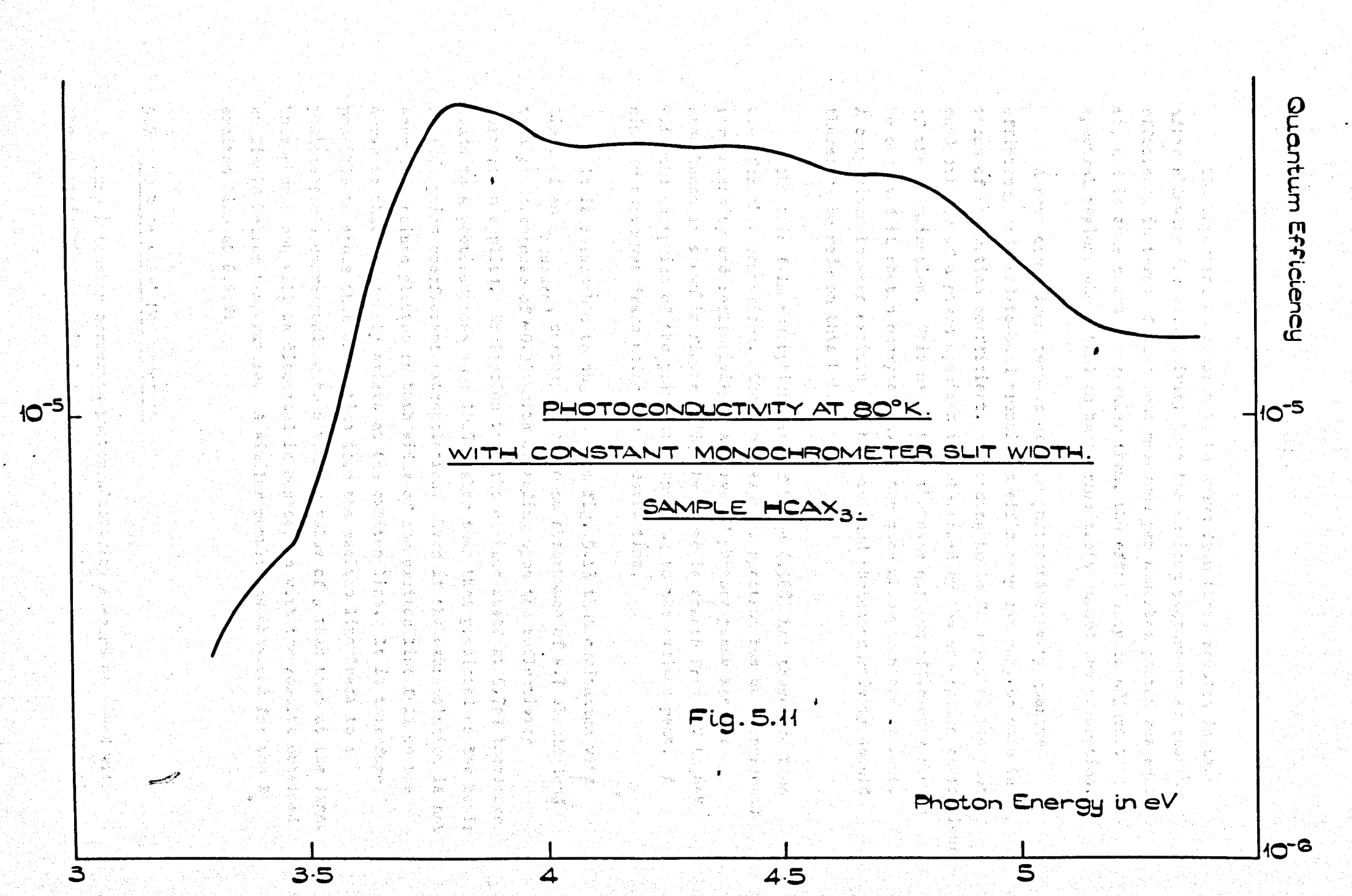
Quantum Efficiency
10^{-5}
10^{-5}
10^{-6}
PHOTOCONDUCTIVITY AT 80°K.
WITH CONSTANT MONOCHROMETER SLIT WIDTH.
SAMPLE HCAX3.
Photon Energy in eV
3
3·5
4
4·5
5

Fig. 5.11

The important conclusion to be drawn from these results is that after allowing for reflectivity loss the exciton photoresponse quantum efficiency in terms of electrons measured per absorbed photon was equal to, and in some cases 20% greater than, the efficiency in adjacent spectral regions where band to band transitions caused the absorption.

A real comparison between exciton photoconductivity quantum efficiency and band-to-band transition efficiency can only be made in terms of absorption coefficient. According to De Vore (1956) the photoconductivity of a given specimen is determined by the absorption coefficient of the illumination. This means that the same quantum efficiency should be observed at photon energies having the same absorption coefficient. A comparison between exciton and band-to-band photoconductivity should therefore be made on this basis.

The thin film absorption data of Tubbs (1968) has therefore been used for this comparison. The photoresponse spectrum has been corrected for intensity and reflectivity. A curve of photoresponse against absorbance is shown in figure 5.13, the curve is smooth from 4eV to 6eV with the exception of the point corresponding to the exciton peak. A similar curve was drawn using the R_1 correction.

It is reasonable to suggest from fig. 5.13 that excitation with light of an $\alpha_{measured}$ corresponding to an absorbance of 4.7 should lead to a photoresponse of ~0.35 units depending upon the reflectivity correction applied. Excitation into the exciton state at 5.7eV therefore leads to a photoresponse some 100% higher than that predicted on the basis of absorption coefficient extrapolation. Even if the extrapolation is not accepted, points plotted on both sides of the exciton line fell on the curve so that an anomaly exists at the exciton line. It is therefore possible to state that excitation into the exciton line leads to a photoresponse corresponding to a smaller value of α than that at the line. This phenomenon will be discussed in connection with the results obtained at liquid helium temperature. A similar result was obtained for the X_4 exciton line at 6.2eV.

5.9 80°K 'c axis' Measurements

Some intensity corrected photoconductivity spectra obtained with the electric field parallel to the c axis are illustrated in fig. 5.14.

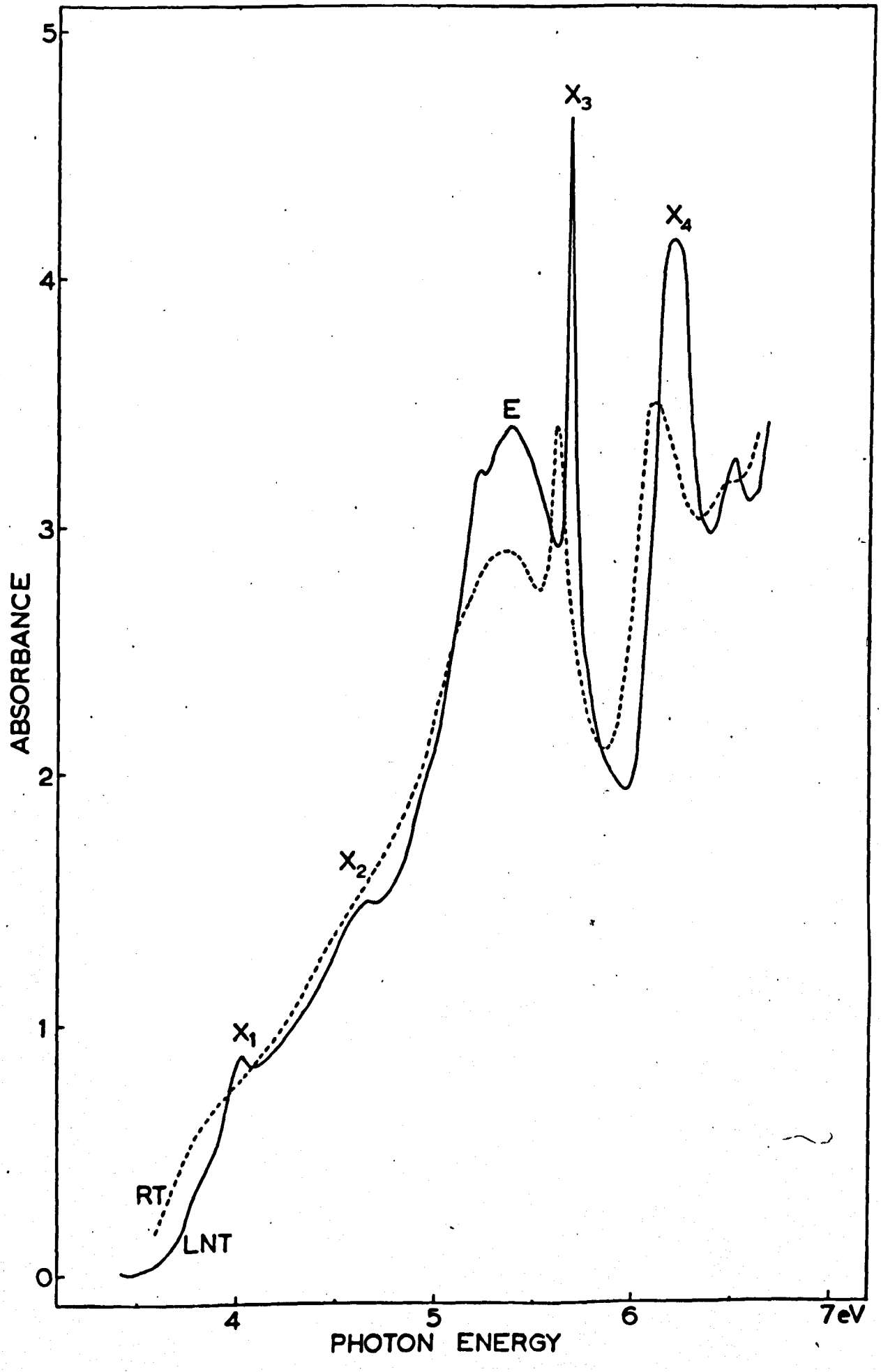

Fig. 5.13

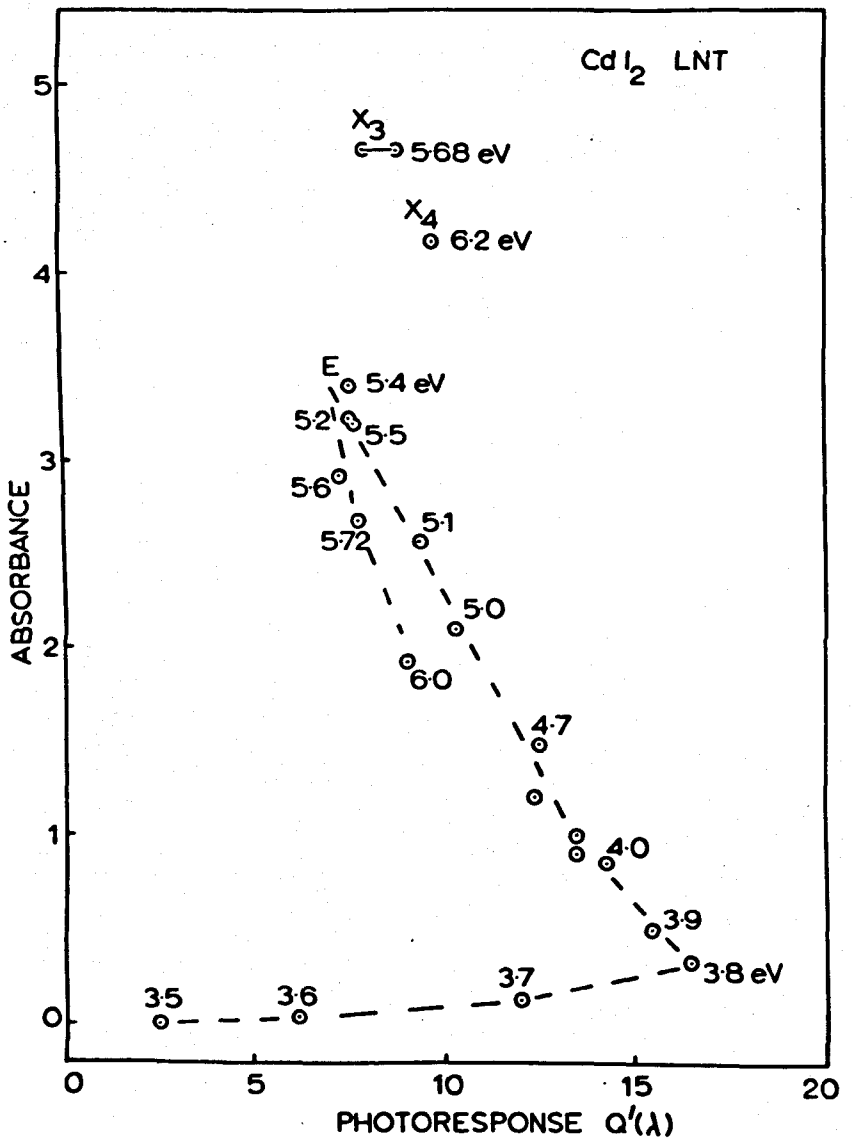
Cd I2 LNT
X3
5·68 eV
X4
6·2 eV
E
5·4 eV
5·2
5·5
5·6
5·72
5·1
5·0
6·0
4·7
4·0
3·9
3·8 eV
3·5
3·6
3·7
ABSORBANCE
PHOTORESPONSE Q'(λ)
0
1
2
3
4
5
0
5
10
15
20

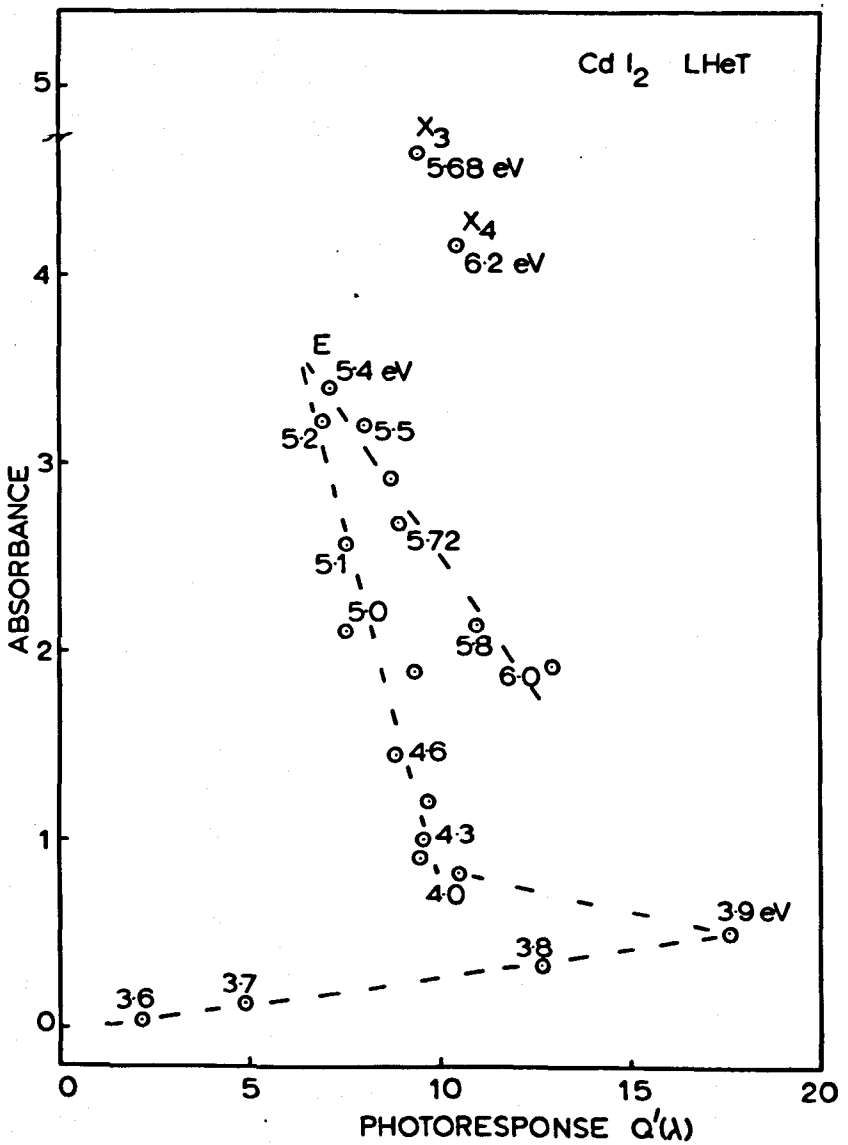
Cd I2 LHeT
X3
5·68 eV
X4
6·2 eV
E
5·4 eV
5·2
5·5
5·72
5·1
5·0
5·8
6·0
4·6
4·3
4·0
3·9 eV
3·8
3·6
3·7
ABSORBANCE
PHOTORESPONSE Q'(λ)
0
1
2
3
4
5
0
5
10
15
20

Fig. 5.13

SPECTRAL DISTRIBUTION OF PHOTOCONDUCTIVITY AT 80°K.

(C AXIS SAMPLE HCCX$_1$)

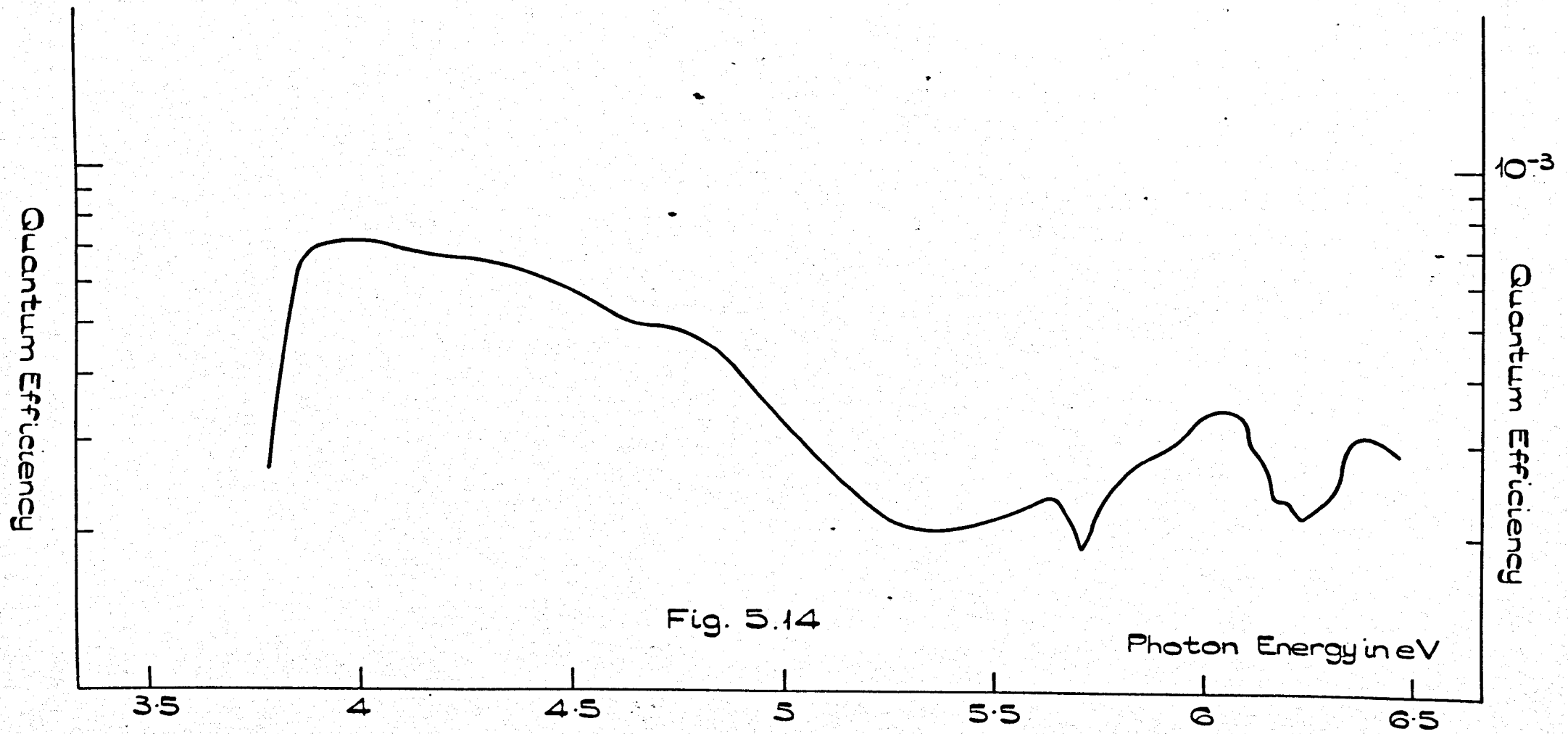

Fig. 5.14

There was some indication of a slight shift 0.01eV between scanning directions due to the response time of the system. There was an appreciable difference at low energies, however, the curve corresponding to scanning from low energies ($\Delta\lambda\theta$) peaked at 3.95eV whereas the curve for the opposite scanning direction ($\Delta\lambda\theta$) peaked at 3.84 and 4eV. This effect has been discussed in Chapter Four and is a polarisation effect. Scanning from low energies shifts the low energy peak to higher energies because of the time constant of the low energy response. Scanning from high energies tends to reproduce the high energy spectrum accurately until at the low energy edge polarisation occurs and the response falls, there is neglibible polarisation at the low energy side of the edge so that the response increases.

The curves have similar forms near the 5.6eV line and after correction for reflectivity loss the dip became a peak of some 25%.

These results show that both 'a' and 'c' axis geometries yield almost identical spectra. This indicates that discrepancies between 'a' and 'c axis' samples found previously were environmental effects probably due to different sample temperatures in the two electrical geometries.

5.10 Liquid Helium Temperature Measurements

Since optical spectra, particularly in exciton regions usually sharpen markedly near liquid helium temperatures, the photoconductivity and reflectivity measurements were extended to this temperature. The photoconductivity measurements were made more difficult by the increased polarisation effects.

The reflectivity spectrum did in fact improve when the temperature was lowered to 10°K. The reflectivity shown in fig. 5.15 rises to 60% at the 5.7eV exciton line and falls to 16% on the high energy side of the line and to 35% on the side of the low energy peak at 5.3eV.

The photoconductivity spectrum measured at 10°K also exhibited sharper structure. Figure 5.16 illustrates results obtained from sample $HCAX_4$; a corresponding spectrum after correction for reflectivity loss is also illustrated in this diagram.

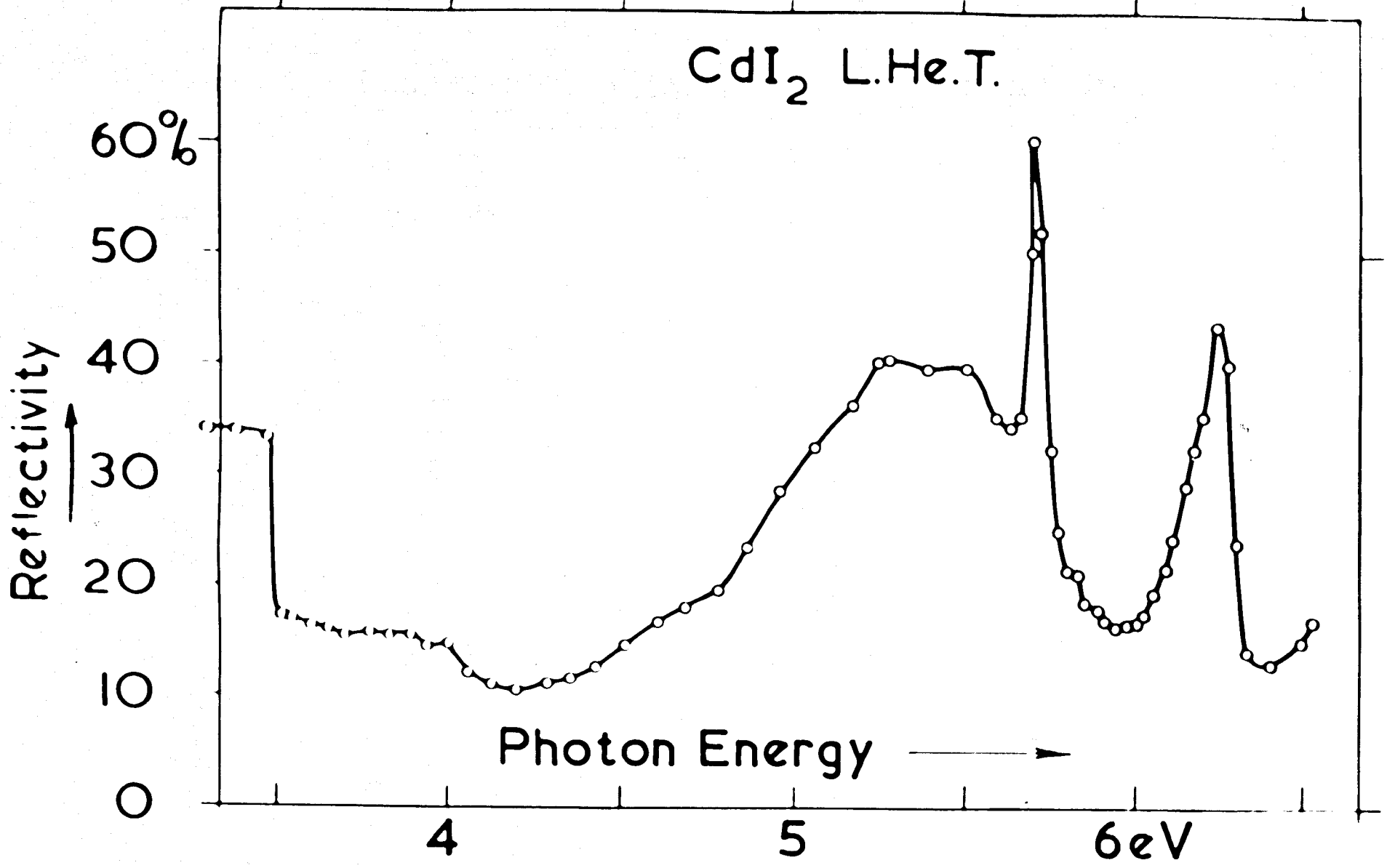
CdI2 L.He.T.
60%
50
40
30
20
10
0
Reflectivity
Photon Energy
4
5
6eV

Fig. 5.15

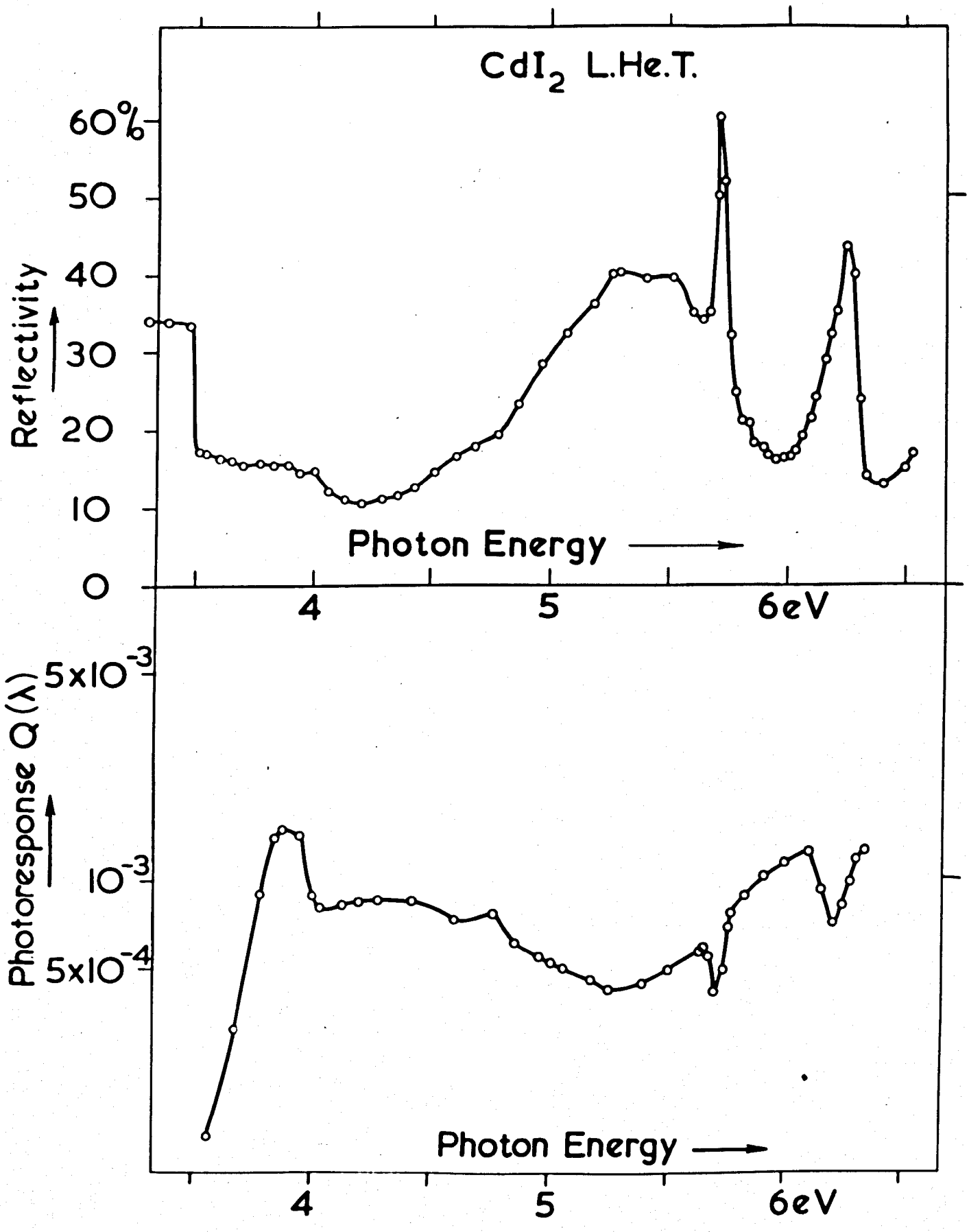
CdI2 L.He.T.
60%
50
40
30
20
10
0
Reflectivity
Photon Energy
4
5
6eV
5x10-3
10-3
5x10-4
Photoresponse Q(λ)
Photon Energy
4
5
6eV

Fig. 5.16

PHOTOCONDUCTIVITY AT 10°K CORRECTED FOR REFLECTIVITY LOSS(R_2).

SAMPLE $HCAX_4$:-

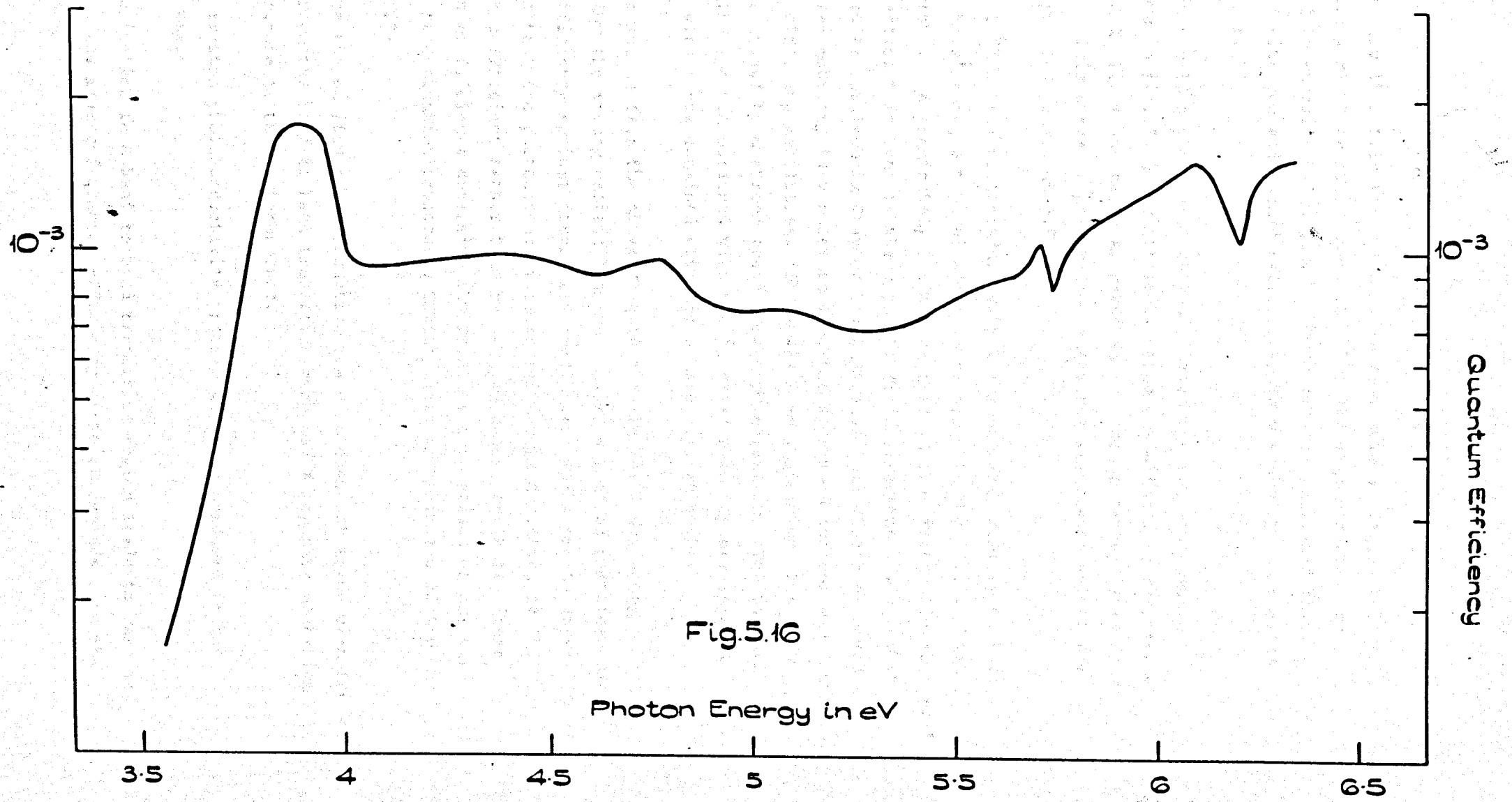

Fig.5.16

The only thin film absorption data available at liquid helium temperature were those of Brahms (1965) but the measurements were restricted to energies below 5.2eV. These results indicated that the liquid nitrogen and liquid helium temperature absorption spectra were similar.

When the $10^{o}K$ photoresponse was plotted against absorbance the curve shown in fig. 5.13 was obtained. Once again the photoresponse at the X_3 and X_4 lines was twice as great as the values extrapolated from the curve. This curve of photoresponse against absorbance was of the De Vore type and peaked at 3.9eV.

The $10^{o}K$ 'c axis' photoconductivity was remarkably similar to that in the 'a axis' case; a typical spectrum is shown in fig. 5.17. The photocurrent was approximately 5 times greater in the 'front electrode +ve' field direction than that in the opposite field direction. The Dember effect results obtained in Chapter Six indicated that electrons moved with greater mobility than holes so that the increased current was not caused by differing mobilities. There was some indication that the effect was caused by a strong space charge polarisation. The overall shape of the spectra obtained with the 'c axis' geometry are in good agreement with those obtained with the a axis configuration.

We conclude from the above results that in the lower energy region below the strong exciton line near 5.7eV a plot of photoresponse quantum efficiency against absorption coefficient was a smooth curve. This means that the photoconductivity efficiency is dominated by the absorption coefficient rather than by the processes involved. These absorption coefficients determine the relative proportions of surface to volume recombination processes, thereby leading to curves of the De Vore type.

Since the exciton photoconductive response does not agree with the value expected from the band to band transition response a separate mechanism must contribute to the photoresponse.

The exciton photoconductivity problem may be considered in the following way.

Illumination in a band to band transition region leads to carrier generation, the measured quantum efficiency of which depends upon the

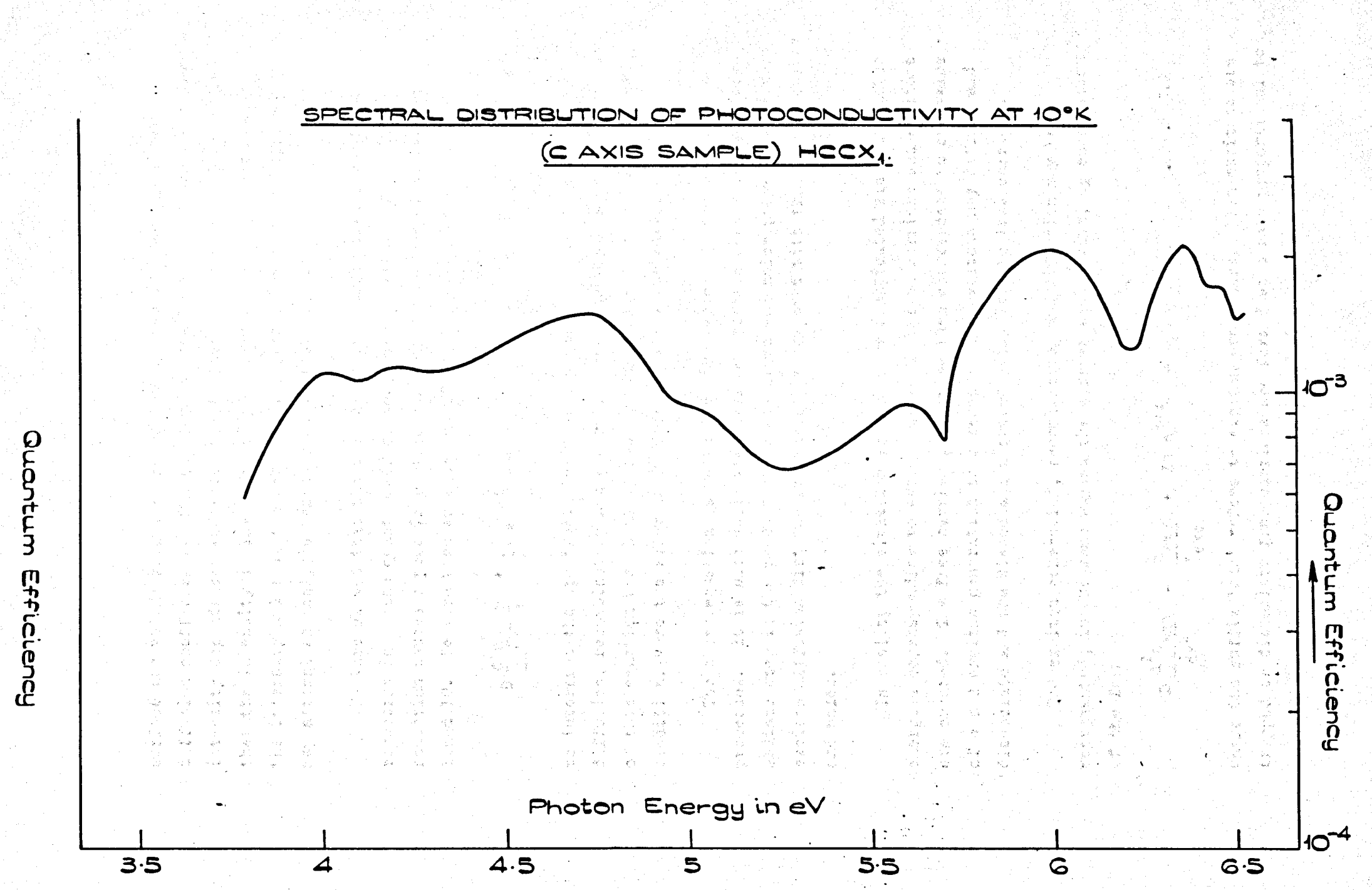
SPECTRAL DISTRIBUTION OF PHOTOCONDUCTIVITY AT 10°K
(C AXIS SAMPLE) HCCX1.
Quantum Efficiency
Quantum Efficiency
10-3
10-4
Photon Energy in eV
3·5
4
4·5
5
5·5
6
6·5

Fig.5.17

surface and volume recombination rates and the relevant lifetimes and diffusion coefficients. The problem is usually complicated by non-linear intensity dependences and reflectivity loss corrections. If we assume that the intensity is low so that the photocurrent is proportional to the intensity and that the reflectivity correction has been applied we may attempt an analysis based on De Vore's theory.

De Vore showed that the surface recombination term leads to a reduction in η, the quantum efficiency, at high values of α. This reduction causes a peak in photoconductivity at values of αd between 1 and 10. De Vore used an equation of the form

$$D \frac{d^2n}{dx^2} - \frac{n}{\tau} + I\alpha e^{-\alpha x} = 0 \quad . \quad . \quad . \quad . \quad . \quad . \quad . \quad . \quad 5.1$$

to interpret the spectrum. The terms in the equation are those of diffusion, recombination and generation respectively. A general solution of this equation was obtained and boundary conditions imposed. These conditions were the relevant surface recombination rates.

The above equation is valid for single-step electron production processes. It is also valid when exciton creation occurs as an intermediate step in the production of electrons and holes provided that the exciton diffusion distance is negligible compared with that for electrons and holes.

In reality the situation is much more complicated since at photon energies corresponding to exciton peaks both free carriers and excitons are created. The free carrier generation then corresponds to one value of α and exciton generation to a second. The excitons may diffuse and dissociate and the dissociation process will lead to free carriers.

The exciton generation, recombination and diffusion may be represented, in the same way as the carrier equilibrium, by an equation of the form

$$D \frac{d^2n_{exc}}{dx^2} - \frac{n_{exc}}{\tau_{exc}} + I\alpha e^{-\alpha x} = 0 \quad . \quad . \quad . \quad . \quad . \quad 5.2$$

where the suffix 'exc' refers to exciton properties. When excitons are trapped or dissociate free carriers are formed at a rate proportional to

$\frac{n_{exc}}{\tau_{exc}}$. A full description of exciton photoconductivity therefore necessitates the inclusion of the above term in the band-to-band transition generated carrier diffusion equation (5.2). Alternatively the two processes may be considered separately, the total carrier density being regarded as the sum of two terms, one from direct carrier generation and the second from exciton dissociation. The latter viewpoint was adopted by Gross (1964) who calculated curves of photoresponse against $(\alpha_o + \alpha)L$ where α_o, α and L are the exciton and band to band transition absorption coefficients and L is the free carrier diffusion length. The exciton surface recombination velocity was nine times greater than that for electron-hole pairs. Four curves were plotted, one for each value of the ratio $\frac{Le}{L}$ where Le is the exciton diffusion length. The photoresponse decreased with increasing values of $\frac{Le}{L}$, the four values of this quantity plotted were 0, 10^{-4}, 10^{-2} and unity. The first curve approached an asymptotic value of ~0.5 at high values of $(\alpha_o + \alpha)L$ whereas the others tended towards a value of ~0.1; the value of $(\alpha_o + \alpha)L$ was then $\approx 10^5$.

This result indicates that when the exciton surface recombination is high compared with that for free carriers increasing exciton diffusion reduces the photocurrent. The surface free carrier recombination rate must therefore be lower than that for the rest of the sample.

Our results indicate the opposite effect to that described above and are interpreted as follows.

Most of the oscillator strength in the exciton line is taken up with exciton formation so that the number of carriers produced directly will be less than the number of excitons produced. If we assume that excitons dissociating near the crystal surface lead to higher electron-hole recombination rates than those diffusing into the crystal bulk then formation of these excitons reduces the surface recombination and therefore increases the number of carriers available for photoconductivity. Since the number of free carriers produced directly is small, then the exciton diffusion coefficient and surface recombination velocity determine the free carrier density and therefore the photoresponse. For a given surface, increasing exciton diffusion increases the number of free carriers by reducing the surface recombination rate.

One method of testing this hypothesis would be to use thin crystals, whose thickness was the same order of magnitude as the exciton diffusion length. Goto (1965) has used this technique on thin film specimens, although there are then difficulties of interpretation because of structural variations with film thickness. The film structure should therefore be determined, for example, by electron diffraction and microscopy, in order to remove this possible difficulty. Some film structure analysis experiments have been performed on CdI_2 by Yu (1968).

Some thin film CdI_2 samples were prepared to investigate the above effects. The techniques used were similar to those described by Huggett and Teegarden (1966). Although these experiments were not performed at liquid helium temperature no photoconductivity could be observed, presumably because of ionic space charge polarisation. If these experiments were to be repeated at liquid helium temperature the ionic current causing the polarisation might be reduced to a negligible value.

The Huggett and Teegarden electrode arrangement used was of the blocking type which was also found to be largely unsuccessful with crystals. The a axis non blocking electrode arrangement was therefore used with thin films. The film of CdI_2 was evaporated onto a quartz substrate onto which gold electrodes had been evaporated in the same vacuum. The photocurrents were many orders of magnitude smaller than those recorded with single crystal samples. It was necessary to use either a deuterium lamp with fully open monochromator slits or a mercury discharge lamp with smaller bandwidth but widely varying intensity. The results obtained and shown in fig. 5.18 are therefore open to the objection that although widely varying intensities were used, no investigation of the intensity dependence of the photocurrent was made. It is gratifying to note that although the mercury lamp spectrum consisted of a series of lines of various strengths there were no large fluctuations in the photocurrent spectrum. There is some evidence of a dip at 5.63eV in the response spectrum but this is not as marked as the dip found in the spectra from single crystal samples before reflectivity correction. It was not possible to correct the thin film spectra for reflectivity loss since no thin film reflectivity spectra were available.

The smaller currents found in thin films are probably caused by the structure of the films which is composed of many small crystallites. These crystallites have the effect of reducing the electron mobility and

SPECTRAL DISTRIBUTION OF PHOTOCONDUCTIVITY
AT 10°K.
THIN FILM SAMPLE HCXF1.

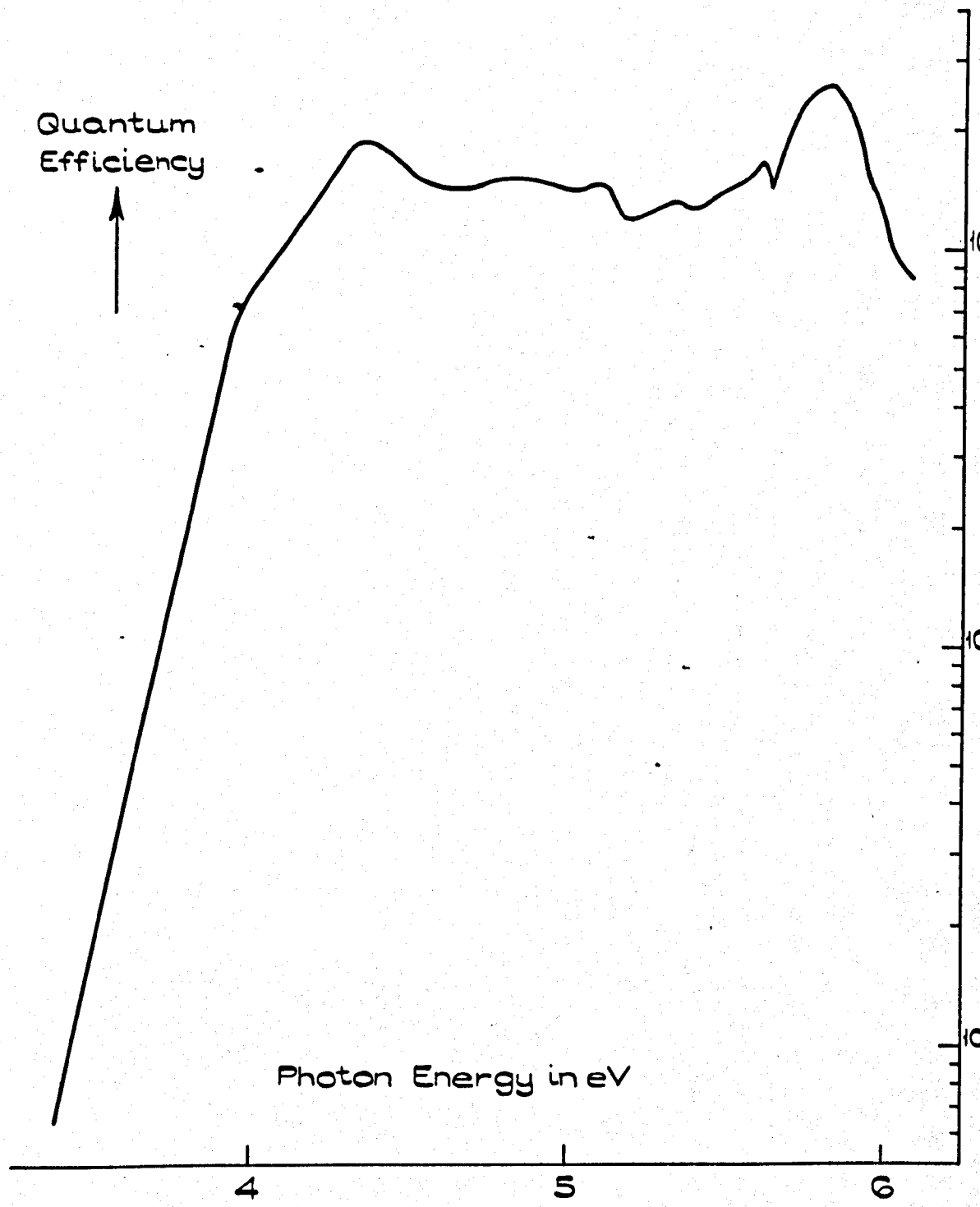

Fig. 5.18

cause polarisation fields inside the illuminated crystallites as well as causing ionic polarisation at higher temperatures.

5.11 Summary

The spectral variation of the photoconductivity quantum efficiency of CdI_2 at RT, 80°K and 10°K has been described. No previous measurements existed at the lower temperatures but the RT results were in agreement with previously published low energy spectra.

The photoconductivity spectra reproduce many of the features of reflectivity and when the photoresponse was corrected for reflectivity loss the sharp dips at exciton energies were smoothed out. When the corrected photocurrent was plotted against absorption coefficient the exciton photocurrent at 5.7 and 6.2eV was greater than that predicted on the basis of absorption. The difference between the band to band and exciton photoconductivity has been interpreted in terms of an exciton diffusion model.

REFERENCES

Brahms, S., 1965, Phys.Lett. 19, 272.

Bube, R.H., Photoconductivity in Solids, Wiley, 1960.

Bube, R.H., 1957, Phys.Rev. 106, 703.

De Vore, H.B., 1956, Phys.Rev. 102, 86.

Goto, T., 1965, J.Phys.Soc.Japan 20, 1654.

Greenaway, D.L. and Nitsche, R., 1965, J.Phys.Chem.Solids 26, 1445.

Gross, E.F., Akopian, J.Kn., Dreingold, F.I., Novikov, B.V., Titor, R.A., and Shekmametiev, R.I., 1964, Proc.Int.Conf. on The Physics of Semiconductors, Paris, p.957.

Huggett, G.R. and Teegarden, K., 1966, Phys.Rev. 141, 797.

Powell, R.L., Bunch, M.D. and Corruccini, R.J., March 1961 Cryogenics 139.

Yu, R.M., 1969, J.Phys.Chem.Solids 30, 63.

CHAPTER SIX

THE DETERMINATION OF TRAPPING ENERGY LEVELS AND THE SIGN OF THE PHOTO-GENERATED CARRIERS IN CADMIUM IODIDE

6.1 Introduction

The preceding chapters have been concerned with the opto-electronic properties of cadmium iodide. It was assumed in the discussion that the properties described were those of ideal single crystals. Real crystals, however, contain large numbers of defects such as impurities, dislocations and surfaces.

In an ideal crystal the lifetimes of electrons and holes are determined by the direct recombination process. In real crystals, however, carrier lifetimes are governed by capture at recombination or trapping centres. In particular, impurity atoms may behave as trapping centres; many experiments have been performed on semiconducting crystals in order to investigate such centres.

Several techniques have been applied to the study of the amount of energy required to excite an electron or hole from a trapping centre to a free state. The required energy is known as the trap depth energy.

6.2 Measurement Techniques

If a crystal is illuminated at a low temperature and warmed by a square temperature pulse the traps, filled by the illumination, will be emptied. The height of the temperature pulse may be varied and the corresponding variation in current due to thermally released carriers studied to give the trapping energy levels. Although this technique has the benefit of simplicity of interpretation there are experimental difficulties because of the requirement of a square temperature pulse.

In an alternative and widely used procedure the temperature is raised in a linear manner with time and the corresponding release of the charge carriers determined. The rate of release of carriers from a given set of traps of given energy is determined by the number of filled traps and the temperature. As the temperature is increased the number of filled traps decreases while the probability of emptying increases. The

variation of the two factors may lead to a peak in the thermally stimulated current against time curve. The thermally released carriers may take part in a radiative recombination process so that luminescence occurs; there will then be a luminescence or "glow" peak at the current peak.

It is also possible to study the trap energy levels by means of optical, instead of thermal, excitation. It is usually necessary to use low energy illumination (usually of infra red frequencies) for this purpose.

If high energy illumination is used to cause intrinsic photoconductivity the photo-generated carriers will be subsequently trapped. Trapping centres therefore play an important part in the rise and decay of photoconductivity. When a trapping centre changes into a recombination level there is a change in the photosensitivity which may be observed by simple photoconductivity measurements. The transition may take place when the temperature or illumination intensity is changed.

In our experiments to measure photoconductivity in CdI_2 high energy ultra-violet illumination was used, this necessitated specialised equipment such as sources and monochromator. The equipment was not suitable for low energy excitation so the method of thermally stimulated currents was used to investigate trapping levels. Since apparatus had been constructed to measure photoconductivity at liquid helium temperatures and above, this was also used for the glow curve determinations.

6.3 Theory of Thermally Stimulated Currents

When a crystal is illuminated at a low temperature with a light flux of sufficient energy to create free carriers some of the generated carriers will be trapped at impurity centres. Prolonged illumination leads to the filling of traps having escape energies greater than $\sim kT$ where T is the specimen temperature at which the illumination is performed.

Consider only electrons and assume that the escape energy associated with a given trap is E. This energy is that required to raise an electron from the trap to the bottom of the conduction band. In the case of holes the excitation is from the trap to the valence band. The probability of escape of an electron will be of the form

$$p = s e^{-E/kT} \quad . \quad . \quad . \quad . \quad . \quad . \quad . \quad . \quad . \quad 6.1$$

where s is the attempt to escape frequency (Randall and Wilkins 1945).

If there are n electrons in the traps at time t and the rate of escape is given by

$$\frac{-dn}{dt} = nse^{-E/kT} \quad \ldots\ldots\ldots\ldots\ldots\ldots\ldots\ldots\ldots\ldots 6.2$$

$$\text{therefore } \log \frac{n}{n_o} = -\int^{T} \frac{1}{\beta} se^{-E/kT} dT \quad \ldots\ldots\ldots\ldots\ldots\ldots 6.3$$

where β is the rate of warming and n_o is the number of traps occupied at $t=0$

$$\text{then } n = n_o e^{-\int^{T} \frac{1}{\beta} se^{-E/kT} dT} \quad \ldots\ldots\ldots\ldots\ldots\ldots 6.4$$

and at a glow peak maximum where $T = T_G$

$$E = kT_G \log s \left[1 + \frac{\log kT_G^2/\beta E}{\log s}\right] \quad \ldots\ldots\ldots\ldots\ldots\ldots 6.5$$

(Heyningen and Brown 1958)

Equation 6.5 enables E to be determined if T_G, s and β are known. Several assumptions are, however, involved in the derivation and these invalidate the treatment in many practical cases.

In practice the electrons released may be retrapped and the term $\frac{dn}{dt}$ should therefore include a retrapping term. Recombination processes may also occur and should be allowed for.

The parameter s is unknown but it is probably temperature dependent. It is possible, using an analysis due to Grossweiner (1953), to eliminate s; this method depends upon the knowledge of the glow peak width, which may have a large uncertainty. Retrapping effects are neglected in this method also.

Haine and Carley-Read (1968) have made a study of different methods of analysis of thermally stimulated current curves and conclude that many of the standard methods used on crystals of CdS are in error by orders of magnitude. They have given an analysis which takes account of retrapping and recombination effects. Their expression is somewhat unweildy, however, and leads to a similar result to that of Bube (1960).

Bube's expression depends upon the thermal equilibrium between electrons in traps and those at the Fermi level. The analysis is similar to that for donor and acceptor levels in semiconductor theory.

The expression is

$$E = kT_{max} \frac{\log N_c e\mu}{\sigma_m} \quad . \quad . \quad . \quad . \quad . \quad . \quad . \quad . \quad . \quad 6.6$$

where μ is the electron mobility, N_c is the density of states at the bottom of the conduction band and σ_m and T_{max} are the peak conductivities and temperature respectively.

T_{max} and σ_m may be determined by plotting glow curves using various warming rates, this leads to two equations.

$$E = kT_a \log \frac{x}{\sigma_a} \quad . \quad . \quad . \quad . \quad . \quad . \quad . \quad . \quad . \quad 6.7$$

$$E = kT_b \log \frac{x}{\sigma_b} \quad . \quad . \quad . \quad . \quad . \quad . \quad . \quad . \quad . \quad 6.8$$

$$\therefore \quad T_a \log \frac{x}{\sigma_a} = T_b \log \frac{x}{\sigma_b} \quad . \quad . \quad . \quad . \quad . \quad . \quad . \quad . \quad 6.9$$

$$\left(\frac{x}{\sigma_a}\right)^{T_a} = \left(\frac{x}{\sigma_b}\right)^{T_b} \quad . \quad . \quad . \quad . \quad . \quad . \quad . \quad . \quad 6.10$$

$$\frac{x^{T_a}}{x^{T_b}} = \frac{\sigma_a^{T_a}}{\sigma_b^{T_b}} \quad . \quad . \quad . \quad . \quad . \quad . \quad . \quad . \quad . \quad 6.11$$

$$\therefore \quad x = \left(\frac{\sigma_a^{T_a}}{\sigma_b^{T_b}}\right)^{\frac{1}{T_a - T_b}} \quad . \quad . \quad . \quad . \quad . \quad . \quad . \quad . \quad 6.12$$

$$E = kT_a \log \left(\frac{\sigma_a^{T_a}}{\sigma_b^{T_b}}\right)^{\frac{1}{T_a - T_b}} \cdot \frac{1}{\sigma_a} \quad . \quad . \quad . \quad . \quad . \quad 6.13$$

If σ_a and σ_b are known at the peak temperatures T_a and T_b, the value of E may be determined. This method assumes that x (and therefore the product $N_c\mu$) is independent of temperature. The chief disadvantage however is the strong dependence of E on $T_a - T_b$.

It was extremely difficult to vary the rate of warming (β) in our apparatus sufficiently to cause significant change in T_{max}. The values of σ_{max} were unreliable because of space charge effects. The expression derived above does however include retrapping effects since it is based

upon thermodynamic equilibrium. Bube (1955) found that in CdS the variation between the trap depths found with this technique and with the one described initially was of the order of 50%. Neither method includes allowancies for recombination.

6.4 Experimental Procedure

There were no thermally stimulated current curves available for CdI_2 so that it was preferable to illuminate at as low a temperature as possible. The samples were therefore illuminated at 10°K with the total output from a high pressure mercury discharge lamp. The illumination caused a current to flow with zero applied field, the illumination continued until a steady current value was attained. The sample was then allowed to warm naturally to 77°K. This warming could be accelerated by removal of the brass top cover of the liquid helium cryostat.

After the liquid helium had evaporated the sample temperature tended towards 77°K, the temperature of the liquid nitrogen reservoir. The warming rate was therefore initially slow, increasing after the liquid helium had all evaporated and falling when the temperature approached 77°K. The latter effect was reduced by the addition of a heating coil to the helium reservoir. The coil was made from Nichrome wire insulated with glass fibre and was heated by means of a "Variac" transformer. The sample holder and temperature measurement devices were as used in the photoconductivity experiments and many of the glow curves were recorded on the same samples as the photoconductivity spectra.

6.5 Experimental Results a axis Geometry

The curve illustrated in fig. 6.1 was recorded with a cleaved solution-grown crystal $HCAX_4$ which had been heated in vacuo to ~150°C before the photoconductivity experiment. The vertical scale of the figure is a current scale and the horizontal axis indicates elapsed time from an arbitrary origin. The warming curve of temperature against time is also plotted on this diagram.

The first peak on this curve was at 54°K, there are many other peaks visible, some of which interact with their neighbours to give double peaks. The peaks were located at 54°K, 70°K, 80°K, 83°K, 88°K, 95°K, 111°K, 118°K, 148°K and at 166°K, corresponding to warming rates of initially

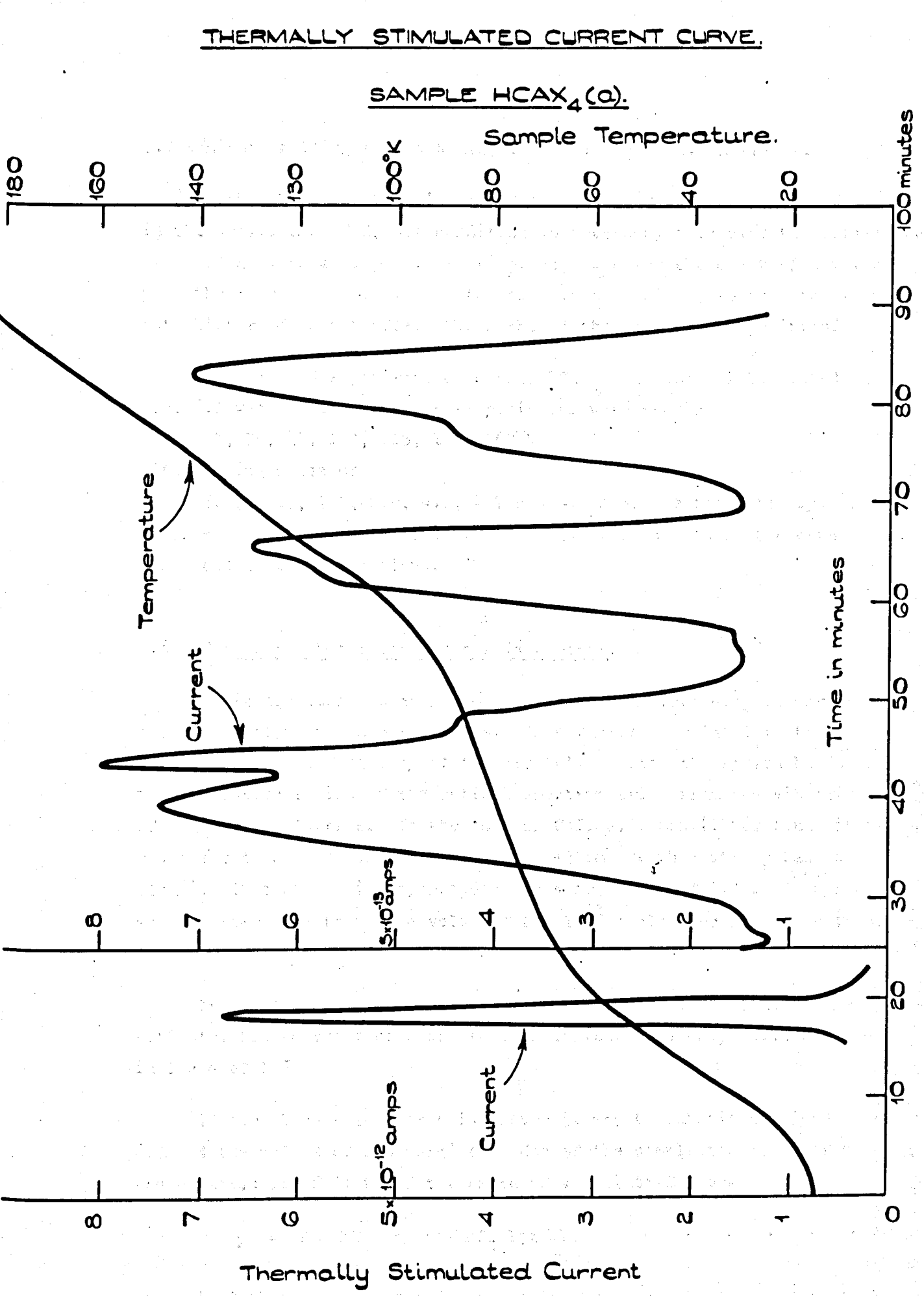
THERMALLY STIMULATED CURRENT CURVE.
SAMPLE HCAX4 (a).
Sample Temperature.
180
160
140
130
100°K
80
60
40
20
100 minutes
90
80
70
60
50
40
30
20
10
0
Temperature
Current
Time in minutes
8
7
6
5x10⁻¹³amps
4
3
2
1
Current
5x10⁻¹²amps
Thermally Stimulated Current

Fig. 6.1

2.7°K/minute falling to 0.8°K/minute and rising to 2.8°K/minute.

Although it has been indicated that a fixed warming rate β is used in the derivation of E, this condition is necessary only over the activation range of a given glow peak. At temperatures below the onset of a given peak the rate of emptying from the trap is negligible, so that the warming rate history does not affect the shape of the peak or its position.

In a second experiment on sample $HCAX_4$ the curve illustrated in fig. 6.2 was obtained. The peak positions were then at

55, 79, 84, 102, 115, 150, 162°K

with warming rates of

3.2, 0.57, 1.0, 2.9, 4.0, 4.7 and 4.7°K/minute respectively. There are remarkable similarities between the two curves both in the shape of the peaks and in their positions.

6.6 Trap Depth Determination a axis Geometry

It is necessary to assume a value for s the frequency factor in order to analyse the above results. This factor is related to the lattice vibration frequency of the crystal. Strong absorption bands in the low energy region of the optical spectrum arise from the vibrations of the crystal lattice. In the case of CdI_2 J.P. Mon (1966) found infra-red absorption bands in the region of $90 \pm 30 cm^{-1}$ with a strong band at $91 cm^{-1}$. This absorption corresponds to a frequency of 2.7×10^{12} cycles/sec, we have therefore assumed a value of 2×10^{12} cycles/sec for s the frequency factor.

It is clear that the value of s for CdI_2 must be an order of magnitude estimate, but an error of 2 orders of magnitude will only cause an error in log s of 10%.

If the above value for s is assume it may be substituted into equation 6.5 and the values of E determined. One of the simplest methods of solving the equation for E is to plot a graph of y against E where

$$y = E - kT_G \log s - kT_G \log \frac{kT_G^2}{\beta E} \quad . \quad . \quad . \quad . \quad . \quad . \quad 6.14$$

Several of these plots are illustrated in fig. 6.3. Various values of E were substituted into equation 6.14 and the y=0 intercept found so that

THERMALLY STIMULATED CURRENT CURVE.

SAMPLE $HCAX_4$ (b).

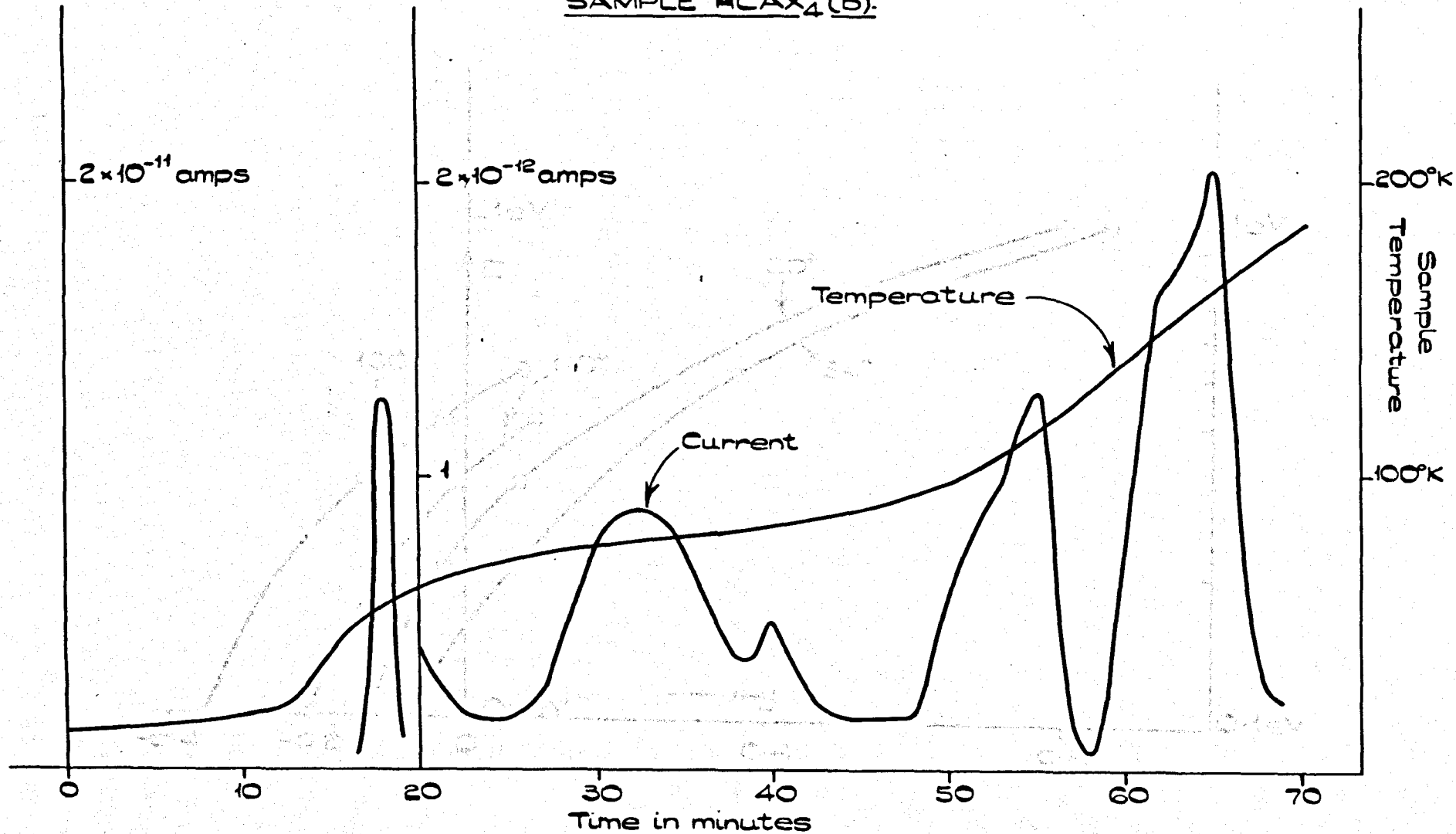

Fig.6.2

PLOT OF E AGAINST y FOR VARIOUS GLOW PEAKS.

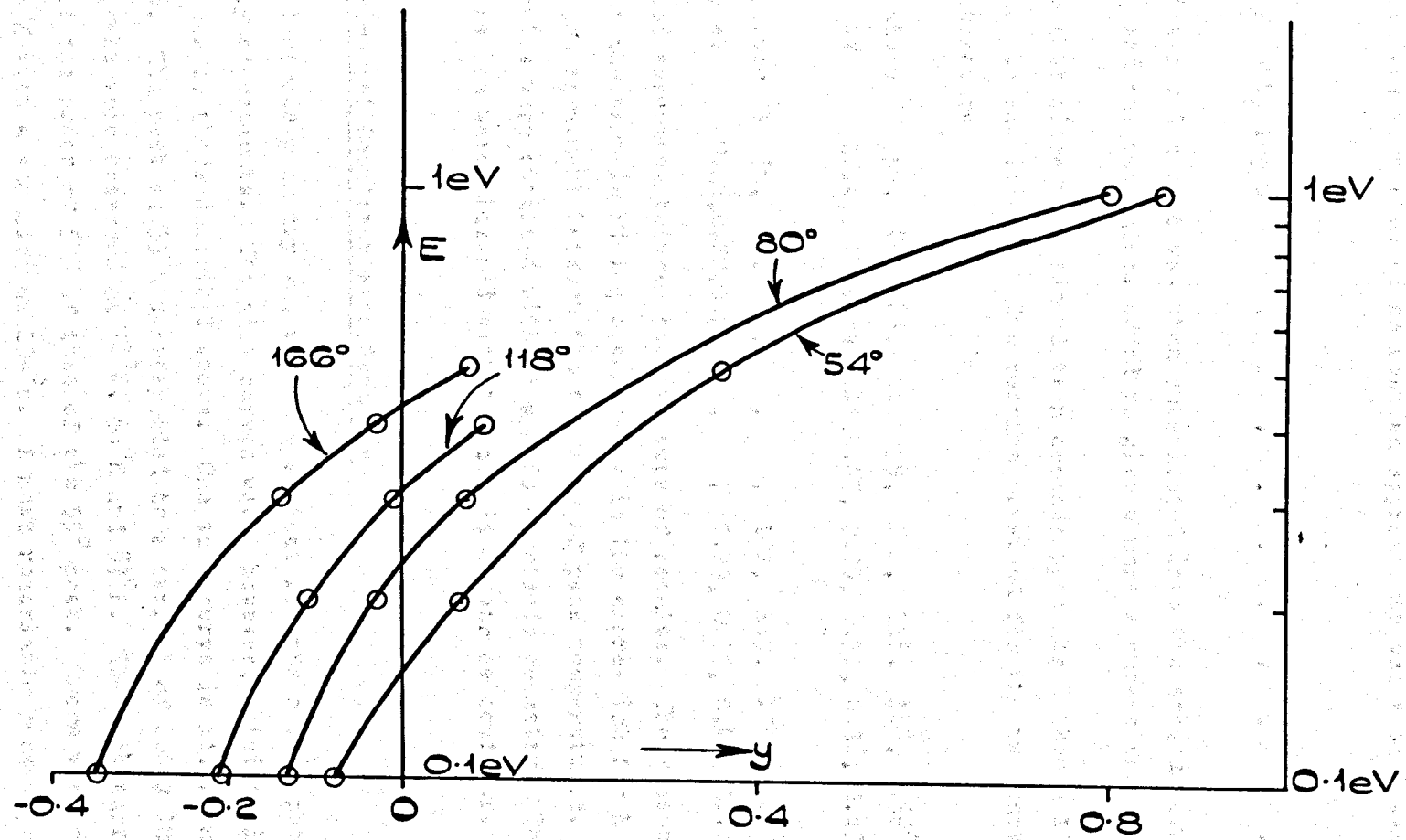

Fig. 6.3

the equation could be solved. It was then clear that the term in $kT_G \log \frac{kT_G^2}{\beta E}$ was generally some 10% of the larger term $kT_G \log s$. The procedure was then changed so that an approximate value of E was found from

$$E \sim kT_G \log s \quad . \quad . \quad . \quad . \quad . \quad . \quad . \quad . \quad . \quad . \quad 6.16$$

The approximate value of E was then substituted into the second term $kT_G \log \frac{kT_G^2}{\beta E}$ and the two values added to give a more accurate value of E. It is clear that since this second term depends upon log E then a 10% error in E will not be significant. The results obtained for the two curves from $HCAX_4$ are therefore

Peak Temperature	°K	54,	80,	83,	88,	95,	111,	118,	148, 166°K
Trap Energy	eV	0.14,	0.23,	0.24,	0.25,	0.27,	0.29,	0.31,	0.38, 0.43 eV

and

Peak Temperature	°K	55,	79,	84,	,	,	102,	115,	156, 168°K
Trap Energy	eV	0.15,	0.22,	0.23,	,	,	0.29,	0.32,	0.41, 0.47 eV

There is good agreement between the two sets of results. The reason for this is that the term in kT log s dominates in the expression for E and there was good agreement between the two sets of peak temperatures. Both sets of results were obtained with an a axis electrode geometry. The remaining results were obtained with the c axis electrode configuration.

6.7 Experimental Results c axis Geometry

The electrode geometry was the same as that for the c axis photoconductivity experiments. The glow curves were, however, obtained in a similar manner to those described above. One such curve is illustrated in fig. 6.4. The peak at 55°K corresponded to a current of 2.4×10^{-12} amps. Secondary peaks were observed at 78°K, 84°K and 87°K. The peak current for these was of the order of 50% of that of the 55° peak. There was another peak at 125°K with a shoulder at 104°K. A most remarkable peak appeared at 178°K with a peak current of 10^{-10} amps. This is in marked contrast with the a axis results where the 53°K peak was 10^{-12} amps and higher temperature peaks were of the same order with a maximum of 2×10^{-12} amps. The high energy peak at 166°K was of some 6.1×10^{-13} amps and was over two order of magnitude smaller than that for $HCCX_1$.

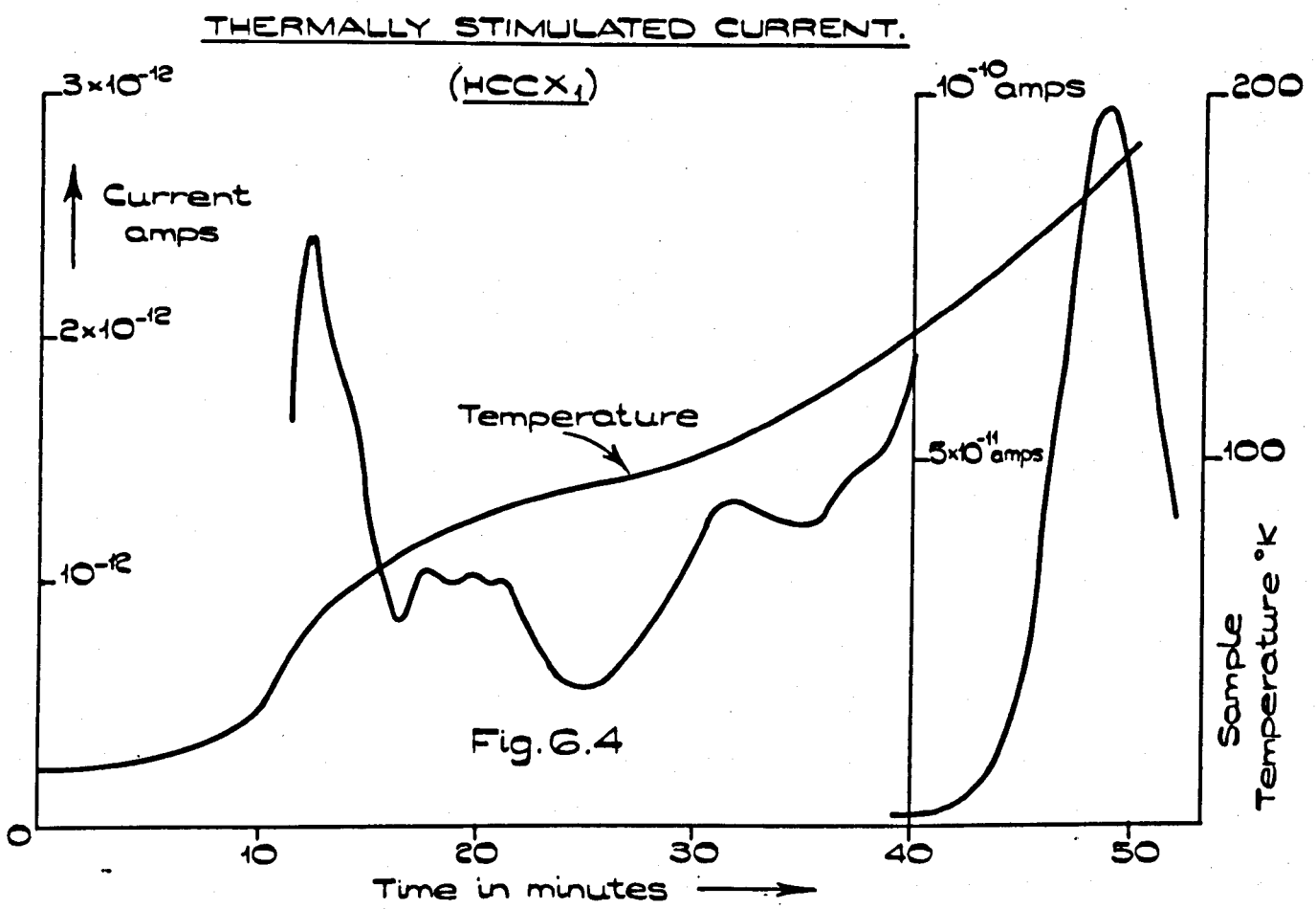
THERMALLY STIMULATED CURRENT.
(HCCX1)
3×10⁻¹²
2×10⁻¹²
10⁻¹²
0
Current amps
Temperature
10⁻¹⁰ amps
5×10⁻¹¹ amps
200
100
Sample Temperature °K
10
20
30
40
50
Time in minutes

Fig.6.4

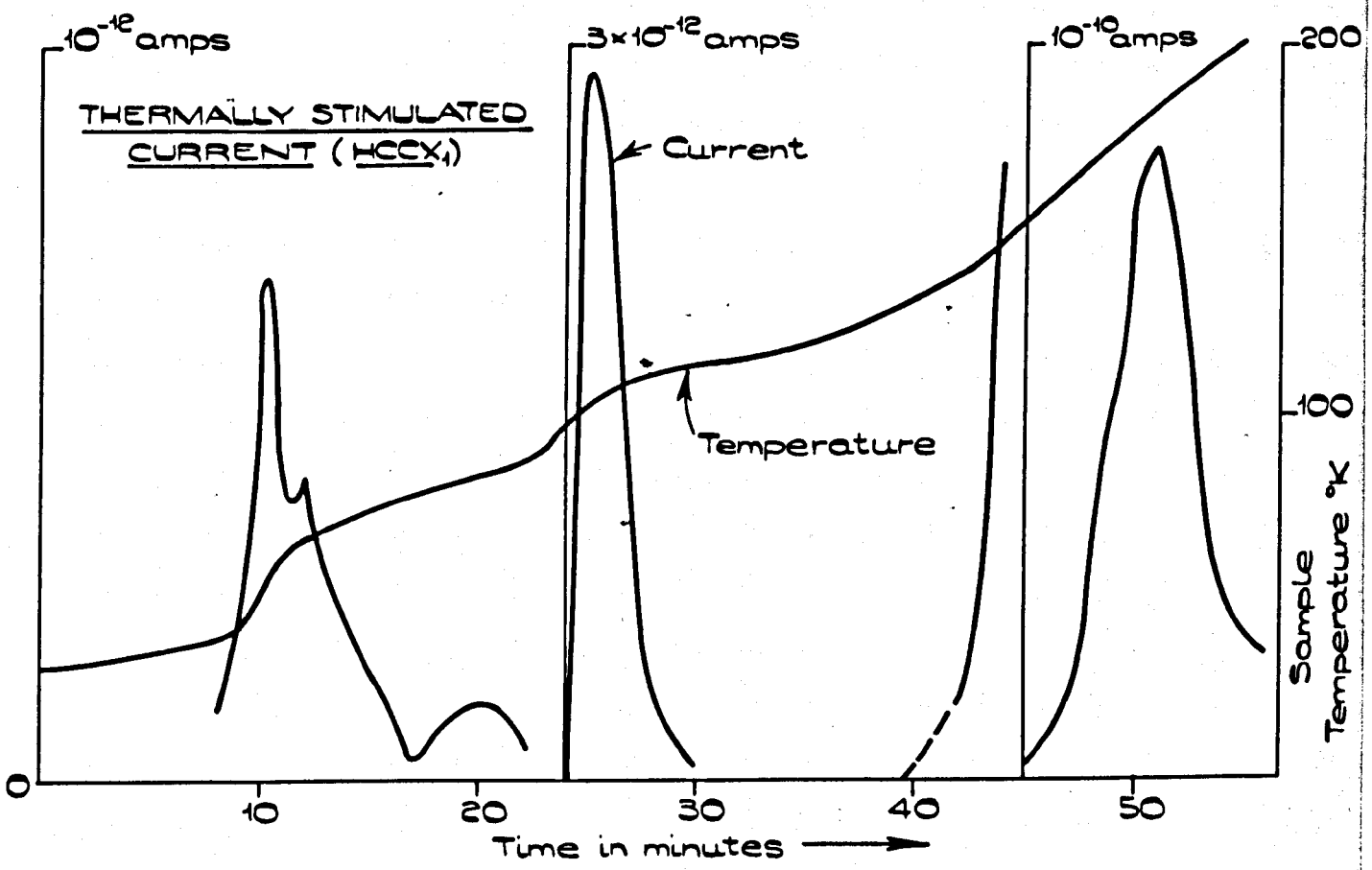
10⁻¹² amps
THERMALLY STIMULATED CURRENT (HCCX1)
3×10⁻¹² amps
Current
Temperature
10⁻¹⁰ amps
200
100
Sample Temperature °K
0
10
20
30
40
50
Time in minutes

Fig.6.5

Repeat experiments were performed on $HCCX_1$ and are illustrated in figs. 6.5 and 6.6. The peak in fig. 6.5 at 56° has a peak current of 6.9×10^{-13} amps. There are smaller peaks at 67° and 83° but the 102° peak has a maximum current of 2.9×10^{-12} amps. The 181°K peak has a maximum current of 9×10^{-11} amps. Similarly fig. 6.6 has a peak at 176° with a current of $\sim 7 \times 10^{-11}$ amps.

The results obtained from the above three runs on the same sample are summarised in Table 6.1. The method used to calculate the peak energies was as described for the a axis sample.

TABLE 6.1

Peak Position	59 ,	78 ,	84 ,	87 ,	105 ,	127 ,	180°K
Peak Energy	0.16,	0.22,	0.24	0.25,	0.31,	0.36,	0.50eV
Peak Position	56 ,	67 ,	83 ,	,	103 ,	,	181°K
Peak Energy	0.15,	0.18,	0.23,	,	0.29,		0.51eV

Peak Position	45 ,	51 ,	74 ,	81 ,	86 ,	107 ,	128 ,	145 ,	180
Peak Energy	0.12,	0.14,	0.21,	0.22,	0.25,	0.30,	0.36,	0.40,	0.50

There is very good agreement between the majority of peak heights between runs.

Similar results were obtained from sample $HCCX_2$ with peaks at

fig. 6.7

Peak Position T_G	49°,	66°,	89°,	109°,	125°,	176°
Peak Energy E	0.13,	0.20,	0.25,	0.31,	0.35,	0.49eV

and for a second run on this sample

fig. 6.8

Peak Temperature T_G °K	55,	72,	90,	108,	130,	152,	182
Peak Energy E eV	0.15,	0.20,	0.26,	0.30,	0.36,	0.42,	0.50

The peak at 50°K was small compared with the second peak which was of a similar size to the 180°K peak.

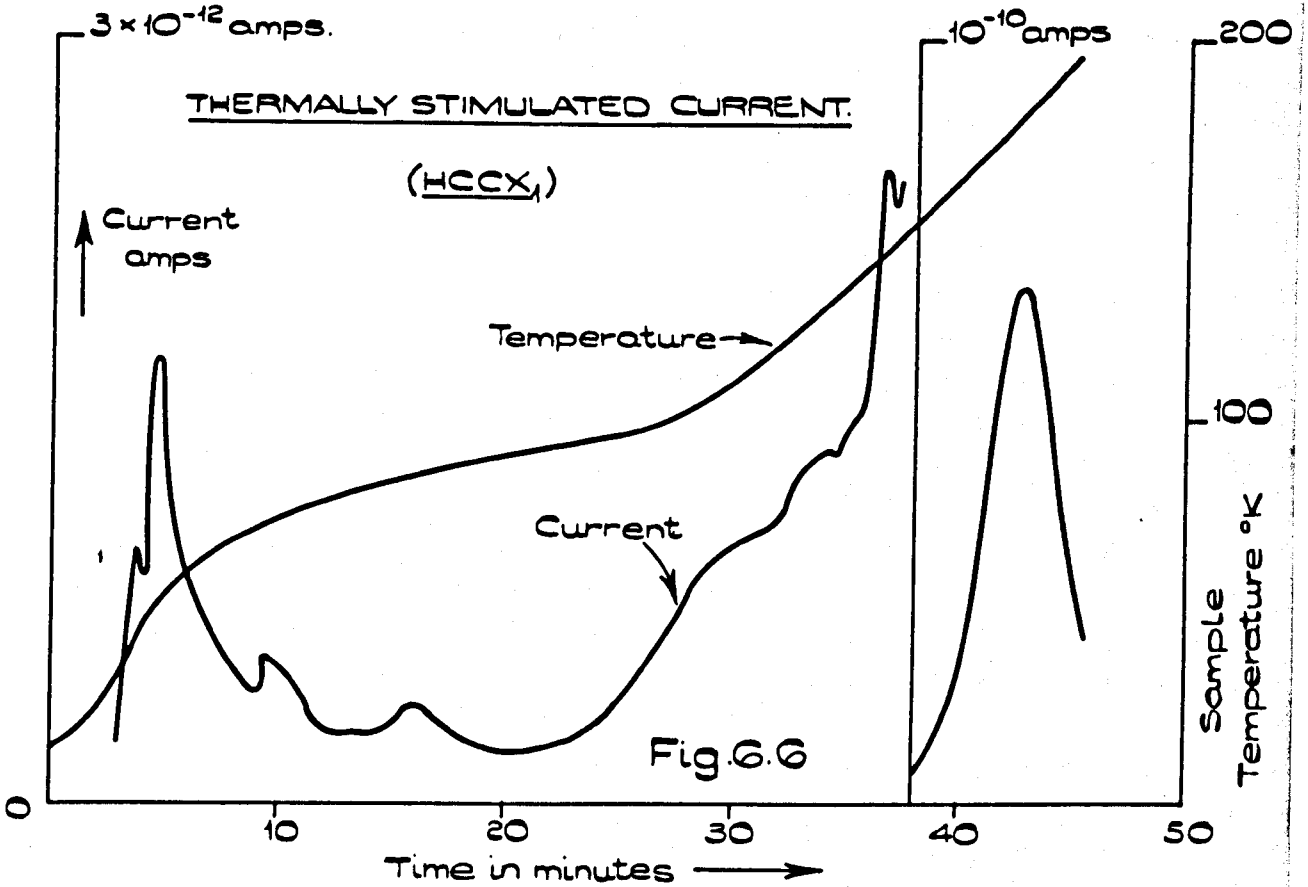
3 × 10⁻¹² amps.
10⁻¹⁰ amps
200
THERMALLY STIMULATED CURRENT.
(HCCX1)
Current amps
Temperature
Current
100
Sample Temperature °K
0
10
20
30
40
50
Time in minutes

Fig.6.6

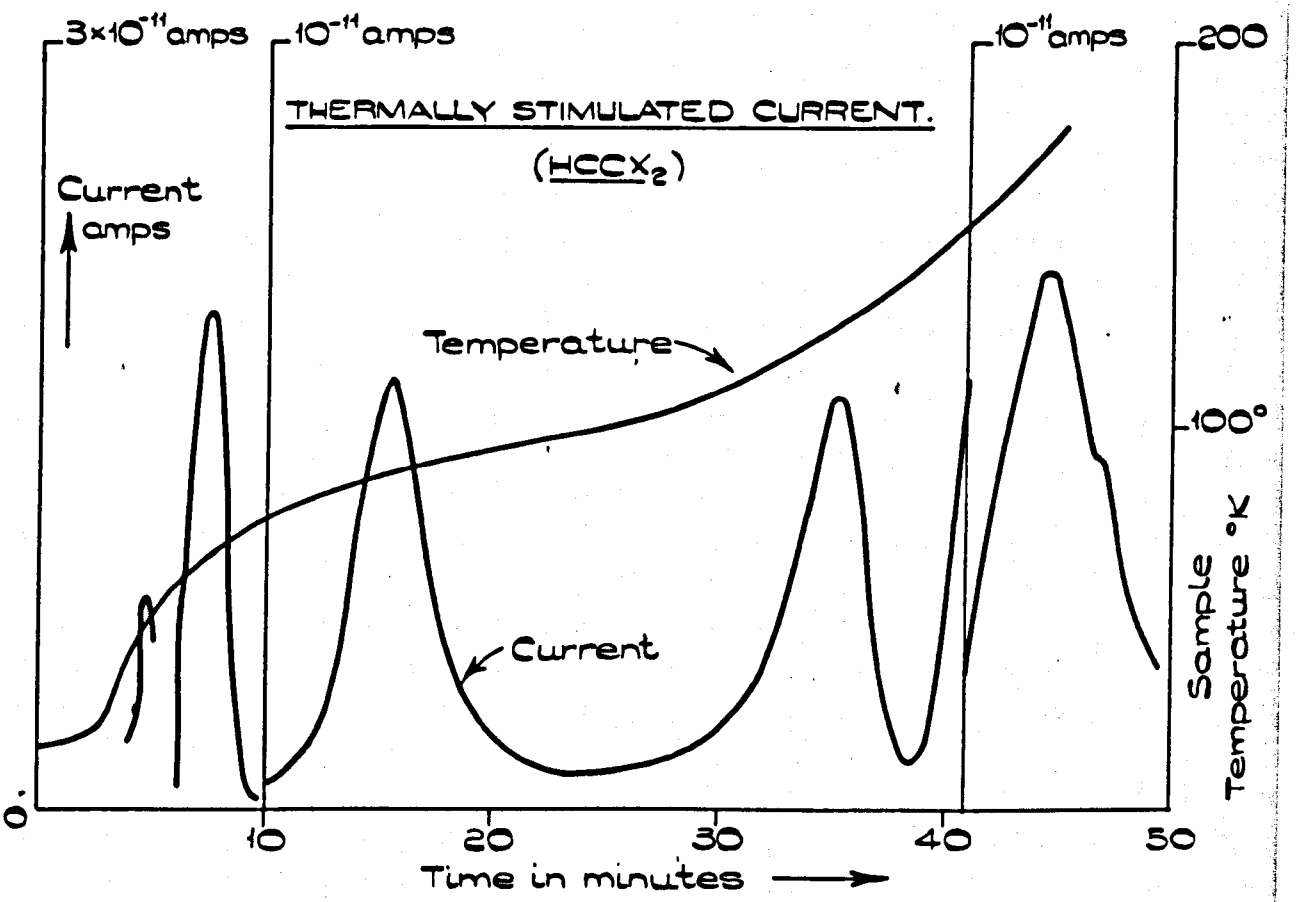
3×10⁻¹¹ amps
10⁻¹¹ amps
10⁻¹¹ amps
200
THERMALLY STIMULATED CURRENT.
(HCCX2)
Current amps
Temperature
Current
100°
Sample Temperature °K
0
10
20
30
40
50
Time in minutes

Fig. 6.7

6.8 Comparison of Results from Both a and c axis Geometries

The above analysis indicates that many of the active traps found in 'a axis' crystals were also present in the 'c axis' samples. There are distinct differences, however, and these appear to be caused by the difference in field geometries. The schematic differencies in the field geometries are illustrated in fig. 6.9. It can be seen that the a axis configuration leads to an increased surface field relative to that in the 'c axis' geometry. The former geometry therefore tends to have an increased surface sensitivity. The 'c axis' geometry is closer to the ideal glow curve determination apparatus since the crystal field tends to be more uniform than that in the a axis configuration.

Since the a axis geometry is more sensitive to surface carriers then any glow peaks enhanced with this system are more likely to be due to surface traps. This argument may be applied to the curves obtained where the 0.15 and 0.20eV traps were enhanced in the 'c axis' geometry. The 0.20eV peak in $HCCX_1$ was relatively small, however, and may have been due to a change in impurity content. The glow peak at 0.5eV was larger in the c axis crystals.

It appears that the peaks below 0.5eV are caused by surface enhanced traps whereas the high energy peak is a volume distributed trapping centre. Comparison of energies of traps found in various samples is justified since a peak at a given temperature certainly corresponds to a given trap energy. The energies are likely to be in error by as much as 50% because of the estimation of the frequency factor s and the neglect of retrapping and recombination. In view of the above errors we have attempted to make use of Bube's method to determine one energy level. In Bube's expression it is necessary to know $Nc\mu$ and T_G to determine E directly. It is however possible to use different heating rates so that the change in T_G and σ_G may be determined and $Nc\mu$ eliminated from the two equations.

Consider the low energy peak at 0.15eV. In the case of $HCAX_4$ the heating rates were 2.7 and 3.2°K/min. The value of E computed from these values was 0.16eV. The 'c axis' samples were used with heating rates that were closer together, so that there was a large error in determining E. The values of E were of the order of 0.1eV however.

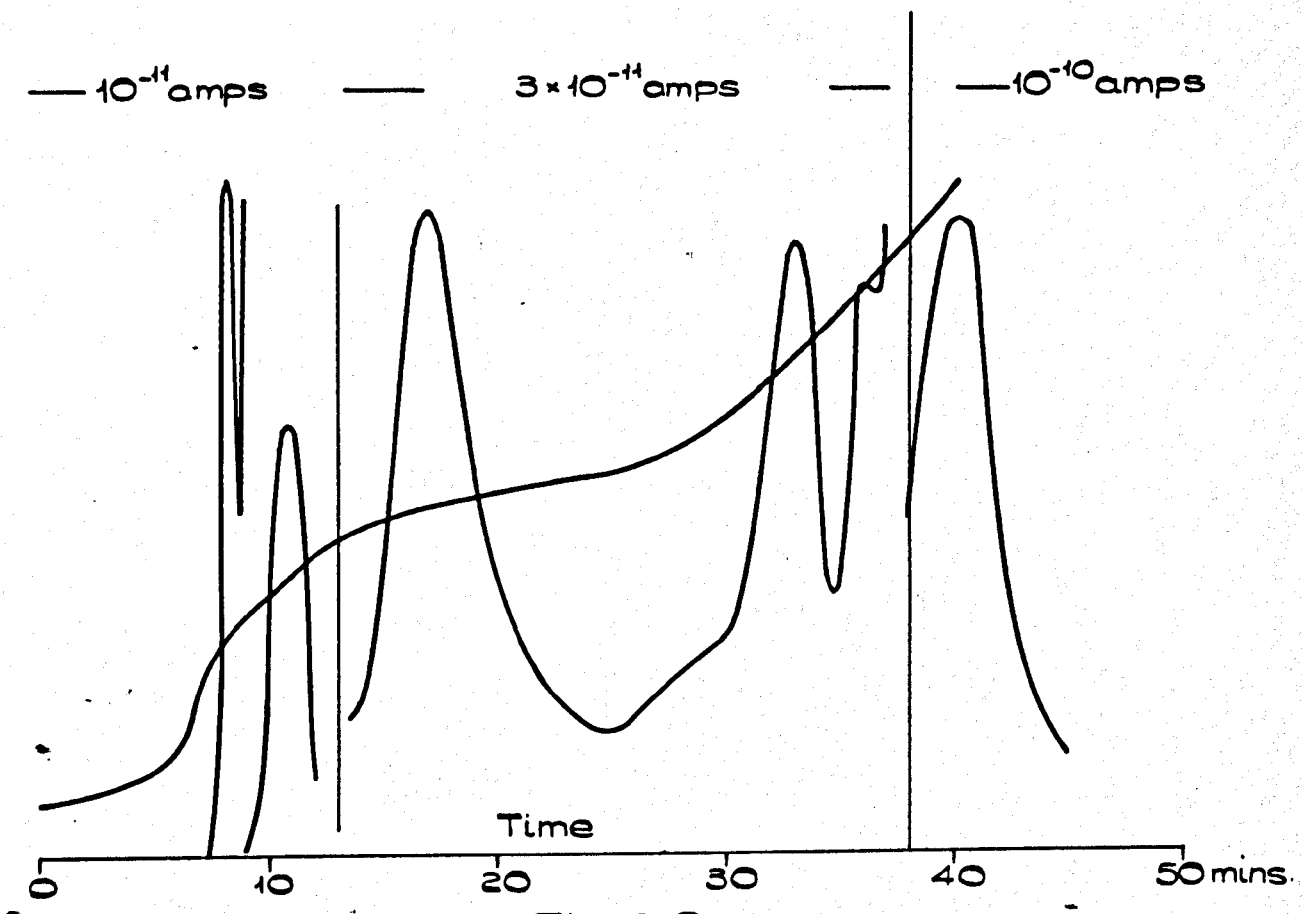

Fig.6.8

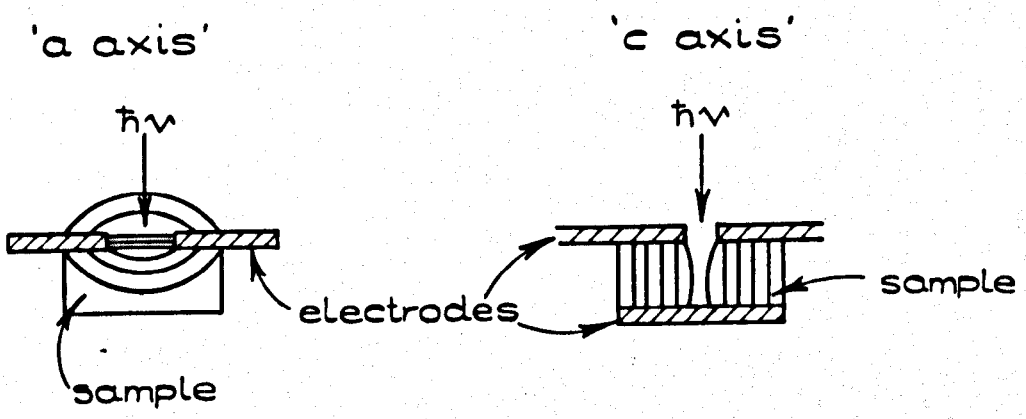

ELECTRODE GEOMETRIES

Fig.6.9

These values are in good agreement with the value of 0.14-0.15eV calculated on the simple theory. It was not possible to use the method of Bube for other trap depth determinations since the heating rates could not be varied sufficiently to change T_G appreciably.

If we consider the high energy glow peak in the 'c axis' samples we find that the peak current was 10^{-10} amps. Now the area under the glow peak gives the total charge flow and hence the number of electrons released assuming no retrapping or recombination. The width of the curve was 2.2 minutes so that the area was some 10^{11} electron charge units. The crystal volume was some 1cm x 1cm x 1mm i.e. 0.1cc but the illuminated volume was probably near 0.01cc so that the trap density when retrapping and recombination were neglected was $10^{13} cc^{-1}$. These processes prevent an accurate assessment but it is possible to determine the trap density by allowing for them using the analysis of Haine and Carley-Read(1968).

6.9 Crystal Purity

In order to assess the impurity content of typical samples an analysis was performed by Johnson Matthey Chemicals Ltd.. The assay is illustrated in fig. 6.10. The chief impurity was found to be iron with a concentration of less than 3 parts per million. This assay illustrates the purification of CdI_2 by the crystallization procedure. The starting material was Analar grade CdI_2 of only 2N purity.

In view of the large number of elements present in very small amounts it is difficult to link particular impurities to trapping levels. It is possible that the high energy peak is connected with the Fe impurity although further evidence is required for a complete assessment. It is usual to use crystals of known impurity content to correlate impurity levels with traps. The doping may be varied and the corresponding changes in the glow curves recorded.

6.10 Summary

CdI_2 has been shown to be a particularly interesting material from the point of view of trapping level determination. Many glow curves have been analysed using a simple model and the trap depths have been determined and compared. These results were also discussed in terms of surface and bulk traps and possible impurity effects.

Reference No.....

Johnson Matthey Chemicals Limited

Analytical Laboratories
Orchard Road Royston Herts
Telephone: Royston 2021

22.10.68.

Certificate of Analysis

To The University of Warwick.

Dear Sir(s),

We have examined the sample of Cadmium Iodide.

.....received from you on the.....and submit the following report:

Element	Estimate of Quantity Present Results as Parts per Million
Bismuth	<1
Calcium	<1
Copper	<1
Iron	3
Magnesium	<1
Silicon	<1
Silver	<1

The following elements were specifically sought but not detected:-
Al, As, Au, B, Ba, Be, Co, Cr, Cs, Ga, Ge, Hf, Hg, In, Ir, K, Li, Mn, Mo, Na, Nb, Ni, Os, P, Pb, Pd, Pt, Rb, Re, Rh, Ru, Sb, Se, Sn, Sr, Ta, Te, Ti, Tl, V, W, Zn, Zr.

for Johnson Matthey Chemicals Ltd.

6·60

F.W. Gerrard

for B. S. COOPER.
Manager, Analytical Laboratories.

Although no previously reported thermally stimulated current curves were available some trap depths determined from luminescence measurements have been reported by Phillipe and Langouet(1967). In their measurements peaks were found at 109°K and 138°K corresponding to traps of 0.08eV and 0.13eV with a value of s of $10^{5\pm1}$. This value of s is to be compared with our value of $2 \times 10^{12} sec^{-1}$. The former value is apparently low in view of the lattice vibration frequencies and the results of Heyningen and Brown for AgCl. If we substitute our value of s this would introduce an energy scaling factor of 2.5 so that Phillipe and Langouets results would indicate trap depths of 0.20eV and 0.32eV for the 109°K and 138°K peaks.

It is possible to determine the mobility of carriers from glow curve experiments using Bube's expression. If E, T_G, N_c and σ_G are known then μ may be determined. N_c, the density of states at the conduction band minimum may not be known so that this will not be possible in many samples. In an anisotropic crystal it should be possible to determine the ratio of the mobilities along crystallographic planes and thereby eliminate N_c. In a layer structured material for example, the mobilities perpendicular to and parallel to the basal plane are μ and μ and are related by

$$E = kT_{\parallel}^{G} \log \frac{N_c e \mu_{\parallel}}{\sigma_{\parallel}^{G}} = kT_{\perp}^{G} \log \frac{N_c e \mu_{\perp}}{\sigma_{\perp}^{G}} \quad . \quad . \quad . \quad . \quad 6.17$$

The anisotropy in μ will then be accompanied by a corresponding change in T^G between the two geometries.

In the case of CdI_2 the high temperature peak at 180°K is located at 167°K in the 'a axis' geometry and at 180°K in the 'c axis' geometry. The peak current in the 'a axis' case was 2×10^{-12} amps with an applied potential of 450V and a thickness of 500 μ. The electrode separation was 0.6cm and the crystal width 1cm.

Hence $$\sigma_{\perp}^{G} = \frac{2 \times 10^{-12} \times 0.6}{0.05 \times 1 \times 450} = 5 \times 10^{-14}\ \Omega^{-1}$$

in the c axis direction the peak current was 10^{-10} amps and therefore

$$\sigma_{\parallel}^{G} = \frac{10^{-10} \times 0.05}{1 \times 1 \times 450} = 10^{-14}\ \Omega^{-1}$$

$$\therefore \quad \sigma_{\perp} = 5 \times 10^{-14}\ \Omega^{-1}\ cm \qquad \sigma_{\parallel} = 10^{-14}\ \Omega^{-1}\ cm$$

then $$167 \log \frac{N_c\, e\, \mu_\perp}{5 \times 10^{-14}} = 180 \log \frac{N_c\, e\, \mu_\parallel}{10^{-14}} = \frac{E}{k}$$

$$\left(\frac{N_c\, e\, \mu_\perp}{5 \times 10^{-14}}\right)^{167} = \left(\frac{N_c\, e\, \mu_\parallel}{10^{-14}}\right)^{180}$$

$$e^{E/kx167} = \frac{N_c\, e\, \mu_\perp}{5 \times 10^{-14}} \qquad e^{E/kx180} = \frac{N_c\, e\, \mu_\parallel}{10^{-14}}$$

$$\therefore \quad \frac{\mu_\perp}{5\mu_\parallel} = \frac{e^{E/kx167}}{e^{E/kx180}} \qquad \log e \frac{}{5} = \frac{E}{k}\left(\frac{1}{167} - \frac{1}{180}\right)$$

$$\therefore \quad \log e \frac{\mu}{5\mu} \sim \frac{0.5}{8.65 \times 10^{-5}} \left(\frac{13}{3 \times 10^{-4}}\right) = 2.5$$

$\mu \sim 50\mu$ which indicates that the mobility in the cleavage plane is 50 times greater than that in the perpendicular direction.

6.11 Thin Film Glow Curve

One experiment was performed on a thin film of CdI_2 and a glow curve determined, this is illustrated in fig. 6.10. There was a quartz cover slip between the film of CdI_2 and the sample holder. It is possible therefore that the film was at a higher temperature than the sample holder for measurements below 77°K. The peak current was of the order of 10^{-13} amps although for some glow peaks the maximum was 10^{-14} amps. The peaks were located at 52, 57, 62, 72, 80, 90, 142, 159 and 199°K. The overall shape of this curve is in good agreement with that for the 'a axis' sample, in particular the peak near 190°K is weak. It is clear that only surface traps will be important in thin film specimens so that strong peaks in their glow curves must be derived from surface traps.

6.12 The Determination of the Sign of the Current Carriers in CdI_2

Although a preliminary discussion of trapping energy levels in CdI_2 has been presented above, the discussion did not include the nature of the trapped charge carriers.

THERMALLY STIMULATED CURRENT CURVE

THIN FILM SPECIMEN HCFA 1:

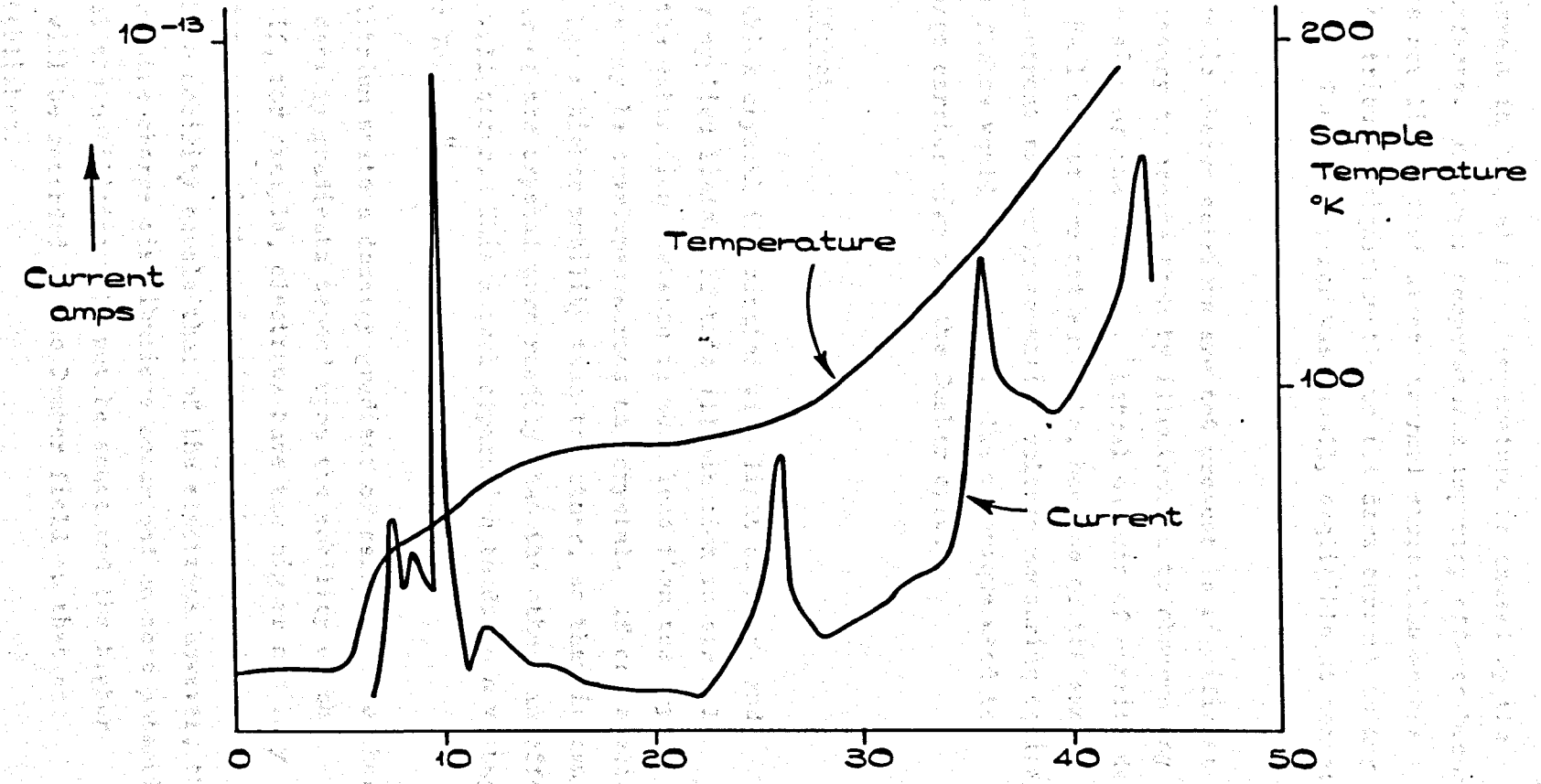

Fig. 6.10

The dark current in CdI_2 at room temperature is caused by the motion of ionic defects. At lower temperatures impurity effects become important. It was not likely that direct thermal excitation across energy band gaps contributed significantly to the dark current in any of the measurements. The dark current was usually negligible at temperatures below R.T..

Since electronic charge carriers are not present in significant numbers it is necessary to create them by illumination to observe any effects due to the sign of the carriers. Normal methods of carrier determination such as the Hall effect are not suitable; because of the small mobility and photocurrent extremely sensitive voltage measuring equipment and high magnetic fields would be required. The technique used to determine the charge carrier sign was the Dember effect.

6.13 The Dember Effect

Consider a thick crystal illuminated with light of $h\nu > E_g$ and with no externally applied field. If this illumination is strongly absorbed so that the extinction distance is much less than the crystal thickness a voltage may be developed across the crystal. If one species of charge carrier has a higher mobility than the other, so that it can diffuse to the rear of the crystal more readily than the other, an effective charge separation will occur. This mutual separation tends to a voltage called the "Dember Voltage".

In the equilibrium state a density gradient of carriers of either sign exists. The density gradients depend upon the mobility of the charge carriers. If, for example, electrons have the higher mobility then there will be a greater electron density near the rear of the crystal. If the hole mobility equals that of the electrons however, then two identically opposite charge distributions occur and no nett potential exists. In general the mobilities will not be equal and the higher mobility carriers will be retarded by the Dember field so that an equilibrium is established.

The Dember Voltage V_D is given by

$$V_D = \frac{(b - 1)\, qL}{\mu_n (n_o + p_o)(1+\alpha)}$$

Where L = diffusion length, b = mobility ratio, $\alpha = \frac{s\tau}{L}$ and s is the surface recombination velocity. q is the photon absorption rate, τ is the carrier lifetime, μ_n is the electron mobility and n_o and p_o are the electron and hole carrier densities.

It is clear that if q, L, s, τ, n_o, p_o, α and μ_n are known then b may be determined from V_D. Since a knowledge of the diffusion parameter is required for this, the equation is more suitable for determining the sign of (b-1). If this quantity is positive then the electron mobility is greater than that for holes, the opposite is true for the negative sign of (b-1).

In principle by illuminating a crystal with light which is strongly absorbed the sign of the Dember voltage enables the carrier of higher mobility to be determined. In practice, however, crystals may not behave as isotropic media and surface states and polarisation effects may mask the Dember effect.

6.14 The Dember Effect in CdI_2

The 'c axis' electrode geometry was used to measure the Dember voltage in CdI_2. Polarisation effects were found to be extremely important however, and a sample was therefore used without previous exposure to illumination or electric field. At low temperatures the absorption edge in CdI_2 is near 3.5eV and photoconductivity is strong near 4eV; the illumination used for the Dember effect was therefore 4.43eV (280mμ). This energy is strongly absorbed but does not come into the strong exciton region near 5.5eV.

The initial experiments were performed upon crystal $HCCX_1$. Fig. 6.11 illustrates the effect of illumination at zero field (fig. a) followed by subsequent illuminations (b and c). When the electric field was applied in the front positive direction the effect was as shown in (d), the opposite effect occurred when the field direction was reversed. Illumination at zero field therefore had the same effect as illumination with an applied field in the front +ve direction. It is also interesting to note that illumination at zero field was determined by the polarity of the previously applied field. This effect may be seen in figs. 6.11(e) and 6.11(i). Crystal $HCCX_2$ was therefore used without previous exposure to light other

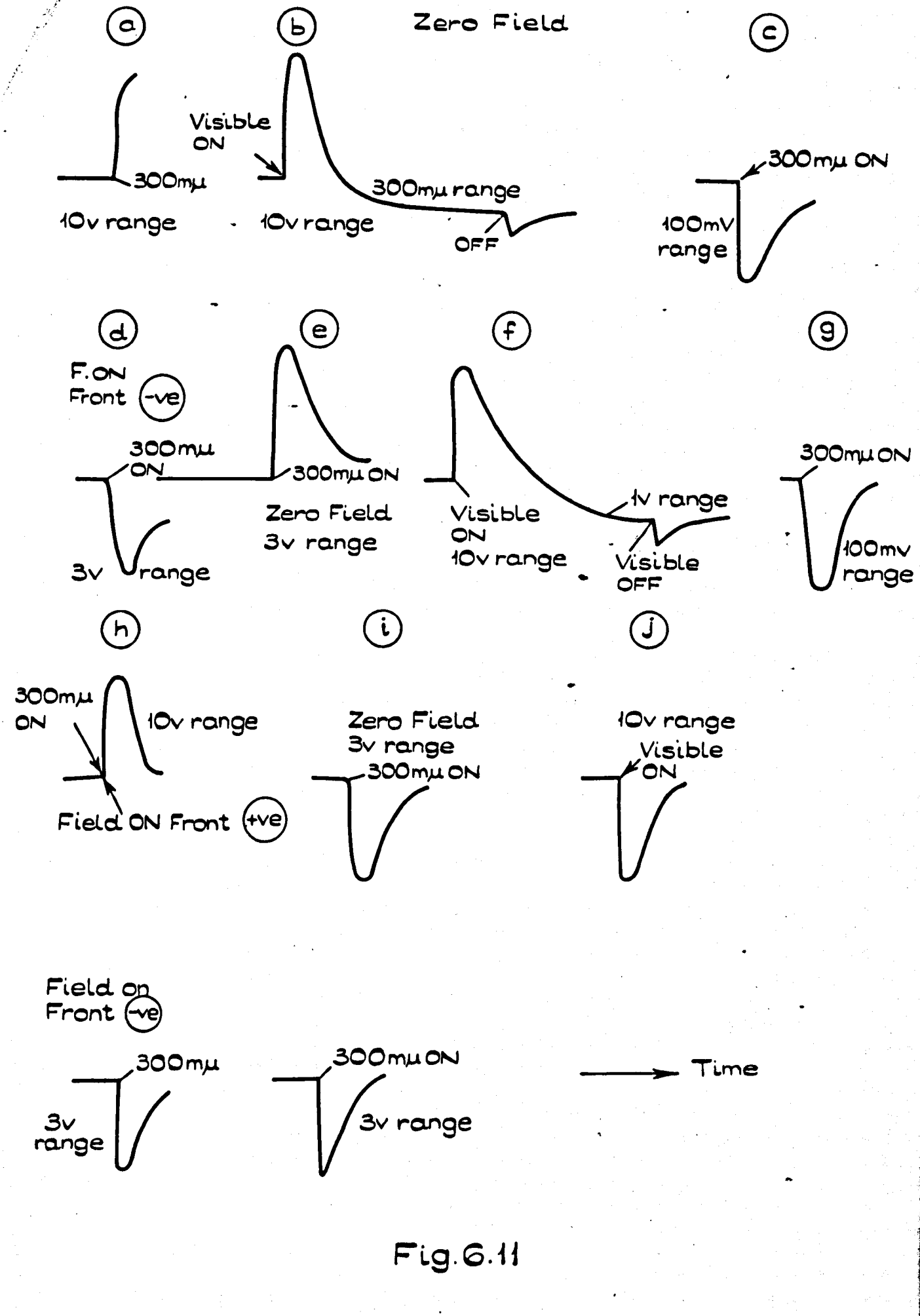
a
b
Zero Field
c
Visible
ON
300mμ
10v range
10v range
300mμ range
OFF
300mμ ON
100mV
range
d
e
f
g
F. ON
Front
-ve
300mμ
ON
3v
range
300mμ ON
Zero Field
3v range
Visible
ON
10v range
1v range
Visible
OFF
300mμ ON
100mv
range
h
i
j
300mμ
ON
10v range
Field ON Front
+ve
Zero Field
3v range
300mμ ON
10v range
Visible
ON
Field on
Front
-ve
300mμ
3v
range
300mμ ON
3v range
Time

Fig. 6.11

than that from a darkroom safe-light. No external field was applied before these measurements.

Illumination at 10°K with zero field produced the effect shown in fig. 6.12. The effect of illumination at zero field was to cause a current in the same direction as illumination with the electric field in the front -ve direction. Illumination with weakly absorption light (360mμ) caused an opposite effect which was then duplicated by the 280mμ illumination (figures a, b and c). A glow curve was then performed with the front -ve polarity and the measurements repeated and illustrated in figures (e) to (h). A second glow curve was performed with reversed polarity and the 280mμ illumination used with zero field, the effect shown in fig. 6.12(j) reproduced the previous results. The effect of the 280mμ illumination at zero field was therefore similar to that produced by illumination with an applied field in the front -ve direction. This means that electrons moved more rapidly than holes towards the rear of the sample, thereby indicating that the mobility of electrons was greater than that of holes at this temperature. Weakly absorbed light (360mμ) tended to reverse this effect, presumably because it produced a photoeffect in the Dember field.

After these experiments the sample was warmed to room temperature to remove polarisations and then cooled to 79°K. The experimental procedure described at 10°K was then repeated. The results obtained were in agreement with those found at 10°K, a similar cycling procedure was adopted to obviate the effects of polarisation.

We conclude from the above results that electrons are more mobile than holes in CdI_2 at both 10°K and 79°K.

The measurements at room temperature were complicated by the ionic current which tended to cause polarisation.. An experiment was performed and the results obtained are illustrated in fig. 6.13. The effect of 280mμ illumination was in the opposite direction to that for the lower temperature experiments. Illumination with light at lower energies produced an effect in the same direction as the 280mμ illumination, but prolonged illumination tended to reverse the effect (figs. 6.13(c) and (d)). When the 380mμ illumination was repeated it remained in the direction opposite to the higher energy illumination direction. Figure 6.13(d) illustrates the opposite effects of 360 and 380mμ illumination. The direction was found to change between 370mμ and 375mμ.

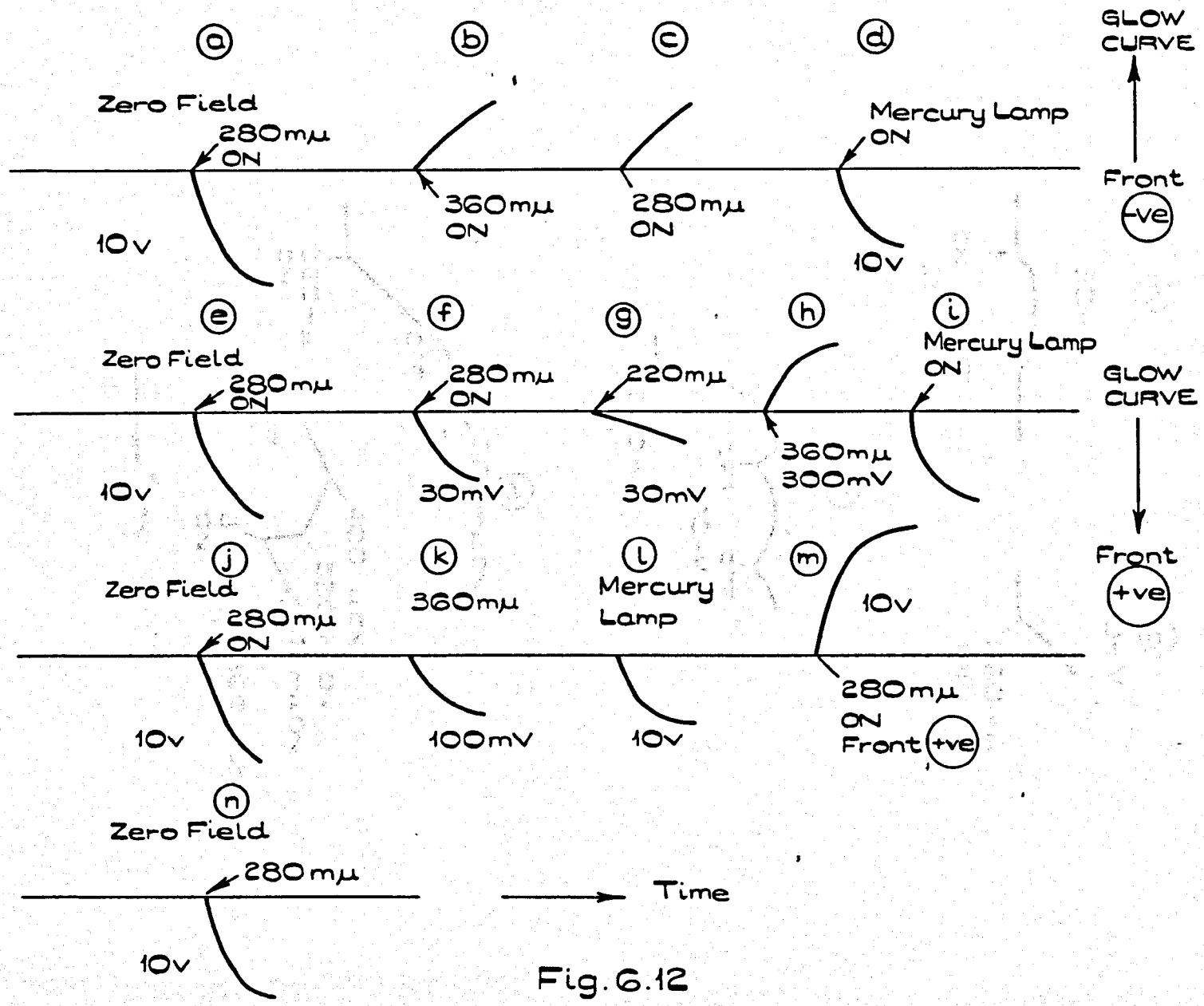
a
Zero Field
280mμ ON
10v
b
360mμ ON
c
280mμ ON
d
Mercury Lamp ON
10v
GLOW CURVE
Front -ve
e
Zero Field
280mμ ON
10v
f
280mμ ON
30mV
g
220mμ
30mV
h
360mμ 300mV
i
Mercury Lamp ON
GLOW CURVE
Front +ve
j
Zero Field
280mμ ON
10v
k
360mμ
100mV
l
Mercury Lamp
10v
m
10v
280mμ ON Front +ve
n
Zero Field
280mμ
10v
Time

Fig. 6.12

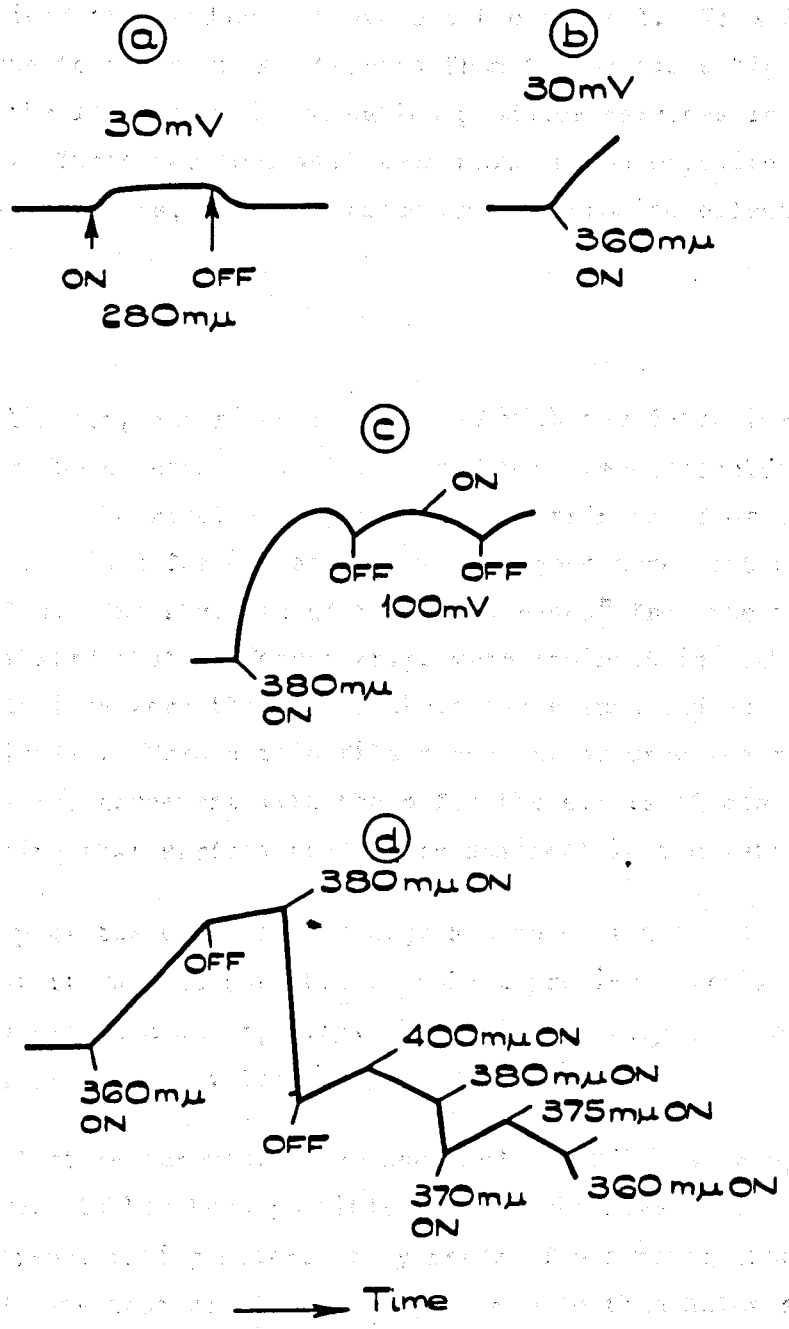
a
30mV
ON
OFF
280mμ
b
30mV
360mμ
ON
c
ON
OFF
OFF
100mV
380mμ
ON
d
380mμ ON
OFF
360mμ
ON
400mμ ON
380mμ ON
375mμ ON
OFF
370mμ
ON
360 mμ ON
Time

Fig. 6.13

Illumination with high energy photons produces carriers near the surface, these may then diffuse and lead to a Dember voltage and field. This situation occurs for 280mμ and 360mμ illumination. At lower energies, however, the absorption coefficient may be low and photo-generated carriers are produced throughout the crystal. If a Dember field exists due to the carriers trapped from the previous high energy illumination, the low energy illumination produces carriers in an electric field. These carriers will then move in the opposite direction to the original carriers, thereby producing the opposite effect.

6.15 Summary

Some preliminary experiments concerned with the determination of trap depths have been described. The trap depths were calculated using a simple model and the results compared with other methods of analysis. The energies determined for one sample were in good agreement with those for other samples. The strength of the "glow peaks" from the two sample geometries indicated that different traps were dominant in each case. Tentative conclusions were then drawn about the volume and surface recombination levels. When a thin film specimen was used the results were in qualitative agreement with those for the a axis single crystal sample, indicating that surface traps were dominant in the latter case.

The purity of the crystals was high and no dominant impurity existed, so that it was not possible to make a precise correlation between a dominant glow peak and an impurity. The main impurity was iron and this may contribute to the volume trap at 0.5eV.

Dember effect measurements have been made in CdI_2 using apparatus of a simple type. It has been possible to make the measurements on this highly self-polarising materials by means of a cycling procedure. The results indicate that electrons are more mobile than holes at $10^{o}K$ and $79^{o}K$ but that at RT a slight reverse effect exists.

REFERENCES

Bube, R.H., 1955, J.Chem.Phys. 23, 18.

Bube, R.H., 1960, Photoconductivity of Solids, Wiley.

Grossweiner, L.I., 1953, J.App.Phys. 24, 1306.

Haine, M.E. and Carley-Read, R.E., 1968, Brit.J.Appl.Phys. , 1257.

Heyningen, R.S. van, and Brown, F.C., 1958, Phys.Rev. 111, 462.

Mon, J.P., 1966, C.R. Acad.Sci. Paris, 262 B, 493.

Phillipe, J. and Langouet, L., 1967, C.R.Acad Sci. Paris, 265 B, 414.

Randall, J.T. and Wilkins, M.H.F., 1945, Proc.Roy.Soc. 184, 366.

CHAPTER SEVEN

STUDIES OF THE EFFECTS OF PHOTDECOMPOSITION OF CADMIUM IODIDE

7.1 Introduction

The preceding chapters have been chiefly concerned with experimental measurements of photoconductivity and reflectivity in single crystals of cadmium iodide. These experiments were designed to yield information on the electronic structure of the material and complemented the optical absorption measurements performed by Brahms (1965), Tubbs (1968) and Greenaway and Nitsche (1965).

Real crystals contain frequent departures from the ideal crystal structure; these departures may be in thermodynamic equilibrium and are therefore intrinsic defects or appear as the result of the preparation of the crystal, for example as defects associated with impurities. Many imperfections extend over more than one lattice site and occur in the form of line, plane or volume defects. Some physical properties are influenced by the concentration of defects, for example many mechanical properties are dependent upon dislocations, whereas the electrical conductivity is often dominated by point defects.

When a crystal is illuminated with light in the region of fundamental absorption leading to photoconductivity, the photo-generated charges are trapped at defects, the nature and abundance of trapping centres therefore has a profound effect upon photoconductivity response. We have therefore performed experiments to investigate the trapping centres in CdI_2 ; the method of thermally stimulating currents was used, these experiments are described in Chapter Six. Although the purity of the samples used was high, so that they contained less than 5p.p.m. of impurity, many different trapping levels were found. It was possible to draw conclusions about the identity of volume and surface traps from these measurements.

Studies of the photoconductivity in ionic crystals are inevitably linked with those of the dark conductivity, since the two components of

the total current may be comparable. It is possible by studying the temperature dependence of the dark current to determine the activation energies of the defects contributing to the ionic current. The temperature dependence of the dark current in CdI_2 has been studied by Yu (1967) who investigated the effect with the electric field both perpendicular to and parallel to the cleavage plane.

All of the above studies were on crystals of high quality. The defects in the crystals were therefore either in thermodynamic equilibrium; or present through unavailable impurities or mechanical strain. Studies of defects may be simplified, however, by the incorporation of varied, measured quantities of defects so that the corresponding change in the physical properties may be observed. In, for example, glow curve determinations the impurity concentration may be varied and the effect on the glow curve measured. It may then be possible to correlate impurity species with specific trapping levels.

Cadmium iodide belongs to a group of materials which decompose when exposed to light in the region of fundamental absorption. Photodecomposition may therefore be used as a means of producing a concentration of defects. The defect concentration may be varied by adjusting the exposure and the temperature.

7.2 Photodecomposition in Crystals of Cadmium Iodide

The photodecomposition of cadmium iodide has been reported by Yu (1967) and by Fotland (1960). These experiments were concerned with the photosensitivity of filter papers soaked in a solution of CdI_2 in water and dried. The sensitivity of CdI_2 paper is sufficient to enable images to be recorded at room temperature. The exposure required to produce perceptible darkening is of the order of 10^{16} quanta of ~3.4eV energy. The photosensitivity of papers is high compared with that for crystals, in the latter case some 10^{20} quanta produced no effect at room temperature. Fotland has suggested that the increased photosensitivity of papers may be due to the smaller crystal size and consequent increase in effective surface area aided by the moisture trapped in the paper.

Although studies of photodecomposition in CdI_2 have not been extensive, many experiments have been reported for PbI_2 which has similar structural and electronic properties. In particular Tubbs (1965) has shown that PbI_2 crystals and films are photosensitive to light in the region of fundamental absorption; the maximum photosensitivity occurs near 190°C so that decomposition does not occur at room temperature. The fundamental optical absorption in PbI_2 begins in the visible region and causes the material to be yellow. Photodecomposition is accompanied by a marked change of colour so that a sharp contrast is observed between the exposed and dark regions. The resolution of this process when used to record images is at least as good as that of available optical systems (e.g. ~1μ).

Cadmium iodide single crystals are colourless and therefore do not exhibit a sharp contrast when decomposition occurs. Temperatures near 250°C were necessary to cause appreciable decomposition even when the total output of a Xenon arc lamp was used. This lamp was found to be particularly advantageous since it had a high output in the ultra violet and strong lines in the infra-red which tended to heat the crystal. When this lamp (with a total emission of ~100mW) was used visible decomposition occurred after several hours at 250°C. When the temperature was increased the crystals began to sublime so that the optimum temperature depended upon the decomposition and evaporation rates.

A typical CdI_2 single crystal as taken from solution is illustrated in fig. 7.1. There is clear evidence of a growth spiral on the surface of the type described by Forty (1951) as well as surface inclusions and small crystallites. The appearance of the crystal was changed markedly by decomposition, fig. 7.2 illustrates this effect, in particular preferential decomposition along the edges of growth spiral steps and at surface irregularities such as small crystallites. Photodecomposition does not appear to have caused appreciable lateral displacement of the growth spiral steps. The penetration of the decomposition along the face of each step appears to have been independent of the width of the faces. The narrower faces have been entirely decomposed, whereas the wider ones have large areas free from decomposition. This seems to indicate that photodecomposition proceeds inwards from the edge of the step, occurring most readily at the edge of a decomposed region. The edges of the decomposed regions are not straight, indicating a non uniform decomposition rate;

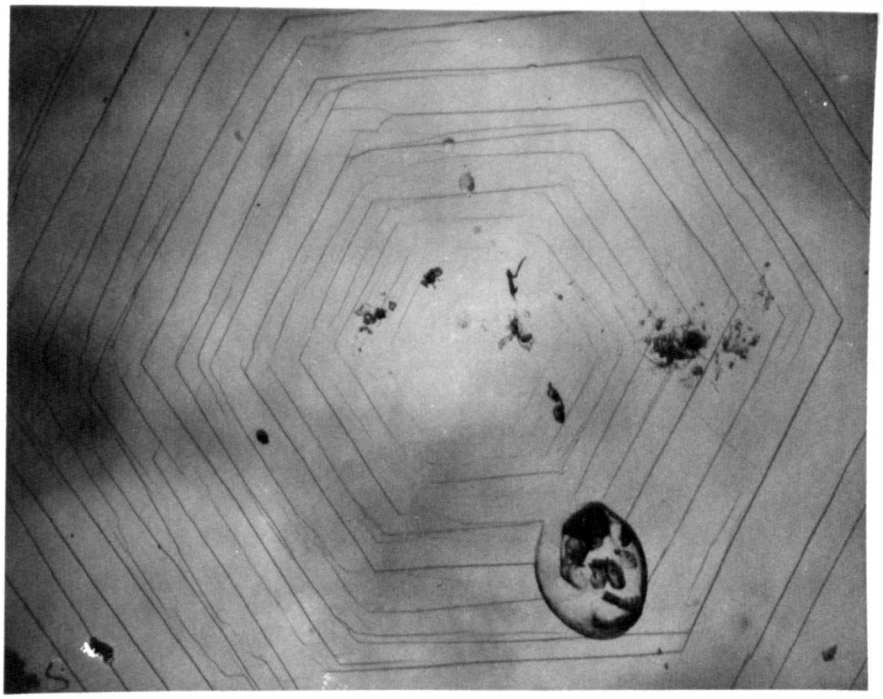

100μ

Fig. 7.1

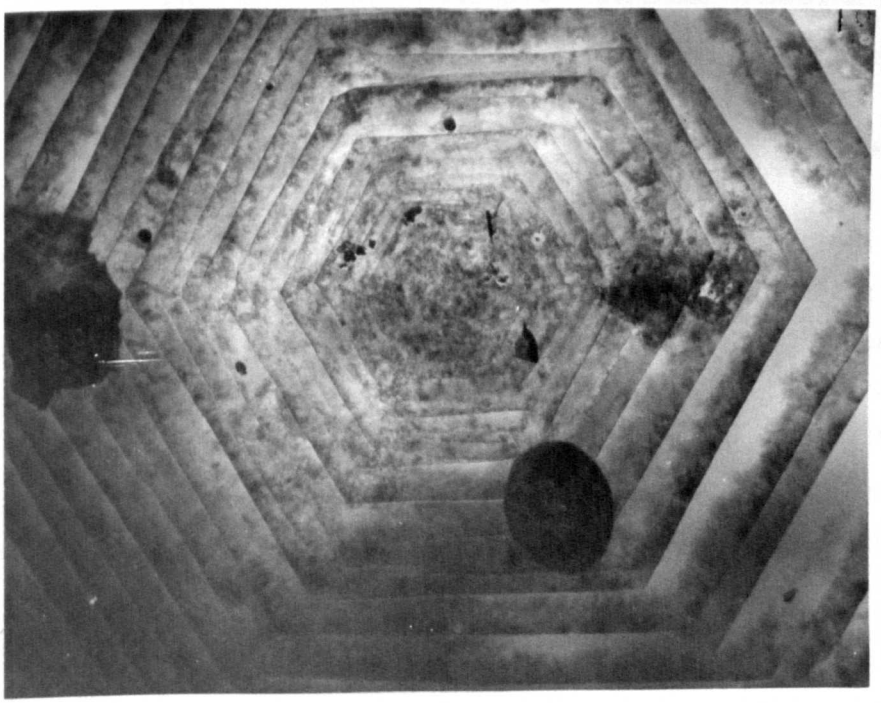

100μ

Fig. 7.2

closer examination, however, reveals that this effect is sometimes due to photodecomposition beginning at less well defined growth steps. The preferential decomposition at step edges may be due to the increased probability of charge trapping at the edge, coupled with the lower formation energy of ionic defects at the edge.

The effect of decomposition was particularly noticeable when a mask was used to prevent photodecomposition of part of the crystal (fig. 7.3). The preferential decomposition is again in evidence but the exposure was greater. There was a sharp dividing line between the exposed and the clear regions. With the increased decomposition there was a tendency to form discrete particles of decomposition products. There was no evidence to suggest a movement of the growth spiral step even with increased magnification (figs. 7.4 and 7.5). At the edge of the masked zone illustrated in fig. 7.5 straight filaments of decomposition products may be observed. These filaments appeared to have grown along crystallographic directions, two main directions had an included angle of 60°. There was some doubt about the formation mechanism of the filament. They could, for example, indicate an early stage in decomposition since they were formed in a region where the illumination intensity was low, or their growth may have been connected with the presence of the heavily decomposed region. It is also possible that grown-in defects such as dislocations had been decorated by the decomposition products.

Preliminary investigations of the spectral variation of photodecomposition have been carried out by Yu (1967) using CdI_2 papers. Images could be formed using photon energies greater than 2.9eV and up to at least 4.9eV. The peak sensitivity was at a somewhat higher energy than the onset of photodecomposition and was probably near 3.4eV. Although the intensities were not measured, the photodecomposition appeared to have a similar spectral variation to the optical absorption spectrum. We have repeated this experiment and obtained similar results. The images placed onto CdI_2 paper were bleached after several weeks so that direct image recording and storage is not possible. The images were apparently more permanent when stored in a dessicator so that water vapour may be connected with the bleaching process.

In the case of lead iodide Tubbs (1965) has shown that photodecomposition and photoconductivity have similar spectral variations for thin film specimens. In the case of CdI_2 no results have been

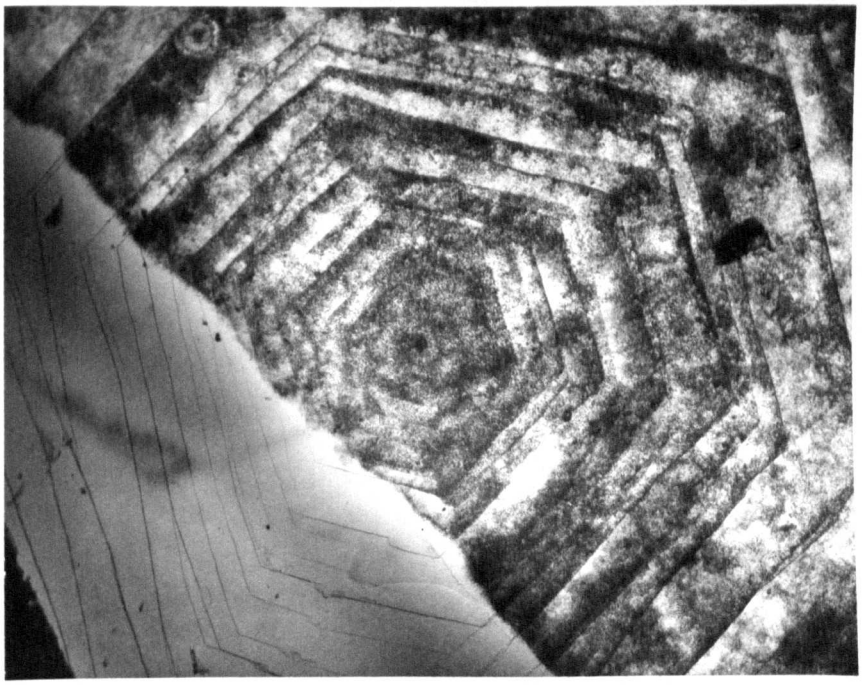

100μ

Fig. 7.3

100μ

Fig. 7.4

10μ

Fig. 7.5

obtained for thin film specimens because of the high temperatures required and consequent evaporation of the film. In the case of single crystals the efficiency of photodecomposition is so low that the spectral variation cannot be determined because of lack of intensity

7.3 The Photoconductivity of Photodecomposed Crystals of CdI_2

Detailed investigations of photodecomposition could not be carried out because of the large exposures at high temperatures necessary to produce visible decomposition. A more sensitive technique was therefore required to determine small amounts of decomposition. This uses the fact that photodecomposition produces defects to change the photoconductivity response, thereby enabling photoconductivity to be used to estimate photodecomposition.

Since photodecomposition involves the heating of the sample to 200°C, experiments were performed to find the effect, if any, of this heat treatment. A photoconductivity experiment was performed, the sample was then heated to the decomposition temperature after which the photoresponse was measured and any change noted. The photodecomposition then took place and the change in photoconductivity was measured.

The cryostat described in Chapter Two was used for the photoconductivity measurements. It was provided with a small 'Nichrome' heating coil so that the decomposition could be performed 'in situ' thereby maintaining the same experimental environment before and after decomposition.

Initially attempts were made to produce photodecomposition in vacuo but these were unsuccessful. When CdI_2 crystals are heated in vacuo to near 180°K they evaporate so that photodecomposition cannot be observed. This effect was clearly demonstrated when sample AX_{11} was heated to ~200°C in vacuo. When the Xenon arc was used to irradiate the specimen the suprasil window on the vacuum vessel became cloudy with evaporated CdI_2.

There was an effect due to the heating which is illustrated in fig. 7.6. The original photoconductivity spectrum at 180°K had a single peak at 3.45eV but after heating to 200°C the peak split into two components.

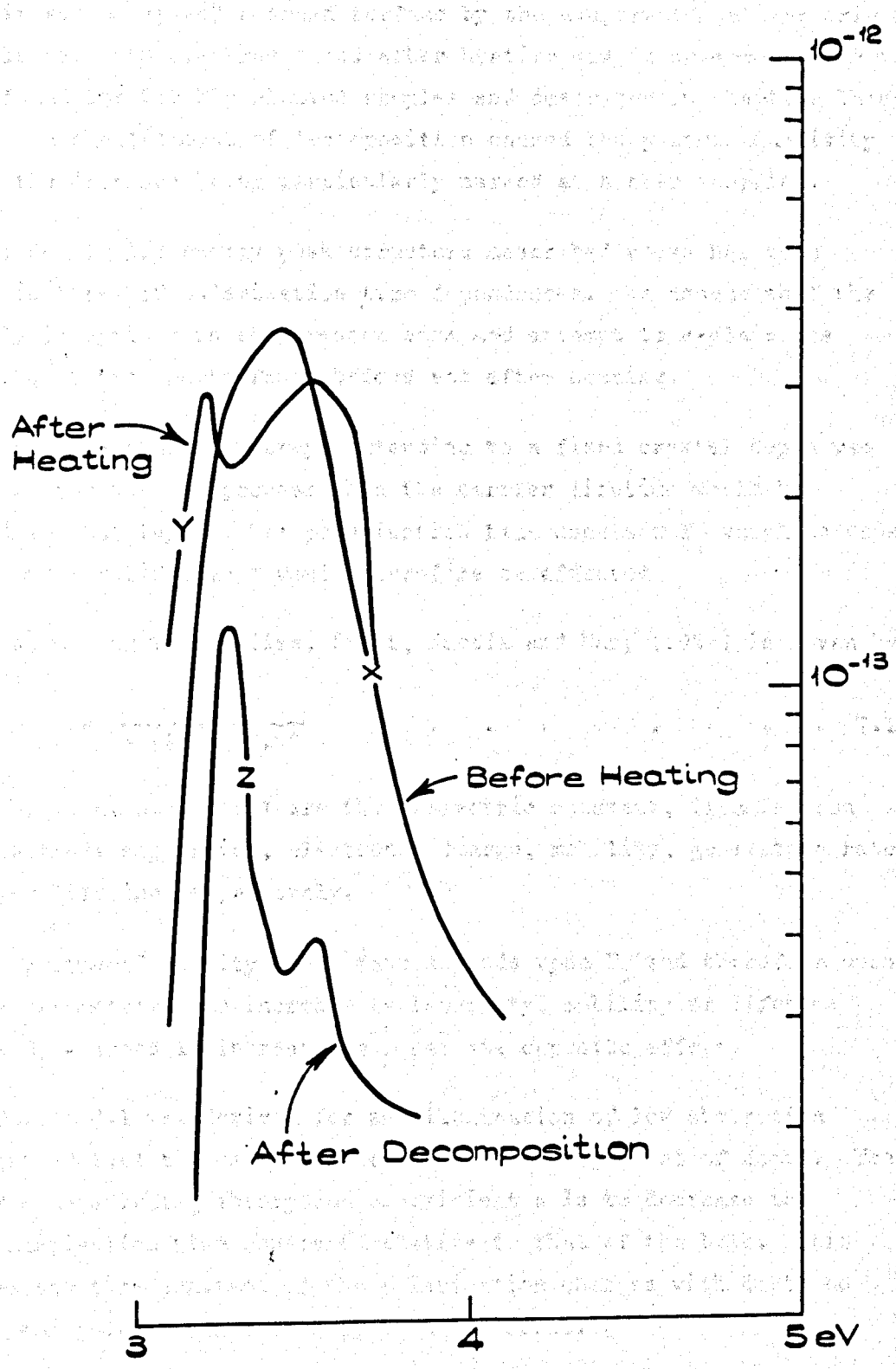
10^{-12}
10^{-13}
After Heating
Y
X
Z
Before Heating
After Decomposition
3
4
5 eV

Fig. 7.6

The effect of the heating may be interpreted in the following way. Heating in vacuo exposed a fresh surface by the evaporation of the original surface layer. The spectrum found after heating was in agreement with the spectra found for freshly cleaved samples and described in Chapters Three and Four. A small amount of decomposition caused the photoconductivity to fall, the decrease being particularly marked at higher energies.

The double low energy peak structure described above has been analysed in terms of polarisation time dependences. We assume that the same analysis applies in the present case and attempt to explain the change between the specta found before and after heating.

If a given number of traps extending to a fixed crystal depth was depleted by the heating process then the carrier lifetime would be increased in that layer. The polarisation time constant T_1 which depends upon the carrier lifetime τ would therefore be affected.

T_1 according to Ben-Sira, Pratt, Harnik and Many (1959) is given by:

$$T_1 = \frac{\epsilon}{4\pi(1 - \frac{b}{L})e\mu\varphi\tau} \qquad \ldots\ldots\ldots 7.1$$

where ϵ, b, L, e, μ, φ and τ are the dielectric constant, illumination width, electrode separation, electronic charge, mobility, generation rate and carrier lifetime respectively.

The photoconductivity decay rate depends upon T_1 and therefore upon the other parameters. An increase in intensity, mobility or lifetime decreases T_1 whereas an increase in $\frac{b}{L}$ has the opposite effect.

Equation 7.1 was derived for an illumination of low absorption coefficient so that the carrier generation was independent of depth. The effect of non-vanishing absorption coefficient α is to decrease the surface polarisation time constant relative to that of the bulk. This means that the time constant of the polarisation changes with depth so that the rear polarises more slowly than the front.

We approximate for non vanishing absorption coefficient in the following way. Consider a crystal illuminated with strongly absorbed light so that $\alpha >> d$ where d is the crystal thickness. The sample then polarises with time constant T_1 given by equation 7.1. The effect of non vanishing polarisation is to reduce the effective depth of illuminated

sample. If the number of carriers generated is independent of absorption coefficient then the electron density will be higher for strongly absorbed illumination. In this case the illumination extends to a cut-off depth of approximately $\frac{1}{\alpha}$ whereas it extends uniformly for weakly absorbed light. The density of generation is therefore approximately proportional to φ.

If the illumination width b at the generation rate φ are constant for illumination of a given α then any change in T_1 is caused by a change in $\mu\tau$. An increase in $\mu\tau$ is therefore accompanied by a decrease in T_1. The polarisation rate is therefore increased by an increase in $\mu\tau$. Both the mobility and the lifetime increase with decreasing trap density; any increase in crystal quality therefore leads to an increase in polarisation. Polarisation is therefore greatest in high quality samples.

We have indicated in Chapter Four that polarisation leads to a splitting of the low energy photoresponse peak, it is now clear that this effect only occurs in high quality samples where τ is large.

The heating of a cleaved crystal in vacuo therefore caused an increase in the polarisation of the photocurrent, a characteristic of high quality crystals.

Initially the a axis electrode geometry was used for photoconductivity measurements. The effect of photodecomposition was often masked by an increase in the dark current since the a axis geometry is particularly sensitive to surface currents. Visible photodecomposition therefore caused an overwhelming dark current. The effect of the photodecomposition on the photocurrent was difficult to detect when the decomposition was reduced. There was some indication of a reduction in the photoresponse after decomposition, but the exact shape of the spectrum could not be reliably determined.

When a quartz-iodine tungsten filament lamp was used, with the monochromator slit set at 1mm, a broad peak appeared in the photoresponse spectrum with its maximum near 650mμ (1.9eV). The shape of the peak could have been caused by the spectral variation of the incident intensity, it is interesting to note, however, that decomposed crystals have a yellow appearance so that some absorption occurs at shorter wavelengths. There is the possibility that photoemission occurs from metallic Cd or its salts into the conduction band of CdI_2.

When large decomposition exposures were used, so that visible discoloration took place, the surface resistance of the crystals fell by many orders of magnitude to a value near $10^6\Omega$ and even as low as $10^3\Omega$. The dark resistance was then independent of temperature over a wide range between ~180°K and ~350°K. The current was carried in the surface layer since when the surface was removed by cleaving the resistance increased to the original value. Photodecomposition therefore causes a conducting layer which prevents 'a axis' photoconductivity measurements. It was therefore apparent that the 'c axis' geometry was more suitable for these measurements since the decomposed surface could be used as part of the front electrode. The decomposed region does not therefore contribute to the dark current in the 'c axis' direction.

The experiments performed using the 'c axis' geometry were similar to those previously described. In this case because of the different sample holder the decomposition took place in air in a separate apparatus.

The photoconductivity spectrum obtained after the preliminary heating is illustrated in figure 7.7. After decomposition the high energy response fell relative to that at lower energies; increases occurred at 330mμ (3.76eV) and 365mμ (3.4eV). The high energy response at RT was also reduced and was observed by the dark current.

The effect of photodecomposition appears to have been a decrease in the high energy photocurrent combined with a marked increase in the dark current. Since the decomposition was confined to the surface region, the dark current did not seriously increase in the 'c axis' direction so that photoconductivity could be measured on heavily decomposed samples with the electric field perpendicular to the cleavage plane.

The increase in the high energy photocurrent may be interpreted in terms of an increase in the number of surface traps relative to those in the volume of the specimen. The increase in photocurrent at low energies, and in particular near 650mμ, is probably caused by photoemission from the decomposition products into the conduction band. A similar effect has been observed when photoelectrons were emitted from Na particles in NaCl and reported by Gyulai (Mott and Gurney 1948). This effect could account for the increase quantum efficiency at energies below the absorption edge of CdI_2. Further investigations are necessary

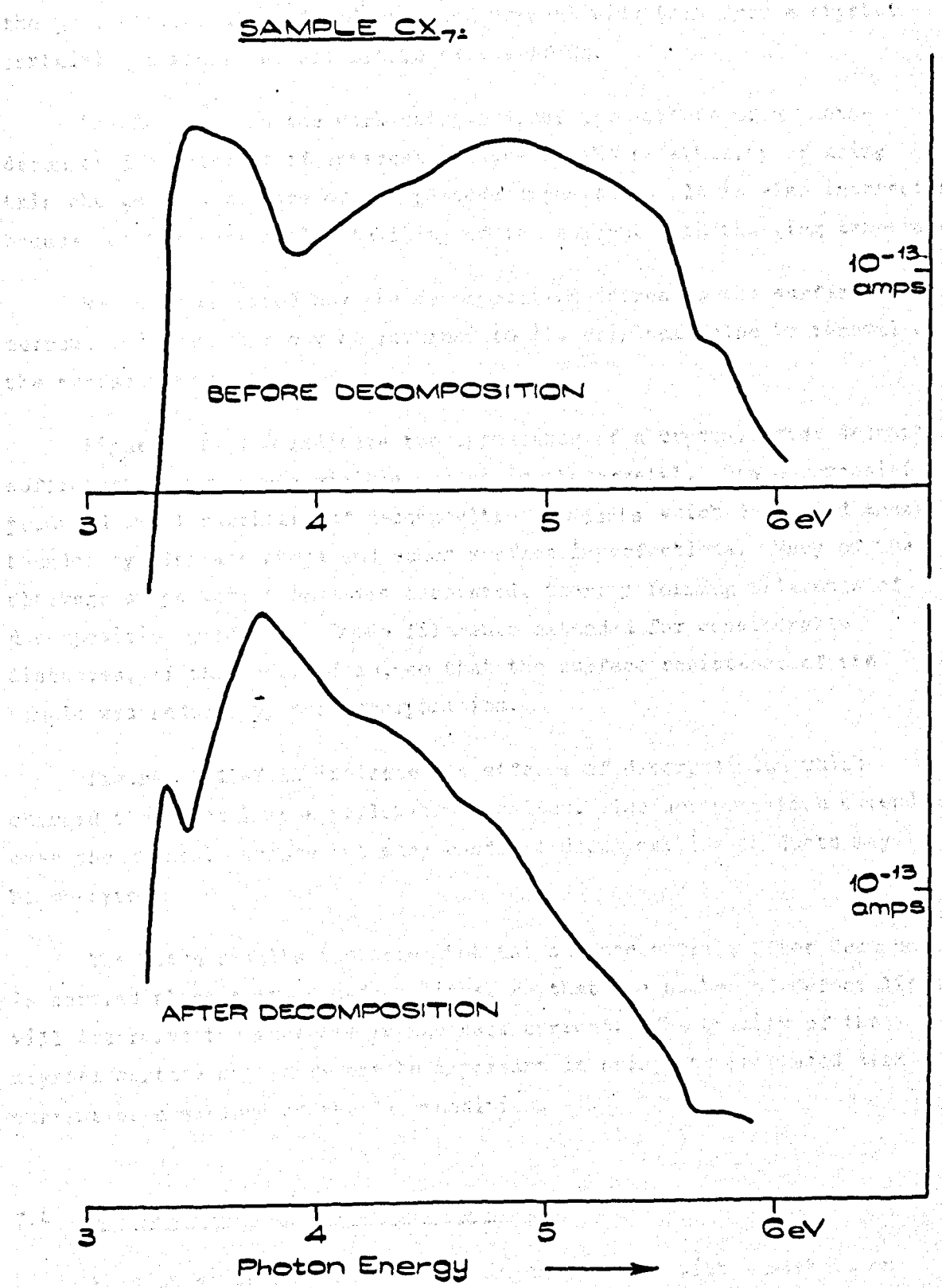
SAMPLE CX7:
BEFORE DECOMPOSITION
10-13 amps
3
4
5
6eV
AFTER DECOMPOSITION
10-13 amps
3
4
5
6eV
Photon Energy

Fig. 7.7

to investigate these possibilities; it would be interesting to determine the stochiometric excess of Cd in a decomposed crystal and to compare the photoconductivity of a decomposed crystal with that from a crystal containing a simple stochiometric excess of Cd.

The increase in the dark current along the surface of a photo-decomposed crystal is of interest because of the possibility of using this change as a measure of the photodecomposition. It is also interesting because of the remarkable stability of the current with changing temperature.

We have indicated how the decomposition increases the surface dark current and that this may be returned to its original value by removal of the surface layer.

Figures 7.8-7.10 indicate the appearance of a crystal after decomposition sufficient to produce a visible change in the crystal. The decomposition produced small particles of decomposition products which decorated areas bounded by cleavage steps and other surface imperfections. Many of the cleavage steps were themselves decorated, thereby forming filaments of decomposition products. These filaments extended for considerable distances, of the order of mm, so that the surface resistance of the sample was reduced by the decomposition.

Figures 7.11-7.12 indicate the effects of decomposition which changed the crystal to a yellow brown colour. The decomposition extended over the crystal surface but many bands of decomposition products may be observed.

The above results indicate that the surface current after decomposition is carried along surface defect lines, so that the number of defect lines will determine the increase in the dark current. The quality of the crystal surface may therefore be important in using the increased dark current as a measure of the decomposition.

7.4 The Movement of Silver through CdI_2

When an applied field was used in conjunction with a mask in an attempt to observe a lateral displacement of the decomposition with applied field no effect could be observed. When the applied potential was connected to the crystal by 'silver dag' electrodes an interesting

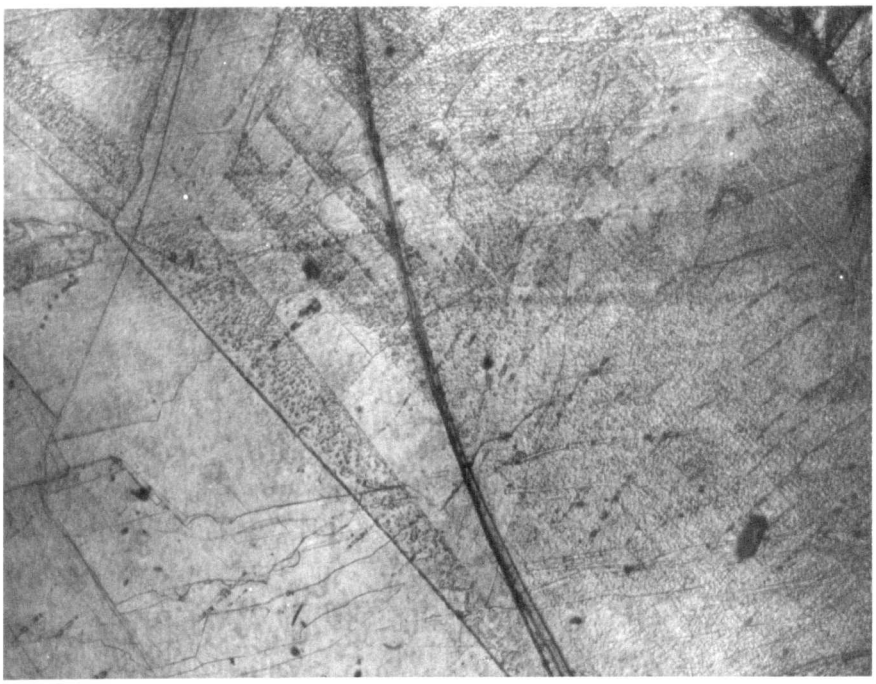

Fig. 7.8

100μ

Fig. 7.9

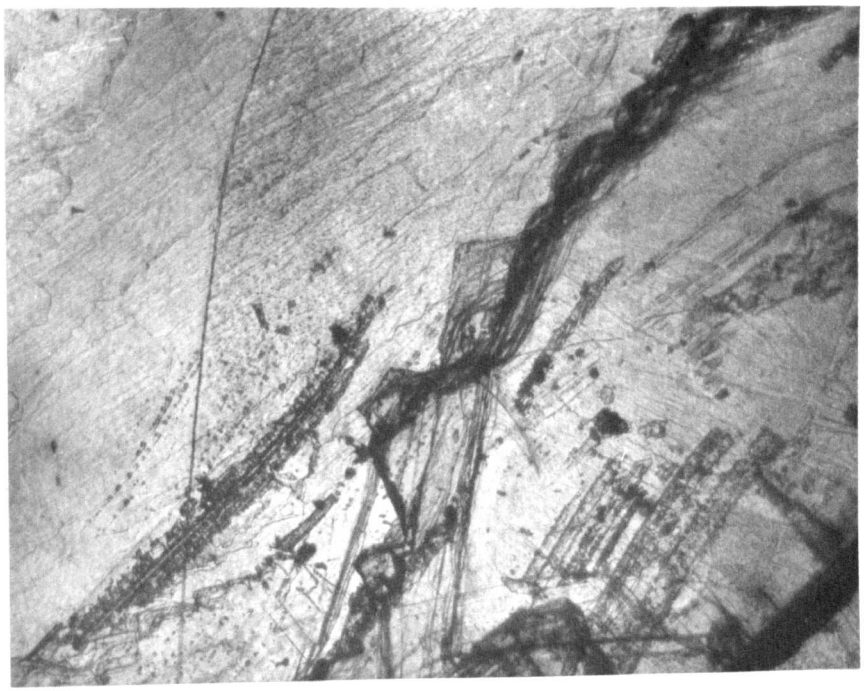

Fig. 7.10

100μ

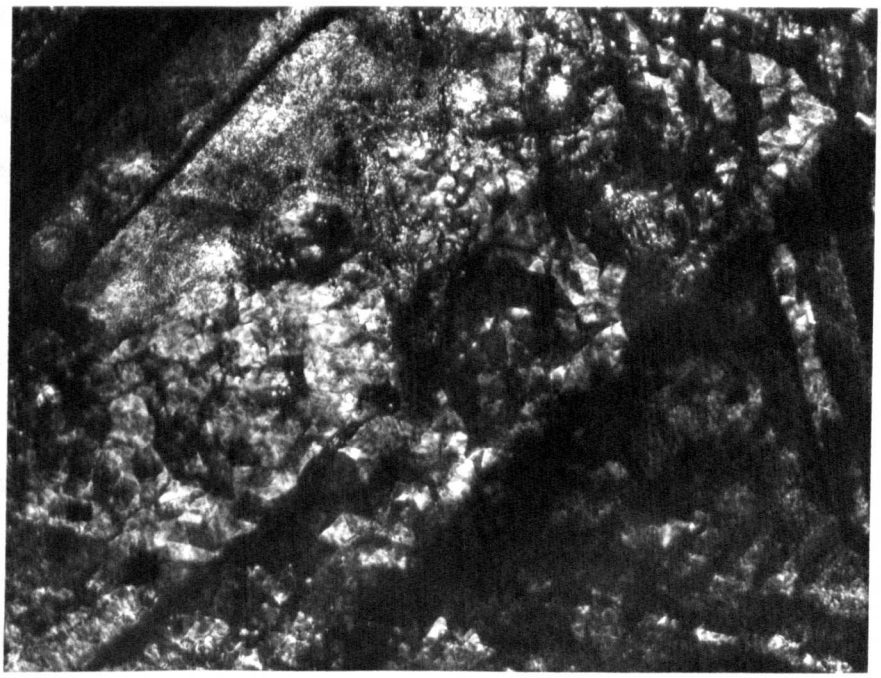

Fig. 7.11

effect was observed. The sample was heated to 250°C and illuminated with the total output of a Xenon arc lamp. The illumination caused a photocurrent of several μA when a field of several hundred volts per cm was applied. There was no polarisation of the photocurrent. The absence of polarisation is attributed to the absence of active traps so that no polarisation field was built up at this temperature.

An irreversible current effect was, however, found in many crystals. The total current through the crystal increased with time and eventually attained such a high value that the crystal was severely damaged. Prolonged application of the electric field in the dark, also caused this effect. Microscopic investigation revealed that branches of silver were growing from the negative electrode towards the positive. When a branch of silver eventually reached the positive electrode a short circuit occurred because of the high conductivity of silver; the crystal was then severely damaged if the applied field was not reduced.

Some typical silver branches are illustrated in fig. 7.13. An interesting interference fringe system was observed around all such branches. The fringes are caused by the wedge system formed when the layers of CdI_2 are forced apart by the silver branch. A double fringe system may be observed in many micrographs indicating that some growth has taken place in a direction perpendicular to the cleavage plane, alternatively, a second branch may have formed at a different level. The branches growing from the electrode in figures 7.13 and 7.14 appear to be growing preferentially from a region of continuous silver, the growth has not occurred as readily in regions where the silver dag is not continuous. When the branches have been growing for an appreciable distance they split into smaller branches, as shown in fig. 7.15. The interference fringes extend over large distances, of the order of mm, indicating that the surface deformation may be extensive.

Although there does not generally appear to be preferential growth along cryatallographic directions some branches do follow cleavage or growth spiral steps. Figure 7.16 illustrates a branch growing along such a step.

The fringe spacing measured at the outer edge of typical systems was $\sim 2\mu$ per fringe so that the wedge angle was approximately 0.1 radians. The thickness of the branches in the direction perpendicular to the cleavage

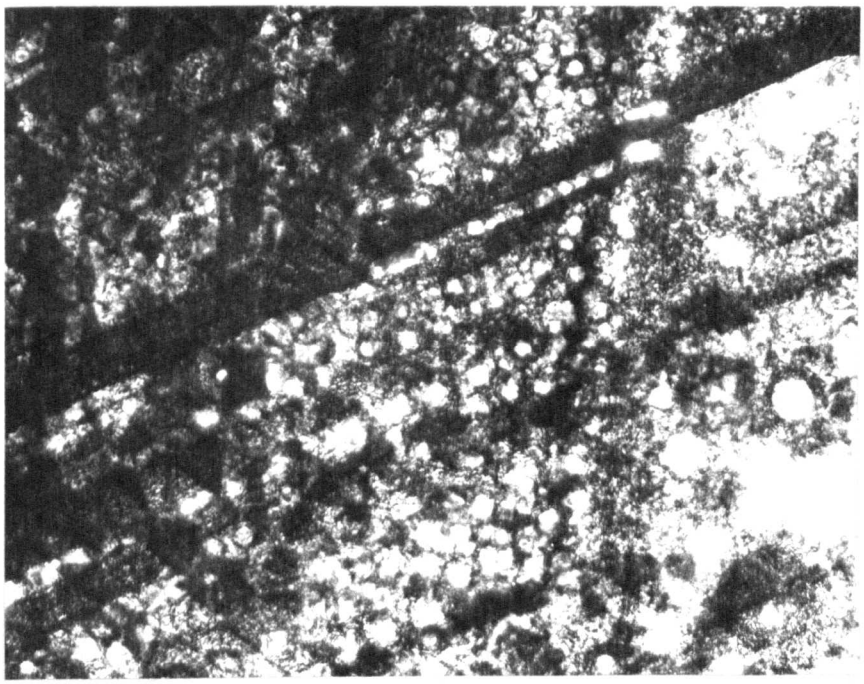

Fig. 7.12

100μ

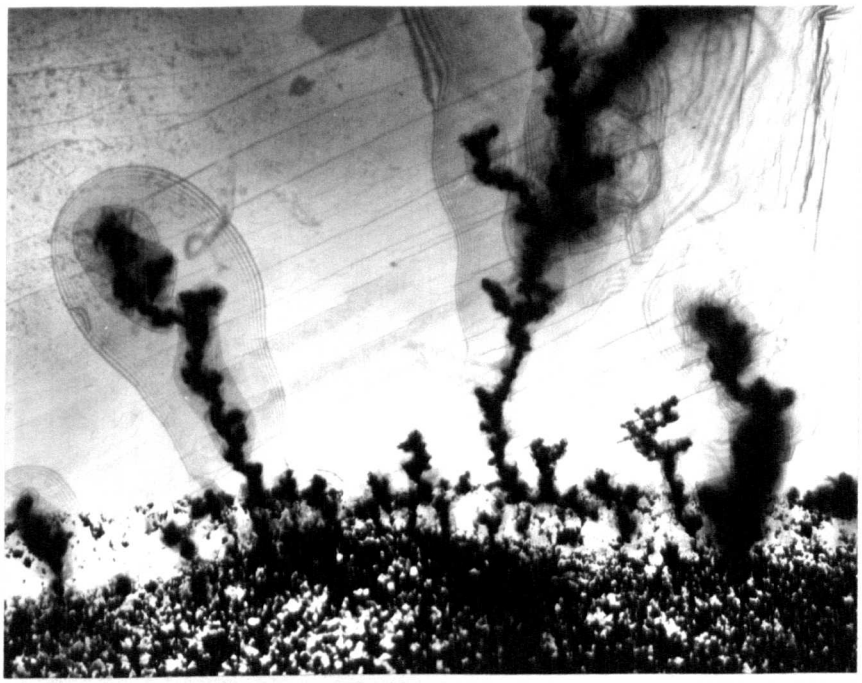

Fig. 7.13

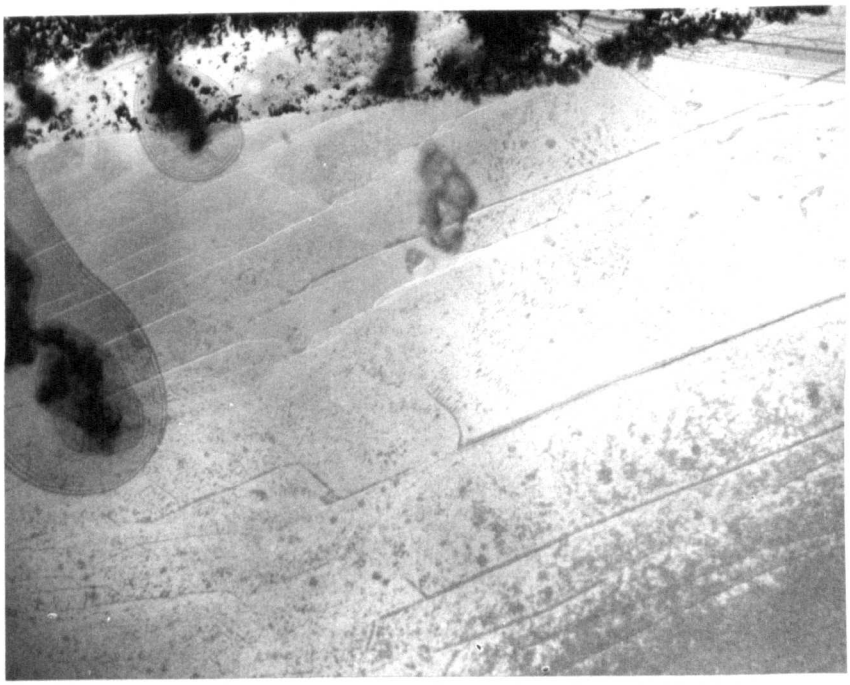

Fig. 7.14

100μ

Fig. 7.15

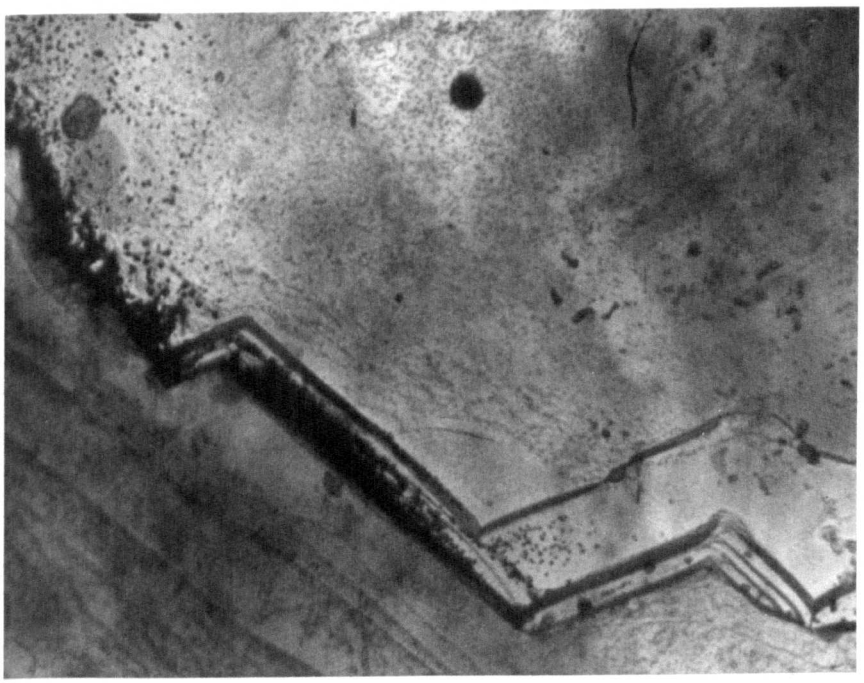

100μ

Fig. 7.16

plane on this basis was therefore ≈1μ. The true thickness was of the order of 10μ; this was determined by the optical microscope using the depth of focus method. The discrepancy was probably due to the non linearity of the wedge sides, in particular the wedge angle will be greater near the branch.

Although the double fringe system indicates a lateral thickness of the branches it does not necessarily indicate branching perpendicular to the cleavage plane. An experiment was therefore performed whereby a sandwich electrode configuration was used. A semi transparent silver dag electrode was painted onto the top surface of the crystal and an opaque electrode of normal thickness on the rear. The electric field was at least 20 times that used in the successful 'a axis' experiments but no silver diffusion could be observed. It was more difficult to observe any growth in this sample but no irreversible current or sample shorting occurred even after many hours at 270°K. This result is evidence for the higher mobility of Ag ions in the cleavage plane compared with that in the perpendicular direction. There is also the possibility that, since silver arms grow within a few microns of the surface, the relative ease of lifting the surface in the a axis case contributes to the rapid growth along the cleavage plane. Typical silver branches grew at the rate of 10μ/sec in the former direction with applied fields of ≈500V/cm.

The effects described above were all observed with 'silver dag' electrodes. Similar effects have been observed with solid silver but the effect was less pronounced because of the poorer contact between the metal and the sample. No effect could be detected with either solid gold or evaporated gold electrodes even when a temperature of 270°C and intense Xenon arc illumination for ~10 hours was used. This result indicates that silver in any form is an unsuitable material for electrodes to measure ionic conductivity in CdI_2, particularly at temperatures above 200°C. Evaporated gold electrodes do not appear to have any undesirable effects at any of the temperatures likely to be used in such experiments.

7.5 Summary

When single crystals of CdI_2 were irradiated with ultra-violet light at 250°C they decomposed and the decomposition was confined to the surface layers.

The surface decomposition occurred preferentially along defect lines thereby increasing the dark current by many orders of magnitude. The increased dark current was largely temperature independent so that the a axis photoconductivity could not be measured with visible photodecomposition. The c axis geometry was therefore adopted, enabling larger amounts of decomposition to be used.

There was an increase in the photoresponse at low energies after the decomposition which may have been caused by photoemission from the decomposition products.

A change in photoconductivity after heating in vacuo has been interpreted in terms of a change in surface quality and consequently change in polarisation time constant.

The results described above indicated that the dark current is more sensitive to photodecomposition than the photocurrent. The dark current after decomposition is carried along surface irregularities so that the increased current depends upon the surface quality of the sample.

When an applied field was used in an attempt to measure any displacement of the photodecomposition products an irreversible effect was observed due to the migration of silver from the silver dag electrodes. This effect suggests that silver dag must not be used for high temperature conductivity measurements in CdI_2. High temperature dark current measurements reported by Fotland (1959) and by Yu (1967) were probably subject to this effect and should be repeated using evaporated gold electrodes.

REFERENCES

Ben-Sira, M.Y., Pratt, B., Harnik, E. and Many, A., 1959, Phys.Rev. 115, 554.

Brahms, S., 1965, Physics Letters 19, 272.

Forty, A.J., 1951, Phil.Mag. 42, 670.

Fotland, R.A., 1959, M.Sc. Thesis, Case Inst. of Technology.

Fotland, R.A., 1960, J.Chem.Phys. 33, 956.

Greenaway, D.L. and Nitsche, R., 1965, J.Phys.Chem. Solids 26, 1445.

Mott, N.F. and Gurney, R.W., 1948, Electronic Processes in Ionic Crystals, Oxford.

Tubbs, M.R., 1965, Proc.Roy.Soc. 284, 272.

Tubbs, M.R., 1968, J.Phys.Chem.Solids 29, 1191.

Yu, R.M., 1967, Ph.D. Thesis, Bristol.

CHAPTER EIGHT

THE OPTICAL AND ELECTRONIC PROPERTIES OF CADMIUM IODIDE

8.1 Introduction

This chapter summarises some of the relevant structural and opto-electronic properties of CdI_2. The properties of pure material will be discussed in the first part; in later sections attention will be directed towards the effects of imperfections on these properties. Some aspects of decomposition in CdI_2 will also be discussed.

8.2 The Crystal Structure of Cadmium Iodide

Cadmium iodide crystallizes in the well-known hexagonal plate habit. This structure has been found in crystals grown from solution, melt or vapour, it may be described in terms of a lattice of close packed iodide ions with the Cd^{++} ions occupying half of the octahedral interstices between alternate planes of iodide ions. The effect of this positioning is to form sandwich-like layers of cadmium ions between layers of the larger iodide ions (figure 8.1). The bonding between oppositely charged layers is mainly ionic, whereas the adjacent layers of iodide ions experience a Van der Waals attraction. The bonding between iodide layers, and therefore between the I-Cd-I sandwiches, is thus greater than that between the cadmium and iodine ions of the sandwiches. The crystal therefore cleaves along the basal plane more readily than in any other direction.

Since the structure of CdI_2 is based upon the close packing of iodide ions it is possible to arrange the packing in various ways.

If the first two layers are packed together as shown in figure 8.2a and 8.2b the third layer may be directly above A when the packing may be designated ABAB, alternatively this layer may be positioned as C and the packing sequence is then ABCABC. The former sequence leads to hexagonal close packing and the latter to cubic. It is clear that successive layers may be packed according to different sequences, each sequence has a different number of layers in its repetition period and is called a polytype.

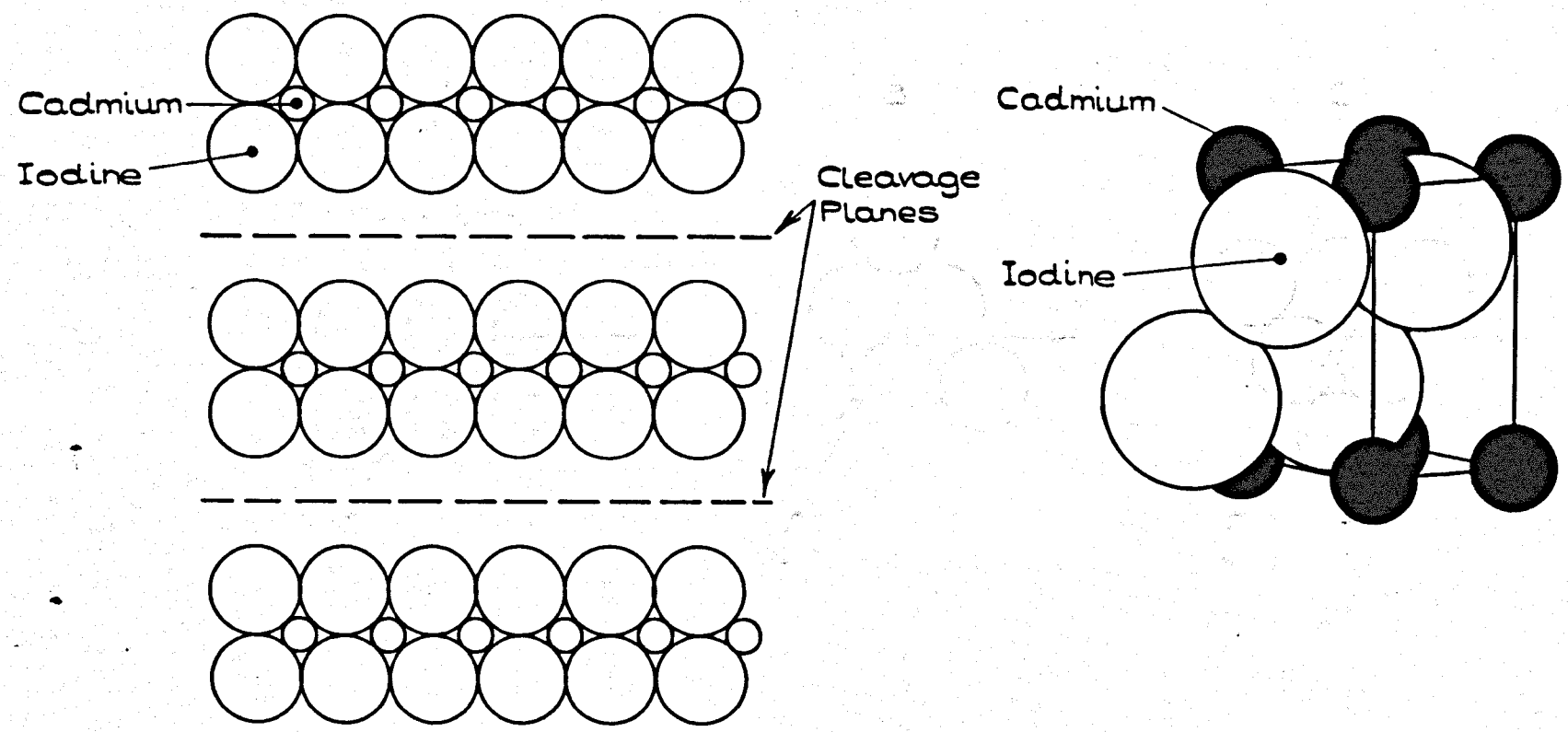

Fig. 8.1

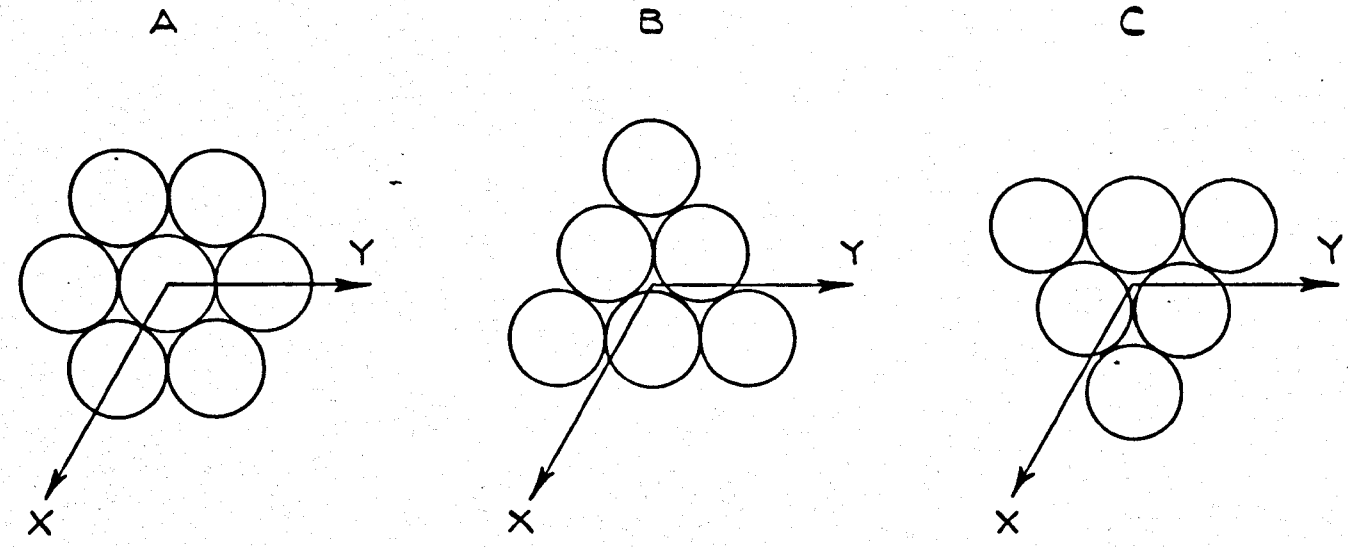

Fig.8.2

Polytypism in CdI_2 was first investigated by Forty (1952) since when many polytypes have been catalogued (Srivastava and Verma 1965). Forty's experiments were concerned with observations of growth spiral step heights by interference microscopy. Growth spirals occur because of crystal growth along screw dislocation lines (Frank 1951). The height of the growth spiral steps was found to be equal to an integral number of polytype periods in many cases. This relationship was not always found, however; Trigunayat and Verma (1962), using both optical and X-ray diffraction techniques, found that a correspondence existed for small period polytypes only.

The majority of crystals grown from solution are of the 4H polytype which has four layers of iodide ions in its polytype period, these are stacked according to |A(Cd)B, C(Cd)B|, where the letters A, B and C refer to iodide ion packing and (Cd) refers to the cadmium ion. Kleber and Fricke (1963) found that 86% of crystals grown in this way had the 4H structure. It is therefore important to remember, when measuring structure sensitive properties, that a significant proportion of crystals grow with other polytype structures. The polytype should therefore be determined, or a significant number of samples used to ensure that the results obtained are not peculiar to a particular polytype.

8.3 Cadmium Iodide Thin Films

The growth and structure of evaporated layers of materials are closely related to the mechanisms of crystal growth.

The optical properties and structure (determined by X-ray diffraction) of thin vacuum deposited films of CdI_2 were found by Best (1963) to be dependent on the substrate temperature during and after deposition. Films prepared on substrates at room temperature appeared to be amorphous whereas those prepared at temperatures near 80°C were crystalline. The optical absorption spectrum, particularly at exciton lines, sharpened considerably when the films changed from the amorphous to the crystalline form.

The texture of vacuum deposited films has been studied recently by Yu (1967) using electron microscopy and electron diffraction. Electron diffraction patterns obtained from films of ~50Å thickness indicated

that the deposited film consisted of randomly distributed particles some 1000Å across. When the film thickness increased to 100Å the particles began to join together and an indication of single crystal diffraction was obtained from some areas. Increasing thickness caused an increase in ordering of the film, so that at 500Å thickness single crystal diffraction patterns were obtained from areas of 100 square microns. The crystalline areas were oriented with their 'c axis' perpendicular to the substrate. The films studied by Yu were all prepared at room temperature, so that the results are not in agreement with those of Best. It is, however, possible that Yu's results were influenced by atmospheric water vapour since the films were exposed to air before measurement.

The optical absorption spectrum of films prepared in vacuo and transferred in vacuo to the measuring cryostat has been investigated by Tubbs (1968). These measurements indicated that film preparation on a substrate at ~80°C gave higher quality films that those prepared at room temperature. The spectrum was also sharpened when the film thickness was increased.

There is strong evidence from Yu's results to indicate that CdI_2 films prepared on substrates at room temperature are largely crystalline, provided that the film thickness is much greater than 200Å. Although this result is not substantiated by Best's experiments, it may be concluded that films of ~1000Å prepared at 80°C are largely crystalline. This result is of some importance since thin film specimens may be necessary for optical absorption measurements in regions of high absorption coefficient. In some parts of the region of fundamental absorption the absorption coefficient may rise to $\sim 10^6$ cm^{-1} so that the maximum specimen thickness that can be used in normal optical transmission experiments is of the order of 1000Å. Single crystals, whose lateral dimensions may be of the order of mm, usually have thicknesses orders of magnitude greater than 1000Å. In the case of CdI_2, crystals of mm width are normally ~100μ thick. Thinner crystals may be obtained from solution by cooling of a saturated solution but manipulation of these is difficult. Evaporated films are therefore the only readily available means of measuring optical absorption at high values of absorption coefficient, (α). Comparison between the absorption spectra of thin films and the reflectivity spectra of single crystals may be made in regions of high absorption coefficient, the reflectivity at high values of α is dominated by the

absorption coefficient, so that there should be good agreement between the two types of spectra at high energies (where α is large).

The films used by Yu (1967) were exposed to the atmosphere between deposition and measurement, there was therefore the possibility of their being affected by atmospheric moisture. This objection could be of some importance in the growth mechanism and future experiments should therefore be performed 'in situ' so that the films are not exposed to the atmosphere.

8.4 The Optical Properties of Cadmium Iodide

The first investigation of the optical absorption spectrum of CdI_2 was conducted by Fesefeldt (1930) who used evaporated films. Fesefeldt's results indicated strong absorption at 3.6eV and 5eV (measured at room temperature).

The observed absorption spectrum was of similar form to that reported for AgCl and TlBr. The material was then studied in single crystal form by Gross and Kapliankii (1955) who reported a narrow absorption band at 3835Å (3.24eV). This band was weak and has not been reported in more recent work on high quality single crystals. Nikitine (1962) duplicated this line using crystals containing a stochiometric excess of iodine and concluded that the line was not an intrinsic feature of the optical spectrum of single crystals of CdI_2. In a recent publication, Yu (1968) indicated that a low energy line has been observed by Greenaway but this line was only observed in crystals containing lead as an impurity.

Great care is therefore necessary in the interpretation of the low energy absorption spectrum of CdI_2. If crystals containing certain impurities are used then the impurity may contribute to the absorption (and to the photoconductivity). This contribution will be small compared with the fundamental absorption but may be significant at low energies, for example in the tail of the indirect absorption edge where $\alpha \lesssim 10^3$ cm^{-1}.

Interest in the region of fundamental absorption at high energies was stimulated by the experiment of Greenaway and Nitsche (1965) on metallic chalcogenides having the CdI_2 structure. Their experiments included measurements of the reflectivity spectrum of CdI_2 single crystals and extended to high energies.

When the optical absorption was measured at low energies and (absorption coefficient)$^{\frac{1}{2}}$ plotted against photon energy linear regions were found indicating that indirect transitions were occurring. The corresponding indirect band edge was found to have a temperature dependence of 1.2×10^{-3}eV/^{o}K; this strong temperature dependence derives from the phonon assistance necessary to conserve electron momentum in the electronic transition.

Features were also reported at 3.8eV and 5.1eV which were thought to correspond to higher energy interband transition thresholds.

The most remarkable features of the reflectivity spectra were the sharp peaks located at 5.6eV and 6.1eV. The strength of these lines and particularly their increase in sharpness with decreasing temperature is typical of exciton line behaviour. These lines were therefore attributed to exciton transitions. It is of particular interest that they occur at some 3eV above the interband edge and in such an anisotropic material.

The work of Greenaway and Nitsche has since been substantiated by the measurements of Brahms (1965) who made measurements at 4.2^{o}K and absorption measurements on evaporated films. The reflectivity peak at 6.2eV was found to have a polarisation dependence so that the peak energy changes by 0.04eV when the polarisation of the light was changed from E$\perp$C to E$\parallel$C.

Tubbs, 1968) has recently made absorption measurements on films of varying thickness prepared under different substrate temperatures. These experiments were part of a programme of research into the optical properties of metallic dihalides. The peaks found in the absorption spectrum of CdI_2 at 3.9eV, 4.6eV, 5.7eV and 6.2eV were designated X_1, X_2, X_3 and X_4 respectively. This nomenclature will be used below.

The X_1 and X_2 peaks were temperature dependent with a coefficient of $\sim 5 \times 10^{-4}$eV/^{o}K, whereas the corresponding figures for the X_3 and X_4 peaks were $\sim 4 \times 10^{-4}$eV/^{o}K. The spectra obtained from thin film absorption and single crystal reflectivity experiments are in good agreement, so that the optical spectrum of CdI_2 is well established. Tubbs has proposed an excitation model to explain the optical spectrum and to correlate it with the spectra of other similar halides.

The optical absorption spectrum of CdI_2 was compared with that for many other iodides and many common features were found.

The low energy peaks, X_1 and X_2, could be observed in the majority of the iodides investigated, but the X_2 peak was absent in ZnI_2. The higher energy peaks X_3 and X_4 were present in Cd, Mn, Pb and Sb iodides.

These results indicated that the peaks were associated with excitation of the iodide ion since they are present for iodides of such a variety of metals. The position of the X_1 peak in the majority of iodides varies linearly with the inverse square of the interionic distance so that the particle in a box model is apparently appropriate. The iodide ion is thought to have excited states $5p^5 6s$ and $5p^6 6p$ which are hybridized by the strong interionic electric field (which exists because an I^- ion has a Cd^{++} on one side and an I^- ion on the other). These levels are then split by the spin-orbit coupling to give four excited levels. These excited levels may then be reached by allowed transitions from the ground state, leading to the experimentally observed peaks X_1-X_4. This model therefore predicts similar temperature dependences for each element of the doublet.

8.5 Cadmium Iodide Band Scheme

The band scheme of CdI_2 derived from the excitation model is shown in figure 8.3, it consists of a pair of spin-orbit split valence bands derived from the iodide ion. The spin orbit splitting is therefore that of this ion and is $\sim$0.6eV. The upper valence band is lifted at $k \neq 0$ to give an indirect band edge in a similar way to that in AgCl and AgBr.

There is also a pair of conduction bands, or alternatively a single band with an extremum at $k \neq 0$. This then allows excitons to be associated with each band or with two extrema of the same band. The sharpness of the X_3 and X_4 exciton peaks indicates that the exciton states have a long lifetime and suggests that the band pair model is appropriate, since it allows exciton transitions associated with conduction band minima. Excitons derived from sadle points at $k \neq 0$ may not form bound states (Duke and Segall (1966), Velicky and Sak (1966). Our evidence for exciton diffusion also indicates that these excitons have finite lifetimes.

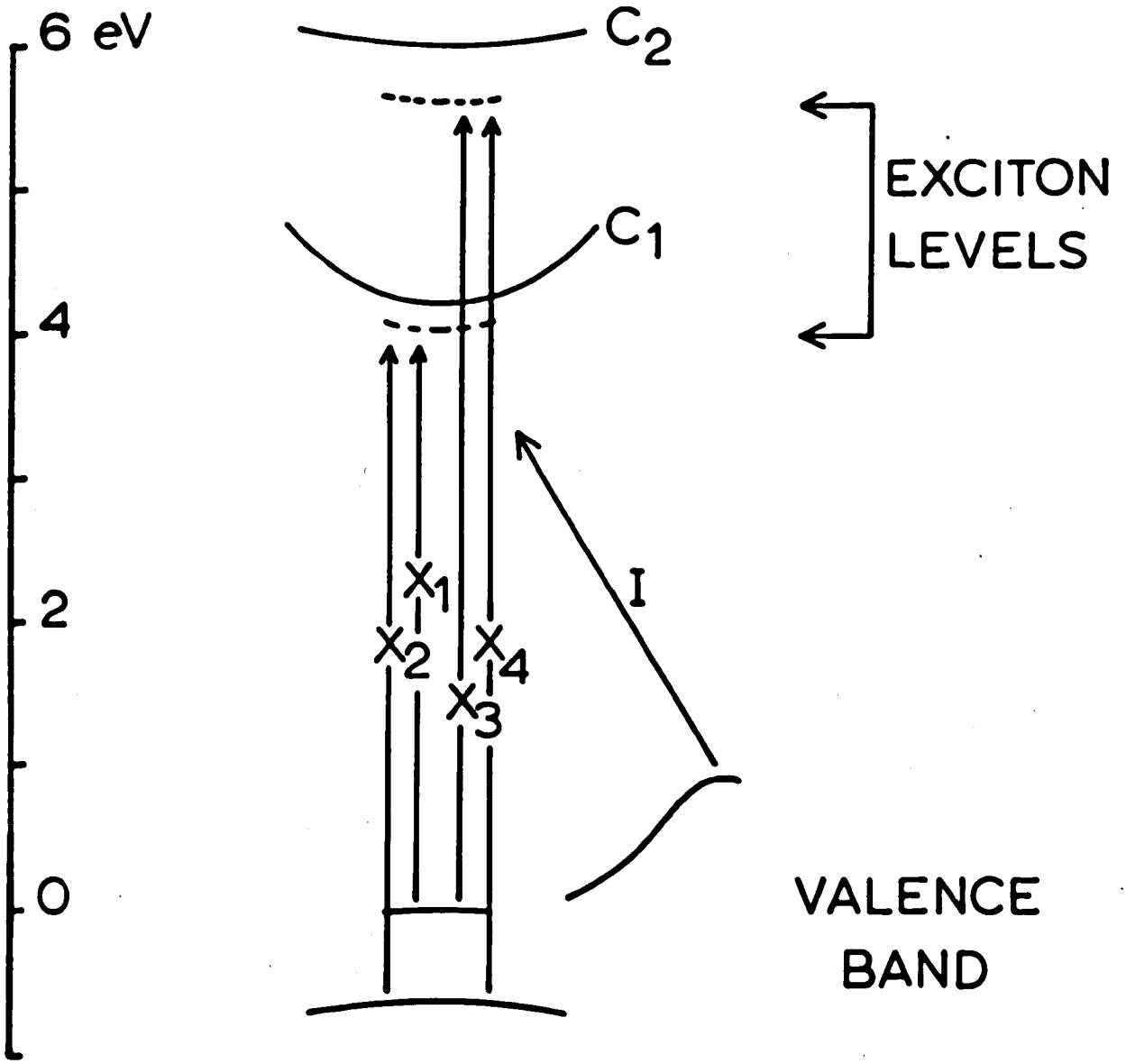

Fig. 8·3

The sharp peaks X_3 and X_4 correspond to transitions from the valence bands to the exciton states derived from the upper conduction band. The shape of these exciton peaks is probably caused by the high density of states near the miminum of the conduction band. There are sharp anti-resonant dips on the high energy side of the peaks which may be caused by the degeneracy of the exciton and interband transition processes, (Brahms 1965).

The low energy exciton peaks X_1 and X_2 are associated with the lower conduction band, the energy difference between the X_1 and X_2 peaks is approximately equal to that between X_3 and X_4. The difference of some 0.1eV between the separations may be due to the differences in binding energies of the excitons.

The semi-empirical model described above accounts for the observed features of the optical absorption and photoconductivity spectra. Remarkable similarities between iodides described by Tubbs (1968) suggests that a band structure calculation for a typical member would be very useful in associating the structure observed in optical absorption experiments with transitions at particular points in the Brillouin Zone.

8.6 Photoconductivity in Cadmium Iodide

When optical absorption takes place in the region of fundamental absorption electrons may be excited into the conduction band. The conduction electrons may then be detected by measuring the corresponding current in an electric field. In principle this technique measures the efficiency of electron production. If the number of incident photons is measured and compared with the number of electrons detected the variation of the quantum efficiency of electron production with wavelength may be determined. In this way absorption processes leading to free electrons and those forming non-conducting states may be distinguished.

It is not possible, however, to measure the number of electrons created directly since many secondary processes occur. The electrons and holes may be trapped at impurities or other defects and take no further part in conduction or the trapping may lead to a recombination of opposite charges. When the absorption coefficient of the illumination is large the generation rate of charge carriers depends upon the depth in the crystal. The distribution of trapping or recombination centres may also

depend upon the distance from the crystal surface. These factors mean that the measured quantum efficiency depends upon the absorption coefficient, the sample purity, the electrode geometry as well as the illumination intensity and the nature of the absorption process.

In the case of CdI_2 we have shown that the quantum efficiency of photoconductivity depends smoothly upon the absorption coefficient. This result is in good agreement with the theoretical model of De Vore (1956), who showed that a low energy peak in photoconductivity was caused by the balance between surface and volume recombination rates. The smooth dependence of photoresponse on absorption coefficient ceases at the X_3 exciton peak where the quantum efficiency is greater than that expected on the absorption coefficient basis. The quantum efficiencies used to plot the curves had been corrected for reflectivity loss.

The apparent increase in quantum efficiency at the exciton lines is surprising since excitons are non conducting states. Excitation into an exciton state leads to equal and opposite bound charges whose collective motion leads to zero total current. Photoconductivity may therefore only occur when excitons dissociate.

Our results indicate that photons absorbed at exciton lines not only lead to photoconductivity but to a higher photoconductivity than band to band transitions at the same absorption coefficient. This result was interpreted in terms of exciton diffusion.

When photons are absorbed at energies corresponding to band to band transitions the electron hole pairs generated contribute to photoconductivity directly.

If the absorption of photons leads to the creation of excitons, however, photoconductivity will only result when the excitons dissociate. The quantum efficiency of the photoresponse of the exciton process will therefore be lower if the two processes have the same absorption coefficient and if no exciton diffusion occurs.

Since the absorption coefficient in the exciton region is large ($\sim 10^6 cm^{-1}$) the direct interband process generates electrons and holes in a layer near the surface of the crystal, these charges may then diffuse, recombine or be trapped.

In the exciton process, excitons are created in the same surface layer and if no diffusion occurs they may annihilate to free electrons and holes, or recombine. The number of charges created for a given number of absorbed photons will therefore be less than that for the interband process. These charges will then be generated in similar conditions to those generated by band to band transitions so that the photoconductivity will be lower.

If the excitons are allowed to diffuse away from the surface layer where the carrier recombination rate may be high, they may travel to a region of relatively low density of recombination centres. The corresponding photoconductivity may then be increased.

Our photoconductivity result is therefore evidence for exciton diffusion. It is also possible that absorption at exciton lines caused re-emission at lower energies and correspondingly lower absorption coefficients. Luminescense could cause this effect but would probably lead to an increased effect at 10°K, which was not observed.

If exciton diffusion occurs it should be possible to estimate their diffusion length by varying the sample thickness. When this falls below the diffusion length the exciton photoconductivity should decrease relative to that in the interband region. For these measurements the properties which influence photoconductivity should not depend upon the specimen thickness. In the case of thin films many physical properties do depend upon the thickness and deposition rate, so that great care is necessary in these experiments.

8.7 The Ionic Conductivity of Cadmium Iodide Single Crystals

When an electric field is applied to a crystal containing charged defects the defects may move in the applied field and contribute to the 'dark current'. The corresponding conductivity is known as the ionic conductivity.

In many crystals, such as narrow band-gap semiconductors, a small amount of energy is sufficient to raise electrons from the valence band into excited states in the conduction band. The material then exhibits electronic conduction with no external excitation provided that the required energy is available from lattice vibrations.

In strongly ionic crystals only a small number of electrons may be thermally excited because of the large band gaps of these materials, so that electronic conduction will not be significant. The dark conductivity will therefore be caused by the motion of ionic defects. These defects may consist of ions or ion vacancies. The number of charge carriers of a given type available at a temperature T will be determined by the energy of formation of that defect. The contribution to the ionic conductivity of a given defect, will also depend upon the energy required to move the defect from one site to an equivalent site displaced by a lattice period. If w is the defect formation energy and u is the energy required to move it from one lattice position to the nearest equivalent one then the contribution to the conductivity is given by

$$\sigma = \frac{\nu A e^2 e}{kT}^{\frac{w+u}{kT}} \quad . \quad . \quad . \quad . \quad . \quad . \quad . \quad . \quad . \quad . \quad . \quad 8.1$$

where A is constant for the particular defect and depends upon the entropy charge due to the defect and upon the lattice parameter, ν is a frequency factor related to the lattice vibration frequencies.

The equation may be written

$$\sigma = 2\nu ABNa^2e^2e^{-(\frac{3u+E}{3kT})} \quad . \quad . \quad . \quad . \quad . \quad . \quad . \quad . \quad . \quad 8.2$$

for a material of the CdI_2 type where σ is the contribution from vacancies and E is the formation energy of a vacancy set, consisting of one Cd^{++} and two I^- vacancies.

If $\log \sigma T$ is plotted against $\frac{1}{T}$ a straight line may be obtained whose slope gives w+u at high temperatures (intrinsic region) where the defect concentration does not depend upon impurities.

A second linear region at lower temperatures is influenced by impurities (extrinsic region), the slope in this region depends upon u only since the defects are not formed by thermal excitation.

Measurements of the ionic conductivity of CdI_2 have been made by Fotland (1959) and by Yu (1967), both using single crystals. Measurements were made along the c axis and in the perpendicular direction. The conductivity perpendicular to the c axis was ~500 times greater than that in the parallel direction. The activation energies of the two orientations were the same, however, so that the curves of

log σ against $\frac{1}{T}$ were parallel. Yu found that the conductivity of solution-grown crystals could be represented by an equation of the form

$$\sigma = \sigma' e^{-\frac{0.8eV}{kT}} + \sigma'' e^{-\frac{0.5eV}{kT}} \quad . \quad . \quad . \quad . \quad . \quad . \quad . \quad 8.3$$

where σ' and σ'' are independent of temperature but dependent upon the orientation.

The first term was dominant at high temperatures and the second at temperatures below 350°C. These measurements did not extend below room temperature. A second set extended from RT to 210°K, but these measurements were confined to the higher conductivity direction. An activation energy of 0.5eV was apparent above ~250°K which increased to 0.9eV below this temperature.

Fotland investigated the higher temperature region and found that the activation energy was 0.3eV for temperatures above 500°K. For T < 500°K this fell to 1.4eV for solution-grown crystals and was apparently 0.8eV for melt grown samples.

There appear to be four different conductivity regions in CdI_2; these are summarised in the table below and compared with similar layer type materials such as PbI_2 (Seith 1933) $PbCl_2$ (De Vries 1965) and $PbBr_2$ (Verwey and Schoonman 1967).

The lower temperature regions indicated depend upon the concentration and nature of the sample impurities.

	Activation Energy eV	Temperature Range °K
CdI_2	3	>500
	0.8 - 1.4	350 - 500
	0.5	250 - 350
	0.9	<250
PbI_2	1.2	>350
	0.38	<350
$PbCl_2$	0.87	>300
	0.35	<300
PbBr	0.77	>200
	0.29	<200

The CdI_2 results may be compared with those reported by Seith (1933) for PbI_2 which has a similar layer structure. A radioactive tracer technique has been used to determine diffusion activation energies in PbI_2. These were in agreement with those for the intrinsic ion conductivity. Pb^{++} intertitials are probably the main current carriers in this region. It is not likely that the larger iodide ions are mobile. Iodide ion vacancies probably contribute to the current in the extrinsic impurity region.

The intrinsic conductivity in $PbBr_2$ and $PbCl_2$ is apparently due to iodide ion vacancies; in the extrinsic region only those impurities which would create iodide ion vacancies increased the ionic current. Interstitial ions were not throught to be significant because of the size of the ions relative to the available interstitial space. The radius of Pb^{++} ions is 1.2Å and those of Br^- and Cl^- are 1.95 and 1.8Å respectively.

In CdI_2 the Cd^{++} ions have a radius of 0.97Å whereas the iodide ion is 2.16Å. There may therefore be a larger number of metallic ion defects in CdI_2 than in the materials described above.

It is possible that the lowest temperature region of the conductivity of CdI_2 is connected with a particular defect or with defect association. The next two higher temperature linear regions are similar to those in the lead dihalides and are probably connected with iodide ion vacancies or with Cd^{++} interstitials. At the highest temperatures the high activation energies of 3eV may be connected with the diffusion of silver ions (see Chapter Seven) since 'silver dag' electrodes were used.

It is clear that a thorough investigation is necessary involving controlled doping and measurements over the entire temperature range. Stable ohmic electrodes such as evaporated gold must be used and particular attention paid to leakage currents at low temperature.

8.8 Photodecomposition in Cadmium Iodide

The phenomenon of photodecomposition is closely related to the optical properties and ionic and electronic conductivities of a given crystal.

The silver halides are the best known and most widely used materials that exhibit photodecomposition. In these materials large exposures are necessary to give print-out images; it is therefore usual to reduce the required exposure by means of a chemical development process. A 'latent' image may then be formed with a very small illumination intensity. The latent images cannot be altered after fixing so that it is therefore difficult to add information to the initial record. The resolution of the process is limited by the grain size of the developed image.

Lead iodide has also been shown to exhibit an interesting photolytic effect. This is a direct print out process with a maximum sensitivity near 190°C. The effect is related to the absorption of light in the intrinsic absorption region and the quantum efficiency of the decomposition has a similar form to that of the optical absorption (Tubbs 1965). The main advantages of the PbI_2 process over the silver halide process are the superior resolution and the absence of chemical development. The chief disadvantages of this material are the poorer constrast, which may be improved by suitable choice of method of observation, and lower technical sensitivity. The latter disadvantage may not be of importance in applications where safe handling and small images are required.

Cadmium iodide also exhibits photodecomposition. Filter papers soaked in CdI_2 solution and allowed to dry are sensitive to light at room temperature. The paper, which is normally white, turns brown or black after strong ultra-violet illumination. Single crystals do not exhibit appreciable sensitivity at room temperature. The increases sensitivity of the CdI_2 papers is thought to be due to water contained in the paper and to the smaller crystallite size, Fotland (1959). It is preferable to study photodecomposition in single crystals or films, however, since these are more likely to give reproducible photo-effects characteristic of the pure material.

In our investigations of photodecomposition in single crystals large exposures were necessary to produce noticeable decomposition. The total output of a Xenon arc lamp (i.e. some 30m watts UV output concentrated into an area some 1cm square) was used with an exposure of several hours to give a marked discoloration. The material appeared to decompose most readily at 250°C; this temperature was the maximum possible because of the sublimation of the crystal at higher temperatures.

Satisfactory decomposition could not be obtained in vacuo because of the evaporation of CdI_2. It was therefore necessary to use an inert gas such as argon for decomposition in an air-free atmosphere.

It is clear from the above results that single crystals of CdI_2 do not have sufficient sensitivity to make the material competitive with other photosensitive materials. It may be possible to increase the sensitivity by doping with, for example, silver in the same way as for PbI_2 (Tubbs, Beasley and Foster 1969). There is no reason to suggest that cadmium iodide would then be any more sensitive than PbI_2 although a feasibility study would be extremely useful.

Several interesting phenomena were observed during the studies of photodecomposition. One experiment was concerned with the effect of an electric field on the position of the photodecomposition products. An electric field was applied during photodecomposition in an attempt to detect any displacement of the decomposition into a masked region. Although no effect could be detected an interesting phenomenon was observed. When silver in the form of 'silver dag' or metallic silver was used as an electrode material tree-like growth of silver were formed inside the crystal. These branches of silver grew from the negative electrode towards the positive. Interference fringes were observed around the branches indicating that the layers of CdI_2 were being forced apart by the metallic silver. This experiment indicated that silver ions diffuse readily in CdI_2 at sufficiently high temperatures. The process occurs most readily parallel to the basal plane, and could not be detected in the perpendicular direction in a much stronger electric field. The silver diffusion anisotropy is in good qualitative agreement with the conductivity anisotropy found by Yu (1967) and by Fotland (1959).

8.9 Polarisation Phenomena in Cadmium Iodide

An interesting feature of the conductivity measurements on CdI_2 is the decay of the current with time. This decay is caused by the polarisation of the sample. In the case of ionic polarisation the application of the electric field causes ionic displacement which leads to an opposite internal field and consequent polarisation. The polarisation field in CdI_2 is probably caused by two components, one from the

dielectric relaxation of the crystal lattice and the other from the space charge formed by the ionic carriers. The increased internal field near the electrode suggests that the space charge exists. Further experiments are necessary to clarify this phenomenon. The anisotropy of the ionic conductivity makes CdI_2 an interesting material for the study of polarisation phenomena because of the possibility of different polarisation rates in the two main crystallographic directions.

The photocurrent was also found to decay with time, indicating that electronic polarisation was taking place. This effect coupled with the ionic polarisation made photoconductivity measurements difficult. The polarisation of the photocurrent could be reduced by the use of low illumination intensity, whereas the ionic conductivity could only be reduced by lowering the sample temperature.

The photoconductivity polarisation arises from trapping of photo-generated carriers at localised sites in the sample. These carriers move in the direction of the internal electric field before being trapped, so that there is a mean displacement between oppositely charged trapped carriers. This displacement creates an internal polarisation field in opposition to the applied field.

The photoconductivity polarisation in CdI_2 depended upon both the energy and the intensity of the illumination, so that great care was necessary in measurements of photoresponse spectra.

8.10 Proposals for Future Work

1. Photoconductivity

The low temperature photoconductivity spectrum of CdI_2 contains sharp dips at high energies corresponding to exciton transitions. When the spectrum was corrected for reflectivity loss these sharp features were smoothed out. The final shape of the photoresponse curve for absorbed photons depended upon the shape of both the photoconductivity and reflectivity curves at that temperature. Ideally both spectra should be recorded simultaneously on the same sample in the same appartus.

In many photoconductivity experiments, particularly those where higher intensities than those used in our experiments are used, the photocurrent is not proportional to the intensity. It is usual in these circumstances to measure the photoconductivity for a constant number of incident photons. A linear photoconductivity-intensity relationship must then be assumed if a correction is to be applied for the reflectivity loss. It would be more satisfactory in many cases to maintain a constant number of absorbed photons and the reflectivity spectrum must therefore be known. An apparatus has therefore been designed to measure photoconductivity and to compensate for the loss by reflection.

In this apparatus (fig. 8.4) an illumination intensity $I_o(\nu)$ is partially reflected from the plate A and transmitted through the second parallel and identical plate B. The photocell P_1 therefore receives an intensity $I_o(\nu)\, R_A(1-R_B)T_B$ where R_A, R_B and T_A and T_B are the relevant reflectivities and transmission coefficients of the plates.

The light transmitted through A has an intensity $I_o(\nu)(1-R_A)T_A$ which is reduced to $I_o(\nu)(1-R_A)T_AR_S$ after reflection from the sample. Reflection from A onto the second photocell (P_2) therefore leads to an intensity $I_o(\nu)(1-R_A)T_AR_SR_A$.

If each photocell has an identical spectral response then the signals may be amplified and subtracted to give a signal of the form

$$S = A\left[I_o(\nu)R_A(1-R_B)T_B - I_o(\nu)(1-R_A)T_AR_SR_A\right]$$

If $R_A = R_B$ and $T_A = T_B$

then

$$S = A\left[I_o(\nu)R_A(1-R_A)T_A\ (1-R_S)\right]$$

which is proportioal to

$$I_o(\nu)R_A(1-R_A)T_A(1-R_S)$$

The number of photons absorbed by the sample is $I_o(\nu)(1-R_S)$ and this quantity must be constant. If R_A and T_A are constant then it is sufficient to make S constant, thereby making the number of photons absorbed constant. This may be accomplished by comparing S with a

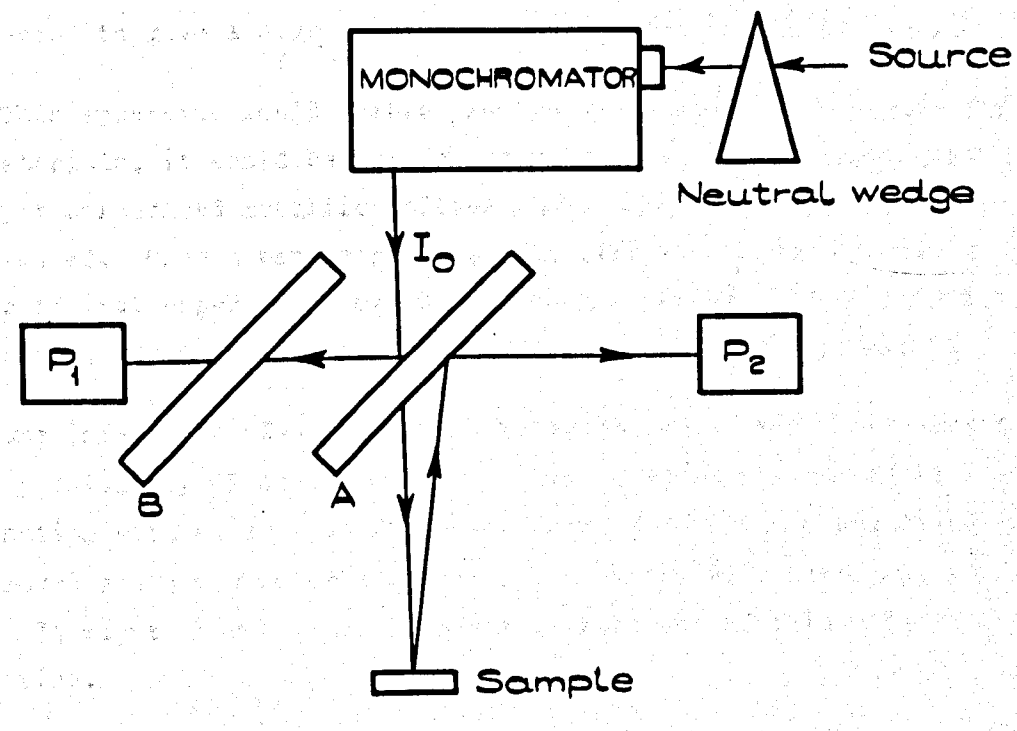

Fig. 8.4

reference signal and the difference fed into a servo system operating a neutral density wedge in the monochromator input. The number of absorbed photons could then be held at a fixed vlaue. If R_A and T_A were not constant it would then be necessary to incorporate wavelength dependent compensation into the photocell output. In many cases, for example 'Suprasil' when used with wavelengths above 200mμ, the values of R_A and T_A vary slowly and would not be significant in regions of rapidly varying sample reflectivity.

An alternative apparatus could utilise a rotating mirror system and one photocell only. The photocell would receive the light from the monochromator during part of a cycle and that reflected from the sample during the next equal part of the cycle. The two signals could then be substracted to give a signal which was proportional to $I_o(\nu)(1-R_S)$.

This apparatus would enable precise measurements to be made for many materials, it would be particularly interesting to investigate the layer structured metallic iodides whose absorption spectra has been studied. Once a band structure calculation has been performed further optical experiments may be necessary. It will be of interest, for example, to study the spectra of mixed crystals of this group.

One interesting feature of the polarisation of the photocurrent is the possibility of charge storage. The polarisation caused by illumination with an applied field persisted when the applied field was removed and could be detected by illumination with zero applied field. It might therefore be possible to make use of this effect in a device.

One of the standard television camera tubes is the "Vidicon" which has a thin film of photoconductor on its upper surface. An electron beam scans this photoconductor which is illuminated by the visual scene. A positive potential applied to a front semi-transparent electrode creates an electric field in the photoconductor when the electron beam negatively charged the rear surface. Illumination then causes a current to flow so that the rear negative charge is reduced. The scanning electron beam removes the effective positive charge thereby causing a potential change at the front electrode. The potential change constitutes the signal.

In a material of the CdI_2 type, semi-transparent electrodes could be used on both front and rear. An electric field could then be applied between the electrodes, when suitable illumination would cause a trapped charge polarisation double layer. This would persist at low temperatures so that the polarisation could be detected by scanning with an electron beam or ultra violet light beam, leading to a current in the opposite direction to the original field. Such a device would not be practicable with pure CdI_2 because of the lack of visible response, but a material having similar electronic properties might be suitable. It might also be possible to use a doped material, thereby changing the spectral response.

As far as the intrinsic properties of photoconductivity are concerned it would be of interest to study the effects of exciton diffusion on the polarisation. This should be reduced if exciton diffusion occurs, so that it would be interesting to study the effect of thickness variation on both photoconductivity and polarisation.

2. Ionic Conductivity

In the case of the ionic conductivity of CdI_2 the results are so far not conclusive. It would be necessary in future experiments to use electrodes that did not diffuse into the sample. Evaporated gold electrodes are suitable for these measurements and would remove doubts about the high temperature conductivity. A more suitable sample holder would then be necessary since PTFE decomposes at temperatures near 250°C. Quartz or alumina would be suitable for these measurements.

At lower temperatures, where impurity effects are important, particular attention should be paid to the insulation of the sample holder since very low currents may be involved.

High purity crystals should be used and subsequently doped with known amounts of impurities, these could for example, be in the form of mono or trivalent metallic iodides which would indicate if iodide ion vacancies were contributing to the current.

REFERENCES

Best, K.J., 1963, Phys.Kondens.Materia. 1,316

Brahms, S., 1965, Phys.Letters 19, 272

De Vore, H.B., 1956, Phys.Rev. 102, 86

Dawood, R.I., Forty, A.J. and Tubbs, M.R., 1965, Proc.Roy.Soc. 284, 272

De Vries, K.J., 1965, Thesis, Utrecht.

Duke, C.B. and Segall, B., 1966, Phys.Rev.Lett. 17, 19.

Fesefeldt, H., 1930, Z.Physik, 64, 741.

Forty, A.J., 1952, Phil.Mag. 43, 377.

Fotland, R.A., 1959, Thesis, Case Inst. of Technology.

Frank, F.C., 1951, Phil.Mag. 42, 1614.

Greenaway, D.L. and Nitsche, R., 1965, J.Phys.Chem.Solids 26, 1445.

Gross, E.F. and Kaplianskii, A.A., 1955, Zhur.Tekh.Fiz. 25, 2061.

Kleber, W. and Fricke, P., 1963, Z.Phys.Chem. 224, 353.

Nikitine, S., 1962, Progress in Semiconductors 6, 233.

Seith, W., 1933, Z.Electrochem. 39, 538.

Srivastava, O.N. and Verma, A.R., 1965, Acta.Cryst. 19, 56.

Trigunayat, G.C. and Verma, A.R., 1962, Acta.Cryst. 15 499.

Tubbs, M.R., 1968, J.Phys.Chem.Solids 29, 1191.

Tubbs, M.R., Beesley, M.J. and Foster, H., 1969, Brit.J.Appl.Phys. 2, 197.

Velicky, B. and Sak, J., 1966, Phys.Stat.Sol. 16, 147.

Verway, J.F. and Schoonman, J., 1967, Physica 35, 386.

Yu, R.M., 1967a, Ph.D. Thesis, University of Bristol.

Yu, R.M., 1967b, Phil.Mag. 16, 1167.

Yu, R.M., 1969, J.Phys.Chem.Solids, 30, 63.